Distance-Based Formation Control of Multi-Agent Systems

Reza Babazadeh

A Thesis
in
The Department
of
Electrical and Computer Engineering

Presented in Partial Fulfillment of the Requirements
for the Degree of
Doctor of Philosophy (Electrical and Computer Engineering) at
Concordia University
Montreal, Quebec, Canada

December 2021

CONCORDIA UNIVERSITY
SCHOOL OF GRADUATE STUDIES

This is to certify that the thesis prepared

By: Reza Babazadeh

Entitled: Distance-Based Formation Control of Multi-Agent Systems

and submitted in partial fulfillment of the requirements for the degree of

Doctor Of Philosophy (Electrical & Computer Engineering)

complies with the regulations of the University and meets the accepted standards with respect to originality and quality.

Signed by the final examining committee:

_____ Chair
Dr. Anjan Bhowmick

_____ External Examiner
Dr. James Richard Forbes

_____ External to Program
Dr. Chun-Yi Su

_____ Examiner
Dr. Shahin Hashtrudi Zad

_____ Examiner
Dr. Kash Khorasani

_____ Thesis Supervisor
Dr. Rastko R. Selmic

Approved by _____
Dr. Wei-Ping Zhu, Graduate Program Director

12/6/2021 _____
Dr. Mourad Debbabi, Dean
Gina Cody School of Engineering and Computer Science

Abstract

Distance-Based Formation Control of Multi-Agent Systems
Reza Babazadeh, Ph.D.
Concordia University, 2021

This Ph.D. dissertation studies the distance-based formation control of multi-agent systems. A new approach to the distance-based formation control problem is proposed in this thesis. We formulated distance-based formation in a nonlinear optimal control framework and used the state-dependent Riccati equation (SDRE) technique as the primary tool for solving the optimal control problem. In general, a distance-based formation can be undirected, where distance constraints between pairs of agents are actively controlled by both adjacent agents, or directed, where just one of the neighboring agents is responsible for maintaining the desired distance. This thesis presents both, undirected and directed formations, and provides extensive simulations to verify the theoretical results.

For undirected topologies, we studied the formation control problem where we showed that the proposed control law results in the global asymptotic stability of the closed-loop system under certain conditions. The formation tracking problem was studied, and the uniform ultimate boundedness of the solutions is rigorously proven. The proposed method guarantees collision avoidance among neighboring agents and prevents depletion of the agents' energy. In the directed distance-based formation control case, we developed a distributed, hierarchical control scheme for a particular class of directed graphs, namely directed triangulated and trilateral Laman graphs. The proposed controller ensures the global asymptotic stability of the desired formation. Rigorous stability analyses are carried out in all cases. Moreover, we addressed the flip-ambiguity issue by using the signed area and signed volume constraints. Additionally, we introduced a performance index for a formation mission that can indicate the controller's overall performance.

We also studied the distance-based formation control of nonlinear agents. We proposed a method that can guarantee asymptotic stability of the distance-based formation for a broad category of nonlinear systems. Furthermore, we studied a distance-based formation control of uncertain nonlinear agents. Based on the combination of integral sliding mode control (ISMC) theory with the SDRE method, we developed a robust optimal formation control scheme that guarantees asymptotic stability of the desired distance-based formation in the presence of bounded uncertainties. We have shown that the proposed controller can compensate for the effect of uncertainties in individual agents on the overall formation.

Acknowledgments

Bellman's principle of optimality:

"An optimal policy has the property that whatever the initial state and initial decision are, the remaining decisions must constitute an optimal policy with regard to the state resulting from the first decision."

I want to express my thankfulness to my supervisor, professor Rastko R. Selmic. Without his guidance, this Ph.D. journey would not be possible. I will always be grateful for all his help, support, and academic freedom he gave to me. Also, I learn much from him in life and academic professionalism. I want to sincerely thank my committee members, Dr. Khorasani, Dr. Hashtrudi Zad, Dr. Su, and Dr. Forbes, for their time and helpful feedback.

Finally, I would like to express my ultimate gratefulness to my family, whom I can not have come along this long journey without their support.

This thesis is dedicated to all unknown mathematicians, scientists, and engineers whose their endless sacrifices bring us all to this point.

Contents

List of Figures ix

List of Tables xiii

List of Abbreviations xiv

List of Publications xv

1 Introduction 1

1.1 Literature Review . . . 1
1.1.1 Formation Control . . . 1
1.1.2 Distance-Based Formation . . . 3
1.1.3 Undirected Formation . . . 4
1.1.4 Directed Formation . . . 6
1.1.5 Formation of Nonlinear Agents . . . 7
1.1.6 Robust Optimal Formation . . . 7
1.2 Contributions . . . 9
1.3 Summary and Dissertation Outline . . . 11

2 Background 13

2.1 Introduction . . . 13
2.2 Problem Statement . . . 13
2.2.1 Notation . . . 14
2.3 Graph Theory . . . 14
2.3.1 Undirected Graphs . . . 14
2.3.2 Directed Graphs . . . 17
2.3.3 Securing Persistence . . . 23
2.3.4 Directed Job Assignment for Formation Topologies . . . 24
2.4 Agent Modeling . . . 28
2.4.1 Single-Integrator Model . . . 28
2.4.2 Double-Integrator Model . . . 28
2.4.3 Agent Energy Model . . . 29

2.4.4 Augmented Agent Model with Energy State . . . 30
2.5 SDRE Method . . . 30
2.5.1 Extended Linearization . . . 31
2.5.2 SDRE Controller . . . 32
2.5.3 Stabilizability and Detectability of SDC Representation . . . 33
2.5.4 SDRE State Tracking . . . 34
2.5.5 SDRE Output Tracking . . . 35
2.5.6 HSDRE Method . . . 36
2.6 Stability of Interconnected Systems . . . 36
2.7 Signed Area and Signed Volume . . . 38

3 Leader-Follower Formation Control **41**
3.1 Introduction . . . 41
3.2 Main Results . . . 41
3.2.1 Single-Integrator Model . . . 41
3.2.2 Double-Integrator Model . . . 44
3.2.3 Selection of Weighting Matrices . . . 46
3.3 Simulation Results . . . 46
3.4 Conclusions . . . 51

4 Undirected Distance-Based Formation Control **53**
4.1 Introduction . . . 53
4.2 Cost Functional . . . 53
4.3 Formation Producing Control . . . 55
4.3.1 Single-Integrator Model . . . 56
4.3.2 Double-Integrator Model . . . 60
4.4 Formation Tracking Control . . . 64
4.4.1 Single-Integrator Model . . . 64
4.4.2 Double-Integrator Model . . . 65
4.5 Simulation Results . . . 67
4.6 Conclusions . . . 76

5 Directed Distance-Based Formation Control **77**
5.1 Introduction . . . 77
5.2 Cost Functional . . . 77
5.3 2-D Space . . . 78
5.3.1 Single-Integrator Model . . . 78
5.3.2 Double-Integrator Model . . . 82
5.3.3 Reflection Prevention and Collision Avoidance . . . 86
5.4 3-D Space . . . 87

5.4.1 Single-Integrator Model . . . 87
5.4.2 Double-Integrator Model . . . 94
5.4.3 Reflection Prevention and Collision Avoidance . . . 100
5.5 Simulation Results . . . 101
5.5.1 2-D Space . . . 101
5.5.2 3-D space . . . 102
5.5.3 Control Performance Function . . . 103
5.6 Conclusions . . . 109

6 Distance-Based Formation Control of Nonlinear Agents 110
6.1 Introduction . . . 110
6.2 Nonlinear Homogeneous Agents in 2-D Space . . . 110
6.2.1 Agent Model . . . 111
6.3 Nonlinear Heterogeneous Agents in 3-D Space . . . 118
6.3.1 Agent Model . . . 118
6.4 Simulation Results . . . 127
6.4.1 2-D Space . . . 127
6.4.2 3-D Space . . . 130
6.5 Conclusions . . . 138

7 Robust Optimal Distance-Based Formation Control 142
7.1 Introduction . . . 142
7.2 Controller Design . . . 142
7.2.1 Matched Uncertainty . . . 149
7.3 Formation Stability . . . 150
7.4 Selection of Weighting Matrices . . . 151
7.5 Simulation Results . . . 152
7.5.1 2-D Space . . . 152
7.5.2 3-D Space . . . 156
7.5.3 Unmatched Uncertainty . . . 159
7.6 Conclusions . . . 162

8 Summary and Future Works 163
8.1 Summary . . . 163
8.2 Future Work . . . 164

Bibliography 166

Appendices 181

A SDC Parametrization 182

B Gradient-Based Controller 183

List of Figures

1.1 Geese fly in "V" shape formation. Picture taken from [1]. 2
1.2 Specifications of different formation control approaches. Figure taken from [2]. 3

2.1 Graph rigidity: nonrigid or flexible graph (a), minimally rigid graph where changing node 1 to 1' makes flip ambiguity (b), and globally rigid graph (c). 16
2.2 Henneberg construction: a minimally rigid graph (a) results in (b) using vertex addition and in (c) using edge splitting. Both constructed graphs preserve minimal rigidity. 18
2.3 Persistency of directed graphs: (a) graph is not constraint consistent because agent #2 has too many constraints to satisfy. While agent #4 can move freely over a circle around agent #3, agent #2 cannot satisfy all its associated desired distances. The graph depicted in (b) is constraint consistent. 18
2.4 Two directed triangular seeds. 22
2.5 Constructing a directed Laman graph: (a) primitive leader-first-follower structure; (b) constructing a new triangulated Laman graph in 2-D, and (c) constructing a new trilateral Laman graph in 3-D using directed vertex addition procedure. 22
2.6 Structural persistency of directed graphs in 3-D: the graph depicted in (a) is not structurally persistent since the agent #1 and #5 can freely move, it is impossible to other agents to preserve their constraints. The graph depicted in (b) is structurally persistent. 23
2.7 Special form of persistence directed graphs: (a) wheel graph, (b) C^2-graph. 24
2.8 Proposed job assignment algorithm: (a) the desired topology of the agents; (b) the corresponding Delaunay triangulation; (c) the out put of the proposed algorithm as a minimally persistent acyclic LFF graph. 25
2.9 Moser spindle: a famous Laman graph. 26

2.10 Proposed algorithm for Moser spindle: (top) the desired topology of the agents; (middle) the respective Delaunay triangulation; (bottom) the out put of the proposed algorithm as a minimally persistent acyclic LFF graph. 27
2.11 Reflection of the desired formation in 2-D space. 39
2.12 Reflection of the desired formation in 3-D space. 40

3.1 Displacement-based formation for $N = 3$ agents. 42
3.2 Leader-follower formation control for $N = 5$ agents modeled by a single-integrator; all followers have the same energy level, $Q = R(0)$ (top); the follower #3 (on the left side) has less initial energy, $R_3(0) = 10$ (middle); the follower #3 has a very low initial energy, $R_3(0) = 100$ (bottom). . . . 47
3.3 Leader-follower formation control for $N = 5$ agents modeled by a single-integrator in 3-dimensional space; all followers have full initial energy level, $Q = R(0)$ (top); the agent #3 (on the right side) has less initial energy, $R_3(0) = 10$ (bottom). 48
3.4 Leader-follower formation control for $N = 5$ agents modeled by a double-integrator model in 2-D; all followers has same initial energy level, Q and $R(0)$ equal to identity matrix (top); the follower #3 has a very low initial energy, $R_3(0) = 100$ (bottom). 49
3.5 Centralized leader-follower formation control for $N = 5$ agents modeled by a double-integrator model in 3-dimensional space; all followers have the same initial energy level, $Q = [I_N, 0_N; 0_N, 0_N]$ and $R(0) = I_N$ (top); the agent on the right side has a lower initial energy level, $R_3(0) = 10$ (bottom). 50
3.6 Comparison of the total energy consumption for the formation governed by various controllers. The formation consists of $N = 5$ agents modeled by the single-integrator model. 51

4.1 Leader-following distance-based formation control where the leader follows desired trajectory and the followers establish the desired formation. . . . 54
4.2 Distance-based optimal formation control for $N = 4$ agents modeled by the single-integrator dynamics; all agents have full initial energy levels (top). The agent #4 has a lower initial energy level, $l_{04} = 0.2$ (bottom). 68
4.3 Convergence of the edge errors to zero, corresponding to the simulations in Figure 4.2. 69
4.4 L_2 norm of the control inputs of the agents corresponding to Figure 4.2. 70
4.5 Collision avoidance in proposed formation control scheme. 71
4.6 Distance-based optimal formation control for $N = 5$ agents modeled by the double-integrator dynamics (top). The corresponding edge errors convergence to zero (bottom). 73

4.7 Distance-based optimal formation tracking control for $N = 4$ agents modeled by the single-integrator model; all agents have full initial energy levels (top). The follower number #4 at the bottom has a lower initial energy level, $l_{04} = 0.1$ (bottom). 74
4.8 3-Dimensional distance-based optimal formation tracking control for $N = 5$ agent modeled by double-integrator dynamics. 75
4.9 Comparison of the total energy consumption for the formation governed by various controllers. The formation consists of $N = 4$ agents modeled by the single-integrator model. 75

5.1 Desired distance-based formation in 2-D. 102
5.2 A distributed distance-based formation for $N = 5$ agents using the proposed controller. The desired formation is given in Figure 5.1. 103
5.3 Simulation result of the proposed controller without signed area constraints (top) and with the signed area constraints that prevents flip ambiguity of the formation (bottom). 104
5.4 Simulation results of the proposed controller for a set of $N = 4$ agents modeled by double-integrator dynamics. 105
5.5 A distributed distance-based formation for $N = 5$ agents using the proposed controller. The desired formation is given in Figure 2.6 (b). 105
5.6 Convergence of the edge errors to zero in the simulation corresponding to Figure 5.5. 106
5.7 Simulation result of the proposed controller without signed volume constraints (top) and with the signed volume constraints that prevents flip ambiguity of the formation (bottom). 107
5.8 Simulation result of the proposed controller for a set of $N = 5$ agent modeled by double-integrator dynamics. 108
5.9 Control performance function for three different controller proposed for distance-based formation control problem. 108

6.1 Desired directed distance-based formation for $N = 4$ agents. 128
6.2 Trajectories of $N = 4$ agents modeled by nonlinear dynamics (6.95) using the proposed control method. 128
6.3 Formation errors for $N = 4$ agents. 129
6.4 Desired directed distance-based formation for $N = 5$ agents. 129
6.5 Trajectories of the set of $N = 5$ agents using the proposed controller. . . 130
6.6 Formation error and control inputs of the agent #2 associated with the simulation of Figure 6.5 131
6.7 Formation errors and control inputs of the agent #3 associated with the simulation of Figure 6.5 132

6.8 Formation errors and control inputs of the agent #4 associated with the simulation of Figure 6.5 . . . 133
6.9 Formation errors and control inputs of the agent #5 associated with the simulation of Figure 6.5 . . . 134
6.10 A distributed directed distance-based formation for $N = 4$ agents using the proposed controller. . . . 136
6.11 Formation errors of the simulation 6.10. . . . 136
6.12 Control inputs of the agent #2, agent #3, and agent #4 corresponding to the formation in Figure 6.10. . . . 137
6.13 Trajectories of the agents for $N = 5$ agents using the proposed controller. 138
6.14 Formation errors assigned to the agent #5. . . . 139
6.15 Input signals of the agent #5. . . . 139
6.16 Simulation result of the proposed controller without signed volume constraints (top) and with the signed volume constraints that prevents flip ambiguity of the formation (bottom). . . . 140

7.1 Desired formation topology for $N = 6$ agents in 2-D. . . . 153
7.2 Trajectories of the agents with only nominal SDRE controller under matched uncertainty. . . . 154
7.3 Corresponding formation errors in simulation Figure 7.2. . . . 154
7.4 Trajectories of the agents with proposed ISMC-SDRE controller under matched uncertainty. . . . 155
7.5 Corresponding formation errors in simulation Figure 7.4. . . . 155
7.6 Agents control signals in simulation Figure 7.4. . . . 156
7.7 Trajectories of the agents using ISMC-SDRE based proposed controller in 3-D space. . . . 158
7.8 Corresponding formation errors in simulation Figure 7.7. . . . 158
7.9 Desired formation topology for $N = 5$ agents in 2-D space. . . . 159
7.10 Trajectories of the agents with proposed ISMC-SDRE controller under unmatched uncertainty. . . . 160
7.11 Agents control signals in simulation of Fig. 7.10. . . . 160
7.12 Desired formation topology for $N = 4$ agents in 2-D space. . . . 161
7.13 Trajectories of the agents with proposed ISMC-SDRE controller under unmatched uncertainty. . . . 161

List of Tables

4.1 Total energy usage for distance-based formations 76

5.1 CPI for different methods 106

List of Abbreviations

CPF	control performance function
CPI	control performance index
DT	Delaunay triangulation or Delaunay trilateration
HSDRE	hybrid state-dependent Riccati equation
ISMC	integral sliding mode control
ISS	input-to-state stable
LFF	leader-first-follower
LMI	linear matrix inequality
LQR	linear quadratic regulator
MAS	multi-agent systems
MIR	minimally infinitesimally rigid
SDC	state-dependent coefficient
SDRE	state-dependent Riccati equation
SMC	sliding mode control
UAV	unmanned aerial vehicles
UGV	unmanned ground vehicles
UUB	uniformly ultimately bounded

List of Publications

[J1]. R. Babazadeh and R. Selmic, "Distance-Based Multi-Agent Formation Control With Energy Constraints Using SDRE"; in *IEEE Transactions on Aerospace and Electronic Systems*, vol. 56, no. 1, pp. 41-56, Feb. 2020.

[C1]. R. Babazadeh and R. R. Selmic, "Distance-Based Formation Control Over Directed Triangulated Laman Graphs in 2-D Space "; in Proc. *59th IEEE Conference on Decision and Control (CDC)*, Jeju Island, Republic of Korea, 2020, pp. 2786-2792.

[C2]. R. Babazadeh and R. Selmic, "Optimal Distance-Based Formation Producing Control of Multi-Agent Systems with Energy Constraints and Collision Avoidance "; in Proc. *58th IEEE Conference on Decision and Control (CDC)*, Nice, France, 2019, pp. 3847-3853.

[C3]. R. Babazadeh and R. Selmic, "Cooperative Distance-Based Leader-Following Formation Control Using SDRE for Multi-Agents with Energy Constraints", in Proc. *57th IEEE Conference on Decision and Control(CDC)*, Miami Beach, FL, 2018, pp. 5008-5014.

[C4]. R. Babazadeh and R. Selmic, "An Optimal Displacement-Based Leader-Follower Formation Control for Multi-Agent Systems With Energy Consumption Constraints", in Proc. *26th Mediterranean Conference on Control and Automation (MED)*, Zadar, Croatia, 2018, pp. 179-184.

[J2]. R. Babazadeh and R. R. Selmic, "Directed Distance-Based Formation Control That Prevents Reflections in 3-D Space"; submitted to *IEEE Transactions on Control of Network Systems*, October, 2021.

[J3]. R. Babazadeh and R. R. Selmic, "Directed Distance-Based Formation Control of Nonlinear Heterogeneous Agents in 3-D Space"; submitted to *Automatica*, May, 2021.

[J4]. R. Babazadeh and R. R. Selmic, "Robust Optimal Distance-Based Formation Control of Uncertain Nonlinear Agents Over Directed Topologies"; submitted to *IEEE Transactions on Automatic Control*, September, 2021.

[C5]. R. Babazadeh and R. R. Selmic, "Formation Control of Nonlinear Agents with Distance Constraints Over Planar Directed Graphs"; submitted to *the 2022 American Control Conference (ACC)*, September, 2021.

[C6]. R. Babazadeh and R. R. Selmic, "Robustness of Distance-Based Formation Control of Nonlinear agents"; will be submitted to *61th IEEE conference on Decision and Control (CDC).*

[C7]. R. Babazadeh and R. R. Selmic, "Job Assignment in Distributed Distance-Based Formation Control Using Delaunay Triangulation "; will be submitted to *61th IEEE conference on Decision and Control (CDC).*

Chapter 1

Introduction

1.1 Literature Review

The collective and cooperative behavior of animals, such as flocking and formation, can be seen and traced in nature for a long time. Cooperative behavior enables groups of animals to reach a sophisticated objective that is not accessible for individual animals [3]. Inspired by nature, cooperative control of multi-agent systems, where a group of autonomous agents act cooperatively, has been widely studied in the control community.

A multi-agent system (MAS) is a set of autonomous agents in which each agent can act individually. There is an increasing need for MAS and their applications nowadays, making it necessary to design reliable and highly effective control techniques for such systems [2]. This chapter presents the introduction, literature review, and thesis outline.

1.1.1 Formation Control

Formation control is one of the most studied areas of cooperative control problems due to its military and engineering applications, such as search and rescue, surveillance, and coverage control. Recently, new interesting applications of formation control have been developed, e.g., the formation control of commercial airplanes and drone light-shows. The concept of formation control stems from nature, where various formation examples can be observed, e.g., flying birds, school of fish, pack of wolves, and more. It is well-known that geese save energy when they fly in a "V" shape formation [4]. A recent study showed that commercial planes could significantly reduce fuel consumption when flying in formation [5].

Formation control aims to develop control methods for a group of agents to conduct a specific mission while maintaining the desired geometric characteristics (shape, distances, angles, etc.). Results have shown that when multiple agents are assigned a particular task, the overall performance and efficiency are improved if agents form a certain geometric shape [2].

Figure 1.1: Geese fly in "V" shape formation. Picture taken from [1].

In literature, formation control problems are classified in several ways. In general, according to the objective of the problem, formation control methods can be categorized into bearing-based, position-based, displacement-based, and distance-based formation control [2], [6]. In bearing-based formation, agents are asked to keep prescribed relative bearings where the distances between agents are flexible [7]. This flexibility in distances is known as the scalability property [8]. In a position-based formation control, the desired formation is specified in terms of a relative displacement of neighboring agents. The objective is to reach the desired formation by controlling the agents' positions. In this method, each agent senses its own position with respect to a global coordinate system and moves towards the desired position (formation). In displacement-based formation, agents control their relative positions while their local coordinate systems have the same orientation. In this way, agents do not need to have access to the information in a global framework [2].

In a distance-based formation control, agents sense relative positions of their neighbors in their local coordinate system, where their local coordinate systems are not required to be aligned in a common direction. The desired formation is specified in terms of intra-agent distances where agents achieve the desired formation by actively controlling the distances between neighboring agents [2], [9]. Figure 1.2 shows the comparative properties of the methods mentioned above.

Also, other classifications of the formation control problems can be seen in the literature, such as formation producing problem, formation tracking problem, vision-based formation, leader-follower approach, behavioral approach, virtual structure approach, centralized approach, and decentralized approach [2]. In a leader-follower formation there is one or more leaders that the rest of agents (followers) follow [10], [11], [12]. Behavioral ap-

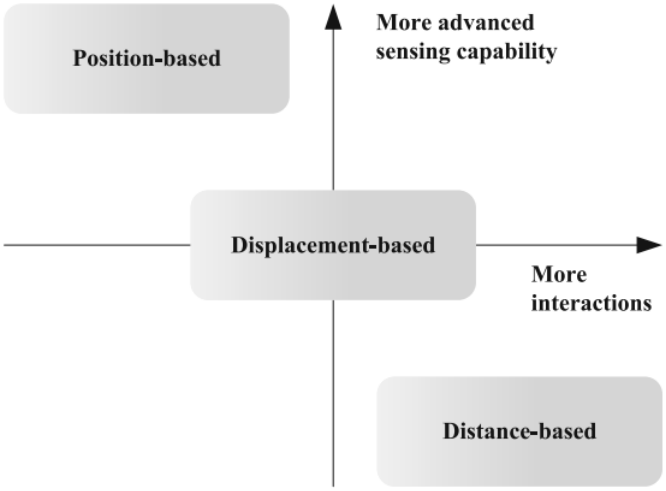

Figure 1.2: Specifications of different formation control approaches. Figure taken from [2].

proach defines a desired behavior such as obstacle or collision avoidance [13], [14]. Virtual structure approach assumes desired formation as a whole virtual rigid structure [15], [16]. There are also other classifications in the literature and can be found in review articles e.g. [2], [6].

1.1.2 Distance-Based Formation

Distance-based formation control of multi-agent systems has recently attracted significant research interest in the control systems community. There has been an increasing focus on distance-based formation control due to its theoretical challenges and plethora of applications [2]. In a distance-based formation control, the desired formation is specified in terms of intra-agent distances where agents aim to reach the desired shape, provided that they have access to their neighbors' relative positions in their local coordinate system [9].

In a distance-based formation, each distance constraint specifies the desired distance between a pair of agents where agents are required to achieve the desired formation shape by controlling their distances to their neighbors [9]. In a distance-based formation, maintaining the distance between a pair of agents can be the responsibility of both adjacent agents or just one of them. The formation is undirected if retaining the desired distance constraint (edge) is allocated to both neighboring agents. Conversely, if only one of the agents is designated as responsible for preserving the edge, the formation is directed [3]. Directed and undirected graphs are appropriate modeling tools in individual and shared responsibility cases, respectively [3].

Rigid graph theory is well developed and maturely used for undirected distance-based formation control where a distance constraint between a pair of neighboring agents is represented by an undirected edge connecting two adjacent vertices. There is a directed

edge from the responsible agent to the other agent in the directed graph case. Only the accountable agent needs to measure the relative position of its neighbor or receive such information via communication links. Directed topologies are shown to have some advantages over undirected ones. It is shown that an undirected distance-based formation can be distorted in 2-D or even drift to infinity in 3-D space if there exist disagreements in measurements of the neighboring agents [17]. It is also shown in [18] that in the directed graph case, the communication and control complexities are reduced by half compared to the undirected graph formations.

While the majority of research in the literature used the gradient-based control method for distance-based formation control problems, few suggested other control approaches. A method based on the Euclidean distance dynamics matrix was proposed for distance-based formation control in [19], [20]. Lin *et al.* in [21] proposed a graph Laplacian-based distributed coordinate-free control scheme for a distance-based formation control over directed networks. Authors in [22] proposed a sliding mode control technique for non-holonomic unicycle agents cyclic formation. A neuro-adaptive formation control method with target tracking was considered in [23].

Other forms of distance-based formation were studied as hybrid sensing graphs containing both unidirectional and bidirectional edges [24] or as hybrid combinations of distance and angle constraints [25]. For instance, authors in [25] divided the neighbor set of an agent into two subsets, namely distance neighbor set that has one member and angle neighbor set that includes the rest. The agent's mission is to control its distance with the former set and its relative bearing regarding the latter one. Reference [26] considered the global stability of the proposed formation control scheme, with both distance and bearing constraints on the plane for agents modeled as single-integrators. Almost global asymptotic stability of a hybrid formation with distance and angle constraints is proven for a set of agents modeled as single-integrators over planar directed graphs, under certain assumptions [27].

1.1.3 Undirected Formation

Inherently, the distance-based control problem is nonlinear and more challenging to solve than displacement-based and position-based formations. The graph rigidity theory is a solid mathematical foundation utilized extensively to solve the distance-based formation control problem. For stability analysis, the center manifold theorem, Lyapunov based approached [28] and LaSalle theorem [29] have been used. The gradient-based control is the most used method for distance-based control problem in the literature [30], [31], [32], [33]. The reference [7] developed an estimator-based, decentralized control scheme to solve the distance-based formation problem. A controller based on the Euclidean distance dynamics matrix is developed in [19] for the case of triangular formation. The expo-

nential stability of distance-based formation over undirected graphs is studied in [32]. Although the global stability of the distance-based formation is achieved for the single-integrator case [34], and the double-integrator dynamics [35], assuring global stability of the distance-based formation for more complicated systems is still an open problem [36].

The graph rigidity approach for distance-based formation is initially proposed in [37]. In [17], it is shown that in the case of the existence of mismatch in the measurement of neighboring agents, a distance-based formation could drift to infinity. Authors in [38] proposed a robust model-free controller for distance-based formation control with assured collision avoidance. Distributed control has several advantages such as independence of agents from the leader, less communication and computation needed, flexibility in adjusting to new tasks, etc. [3], [39]. Reference [40] proposed a distributed control scheme for combined formation control and flocking. Distance-based undirected formation of both single and double integrator dynamics have been studied for n-dimensional spaces in [31]. Deghat *et al.* combined the flocking and distance-based shape control in [41].

Distance-based formations are usually supposed to be invariant with respect to translation, rotation, and reflection. Recently, there have been attempts to uniquely determine the desired distance-based formation with regard to reflection. The most common approach for planar topologies is using signed area constraints [42], [43]. The aim of adding area constraints is to eliminate reflected configurations from the equilibria set. Distance-based formation control with signed area constraints is discussed in [44], where four agents on a planar undirected graph have been considered. The area constraints were also utilized for hybrid, undirected, distance- and angle-based formation control over planar graphs [45]. Reference [27] proposed a combination of distance- and angle-based formation control method for rigid formations in 2-D. A distance-based formation control with signed area constraints is discussed in some recent work [44], [46].

Sugie *et al.* in [47] proposed a hierarchical control strategy that precludes reflection ambiguities of a triangulated distance-based formation in 2-D. While the method in [47] is limited to equilateral triangles, the reference [48] extended the results to the general triangulation case. The global stabilization for a set of target configurations for triangulated formations is discussed in [49] to make undesired equilibria unstable. However, the method cannot preclude the undesired equilibria that are equivalent but not congruent configurations.

In 3-D space, reflection prevention is more challenging. Reference [50] proposed the utilization of the volume constraints for undirected distance-based formation control of multi-agents modeled as double-integrators in 3-D. The issue with the proposed control is that each agent needs to take care of the volume constraints of all possible tetrahedrons that make control law complicated and computationally complex. Also, this control method highlights the problem of measurement disagreement of neighboring agents. Furthermore, in stability analysis, it showed that the proposed controller steers the swarm

to an invariant set that includes undesired stable equilibria. Reference [51] used an adaptive potential field control over undirected graphs and considered planar and volume constraints. The number of planar and volume constraints rises significantly with the number of edges that are incident to the agent. Signed constraints, including angle and normalized volume, applied on formation shape control have been proposed in [45] for the single-integrator case.

1.1.4 Directed Formation

In order to model a directed distance-based formation topology, directed graph theory is used where each agent is represented by a vertex and each distance constraint is represented by a directed edge from the responsible agent to the other one [52]. Only the accountable agent needs to measure the relative position of its neighbor. Directed topologies are shown to have some advantages over undirected ones. For instance, mismatching in measurements of the neighboring agents in undirected topologies can distort the formation [17] while this is not a concern in directed formations. Also, the communication and control complexities in the directed formations are halved compared to the corresponding undirected formations [18].

A graph-theoretic framework for distance-based formation over directed graphs is developed in [52]. Distance-based formation control over a cycle-free directed graphs is studied in [53]. Distance-based formation control with signed area constraints is discussed in [44]. The aim of adding area constraints is to eliminate reflected configurations from the equilibria set. A distance-based formation over minimally persistent directed graphs with the leader-first-follower structure is considered in [54]. A directed distance-based formation over acyclic planar persistent graphs for single-integrator dynamics is discussed in [53]. Directed cyclic distance-based formation problems have been studied in [55]. A directed distance-based formation for a triangle with a single moving leader, modeled as single-integrator dynamics, is analyzed in [10].

There is a rich body of research on planar directed distance-based formation control [54], [53], [55], [10], to name a few. Authors in [56] studied the problem of distance-based formation control over directed, acyclic, minimally persistent graphs in 3-D space for a set of agents modeled by the single-integrator dynamics where they proposed a gradient-based control law. They did not exclude equivalent configurations nor undesired equilibria of the controlled system. Authors in [57] considered translational and rotational movements of the directed topologies in 3-D space, namely formation marching and formation rotating control problems, for single-integrator dynamics.

A directed distance-based formation control with reference tracking in 2-D is studied in [58], where an adaptive estimator is utilized to estimate the leader's velocity. Reference [59] considered leader-follower formation control problem using dynamic games. A

formation and fault accommodation algorithms for autonomous underwater vehicles have been developed in [60].

Liu *et al.* in [42] developed a distance-based formation control method for directed minimally persistent graphs in 2-D with an acyclic structure for a set of agents modeled as single-integrators. Reference [61] proposed a gradient-based control law for the distance-based formation control problem over minimally persistent directed graphs for the single-integrator case. It used the theory of interconnected systems for proving asymptotic stability of the formation while it lacks the stability analysis when the primitive triangle is cyclic. The authors extended the results for the planar second-order agents' case in [62]. Planar directed distance-based formation is also discussed in [63], where the experimental results are presented for a set of quadcopters.

1.1.5 Formation of Nonlinear Agents

Due to the highly nonlinear and complex nature of the distance-based formation control problem, the majority of the research in the literature considered very simple models [56]. Distance-based formation control for a set of agents modeled as single-integrators has been studied in [64], [65], [42], while few studies also considered the double-integrator case, e.g., [62], [35]. The unicycle model has been studied in [66], [67].

Authors in [68] considered the second-order nonlinear dynamics where they showed the uniform ultimate boundedness of the formation. The multi-layered formation of autonomous marine vehicles was studied in [69] for a particular class of nonlinear, double-integrator models.

1.1.6 Robust Optimal Formation

There are many proposed solutions for displacement-based formation control problems in the literature, including optimal control methods. Such a control optimizes a given cost functional and achieves the system stability in the formation control sense. In [70] the author used an optimal control framework to solve the formation control problem by formulating the problem as a Linear Quadratic (LQ) optimal control problem. A Linear Quadratic Regulator (LQR)-based optimal controller has been proposed for the leader-follower formation in [71] and for formation reconfiguration and collision avoidance in [72]. Various cost/objective functions were proposed for formation control problems and solved in standard optimal control framework, e.g., [13], [14], [73], [74], [75], [76], [77]. The desired objective can include preserving formation, tracking, obstacle avoidance, minimizing time, and control effort.

A leader-follower formation control using state-dependent Riccati equation (SDRE) control method was proposed in [12], [78] which in general produces a sub-optimal controller for nonlinear systems. A recurrent neural network was used in [73] for an optimal

formation control. The objective is to find a desired formation from a feasible formation set, which has the minimum distance to the initial formation of the multi-robot system. A control method that minimizes time to reach the desired formation is given in [79].

A distributed optimization problem has also received extensive interest in the research community recently [80]. Distributed optimal control of multi-agent systems due to the dependency of the problem to the neighbors' dynamics is more challenging than centralized optimal control problem to solve [81], [82]. There are efforts in literature to develop distributed LQR controller for linear systems [83], [83], [84]. In [85], an inverse optimal approach is used to develop a distributed cooperative optimal controller for multi-agent systems. A distributed receding horizon control scheme is presented in [86] and distributed subgradient optimization methods is proposed in [87]. Moreover, the reference [88] developed a distributed control scheme for linear multi-agent systems, which is globally optimal.

Uncertainty and disturbances are real challenges in control systems. Recently, robust formation control gained research attention. Reference [89] proposed an output feedback algorithms-based robust control scheme for vision-based formation. Robust displacement-based formation control problem have been studied in several recent studies, to name a few: [90], [91], [92], [93], [94]. Robust displacement-based formation control of general linear systems with matched uncertainty is discussed in [95] where the proposed method requires full-rankness of the input matrix. They showed the boundedness of the formation error. Reference [96] proposed a neural network-based robust adaptive controller for a displacement-based formation of surface vehicles where the stability of the formation error is shown via Lyapunov theory. A continuous-time sliding mode-based robust controller is designed for a set of uncertain quadrotors where the formation is a time-varying displacement-based [97]. Robust displacement-based formation control for underactuated quadrotors is proposed in [98] based on reinforcement learning.

A robust adaptive control protocol for a set of quadcopters is presented in [99] where the desired formation is described in terms of displacement constraint. They showed the stability and boundedness of the formation error signals. A robust control scheme is proposed for displacement-based formation control of a set of multi-agent systems with state constraints in [100]. Uniform ultimate boundedness of displacement-based formation in leader's coordinate for a group of underactuated autonomous surface vessels, subject to disturbance, is achieved via a robust adaptive controller based on minimal learning parameter (MLP) algorithm and the disturbance observer (DOB) in [101]. A robust controller for a combined distance and orientation-based formation control of a set of second-order systems is proposed in [38]. Robust displacement formation of a set of second-order nonholonomic agents is studied in [102] where a controller based on parametric Lyapunov-like barrier functions is designed. A robust fault-tolerant controller was proposed for a displacement-based formation of a set of tail-sitters in [103] where bound-

edness of the formation error signals have been shown. A model-free robust controller has been designed in reference [104] for a set of nonlinear scalar agents. Authors in [105] proposed a robust formation control protocol for a displacement-based formation of a group of second-order systems with mismatched uncertainty that guarantees ultimate boundedness of the errors.

The robustness of distance-based formation control over undirected graphs was studied in [106], where the agents are modeled as single-integrators with additive exogenous disturbance. The authors proposed a linear matrix inequality-based approach for disturbance attenuation. A robust distance-based formation control with prescribed performance that handles connectivity maintenance and collision avoidance for single-integrator dynamics has been studied in [107]. A flocking and distance-based formation control of a set of heterogeneous, second-order agents with parametric uncertainty was considered in [34] where a distributed adaptive control scheme has been developed for leader-first-follower (LFF) directed topologies. In combination with flocking, an angle-based formation control has been studied in [108] for the second-order agents where authors considered angle rigidity of planar graphs. A distance-based formation tracking control over planar acyclic directed graphs, where the leader's velocity is unknown but bounded, has been studied in [109].

1.2 Contributions

The contributions of this Ph.D. dissertation can be summarized in several categories. We developed a new optimal framework for a distance-based formation control. While the majority of the research used the famous gradient-based control for distance-based formation, we developed a nonlinear optimal control methodology for distance-based formation control. Additionally, we introduced new energy dynamic models for multi-agent systems. The proposed energy model is developed for the network of unmanned ground vehicles (UGVs). The model is also applicable to a broad range of unmanned aerial vehicles (UAVs) without hovering capabilities, e.g., fixed-wing UAVs, when external disturbances can be neglected. Simulation results offer deep underestimating of optimality in multi-agent systems and revealed interesting behaviors of the group.

In graph theory, the contribution of this dissertation is threefold. First, we introduced the normalized rigidity matrix for undirected graphs, which is a particular form of rigidity matrix. The normalized rigidity matrix has been used for formation purposes later. Second, we introduced a specific class of directed graphs, namely directed triangulated Laman graphs in 2-D space and directed trilateral Laman graphs in 3-D space, that can be constructed by triangulation and trilateration procedures, respectively. As a connection bridge between undirected and directed topologies, we proposed an algorithm based on Delaunay triangulation that can convert a given distance-based framework to a corre-

sponding directed Laman topology. Since the directed topologies have some advantages over undirected topologies, the proposed algorithm provides an effective way to assign a direction for each edge that can guarantee the persistence of the directed formation.

We developed a formation control scheme for undirected topologies. In undirected formation, we showed that the given control law results in the global asymptotic stability of the closed-loop system under certain conditions. Also, we extend the results to guarantee collision avoidance among neighboring agents. Finally, to prevent depleting of agent's energy, the proposed method considers the agents' energy level as a weighting factor in the cost functional. In addition, by including the energy level of agents in the proposed method, we investigate the effect of the lower energy level of weak agents on the swarm's behavior. Furthermore, the developed SDRE-based controller can address performance directly by online adjustment of weighting factors. The advantages of the proposed method include: (1) being systematic; (2) assuring global asymptotic stability; (3) reduction in energy consumption; (4) prevention of agent's energy depletion; (5) collision avoidance;

We presented a distributed formation control for directed distance-based formation control where only one of the neighboring pairs of agents is assigned to preserve the desired distance. We developed a novel distributed distance-based formation control scheme for a class of directed graphs. It is shown that the distance-based formation control over directed graphs has several advantages compared to the undirected graph configurations. We formulated the distance-based formation control problem over directed triangulated and directed trilateral Laman graphs. The proposed controller ensures the global asymptotic stability of the desired formation. Furthermore, an additional problem in distance-based formation control is the existence of reflected configurations that satisfy the distance constraints while the framework is not the desired one. We introduced a method based on the concept of a barrier function that prevents such flip-ambiguous configurations considering signed area and signed volume constraints. Additionally, we present a performance index for a control mission that indicates the system's overall performance and can be used for comparison purposes.

Distance-based formation control is mathematically complex and nonlinear. Due to the highly nonlinear and complex nature of the distance-based formation control problem, the majority of the research in the literature considered elementary models. To the best of the author's knowledge, this work is one of the first works on the distance-based formation of affine, nonlinear systems. We studied the distance-based formation control of nonlinear systems. We proposed a method that can guarantee asymptotic stability of the distance-based formation for a broad class of nonlinear systems. We developed the results for both 2-D and 3-D spaces as well as homogeneous and heterogeneous agents.

Physical systems are subjected to uncertainties due to imperfections in modeling, internal noise, disturbances, etc. We studied a distance-based formation control of un-

certain nonlinear agents. For a set of nonlinear agents with additive uncertainty, we developed a robust optimal formation control scheme that guarantees asymptotic stability of the desired distance-based formation in the presence of bounded uncertainty. The target formation is supposed to be a directed triangulated Laman graph in 2-D space or a directed trilateral Laman graph in 3-D space. We have shown that the proposed controller can completely compensate for the effect of matched uncertainty on the formation. The proposed control scheme is based on the integral sliding mode control (ISMC) theory combined with the state-dependent Riccati equation (SDRE) method.

1.3 Summary and Dissertation Outline

This dissertation is organized into eight chapters as follows:

- **Chapter 1:** This chapter presents the introduction, literature review, and outline of this dissertation.

- **Chapter 2:** This chapter presents background on graph theory, nonlinear optimal control theory, and stability analysis of cascade interconnected systems. We introduced a new dynamic model for the energy of the agents in this chapter. Also, we introduced directed triangulated Laman graphs in 2-D space and directed trilateral Laman graphs in 3-D space. Furthermore, an algorithm is proposed to transfer the desired topology to a corresponding directed Laman graph using Delaunay triangulation. The corresponding parts of this chapter have been published as [J2], [C4], and [C7].

- **Chapter 3:** This chapter provides a brief discussion on optimal leader-follower, displacement-based formation control of multi-agent systems. The results of this chapter are published as [C4].

- **Chapter 4:** This chapter presents the main results of this dissertation on undirected distance-based formation control, where we introduced the normalized rigidity matrix and proved the global asymptotic stability of the distance-based formation. Also, a hybrid SDRE control scheme is proposed for formation tracking of the multi-agent systems that guarantee practical stability of the formation and tracking error. The energy depletion and collision avoidance problems are addressed here. This chapter has been published as articles [J1], [C2], and [C3].

- **Chapter 5:** The results of directed distance-based formation control of single and double integrator systems are presented in this chapter. Global asymptotic stability of the formation for single-integrator agents is proven. Also, the reflection prevention problems in 2-D and 3-D spaces are solved in this chapter. The corresponding publications are [J2] and [C1].

- **Chapter 6:** One of the first studies of the distance-based formation for autonomous, affine, nonlinear systems is developed in this chapter. The directed Laman topologies are used for this aim. The results have appeared in [J3] and [C5].

- **Chapter 7:** The distance-based formation of uncertain nonlinear systems is discussed in this chapter. As a novel study on the robustness of distance-based formation, we developed a robust optimal distance-based formation control scheme based on a combination of integral sliding mode control and state-dependent Riccati equation methods. The results of this chapter appear in [J4] and [C6].

- **Chapter 8:** In this chapter, a summary of the dissertation is given, and possible future works have been discussed.

Chapter 2

Background

2.1 Introduction

In this section, the background materials are presented. First, the formation problem is stated. Second, the fundamentals of graph theory are discussed for directed and undirected graphs. Concepts of rigidity and persistency are presented, and directed Laman graphs are introduced. A new model is developed for agent's energy consumption which can be used for a broad class of multi-agent systems. Then, the typical agent's dynamic models are introduced and combined with the proposed energy dynamics. Finally, the fundamentals of nonlinear optimal control methods and some stability results are provided.

2.2 Problem Statement

A formation control problem can be defined as follows: consider a set of N agents that can be described by

$$\dot{x}_i = f_i(x_i, u_i) \tag{2.1a}$$

$$y_i = g_i(x_i), \tag{2.1b}$$

where $x_i \in \mathbb{R}^q$, $u_i \in \mathbb{R}^p$, and $y_i \in \mathbb{R}^r$ denote the state, input, and output vectors of the agent $i \in \{1, ..., N\}$ respectively. Here q, p and r are dimensions of the state, input, and output vectors respectively, and $f_i : \mathbb{R}^{q\times p} \to \mathbb{R}^q$, $g_i : \mathbb{R}^{q\times p} \to \mathbb{R}^r$. Let us define the swarm output vector as $\mathbf{y} = [y_1^T, ..., y_N^T]^T \in \mathbb{R}^{rN}$. A desired formation for the set of agents can then be described by M-constraints

$$F(\mathbf{y}) = F(\mathbf{y}^*), \tag{2.2}$$

where $F : \mathbb{R}^{rN} \to \mathbb{R}^M$, for a given $\mathbf{y}^* \in \mathbb{R}^{rN}$. A formation control problem for the set of agents (2.1) is to design a set of control law u_i such that the set

$$E_{\mathbf{y}^*} = \left\{ [x_1^T, ..., x_N^T]^T : F(\mathbf{y}) = F(\mathbf{y}^*) \right\} \tag{2.3}$$

becomes asymptotically stable. It should be noted that, in general, the objective is not $\mathbf{y} \to \mathbf{y}^*$, but to achieve $F(\mathbf{y}) \to F(\mathbf{y}^*)$. Further, the constraint (2.2) is usually defined by a specified problem setup [2].

2.2.1 Notation

The following notations are used throughout this thesis. Let $\mathbb{R}$ denote the real numbers set, $\mathbb{N}$ denote the natural numbers set, and $\mathbb{Z}$ be used for integer numbers. The positive real numbers set is denoted by $\mathbb{R}_+$. Let $\mathbb{R}^n$ denote an n-dimensional Euclidean space and $\mathbb{R}^{n\times m}$ denote $n \times m$ real matrices. Let I_n denote $n \times n$ identity matrix and $\mathbf{0}_{n\times m}$ denote the $n \times m$ zero matrix. We use $\mathbf{0}_n$ and $\mathbf{1}_n$ for column vectors of size n with all entries equal to zero and one, respectively. With diag$[a_i]$ we denote a block diagonal matrix with matrices a_i on its diagonal. Also, rank(A) represents the rank of a matrix A. Let $\otimes$ denote the Kronecker product. By $\|.\|_i$ we denote the l_i-norm and by $\Theta(A)$ we denote the set of eigenvalues of matrix A, also known as spectrum of matrix A. Mathematical signum function, commonly referred as sign function and denoted by sgn(x), is defined as

$$\text{sgn}(x) = \begin{cases} -1 & x < 0 \\ 0 & x = 0 \\ 1 & x > 0 \end{cases} . \tag{2.4}$$

The sign of a vector $\mathbf{x} = [x_1, ..., x_n]$ is denoted by $\text{sgn}(\mathbf{x}) = [\text{sgn}(x_1), ..., \text{sgn}(x_n)]$.

2.3 Graph Theory

This section gives the essential mathematical background on graph theory, rigidity, and persistency as core concepts in distance-based formation control. First, we will present the fundamentals of undirected graphs following by the theory of directed graphs.

2.3.1 Undirected Graphs

A formation of N agents can be represented by an undirected graph $G = (V, E)$, where $V = \{v_1, ..., v_N\}$ is the set of vertices with v_i representing the agent i and $E \subset V \times V$ is an edge set where any of its elements represents a direct connection between a pair of agents. Note that $(i, j) \in E$ if agents i and j are adjacent. Moreover, $(j, i) \in E$ if and only if $(i, j) \in E$. The topology of an inter-agent network can be modeled with an

adjacency matrix $A = [a_{ij}]$, where a_{ij} represents a distance constrain between a pair of agents. The element $a_{ij} = 1$, if there exists an edge between vertices (agents) i and j; otherwise $a_{ij} = 0$. A graph without multiple edges and loops is called a simple graph. In this dissertation, all graphs are supposed to be simple. Cardinality of sets V and E ($|V|$ and $|E|$, respectively) is the number of vertices and edges of the graph G. For agent i, the neighboring set N_i is defined as a set of agents that are adjacent to it [110].

Given a graph $G(V, E)$, a realization is defined as a function that maps the vertices of the graph to a set of points in the Euclidean space. Obviously, graph G can have several realizations in $\mathbb{R}^n$ where $n \in \{2, 3\}$ is the dimension of the space. A framework $\mathcal{F}(G, \mathbf{p})$ is a realization of $G(V, E)$ at given points $\mathbf{p} = [p_1^T, ..., p_N^T]^T \in \mathbb{R}^{nN}$, where $p_i \in \mathbb{R}^n$ is the corresponding position of the vertex v_i. An edge function $\mathcal{E} : \mathbb{R}^{nN} \to \mathbb{R}^{|E|}$ of the framework $\mathcal{F}(G, \mathbf{p})$ is defined by

$$\mathcal{E}_G(\mathbf{p}) = \Big(..., \|p_i - p_j\|^2, ...\Big), \quad (i, j) \in E. \tag{2.5}$$

For a realization $\mathcal{F}(G, \mathbf{p})$, the rigidity matrix $\mathcal{R}(\mathbf{p}) : \mathbb{R}^{nN} \to \mathbb{R}^{|E| \times nN}$ is defined as

$$\mathcal{R}(\mathbf{p}) = \frac{1}{2} \frac{\partial \mathcal{E}_G(\mathbf{p})}{\partial \mathbf{p}}. \tag{2.6}$$

Frameworks $\mathcal{F}(G, \mathbf{p})$ and $\mathcal{F}(G, \mathbf{q})$ are said to be equivalent if $\mathcal{E}_G(\mathbf{p}) = \mathcal{E}_G(\mathbf{q})$. In addition, they are congruent if $\|p_i - p_j\| = \|q_i - q_j\|$ for all $(i, j) \in V$. Note that rotations and translations of the whole framework are congruent transformations, and normally we exclude them. Two frameworks are called flip ambiguous if they are equivalent but not congruent.

Rigidity is an important feature in formation control, whereas a consistent formation requires the corresponding graph to be rigid. Rigidity is defined in [111] as follows:

Definition 2.1. Let $G(V, E)$ be a desired graph and $C(V, E')$ be the complete graph with $|V|$ vertices. A framework $\mathcal{F}(G, \mathbf{p})$ in $\mathbb{R}^n$ is rigid if there exists a neighborhood U_p of $\mathbf{p}$ in $\in \mathbb{R}^{nN}$ such that

$$\mathcal{E}_G^{-1}(\mathcal{E}_G(\mathbf{p})) \cap U_p = \mathcal{E}_C^{-1}(\mathcal{E}_C(\mathbf{p})) \cap U_p. \tag{2.7}$$

We call $\mathcal{F}(G, \mathbf{p})$ flexible if it is not rigid. In other words, the framework $\mathcal{F}(G, \mathbf{p})$ is called flexible if it can be continuously deformed to $\mathcal{F}(G, \hat{\mathbf{p}})$ while keeping all desired distances constant; otherwise, it is rigid [112]. A realization $\mathcal{F}(G, \mathbf{p})$ is globally rigid if every equivalent realization is also congruent. Thus, a globally rigid graph has a unique realization irrespective of translation and rotation. The following well-known Laman theorem provides an effective way to check graph rigidity.

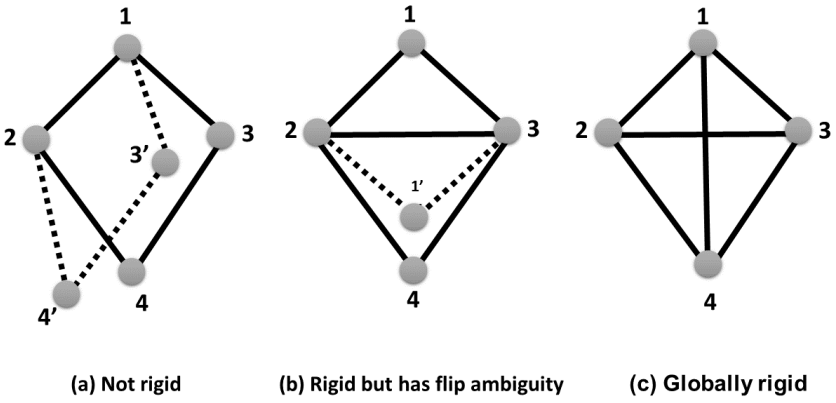

Figure 2.1: Graph rigidity: nonrigid or flexible graph (a), minimally rigid graph where changing node 1 to 1' makes flip ambiguity (b), and globally rigid graph (c).

Theorem 2.1 ([113]). *A graph $G = (V, E)$ is rigid in 2-D (respectively in 3-D) if and only if there exists a subgraph $\bar{G} = (V, \bar{E})$, $\bar{E} \subset E$ with $|\bar{E}| = 2|V| - 3$ (respectively $|\bar{E}| = 3|V| - 6$), and for any other $\bar{V} \subset V$, the associated induced subgraph $\bar{\bar{G}} = (\bar{V}, \bar{\bar{E}})$ of $\bar{G}$ with $\bar{\bar{E}} \subset \bar{E}$, satisfies $|\bar{\bar{E}}| \leq 2|\bar{V}| - 3$ (respectively $|\bar{E}| = 3|V| - 6$).*

Corollary 2.1.1 ([113]). *A graph is minimally rigid if it is rigid and if by removing any of its edges it loses rigidity. In addition, a rigid graph $G = (V, E)$ is minimally rigid in 2-D if and only if $|E| = 2|V| - 3$. For 3-D it is minimally rigid if and only if $|E| = 3|V| - 6$.*

In other words, a graph is rigid if and only if it contains a minimally rigid subgraph.

Remark 2.1. A minimally rigid graph in $\mathbb{R}^2$ is called a Laman graph [114].

The framework $\mathcal{F}(G, \mathbf{p})$ is infinitesimally rigid if every possible motion of the framework that satisfies

$$(p_i - p_j)^T(\dot{p}_i - \dot{p}_j) = 0, \quad \forall (i, j) \in E \tag{2.8}$$

consists of just rotation and translation of the whole framework. Thus, $\mathcal{F}(G, \mathbf{p})$ is infinitesimally flexible if it is not infinitesimally rigid [41]. A framework $\mathcal{F}(G, \mathbf{p})$, where $N > n$ and $\mathbf{p}$ is a regular point of G, is infinitesimally rigid if and only if $rank(\mathcal{R}(\mathbf{p})) = Nn - \binom{n+1}{2}$, [9], [111], [115].

Corollary 2.1.2 ([28]). *For a minimally and infinitesimally rigid (MIR) framework $\mathcal{F}(G, \boldsymbol{p})$, the rigidity matrix $\mathcal{R}(\boldsymbol{p})$ has full row rank.*

Also, for MIR graphs, we have the following lemma presented in the literature.

Lemma 2.1 ([32]). *For a MIR framework $\mathcal{F}(G, \boldsymbol{p})$, the matrix $\mathcal{R}(\boldsymbol{p})\mathcal{R}(\boldsymbol{p})^T$ is positive definite, hence invertible.*

Roughly speaking, there are operations for building a new graph that preserves the rigidity property of the primitive graph. The following lemma gives an essential result on the rigidity of a graph that is obtained from another graph.

Lemma 2.2 ([18]). *A graph $\bar{G} = (\bar{V}, \bar{E})$ in $\in \mathbb{R}^n$ obtained by adding a vertex with n edges to a graph $G = (V, E)$, is (respectively minimally) rigid if and only if $G = (V, E)$ is (respectively minimally) rigid.*

Henneberg construction is a systematic and iterative way to construct minimally rigid graphs in 2-D [3]. Henneberg construction consists of two possible operations: (1) vertex addition and (2) edge splitting. Vertex addition is a procedure of adding a new vertex with two edges to an existing graph. Edge splitting is a procedure of adding a new vertex with three edges while removing one existing edge. It should be noted that the vertices that were incident to the removed edge should be adjacent to the added vertex. Figure 2.2 illustrates Henneberg construction procedures. For more detailed information on Henneberg construction, the reader may refer to [116]. It is well-known that having a minimally rigid framework, adding another vertex to it via Henneberg construction, the resulting graph is also minimally rigid. Furthermore, it is shown that every minimally rigid graph can be obtained by a sequence of Henneberg construction applied to a complete graph with two vertex [37]. The following lemma states this.

Lemma 2.3 ([52]). *A minimally rigid graph in 2-D, can be constructed using Henneberg construction starting from a complete graph of two vertices with one edge.*

Also, as a consequence of Lemma 2.3, every minimally rigid graph can be deconstructed using the inverse of Henneberg construction to end up in the complete graph of two [3]. The 3-dimensional version of constructing a minimally rigid graph known as *trilateration* operation is discussed in [117]. Starting from a complete graph of three vertices, a graph which is obtained by a sequence of adding a vertex with three edges are minimally rigid. This is a direct consequence of Lemma 2.2.

Remark 2.2. A minimally rigid graph in 2-D that is obtained by the Henneberg vertex addition procedure is called a triangulated Laman graph [114].

2.3.2 Directed Graphs

The connection between agents can be unidirectional. In this sense, the agent i can measure the relative position or receive the data from agent j while the reverse is not true. This is quite a common phenomenon in distributed multi-agent applications. A communication topology or desired formation among N agents can be represented by a directed graph (also known as digraph) $\mathcal{G} = (\mathcal{V}, \mathcal{E})$, where $\mathcal{V} = \{v_1, ..., v_N\}$ is the set of vertices and $\mathcal{E} \subset \mathcal{V} \times \mathcal{V}$ is an edge set where any of its elements represents a distance

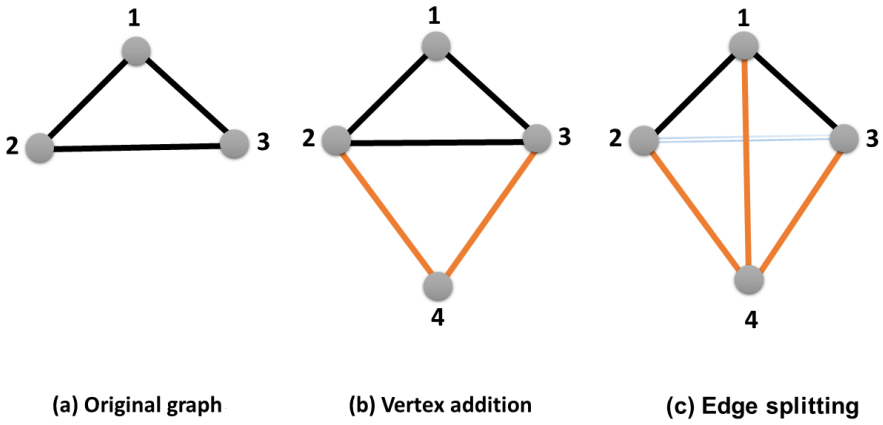

Figure 2.2: Henneberg construction: a minimally rigid graph (a) results in (b) using vertex addition and in (c) using edge splitting. Both constructed graphs preserve minimal rigidity.

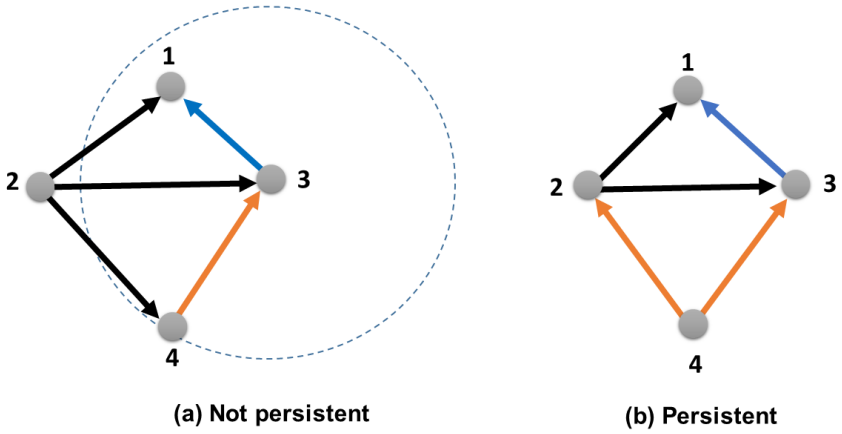

Figure 2.3: Persistency of directed graphs: (a) graph is not constraint consistent because agent #2 has too many constraints to satisfy. While agent #4 can move freely over a circle around agent #3, agent #2 cannot satisfy all its associated desired distances. The graph depicted in (b) is constraint consistent.

constraint. Note that $(i,j) \in \mathcal{E}$ means that there is a flow of information from agent j to agent i. In other words, agent i can receive the information from agent j or it can measure the relative position of agent j. The edge $e_{ij} = (i,j) \in \mathcal{E}$ is shown by an arrow with the head in vertex j and the tail in vertex i, respectively. The agent j is called *sink* while the vertex i is the *source* of the edge e_{ij}. The topology of an inter-agent network can be defined using an adjacency matrix $A = [a_{ij}]$, where a_{ij} represents a directed connection between a sink and a source. The element $a_{ij} = 1$ if there exist a information flow from agent j to agents i; otherwise $a_{ij} = 0$.

A matrix which provides the relationship between vertices and edges is known as an incidence matrix $H = [h_{ij}]$ [110]. The elements of incidence matrix for a directed graph are defined as

$$h_{ij} = \begin{cases} -1 & \text{if vertex } i\text{th is the tail of edge } j \\ 1 & \text{if vertex } i\text{th is the head of edge } j \\ 0 & \text{otherwise.} \end{cases} \tag{2.9}$$

Note that incidence matrix also can be defined for undirected graphs with associating an arbitrary orientation for each edge.

For the agent i in a directed graph, the neighboring set $\mathcal{N}_i$ is defined as a set of agents that their positions can be sensed by agent i [110]. Out-degree of vertex i is defined as $dg_i^+ = |\mathcal{N}_i|$. Consequently, for a directed graph $\mathcal{G}$ the out-degree matrix is defined as $\mathcal{D}_\mathcal{G} = diag[dg_1^+, ..., dg_N^+]$.

In the case of directed formation, the rigidity of the underlying undirected graph (which is obtained after replacing all directed edges with undirected ones) is not sufficient for feasibility of the formation [2]. For directed graphs, the counterpart condition to rigidity is persistency. A directed graph is said to be persistent if it is constraint consistent and the underlying undirected graph is rigid [52]. Roughly speaking, a formation is constraint consistent if every agent is able to satisfy all its distance constraints while all other agents are trying to do so. In other words, if the responsibility of an agent for keeping desired distances is too much such that the agent can not fulfill it, then the directed formation is not constraint consistent [52]. Figure 2.3 shows constraint consistency of a directed graph. The following theorem provides the definition of being persistent.

Theorem 2.2 ([117]). *A directed graph $\mathcal{G} = (\mathcal{V}, \mathcal{E})$ is persistent if and only if it is constraint consistent and the underlying undirected graph is rigid.*

There are some definitions for constraint consistency of a directed graph. Reader may refer to [3], [52] fo more details. However, here we are giving a criteria to check the constraint consistency of a directed graph in the following lemma.

Lemma 2.4 ([3]). *A directed graph in n-dimensional space is constraint consistent if none of its vertices has an out-degree greater than n,*

$$max(dg_i^+) \leq n \quad for\ all\ i \in \{1, ..., N\}. \tag{2.10}$$

Similarly to minimal rigidity, we can define minimal persistency for a directed graph as follows.

Definition 2.2 ([52]). A directed graph $\mathcal{G} = (\mathcal{V}, \mathcal{E})$ is minimally persistent if it is persistent and if by removing any of its edges, it loses persistency.

A simple way to check the minimal persistency of a directed graph is given in the following.

Proposition 2.1 ([118]). A directed graph $\mathcal{G} = (\mathcal{V}, \mathcal{E})$ is minimally persistent if and only if its underlying undirected graph is minimally rigid and for all vertices we have

$$max(dg_i^+) \leq n \quad \text{for all } i \in \{1, ..., N\}. \tag{2.11}$$

Lemma 2.4 states that a directed graph in 3-D is constraint consistent if every vertex of the graph has at most three neighbors. First, let us define degree of freedom of a vertex in n-dimensional space where $n \in \{2, 3\}$ as following:

Definition 2.3. For a vertex i in a directed graph $\mathcal{G} \in \mathbb{R}^n$, the degree of freedom (df_i) is

$$df_i = \begin{cases} n & \text{if} \quad dg_i^+ = 0 \\ n-1 & \text{if} \quad dg_i^+ = 1 \\ n-2 & \text{if} \quad dg_i^+ = 2 \\ 0 & \text{otherwise.} \end{cases} \tag{2.12}$$

Based on degree of freedom we can state the following lemma which relates graph's pesistency to the sum of degree of freedom of vertices.

Lemma 2.5 ([18]). *For a persistent directed graph in n-dimensional space where $n \in \{2, 3\}$, the following inequality is valid*

$$\sum_{N}^{i=1} df_i \leq \frac{n(n+1)}{2}. \tag{2.13}$$

Henneberg operation also is defined for directed graphs. Directed vertex addition can be stated as follows.

Definition 2.4. Henneberg directed vertex addition to a directed graph in n-dimensional space where $n \in \{2, 3\}$, is adding a vertex with n directed edges to an existing directed graph provided that the added vertex is the source of the added edges.

Henneberg directed vertex addition in 2-D and 3-D spaces are known as triangulation and trilateration operations, respectively. Furthermore, we can state the following lemma about the persistency of a constructed graph.

Lemma 2.6 ([18]). *A directed graph $\bar{\mathcal{G}} = (\bar{\mathcal{V}}, \bar{\mathcal{E}})$ in $\mathbb{R}^n$ obtained by Henneberg directed vertex addition to a graph $\mathcal{G} = (\mathcal{V}, \mathcal{E})$, is (respectively minimally) persistent if and only if $\mathcal{G} = (\mathcal{V}, \mathcal{E})$ is (respectively minimally) persistent.*

Not all minimally persistent directed graphs can be obtained by Henneberg sequence since there are some counterexamples [52]. The following corollary offers important results on the structure of minimally persistent directed graphs which is constructible using Henneberg sequence.

Corollary 2.2.1 ([52]). *A minimally persistent directed graph which has no cycle (cycle-free or acyclic), always has a Leader-First-Follower structure and hence can be obtained via Henneberg directed vertex addition starting from a graph of two vertices connected with single edge.*

Similar to undirected case we define a directed triangulated Laman graph as following.

Definition 2.5. A minimally persistent graph in 2-D which is obtained by Henneberg directed vertex addition starting from a LFF structure, is called a directed triangulated Laman graph.

Being persistent is not sufficient for the feasibility of formation in 3-D as shown in [3]. For the sake of having feasible formation, a directed graph in 3-D needs to be structurally persistent. Figure 2.6 shows structural persistency of a directed graph in 3-D space. To be more specific, we can state the following lemma.

Lemma 2.7 ([3]). *A directed graph in 3-D is structurally persistent if it is persistent and if it has at most one vertex with $df_i = 0$.*

Corollary 2.2.2 ([117]). *A minimally persistent directed graph in $\mathbb{R}^3$ can be obtained via directed trilateration operation starting from a graph of directed triangular with three vertices connected with three edges in form of LFF or balanced triangle (that each agent has $dg^+ = 1$).*

Figure 2.4 depicts two possible starting triangular for constructing a minimally persistent graph in 3-D.

Remark 2.3. A minimally persistent graph in 3-D which is obtained by trilateration sequence is called trilaterated minimally persistent graph.

Figure 2.5(a) shows leader-first-follower structure while Figure 2.5(b) depicts the procedure of construction of a directed triangulated Laman graph.

Note that for directed graphs in 3-D, trilateration operation equals to directed vertex addition.

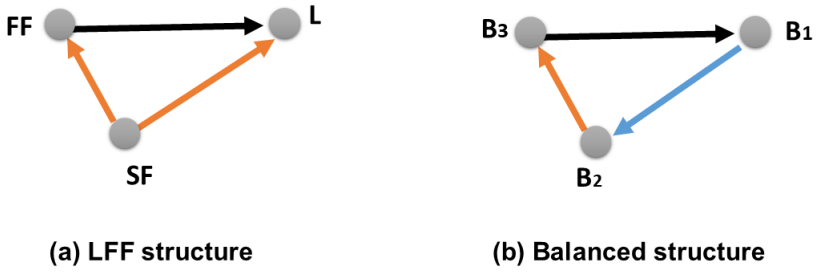

Figure 2.4: Two directed triangular seeds.

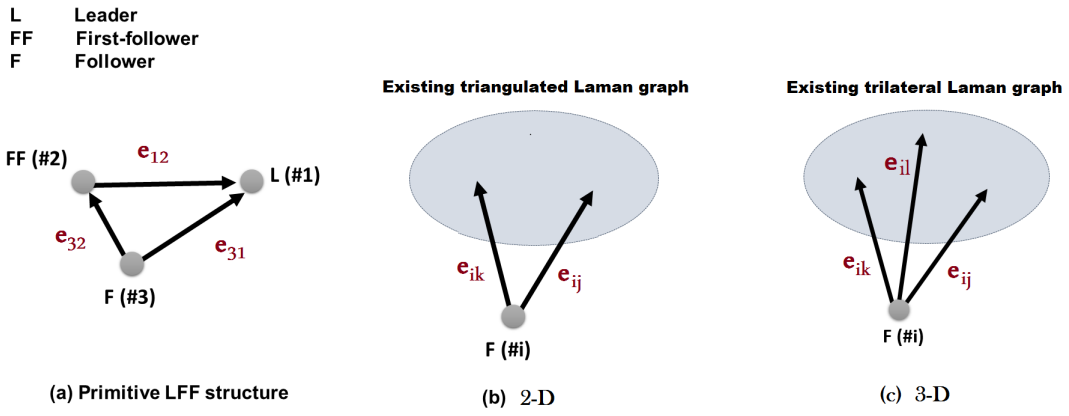

Figure 2.5: Constructing a directed Laman graph: (a) primitive leader-first-follower structure; (b) constructing a new triangulated Laman graph in 2-D, and (c) constructing a new trilateral Laman graph in 3-D using directed vertex addition procedure.

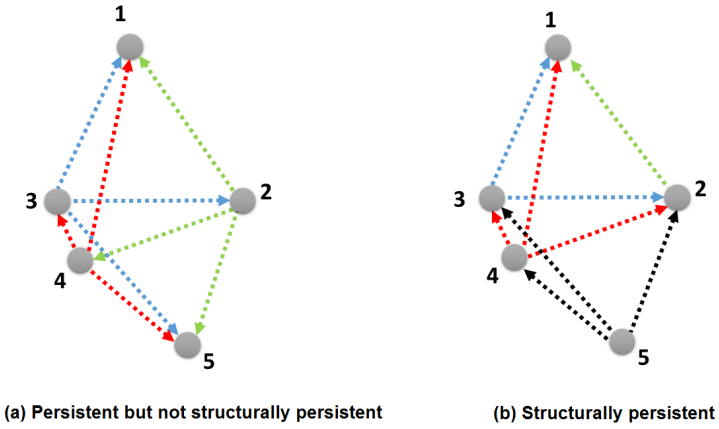

Figure 2.6: Structural persistency of directed graphs in 3-D: the graph depicted in (a) is not structurally persistent since the agent #1 and #5 can freely move, it is impossible to other agents to preserve their constraints. The graph depicted in (b) is structurally persistent.

Definition 2.6. A minimally structurally persistent graph in 3-D that is obtained via trilateration sequence from a starting LFF triangle is called directed trilateral Laman graph.

Figure 2.5(c) shows construction of directed trilateral graphs.

2.3.3 Securing Persistence

Considering the relation between undirected and directed graphs, there is an important question here: for a given undirected graph, can we assign a direction to each edge such that the resulting directed graph is persistent? This problem in general form is unsolved [18]. However, for special cases such as complete graphs, bilateration and trilateration graphs, wheel graphs, C_2, and C_3-graphs, there are some methods proposed in the literature [3]. The following lemma states the possibility of securing persistence for minimally rigid graphs [52].

Lemma 2.8 ([3]). *A minimally rigid graph can be assigned directions to its edges such that the resulting directed graph be minimally persistent.*

Using Henneberg construction, we can deconstruct any minimally rigid graph to its primitive complete graph of two or three in 2-D or 3-D, respectively. A C^2-graph is a square of the corresponding cycle graph, which is obtained by adding edges between every two vertices with a common neighbor. Both wheel and C^2-graphs are interesting structures in formation control due to their particular structures. Furthermore, it is shown that both wheel graphs and C^2-graphs are robust in terms of remaining persistent in case of losing a vertex (rather than leader vertex for wheel graph) or an edge [3].

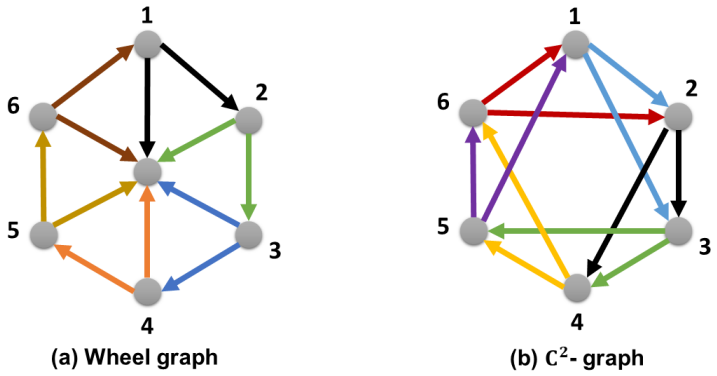

Figure 2.7: Special form of persistence directed graphs: (a) wheel graph, (b) C^2-graph.

2.3.4 Directed Job Assignment for Formation Topologies

Assume that the desired distance-based formation shape is given. The objective is to find an algorithm for job assignment procedure such that the resulted directed topology be a persistent graph. At the same time, for stability purposes and the advantages that leader-first-follower structure has, it is desired that the final topology be in acyclic LFF form. In this subsection, we propose an algorithm that can solve this problem.

Triangulation (respectively trilateration) of a given set P on N points in 2-dimensional (respectively in 3-dimensional) space is a simplicial decomposition of the hull in a way that:

1. Vertices of triangles (respectively tetrahedrons) belong to P.
2. Intersection of two triangles (respectively tetrahedrons) is either empty or a vertex or an edge (or a face).

A triangulation in 2-D is a Delaunay triangulation (DT) if and only if the circle circumscribing each triangle does not contain any point of the set P.

A trilateration in 3-D is a Delaunay trilateration (DT) if and only if the circumsphere circumscribing each tetrahedron does not contain any point of the set P.
Given a desired geometric shape for a set of N agents, perform the following steps:

- **Step 1.** Perform the Delaunay operation (DT) for a given set of points.
- **Step 2.** For a resulted graph, select an appropriate leader agent (#1).
- **Step 3.** From the neighboring set of the leader(N_1), select first follower (#2).
- **Step 4.** Connect the first follower to the leader with a directed outgoing edge (e_{21}).
- **Step 5.** From the set $N_1 \cap N_2$ select follower #3.

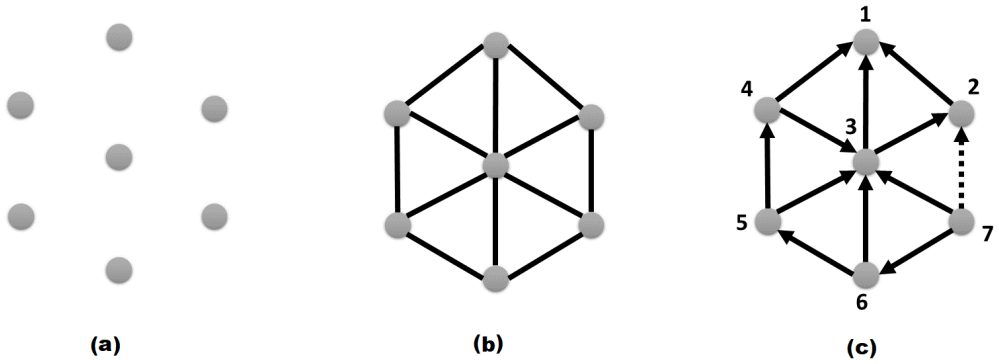

Figure 2.8: Proposed job assignment algorithm: (a) the desired topology of the agents; (b) the corresponding Delaunay triangulation; (c) the out put of the proposed algorithm as a minimally persistent acyclic LFF graph.

- **Step 6.** Connect follower #3 to the leader and first follower with two outgoing edges e_{31} and e_{32}, respectively.
- **Step 7.** Select next follower $\#i$ where $4 \leq i \leq N$ as $N_i \subset \Lambda_{i-1}$ where $\Lambda_{i-1} = \{1, ..., i-1\}$.
- **Step 8.** Arrange the incidents edges of the agent i from the shortest to longest length (Euclidean distance)
- **Step 9.** Connect the follower $\#i$ to the the graph with directed triangulation (respectively trilateration in 3-D) through the shortest length edges.
- **Step 10.** Repeat step 7 for the next agents until all agents are connected to the graph.

The resulted directed graph is an acyclic LFF structured graph. It is worth mentioning that the resulted directed graph is not unique. However, it is in an LFF form, and the formation is persistent. This job assignment is compatible with flocking, directed distance-based formation, and vision-based formation control, where an agent is required to preserve its position about its nearest neighbors.

Figure 2.8 shows the proposed algorithm's application where the desired topology of agents is given in Figure 2.8(a). Implementing the Delaunay triangulation for a given set of points in (a), the output of Delaunay triangulation is shown in (b). The resulted directed LFF minimally persistent graph is depicted in (c). As another example, we implemented the proposed algorithm for a Moser graph depicted in Figure 2.9. The procedure and the resulted directed graph are shown in Figure 2.10.

Algorithm 1 The proposed job assignment algorithm using DT

Require: The desired framework $\mathcal{F}(G, \mathbf{p})$

Perform DT on set of points $\mathbf{p}$
Select an appropriate leader (agent#1)
Select first-follower (agent#2) such that $2 \in N_1$
Connect the first follower to the leader with a directed outgoing edge (e_{21})
Select follower #3 such that $3 \in N_1 \cap N_2$
Connect follower #3 to the leader and first follower with outgoing edges e_{31} and e_{32}
for $4 \leq i \leq N$ **do** ▷ $N = |V|$
    Select next follower $\#i$ such that $N_i \subset \Lambda_{i-1}$ where $\Lambda_{i-1} = \{1, ..., i-1\}$
    Arrange the incidents edges of the agent i from the shortest to longest length (Euclidean distance)
    if $n = 2$ **then**
        Connect the follower $\#i$ to the the digraph with directed triangulation via the shortest length edges.
    else if $n = 3$ **then**
        Connect the follower $\#i$ to the the digraph with directed trilateration via the shortest length edges.
    end if
end for
    return Corresponding directed Laman graph $\mathcal{G} = (\mathcal{V}, \mathcal{E})$

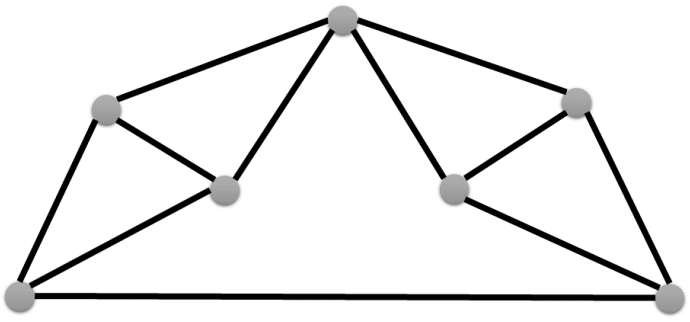

Figure 2.9: Moser spindle: a famous Laman graph.

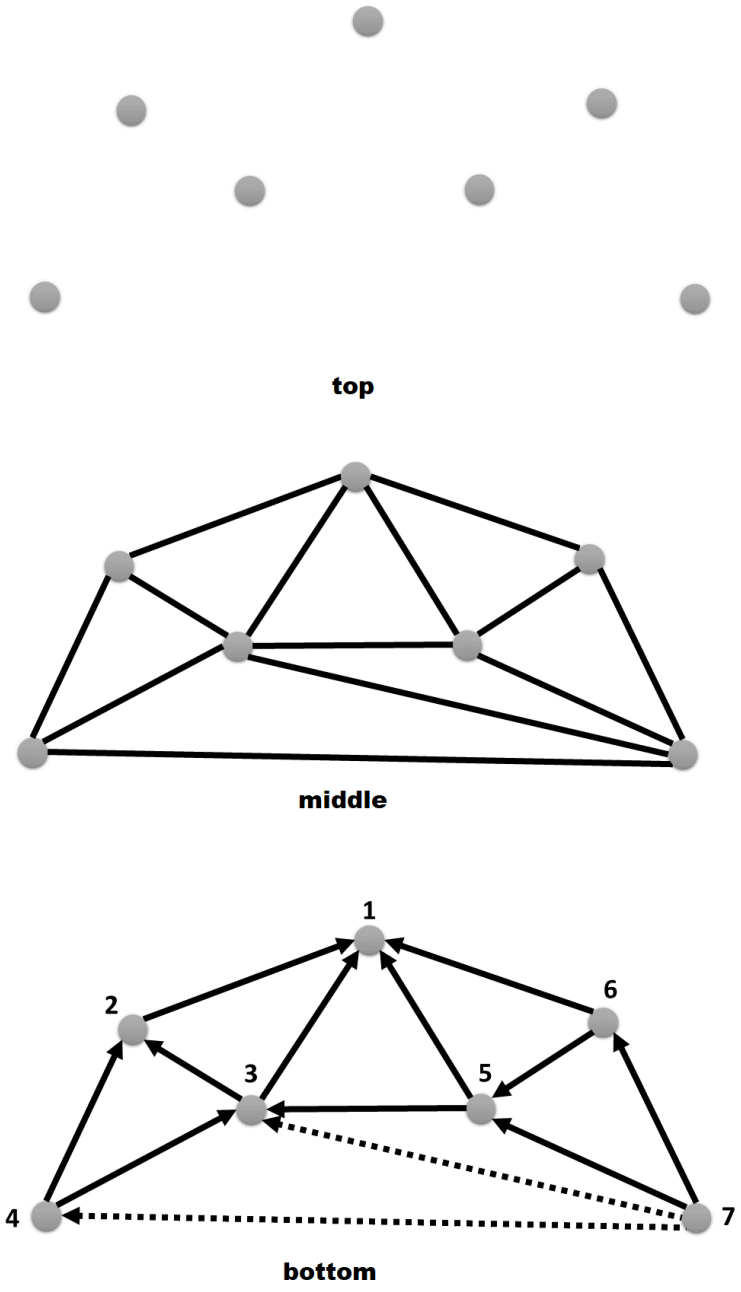

Figure 2.10: Proposed algorithm for Moser spindle: (top) the desired topology of the agents; (middle) the respective Delaunay triangulation; (bottom) the out put of the proposed algorithm as a minimally persistent acyclic LFF graph.

2.4 Agent Modeling

There are variety of dynamical models of multi-agents used in the literature (e.g., see [2] for a survey of models). The most common model of agents that are used in distance-based formation control is the single-integrator and the double-integrator models [2], [9].

2.4.1 Single-Integrator Model

The agent model is given by

$$\mathcal{W}_s : \quad \dot{p}_i = u_i, \tag{2.14}$$

where $p_i \in \mathbb{R}^n$ and $u_i \in \mathbb{R}^n$ denote the position and control input of agent i in an n-dimensional space, $n \in \{2, 3\}$, with respect to a global coordinate system. Forming the aggregate state vector for a set of N agents as $\mathbf{x}_s = \mathbf{p}$ where $\mathbf{p} = [p_1^T, ..., p_N^T]^T$, and aggregate input vector as $\mathbf{u} = [u_1^T, ..., u_N^T]^T$, the model for the set of N agents modeled by the single-integrator dynamics is given by

$$\dot{\mathbf{x}}_s = B_s \mathbf{u}, \tag{2.15}$$

where

$$B_s = I_N \otimes I_d. \tag{2.16}$$

2.4.2 Double-Integrator Model

The agents are modeled by

$$\mathcal{W}_d : \begin{cases} \dot{p}_i = v_i \\ \dot{v}_i = u_i, \end{cases} \tag{2.17}$$

where $v_i \in \mathbb{R}^n$ denotes the velocity of the agent i with respect to a global coordinate system. Let $\mathbf{v} = [v_1^T, ..., v_N^T]^T$ be the swarm velocity vector. Then, input vector elements are accelerations of the agents. Defining the aggregate state vector as $\mathbf{x}_d = [\mathbf{p}^T, \mathbf{v}^T]^T$, the state-space model for a set of N agents modeled by the double-integrator dynamics is given by

$$\dot{\mathbf{x}}_d = A_d \mathbf{x}_d + B_d \mathbf{u}, \tag{2.18}$$

with

$$A_d = \begin{bmatrix} \mathbf{0}_{N\times N} & I_N \\ \mathbf{0}_{N\times N} & \mathbf{0}_{N\times N} \end{bmatrix} \otimes I_d \tag{2.19a}$$

$$B_d = \begin{bmatrix} \mathbf{0}_{N\times N} \\ I_N \end{bmatrix} \otimes I_d, \tag{2.19b}$$

where $\mathbf{x}_d \in \mathbb{R}^{2nN}$ and $\mathbf{u} \in \mathbb{R}^{nN}$ are the aggregate state and control input of all agents respectively.

2.4.3 Agent Energy Model

In real-life multi-agent applications, there are always constraints on energy usage. Here we propose an energy model for agents that will be used in the formation control algorithm. In general, the energy consumption of agents with electric energy sources is a function of several parameters such as speed of electric motors, aerodynamic shape of the agent, agent's weight, electric efficiency, external disturbances such as wind speed, etc. The energy level of an agent i can be modeled as

$$\dot{l}_i(t) = \mathcal{L}_i(v_i, u_i), \tag{2.20}$$

where $l_i(t) \in \mathbb{R}_+$ is the energy level at time t, $v_i \in \mathbb{R}^n$ and $u_i \in \mathbb{R}^m$ are velocity and control inputs respectively, and $\mathcal{L}_i : \mathbb{R}^{n\times m} \to \mathbb{R}$ is a nonlinear mapping. In modeling of an energy consumption we focus on agents where the energy consumption depends on traveled distance. We assume that agents use no energy when they are stationary (no hovering). For simplicity, we assume that the gear ratio between electric motor and wheels is one. Suppose $l_{0i} \in \mathbb{R}_+$ is an initial energy level of the agent i at initial time t_0, expressed as a percentage of maximum energy storage capacity (current energy level over maximum energy that can be stored) and α_i is the normalized energy consumption rate per traveled distance unit. Then $l_i(t)$ can be described by

$$l_i(t) = l_i(0) - \alpha_i \int_{t_0}^{t} \|\dot{p}_i\| dt. \tag{2.21}$$

Considering that time derivative of position is velocity, we can write

$$l_i(t) = l_i(0) - \alpha_i \int_{t_0}^{t} \|v_i\| dt. \tag{2.22}$$

The total consumed energy of agent i can be expressed as

$$l_i(0) - l_i(t_f) = \alpha_i \int_{t_0}^{t_f} \|v_i\| dt, \tag{2.23}$$

where t_f is final time. Consequently, from the equation (2.22) the agent energy dynamic can be written as

$$\begin{cases} \dot{l}_i(t) = -\alpha_i \|v_i\| \\ l_i(t_0) = l_i(0). \end{cases} \tag{2.24}$$

Remark 2.4. Although more complex mathematical models for energy dynamics of mobile robots have been suggested in the literature (e.g., [119], [120]), the experimental results from [121] and [122], justify using of the proposed model (2.24).

Remark 2.5. The proposed energy model is developed for the network of Unmanned Ground Vehicles (UGVs) for cases when the external disturbances such as wind and road bumps can be neglected. The model is also applicable to a broad range of Unmanned Aerial Vehicles (UAVs) without hovering capabilities, e.g., fixed-wing UAVs in cases when external disturbances can be neglected.

2.4.4 Augmented Agent Model with Energy State

Adding the energy dynamics as an extra state to the agent's model results in an augmented dynamic model. For the single-integrator model, the augmented state vector is $\hat{\mathbf{x}}_{s_i} = [p_i^T, l_i]^T$ and the state-space model is given by

$$\hat{\mathcal{W}}_s : \begin{cases} \dot{p}_i = u_i \\ \dot{l}_i = -\alpha_i \|u_i\|. \end{cases} \tag{2.25}$$

Similarly, for the double-integrator model, the augmented state vector is $\hat{\mathbf{x}}_{d_i} = [p_i^T, v_i^T, l_i]^T$ and the state-space model is

$$\hat{\mathcal{W}}_d : \begin{cases} \dot{p}_i = v_i \\ \dot{v}_i = u_i \\ \dot{l}_i = -\alpha_i \|v_i\|. \end{cases} \tag{2.26}$$

Equations (2.25) and (2.26) are augmented single and double-integrator models of an agent, respectively.

2.5 SDRE Method

There are two common approaches for solving optimal control problems – either by Pontryagin's maximum principle (PMP) or by Hamilton–Jacobi–Bellman (HJB) equation. For linear systems with a quadratic cost functional, optimal control results in a well-known linear quadratic regulator (LQR) method. There were attempts to mimic the

LQR controller for nonlinear systems resulting in the state-dependent Riccati equation (SDRE) method. The underlying idea is to generalize well-developed linear control techniques for nonlinear systems to treat the nonlinear system like a linear one. In fact, the SDRE method can be used to design a nonlinear state-feedback controller in a very effective way for a broad class of nonlinear systems [123], [124].

Suppose a system that is nonlinear in the state, but affine in control is given by

$$\dot{\mathbf{x}} = f(\mathbf{x}) + B(\mathbf{x})\mathbf{u}, \tag{2.27}$$

where $\mathbf{x} \in \mathbb{R}^q$ and $\mathbf{u} \in \mathbb{R}^p$ are the state and input vectors of the system, respectively. Note that $f(\mathbf{x}) : \mathbb{R}^q \to \mathbb{R}^q$ is a nonlinear mapping and $B(\mathbf{x}) \in \mathbb{R}^{q\times p}$ is a matrix-valued, state-dependent input matrix. The system (2.27) can be rewritten in a linear-like form using extended linearization as described next.

2.5.1 Extended Linearization

Extended linearization, also known as state-dependent coefficient (SDC) factorization, is a way of rewriting nonlinear equations in a linear-like form that absorbs nonlinearities in the state and input matrices. Under the assumption that $f(\mathbf{x}) \in C^1$, we can write (2.27) in a linear-like form

$$\dot{\mathbf{x}} = A(\mathbf{x})\mathbf{x} + B(\mathbf{x})\mathbf{u}, \tag{2.28}$$

where $A : \mathbb{R}^q \to \mathbb{R}^{q\times q}$ is a matrix valued function and is non-unique for non-scalar systems [123].

The representation (2.28) is called a SDC representation of the system (2.27) where the matrix $A(\mathbf{x})$ is SDC state matrix.

Remark 2.6. There are several proposed methods for finding $A(\mathbf{x})$ in the literature. Note that non-uniqueness of $A(\mathbf{x})$ results in extra degrees of freedom in control design procedure. The reader may refer to [123], [125], [126] for more details.

Remark 2.7. If $A(\mathbf{x})$ is a SDC representation of the nonlinear system (2.27) such that $f(\mathbf{x}) = A(\mathbf{x})\mathbf{x}$ then, $\hat{A}(\mathbf{x}) = A(\mathbf{x}) + E(\mathbf{x})$ for every $E(\mathbf{x})$ that satisfies $E(\mathbf{x})\mathbf{x} = 0$, is also a SDC representation of the system (2.27).

Remark 2.8. If $A_1(\mathbf{x})$ and $A_2(\mathbf{x})$ are a SDC representation of the nonlinear system (2.27), then $\hat{A}(\mathbf{x}) = \alpha A_1(\mathbf{x}) + (1-\alpha)A_2(\mathbf{x})$ for any $0 \leq \alpha \leq 1$ is also a SDC representation of the system (2.27).

2.5.2 SDRE Controller

Suppose a cost functional with state-dependent weighting matrices is given by

$$J(\mathbf{x}_0, \mathbf{u}) = \frac{1}{2}\int_{t_0}^{\infty} \{\mathbf{x}(t)^T Q(\mathbf{x})\mathbf{x}(t) + \mathbf{u}(t)^T R(\mathbf{x})\mathbf{u}(t)\}dt, \tag{2.29}$$

where $\mathbf{x}_0$ is the initial state of the system at the initial time t_0. Here $Q : \mathbb{R}^q \to \mathbb{R}^{q\times q}$ is a non-negative, symmetric matrix-valued function and $R : \mathbb{R}^q \to \mathbb{R}^{p\times p}$ is a positive definite, symmetric matrix-valued function. The objective of the optimal control problem is to find a control $\mathbf{u}$ for the system (2.28) such that it minimizes the cost functional (2.29), while stabilizing the closed-loop system. The desired optimal control will be in the state feedback form $\mathbf{u}(\mathbf{x}) = -k(\mathbf{x})\mathbf{x}(t)$, with $k(\mathbf{x})$ being the optimal feedback gain.

For solution feasibility of the SDRE control method, the following conditions are required:

- Condition 1: The function $f(\mathbf{x})$ is continuously differentiable ($f(\mathbf{x}) \in C^1$) and $B(\mathbf{x})$ is a matrix valued function such that $B(\mathbf{x}) \in C^0$.
- Condition 2: The origin ($\mathbf{x} = 0$) is an equilibrium of the system with zero input such that $f(0) = 0$.
- Condition 3: The pair $\{A(\mathbf{x}), B(\mathbf{x})\}$ is point-wise stabilizable and the pair $\{C(\mathbf{x}), A(\mathbf{x})\}$ is point-wise detectable in linear sense for all $\mathbf{x}$ in some nonempty neighborhood of the origin Ω, where $C^T(\mathbf{x})C(\mathbf{x}) = Q(\mathbf{x})$.

The following lemma presents the main results in SDRE theory and can be found in [123], [124].

Lemma 2.9 ([124]). *Given that the nonlinear system (2.27) meets Conditions 1-3, there exists a state feedback control law*

$$\boldsymbol{u}(\boldsymbol{x}) = -k(\boldsymbol{x})\boldsymbol{x}(t), \tag{2.30}$$

where feedback gain $k(\boldsymbol{x})$ is given by

$$k(\boldsymbol{x}) = R^{-1}(\boldsymbol{x})B^T(\boldsymbol{x})S(\boldsymbol{x}), \tag{2.31}$$

and $S(\boldsymbol{x})$ is a unique, symmetric, and positive-definite solution of the following corresponding state-dependent Riccati equation

$$Q(\boldsymbol{x}) + A^T(\boldsymbol{x})S(\boldsymbol{x}) + S(\boldsymbol{x})A(\boldsymbol{x}) - S(\boldsymbol{x})B(\boldsymbol{x})R^{-1}(\boldsymbol{x})B^T(\boldsymbol{x})S(\boldsymbol{x}) = 0. \tag{2.32}$$

The control law (2.30) asymptotically minimizes the cost functional (2.29) and guarantees local asymptotic stability of the closed-loop system.

Remark 2.9. The SDRE control law (2.30) becomes optimal if it satisfies additional constraints presented in [124].

Remark 2.10. Substituting control law (2.30) in the system (2.28), then, the closed-loop dynamics is

$$\dot{\mathbf{x}} = A_{CL}(\mathbf{x})\mathbf{x} \tag{2.33a}$$

$$A_{CL}(\mathbf{x}) = A(\mathbf{x}) - B(\mathbf{x})R^{-1}(\mathbf{x})B^T(\mathbf{x})S(\mathbf{x}), \tag{2.33b}$$

where $A_{CL}(\mathbf{x})$ is called a closed-loop SDC matrix [127].

Lemma 2.10 ([128]). *Assume that the system (2.28) satisfies Conditions 1-3 and $A_{CL}(\boldsymbol{x})$ is symmetric for all $\boldsymbol{x}$, then SDRE control law (2.30) results in the global asymptotic stability of the closed-loop system.*

Remark 2.11. As a consequence of Lemma 2.10, for scalar systems, the SDRE control law is globally asymptotically stabilizing [128].

Remark 2.12. Conditions 1-3, known as the SDRE feasibility conditions, are common assumptions for general systems in the literature that guarantees existence and uniqueness of the solution of the Riccati equation and SDRE controller [123], [124].

Remark 2.13. Although we supposed that the system (2.27) is autonomous and affine in control, there are studies that extended the SDRE method for non-affine systems [129] and nonautonomous systems [130].

Remark 2.14. Finding the exact solution of the Riccati equation is not possible except for very simple systems. However, there are effective numerical solutions for implementation of SDRE controller in the literature [124], [131].

2.5.3 Stabilizability and Detectability of SDC Representation

The SDC representation of the system (2.27) where $q > 2$ is not unique. The stabilizability and detectability of a SDC representation can be checked by forming the controllability and observability matrices and checking their ranks throughout the state trajectories. The existence and uniqueness of the SDRE solution is an important question [132]. For an affine nonlinear system, Conditions 1-3 known as SDRE feasibility conditions are common assumptions in the literature that guarantees the existence and uniqueness of the solution of the Riccati equation and SDRE controller [123], [124]. However, there is no established way to propose a stabilizable and detectable representation of a system. The following lemma presents important results on the existence of such a representation.

Lemma 2.11 ([133]). *For the system (2.27) always there exist a stabilizable and detectable SDC representation unless $(\boldsymbol{x}, f(\boldsymbol{x}))$ are linearly dependent and $C(\boldsymbol{x})\boldsymbol{x} = 0$.*

Since the state weighting matrix $Q(\mathbf{x})$ is selective, we can select a $Q(\mathbf{x})$ in a way that the state $\mathbf{x}$ does not belong to the null space of $C(\mathbf{x})$ therefore $C(\mathbf{x})\mathbf{x} \neq 0$. This guarantees the existence of a stabilizable and detectable SDC representation of the system (2.27).

Remark 2.15. By choosing a positive definite $Q(\mathbf{x})$, detectability of the pair $\{C(\mathbf{x}), A(\mathbf{x})\}$ is guaranteed [127].

Remark 2.16. The stabilizability of the pair $\{A(\mathbf{x}), B(\mathbf{x})\}$ greatly depends on the selection of SDC matrices [134]. In particular, the flexibility of selecting $A(\mathbf{x})$ can guarantee the optimality of the solution and enhance the stabilizability of the SDC representation [135]. There are several studies in the literature on optimal selection of SDC matrix [130], and how to choose the SDC matrices for a better stabilizability [133], [135].

The region of attraction (ROA) is also important in some applications. The reference [136] proposes a method for estimation of the region of attraction of the controller. The region of exponential stability of SDRE controllers are studied by Chang and Chung in [137].

2.5.4 SDRE State Tracking

For the state tracking problem using SDRE controller, several methods are proposed in the literature. In [138], the so-called "integral servomechanism method" is introduced. Assume that $\mathbf{x}_R$ is the state to track, corresponding to the desired reference command $\mathbf{r} \in \mathbb{R}^\tau$. The state vector can be written as $\mathbf{x} = [\mathbf{x}_R^T, \mathbf{x}_N^T]^T$. Define $\mathbf{x}_I$ as the integral state of $\mathbf{x}_R$; the augmented state vector is then $\tilde{\mathbf{x}} = [\mathbf{x}_I^T, \mathbf{x}_R^T, \mathbf{x}_N^T]^T$. Hence, the augmented system is given by

$$\dot{\tilde{\mathbf{x}}} = \tilde{A}(\tilde{\mathbf{x}})\tilde{\mathbf{x}} + \tilde{B}(\tilde{\mathbf{x}})\mathbf{u}, \tag{2.34}$$

where

$$\tilde{A}(\tilde{\mathbf{x}}) = \begin{bmatrix} 0 & [I_\tau, 0] \\ 0 & A(\mathbf{x}) \end{bmatrix} \tag{2.35a}$$

$$\tilde{B}(\tilde{\mathbf{x}}) = \begin{bmatrix} 0 \\ B(\mathbf{x}) \end{bmatrix}. \tag{2.35b}$$

Consequently, the integral servomechanism SDRE control law is

$$\mathbf{u}(\tilde{\mathbf{x}}) = -\tilde{R}^{-1}(\tilde{\mathbf{x}})\tilde{B}^T(\tilde{\mathbf{x}})\tilde{S}(\tilde{\mathbf{x}}) \begin{bmatrix} \mathbf{x}_I - \int \mathbf{r} dt \\ \mathbf{x}_R - \mathbf{r} \\ \mathbf{x}_N \end{bmatrix}, \tag{2.36}$$

where $\tilde{S}(\tilde{\mathbf{x}})$ is a solution of the corresponding algebraic Riccati equation

$$\tilde{Q}(\tilde{\mathbf{x}}) + \tilde{A}^T(\tilde{\mathbf{x}})\tilde{S}(\tilde{\mathbf{x}}) + \tilde{S}(\tilde{\mathbf{x}})\tilde{A}(\tilde{\mathbf{x}}) - \tilde{S}(\tilde{\mathbf{x}})\tilde{B}(\tilde{\mathbf{x}})\tilde{R}^{-1}(\tilde{\mathbf{x}})\tilde{B}^T(\tilde{\mathbf{x}})\tilde{S}(\tilde{\mathbf{x}}) = 0, \tag{2.37}$$

in which $\tilde{Q}(\tilde{\mathbf{x}})$ and $\tilde{R}(\tilde{\mathbf{x}})$ stand for weighting matrices associated with the corresponding cost functional. It should be noted that for the sake of pointwise detectability of the augmented system, the associated weighting element for $\mathbf{x}_I$ has to be nonzero in $\tilde{Q}(\tilde{\mathbf{x}})$ [123].

2.5.5 SDRE Output Tracking

Suppose we have a nonlinear input-affine system given by (2.28) with the output $\mathbf{y} = H(\mathbf{x})(\mathbf{x})$. Define the output tracking error as

$$\mathbf{e} = \mathbf{z} - \mathbf{y} = \mathbf{z} - H(\mathbf{x})\mathbf{x}, \tag{2.38}$$

where $\mathbf{z} \in \mathbb{R}^n$ is the desired output reference. The objective is to minimize the cost functional

$$J = \frac{1}{2}\int_{t_0}^{\infty} \{\mathbf{e}(t)^T Q(\mathbf{x})\mathbf{e}(t) + \mathbf{u}(t)^T R(\mathbf{x})\mathbf{u}(t)\}dt \tag{2.39}$$

with respect to (2.28) such that the output $\mathbf{y}$ tracks the reference signal $\mathbf{z}$. The following result provides the SDRE-based control law that is the solution of the output tracking problem.

Lemma 2.12 ([139]). *Under feasibility conditions, there exists a control law in the feedback form*

$$\boldsymbol{u}(\boldsymbol{x}) = -R^{-1}(\boldsymbol{x})B^T(\boldsymbol{x})[S(\boldsymbol{x})\boldsymbol{x}(t) - P(\boldsymbol{x})], \tag{2.40}$$

where $S(\boldsymbol{x})$ is a unique, symmetric, and positive-definite solution of the following state-dependent Riccati equation

$$H^T(\boldsymbol{x})Q(\boldsymbol{x})H(\boldsymbol{x}) + A^T(\boldsymbol{x})S(\boldsymbol{x}) + S(\boldsymbol{x})A(\boldsymbol{x}) - S(\boldsymbol{x})B(\boldsymbol{x})R^{-1}(\boldsymbol{x})B^T(\boldsymbol{x})S(\boldsymbol{x}) = 0, \tag{2.41}$$

and $P(\boldsymbol{x})$ is a solution of following linear vector equation

$$P(\boldsymbol{x}) = -\big([A(\boldsymbol{x}) - B(\boldsymbol{x})R^{-1}(\boldsymbol{x})B^T(\boldsymbol{x})S(\boldsymbol{x})]^T\big)^{-1}H^T(\boldsymbol{x})Q(\boldsymbol{x})\boldsymbol{z}, \tag{2.42}$$

that asymptotically minimizes the cost functional (2.39) alongside the closed-loop stability of the output tracking system.

2.5.6 HSDRE Method

SDC parametrization provides a flexible tool for control system design. However, for some systems, the feasibility conditions cannot be satisfied at some points in their domain. The following lemma provides the hybrid state-dependent Riccati equation (HSDRE) control law for this kind of system and guarantees the local stability of the corresponding closed-loop system.

Lemma 2.13 ([128]). *Assume that the system (2.28) satisfies Conditions 1-2 and is stabilizable and detectable everywhere except at the origin. Then for sufficiently small $\varepsilon > 0$, the following HSDRE control law*

$$HSDRE: \begin{cases} SDRE\ control\ law & whenever \quad \|\boldsymbol{x}\| > \varepsilon \\ \boldsymbol{u} = 0 & whenever \quad \|\boldsymbol{x}\| \leq \varepsilon \end{cases} \tag{2.43}$$

results in uniform ultimate boundedness of the closed-loop system's solution with ε being the ultimate bound.

Remark 2.17. A closed-loop system that all its solutions are uniformly ultimately bounded (UUB) within a selective ultimate bound is called a practically stable system [140].

2.6 Stability of Interconnected Systems

Stability analysis of distributed multi-agent systems is challenging due to the coupled dynamics of agents. Therefore, this section presents a brief discussion on the stability of cascade interconnected systems, which is a core idea of the stability analysis of the later results.

Definition 2.7 ([140]). The origin of the system

$$\dot{x} = f(x), \tag{2.44}$$

where $f(.)$ is a locally Lipschitz, is exponentially stable if there exist positive constants α, λ and d such that the following is satisfied

$$\|x(t)\| \leq \alpha \|x(0)\| e^{-\lambda t}, \tag{2.45}$$

for any initial condition $\|x(0)\| < d$. The results are global if the conditions are satisfied globally.

Theorem 2.3 ([141]). *The origin of the system (2.44) is exponentially stable if there exists continuously differentiable function $V(x)$, over some neighborhood of origin Ω,*

satisfying

$$k_1||x||^p \leq V(x) \leq k_2||x||^p \tag{2.46a}$$

$$\dot{V}(x) \leq -k_3||x||^p, \tag{2.46b}$$

is which k_1, k_2, k_3, and p are positive constants. The result is global if the conditions hold globally.

Definition 2.8 ([140])**.** The system

$$\Xi_0 : \quad \dot{x} = f(x, u), \tag{2.47}$$

where f is a locally Lipschitz nonlinear mapping, is input-to-state stable (ISS) if there exist class $\mathcal{KL}$ and class $\mathcal{K}$ functions σ and ψ, respectively, such that the following is satisfied

$$\|x(t)\| \leq \sigma(\|x(0)\|, t) + \psi\Big(\sup_{0\leq\tau\leq t} \|u(\tau)\|\Big), \tag{2.48}$$

for any bounded input u and initial condition $x(0)$. The results are local if the conditions are hold only in some neighborhood of the origin.

Remark 2.18. For the system (2.47), the unforced system is $\dot{x} = f(x, 0)$.

Theorem 2.4 ([142])**.** *Suppose that the origin of unforced system (2.47) is asymptotically stable provided that $f \in C^1$. Then, the system (2.47) is locally input-to-state stable.*

Theorem 2.5 ([141])**.** *The system (2.47) is input-to-state stable if the origin of the unforced system is globally exponentially stable and $f \in C^1$ is globally Lipschitz in (x,u).*

Theorem 2.6 ([140])**.** *If the system*

$$\Xi_1 : \quad \dot{\omega} = h(\omega, z), \tag{2.49}$$

is input-to-state stable with respect to z as the input and the system

$$\Xi_2 : \quad \dot{z} = g(z, u), \tag{2.50}$$

is input-to-state stable with respect to u as the input, then the interconnected system

$$\Xi_3 : \begin{cases} \dot{\omega} = h(\omega, z) \\ \dot{z} = g(z, u), \end{cases} \tag{2.51}$$

is input-to-state stable.

Lemma 2.14 ([140]). *Assume that the origin of unforced system (2.49) is locally asymptotically stable and the origin of unforced system (2.50) is locally asymptotically stable. Then, the origin of the unforced interconnected system (2.51) is locally asymptotically stable.*

Lemma 2.15 ([142]). *Assume that the origin of the system (2.49) is locally input-to-state stable with respect to z as an input and the origin of unforced system (2.50) is locally asymptotically stable. Then, the origin of the unforced interconnected system (2.51) is locally asymptotically stable.*

Lemma 2.16 ([140]). *Assume that the system (2.49) is input-to-state stable with respect to input z and the origin of unforced system (2.50) is globally asymptotically stable. Then, the origin of the unforced interconnected system (2.51) is globally asymptotically stable.*

Theorem 2.7 ([143]). *The origin of the system*

$$\dot{x}_1 = f_1(x_1) \tag{2.52a}$$

$$\dot{x}_2 = f_2(x_2, x_1) \tag{2.52b}$$

$$\vdots$$

$$\dot{x}_i = f_i(x_i, x_{i-1}, \ldots, x_1), \tag{2.52c}$$

is locally (respectively globally) asymptotically stable equilibrium point if the origin of the system (2.52a) is locally (respectively globally) asymptotically stable and all subsystems $x_j = f_j(.)$ where $1 < j \leq i$, is locally (respectively globally) ISS with respect to the all x_k where $k < j$.

2.7 Signed Area and Signed Volume

For a triangular formation prescribed by the length of edges, there is one ambiguous formation rather than translation and rotation of the original shape, known as reflection. In other words, reflection inverses the sign of the triangulated area while translation and rotation keep the sign same. The Figure 2.11 depicts this situation. Although these two representations are congruent and both satisfy the desired distance constraints, it is well known that the area of the two triangles is different in sign. A signed area of a triangle between a three agents i, j, and k located at p_i, p_j, and p_k is given by [42]and [44]:

$$\mathbb{A} = \frac{1}{2} det \begin{bmatrix} 1 & 1 & 1 \\ p_i & p_j & p_k \end{bmatrix}. \tag{2.53}$$

The set of (i, j, k) is called a clique [48]. The value of $\mathbb{A}$ is positive or negative depending on the order of points around the center of the triangle whether is clockwise or

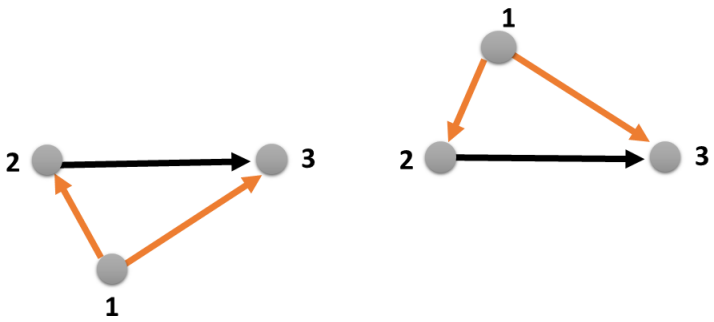

(a) Desired triangle (b) Flipped triangle

Figure 2.11: Reflection of the desired formation in 2-D space.

counterclockwise. Using simple algebraic manipulation, we can write

$$\mathbb{A} = \frac{1}{2} det \begin{bmatrix} p_j - p_i & p_k - p_i \end{bmatrix} \tag{2.54a}$$

$$= \frac{1}{2}(p_k - p_i)^T \begin{bmatrix} 0 & 1 \\ -1 & 0 \end{bmatrix} (p_k - p_j). \tag{2.54b}$$

It is shown that for any rotation of the triangle the signed area, $\mathbb{A}$, remains unchanged [44].

Suppose that a clique (i, j, k, l) is deployed in the space. The signed volume of tetrahedron that formed is between the agents located in p_i, p_j, p_k, and p_l in 3-D is given by [144]:

$$\mathbb{V} = \frac{1}{6} det \begin{bmatrix} x_i & y_i & z_i & 1 \\ x_j & y_j & z_j & 1 \\ x_k & y_k & z_k & 1 \\ x_l & y_l & z_l & 1 \end{bmatrix}. \tag{2.55}$$

Using mathematical manipulation it can be simplified as

$$\mathbb{V} = \frac{1}{6} det \begin{bmatrix} x_i - x_l & y_i - y_l & z_i - z_l \\ x_j - x_l & y_j - y_l & z_j - z_l \\ x_k - x_l & y_k - y_l & z_k - z_l \end{bmatrix}. \tag{2.56}$$

Equivalently, the volume of a pyramid spanned by vectors $\mathbf{u}$, $\mathbf{v}$, and $\mathbf{w}$ is denoted by

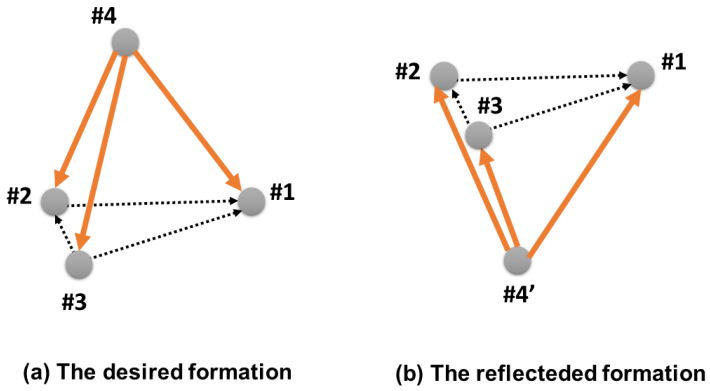

Figure 2.12: Reflection of the desired formation in 3-D space.

$\mathbb{V} = \langle \mathbf{uvw} \rangle_3$ and given by

$$\begin{aligned} \mathbb{V} &= \frac{1}{6}(\mathbf{u} \times \mathbf{v}).\mathbf{w} \\ &= \frac{1}{6} det \begin{bmatrix} w_1 & w_2 & w_3 \\ u_1 & u_2 & u_3 \\ v_1 & v_2 & v_3 \end{bmatrix}. \end{aligned} \tag{2.57}$$

The value of $\mathbb{V}$ could be positive or negative depending on the two possible realizations. Figure 2.12 illustrates the possible two situation. The agent #4 locates in its desired position satisfying all the associated distance constraints in Figure 2.12(a). The agent can locate at the position #4', which is the reflection of the desired position shown in Figure 2.12(b). Although the follower at position #4' satisfies all its associated distance constraints, the formation is not the desired one.

Chapter 3

Leader-Follower Formation Control

3.1 Introduction

This chapter presents an optimal displacement-based leader-follower formation control of multi-agent systems with energy consumption constraints. The leader-follower formation control problem is formulated as a displacement-based formation, and solved using the SDRE control approach, where we proved the asymptotic stability of the formation. We choose the weighting matrices of the cost functional to be dependent on the energy level of the agents, thus allowing for autonomous adjustment of the agents' trajectories that preserve the integrity of the overall formation despite energy levels.

3.2 Main Results

In the leader-follower formation control, two main objectives are tracking performance and preserving the desired formation. Other aims such as energy consumption, collision avoidance, obstacle avoidance, time of operation, control effort, etc., can also be included in the cost functional. Here, we formulated the problem such that the obtained optimal control law preserves formation and satisfies required tracking performance.

Consider a formation of N agents where the first agent is the leader and others are followers. The leader is assigned a reference trajectory $p^\star$ to follow. Also, it can sense the followers' relative position.

3.2.1 Single-Integrator Model

We define the desired formation in a displacement-based form where desired followers' positions are vectors with regard to the leader's local coordinate frame. For a set of agents modeled as augmented single-integrators $\hat{\mathcal{W}}_s$, the formation vector in n-dimensional space,

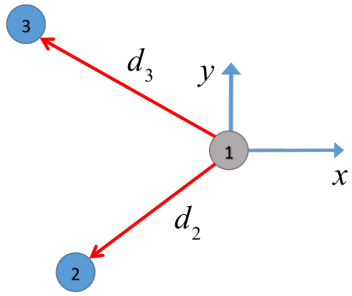

Figure 3.1: Displacement-based formation for $N = 3$ agents.

with the first agent being the leader, is given by

$$\hat{\mathbf{d}}_1 = [0_n^T, d_2^T, ..., d_N^T]^T, \tag{3.1}$$

where

$$d_i = p_i^\star - p_1^\star, \qquad i \in \{2, ..., N\}. \tag{3.2}$$

Note that $p_i^\star$ is the desired position of the agent i in the global coordinate frame. Figure 3.1 shows the desired formation for $N = 3$ agents.

We propose a cost functional that includes three parts related to tracking, formation stability, and energy consumption:

$$J = J_{tr} + J_{fm} + J_{en}. \tag{3.3}$$

The cost functional components are given by

$$J_{tr} = \frac{1}{2}\int_{t_0}^{\infty} (p_1 - p^\star)^T Q_1 (p_1 - p^\star) dt, \tag{3.4}$$

$$J_{fm} = \frac{1}{2}\sum_{i=2}^{N}\int_{t_0}^{\infty} (p_i - p_1 - d_i)^T Q_i (p_i - p_1 - d_i) dt, \tag{3.5}$$

$$J_{en} = \frac{1}{2}\sum_{i=1}^{N}\int_{t_0}^{\infty} (\alpha_i u_i)^T R_i (\alpha_i u_i) dt. \tag{3.6}$$

Let define the error vector as

$$\hat{\mathbf{e}}_1 = [e_1^T, e_2^T, ..., e_N^T]^T, \tag{3.7}$$

where e_1 is the leader's reference tracking error given by

$$e_1 = p_1 - p^\star. \tag{3.8}$$

The formation errors are

$$e_i = p_i - p_1 - d_i, \qquad i \in \{2, ..., N\}. \tag{3.9}$$

The error dynamics is then given by

$$\dot{e_1} = \dot{p_1} = u_1 \tag{3.10a}$$

$$\dot{e_i} = \dot{p_i} - \dot{p_1} = u_i - u_1. \tag{3.10b}$$

The cost functional (3.3) can now be written in the quadratic form. Thus, the optimal control problem can be stated as

$$\begin{aligned} J =& \min \frac{1}{2} \int_{t_0}^{\infty} (\hat{\mathbf{e}}_1^T Q_s(\mathbf{x}) \hat{\mathbf{e}}_1 + \mathbf{u}^T R_s(\mathbf{x}) \mathbf{u}) dt \\ &\text{s.t.} \\ &\dot{\hat{\mathbf{e}}}_1 = \hat{B}_1 \mathbf{u} \\ &Q_s(\mathbf{x}) = \text{diag}[Q_1, ..., Q_N] \geq 0 \\ &R_s(\mathbf{x}) = \text{diag}[R_1, ..., R_N] > 0, \end{aligned} \tag{3.11}$$

where

$$\hat{B}_1 = \begin{bmatrix} 1 & 0_{N-1}^T \\ -1_{N-1} & I_{N-1} \end{bmatrix} \otimes I_n. \tag{3.12}$$

Note that in the optimal control problem (3.11) the error dynamic is linear and only the weighting matrices of cost functional are state-dependent. The notation $Q_s(\mathbf{x})$ and $R_s(\mathbf{x})$ are used for showing state-dependency. As a result, by proper selection of $Q_s(\mathbf{x})$ we can ensure satisfaction of Conditions 1-3 of Lemma 2.9. Then based on Lemma 2.9, we conclude that the sub-optimal state-dependent feedback control law that minimizes the cost functional in (3.11) and locally asymptotically stabilize the closed-loop system is

$$\mathbf{u}^\star = -k \hat{\mathbf{e}}_1, \tag{3.13}$$

where k is a state feedback gain given by

$$k = R_s(\mathbf{x})^{-1} \hat{B}_1^T S, \tag{3.14}$$

and S is the positive definite solution of the following state-dependent Riccati equation

$$S \hat{B}_1 R_s(\mathbf{x})^{-1} \hat{B}_1^T S = Q_s(\mathbf{x}). \tag{3.15}$$

Theorem 3.1. *Select the state weighting matrix as*

$$Q_s = K \times I, \tag{3.16}$$

where K is a positive scalar. Then, for a set of agents described by the single-integrator model, the proposed control law (3.13) results in global asymptotic stability of the closed-loop system.

Proof. Substituting (3.13) in error dynamic, the closed-loop error dynamics of the system is

$$\dot{\hat{\mathbf{e}}}_1 = A_{CS}\hat{\mathbf{e}}_1, \tag{3.17}$$

where

$$A_{CS} = -\hat{B}_1 R_s(\mathbf{x})^{-1}\hat{B}_1^T S. \tag{3.18}$$

Rearranging equation (3.15) yields

$$A_{CS} = -S^{-1}Q_s. \tag{3.19}$$

Since S as a solution of Riccati equation is symmetric, by selecting Q_s as proposed in equation (3.16), the closed-loop SDC matrix A_{CS} will be symmetric for all $\mathbf{e}_1$. According to Lemma 2.10, this implies global asymptotic stability of the closed-loop system. □

Theorem 3.1 provides a sufficient condition for the global stability of the closed-loop system in case of the single-integrator dynamics.

Remark 3.1. Choosing constant weighting matrix, the optimal control problem (3.11) reduces to standard LQR that guarantees global asymptotic stability of the closed-loop system.

3.2.2 Double-Integrator Model

In case of a double-integrator model where agents are modeled as $\hat{\mathcal{W}}_d$, we define the state vector as $\mathbf{x}_d = [p_1^T, ..., p_N^T, v_1^T, ..., v_N^T]^T$. Similarly to (3.1), N agents in a formation can be defined by a constant formation vector

$$\hat{\mathbf{d}}_2 = [0_n^T, d_2^T, ..., d_N^T, 0_{nN}^T]^T, \tag{3.20}$$

where d_i for $i \in \{2, ..., N\}$ is given by (3.2). Defining the error vector we have

$$\hat{\mathbf{e}}_2 = [e_1^T, ..., e_N^T, v_1^T, v_2^T - v_1^T, ..., v_N^T - v_1^T]^T, \tag{3.21}$$

where components e_1 and e_i are defined in (3.8) and (3.9). Derivatives are then given by

$$\dot{e_1} = \dot{p_1} = v_1 \tag{3.22a}$$
$$\dot{e_i} = \dot{p_i} - \dot{p_1} = v_i - v_1 \tag{3.22b}$$
$$\dot{v_i} - \dot{v_1} = u_i - u_1. \tag{3.22c}$$

Then we can rewrite the system equations as

$$\dot{\hat{\mathbf{e}}}_2 = \hat{A}_2\hat{\mathbf{e}}_2 + \hat{B}_2\mathbf{u}, \tag{3.23}$$

with

$$\hat{A}_2 = \begin{bmatrix} 0_{N\times N} & I_N \\ 0_{N\times N} & 0_{N\times N} \end{bmatrix} \otimes I_n \tag{3.24a}$$
$$\hat{B}_2 = \begin{bmatrix} 0_{N\times N} \\ \hat{I} \end{bmatrix} \otimes I_n, \tag{3.24b}$$

and

$$\hat{I} = \begin{bmatrix} 1 & 0_{N-1}^T \\ -1_{N-1} & I_{N-1} \end{bmatrix}. \tag{3.25}$$

Now we can formulate an optimal control problem for the double-integrator model as

$$\begin{aligned} J = &\min \frac{1}{2}\int_{t_0}^{\infty} (\hat{\mathbf{e}}_2^T Q_d(\mathbf{x})\hat{\mathbf{e}}_2 + \mathbf{u}^T R_d(\mathbf{x})\mathbf{u})dt \\ &\text{s.t.} \\ &\dot{\hat{\mathbf{e}}}_2 = \hat{A}_2\hat{\mathbf{e}}_2 + \hat{B}_2\mathbf{u} \\ &Q_d(\mathbf{x}) = \text{diag}[Q_1, ..., Q_{2N}] \geq 0 \\ &R_d(\mathbf{x}) = \text{diag}[R_1, ..., R_N] > 0. \end{aligned} \tag{3.26}$$

Since the error dynamic in (3.23) is linear, proper choice of $Q_d(\mathbf{x})$ guarantees feasibility of SDRE solution. Then, sub-optimal control law is given by Lemma 2.9 as

$$\mathbf{u}^\star = -k_2\hat{\mathbf{e}}_2, \tag{3.27}$$

yields in local asymptotic stability of the closed-loop system. Note that the feedback gain k_2 is given by

$$k_2 = R_d(\mathbf{x})^{-1}\hat{B}_2^T S, \tag{3.28}$$

where S is the positive definite solution of the following SDRE

$$Q_d(\mathbf{x}) + \hat{A}_2^T S + S\hat{A}_2 - S\hat{B}_2 R_d(\mathbf{x})^{-1}\hat{B}_2^T S = 0. \tag{3.29}$$

Note that according to equation (2.26) the energy usage can be modeled using agents' velocity. For the double-integrator agent model, the velocity appears in the state vector and the energy weighting factors can be adjusted in matrix $Q_d(\mathbf{x})$.

Remark 3.2. Selecting constant weighting matrix $Q_d(\mathbf{x})$ and $R_d(\mathbf{x})$, results into a standard LQR problem that guarantees global asymptotic stability of the closed-loop system.

3.2.3 Selection of Weighting Matrices

Although constant weighting matrices are widely used, our aim is to relate the weighting matrix of the cost functional to energy levels of each agent and thus include the energy model into the control algorithm. We propose that the control weighting factor R_i (an element on the i-th row, i-th column of diagonal weighting matrix R) is a function of the energy level of each agent

$$R_i(t) = \frac{1}{l_i(t)}. \tag{3.30}$$

The weighting factor (3.30) is a time-varying and state (energy) dependent, resulting in an optimal controller that is state-dependent with continuous tuning throughout the state trajectory.

3.3 Simulation Results

Here, we present the results of simulations based on the proposed control methods. For simplicity, we choose $\alpha_i = 0.01$ in all simulations.

Figure 3.2 (top) shows the result of the optimal formation control law that (3.13) for a set of $N = 5$ agents that are modeled by the single-integrator dynamics in 2-D. We first simulated the scenario where all followers have fully charged batteries (all $l_{0i} = 1$) and we selected $Q = R(0) = I_n$ (top). Note that with $R(0)$ we indicated the initial value of weighting matrix. In case when one follower (agent #3 on the left side) has less initial energy than other agents $l_{03} = 0.1$, we selected $R_3(0) = 10$ according to (3.30). The result are shown in Figure 3.2 (middle). In case of a very low initial energy level, $l_{03} = 0.01$, the simulation results are in Figure 3.2 (bottom) with $R_3(0) = 100$.

Figure 3.3 (top) shows the result of the proposed formation control law for a set of single-integrators in 3-D. We first simulated the scenario where all followers have fully charged batteries (all $l_{0i} = 1$) and we selected $Q = R(0) = I_n$ (top). In case when one follower (agent #3 on the right side) has less initial energy than other agents $l_{03} = 0.1$, we selected $R_3(0) = 10$. The result is shown in Figure 3.3 (bottom).

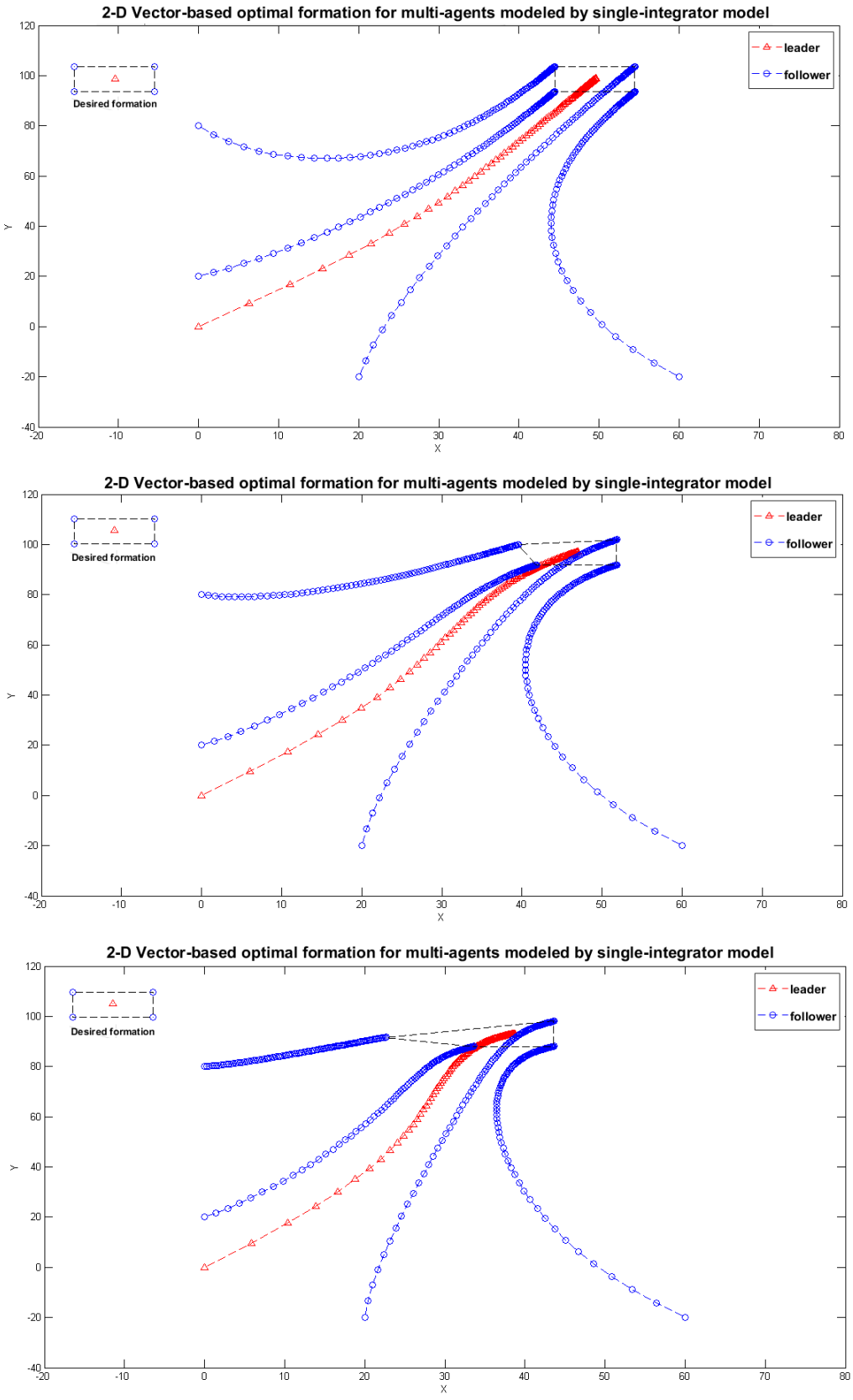

Figure 3.2: Leader-follower formation control for $N = 5$ agents modeled by a single-integrator; all followers have the same energy level, $Q = R(0)$ (top); the follower #3 (on the left side) has less initial energy, $R_3(0) = 10$ (middle); the follower #3 has a very low initial energy, $R_3(0) = 100$ (bottom).

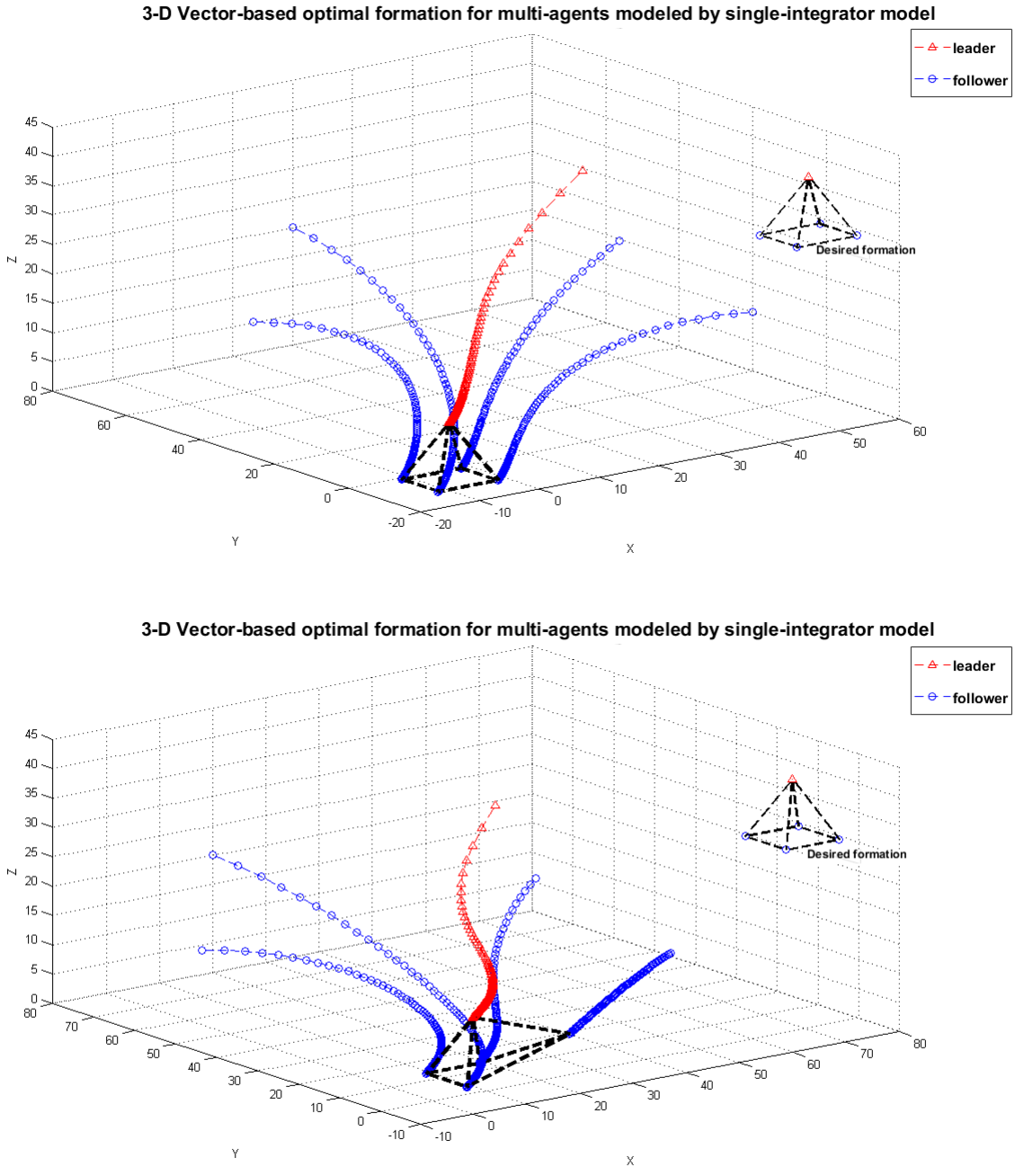

Figure 3.3: Leader-follower formation control for $N = 5$ agents modeled by a single-integrator in 3-dimensional space; all followers have full initial energy level, $Q = R(0)$ (top); the agent #3 (on the right side) has less initial energy, $R_3(0) = 10$ (bottom).

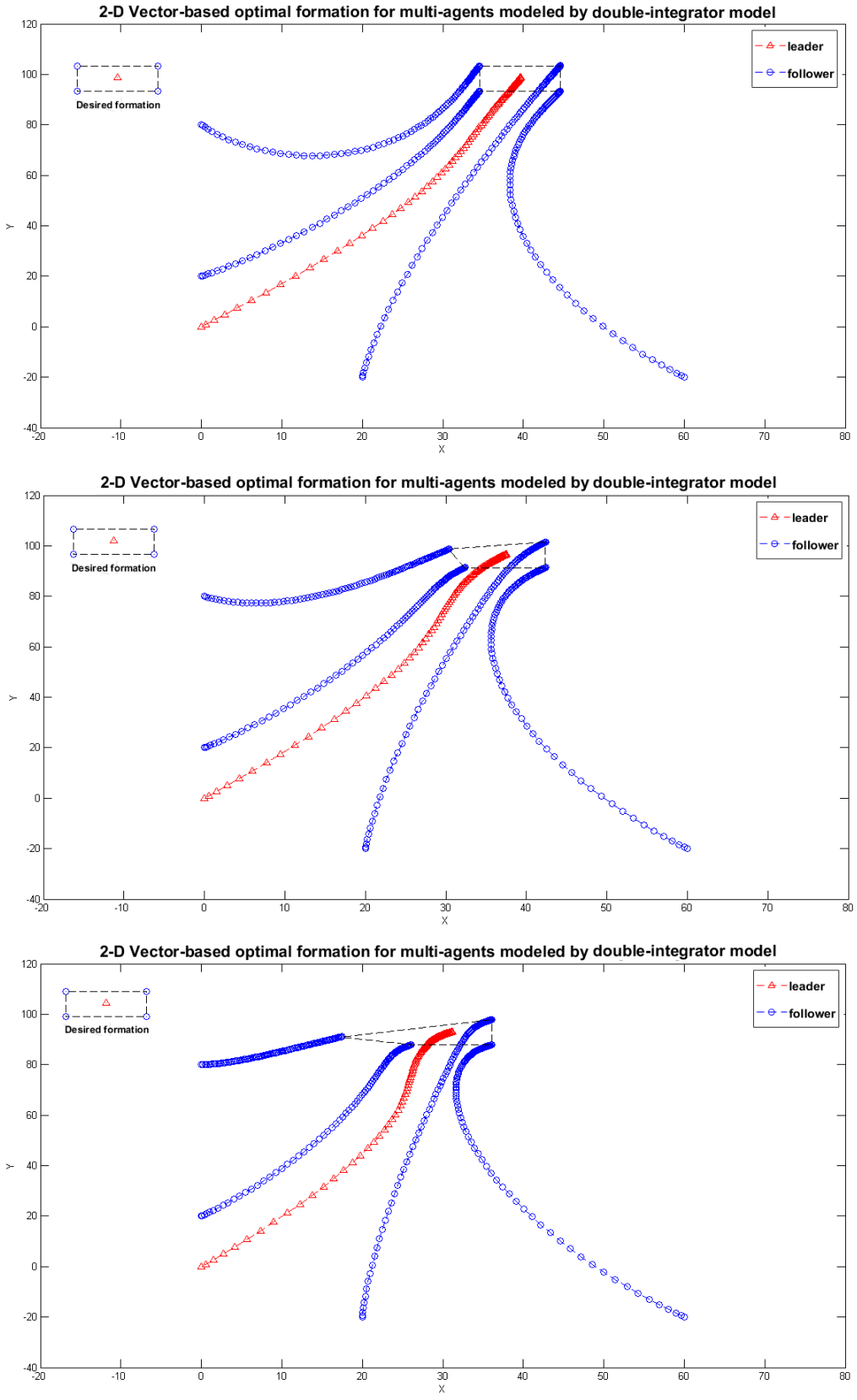

Figure 3.4: Leader-follower formation control for $N = 5$ agents modeled by a double-integrator model in 2-D; all followers has same initial energy level, Q and $R(0)$ equal to identity matrix (top); the follower #3 has a very low initial energy, $R_3(0) = 100$ (bottom).

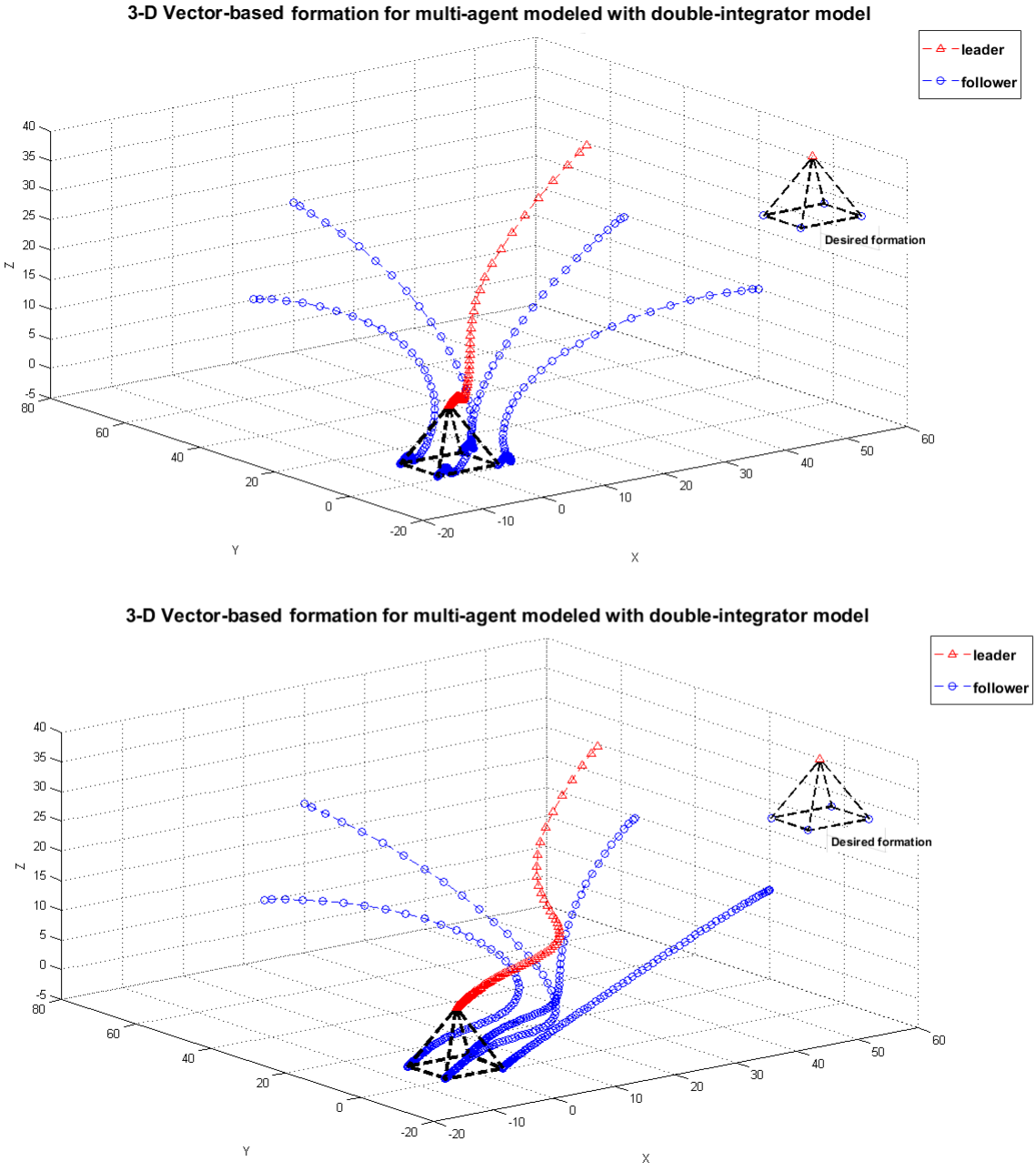

Figure 3.5: Centralized leader-follower formation control for $N = 5$ agents modeled by a double-integrator model in 3-dimensional space; all followers have the same initial energy level, $Q = [I_N, 0_N; 0_N, 0_N]$ and $R(0) = I_N$ (top); the agent on the right side has a lower initial energy level, $R_3(0) = 10$ (bottom).

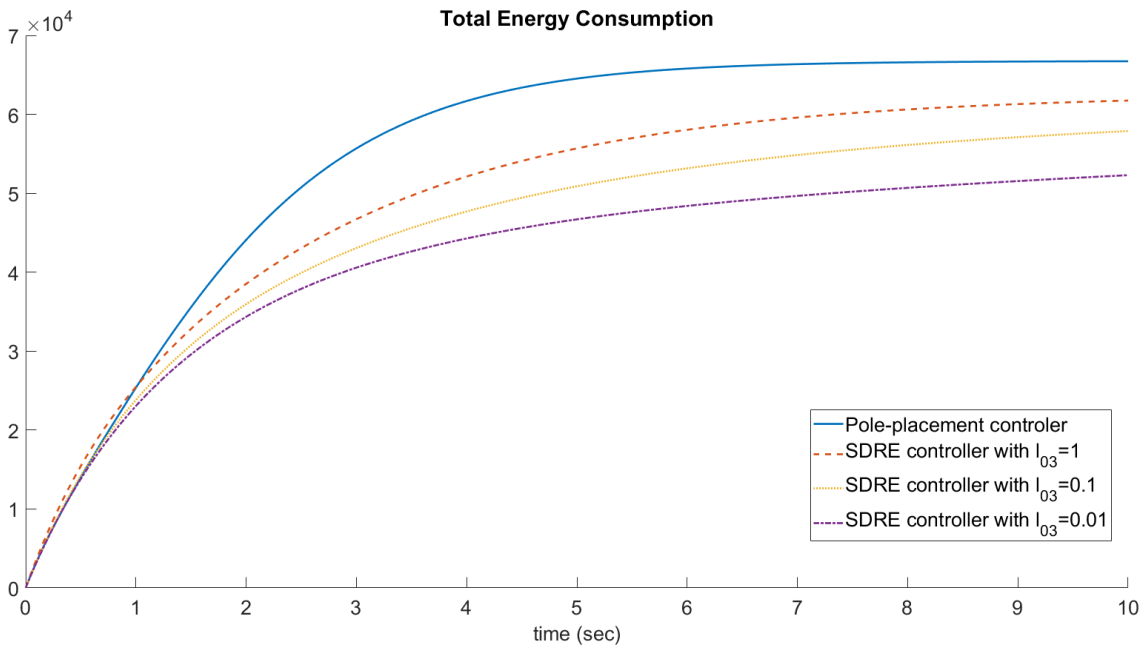

Figure 3.6: Comparison of the total energy consumption for the formation governed by various controllers. The formation consists of $N = 5$ agents modeled by the single-integrator model.

Figure 3.4 shows the results of the proposed optimal formation control law (3.27) for a set of agents modeled by the double-integrator dynamics. All followers have initially fully charged batteries ($l_{0i} = 1$), and we selected Q and $R(0)$ equal to identity matrices, Figure 3.4 (top). Then we consider the case where one of the followers (agent #3 on the left side) has lower initial energy charged than others ($l_{03} = 0.01$) with selected $R_3(0) = 100$, Figure 3.4 (bottom). Note that the agents adjust their paths to preserve formation concerning the "weak" agent as a result of the control algorithm. Figure 3.5 shows the optimal formation control of agents with double-integrator model in 3-D.

In comparison with the linear pole-placement controller, the proposed method shows a significant reduction in energy consumption. Figure 3.6 shows that the SDRE controller saves more than 7.47 percent energy usage compared to a pole-placement controller with all poles placed at $s = -1$. The saved energy rate reaches 22 percent in the case of selecting $l_{03} = 0.01$ as the initial energy for agent #3.

3.4 Conclusions

In this chapter, an optimal leader-follower formation control problem is considered. We developed a displacement-based, leader-follower control scheme for a set of agents which asymptotically minimizes energy usage while satisfying tracking and formation performances. We also proposed a solution that results in the global asymptotic stability of the

closed-loop system. The simulation results show the effectiveness of the proposed solution and reveal an interesting behavior of the group (swarm) when some agents become "weak" while maintaining the desired formation. Simulation results show a significant reduction in energy consumption.

Chapter 4

Undirected Distance-Based Formation Control

4.1 Introduction

In this chapter, the distance-based formation control problem over undirected graphs is presented. We use the nonlinear optimal control methods to optimize a predefined cost functional, including formation and energy costs. We developed an SDRE-based control scheme. We first formulated a distance-based formation control problem for the single and double-integrator agent models. Then, we considered the leader tracking with the formation control problem and provided results for the distance-based formation tracking problem.

4.2 Cost Functional

Distance-based formation control problem, where agents need to keep desired distances between the pair of neighbors, is an active research field during recent years. Although formation is the prime objective, we also consider the leader-tracking capability. In the leader-following formation control, two main goals are tracking performance and preserving the desired formation. Other objectives such as energy consumption, collision avoidance, obstacle avoidance, time of operation, and control effort also can be included in the cost functional. Here, we formulated the problem such that the obtained optimal control law preserves the formation and satisfies required tracking performance. Reference [75] proposed a cost functional with two terms that are related to the error vector and the control input. In [145], the authors offered a cost functional, which includes three elements representing the consensus formation cost, obstacle and/or collision avoidance, and tracking cost.

Figure 4.1 depicts the leader-following formation with $N = 3$ agents where the first

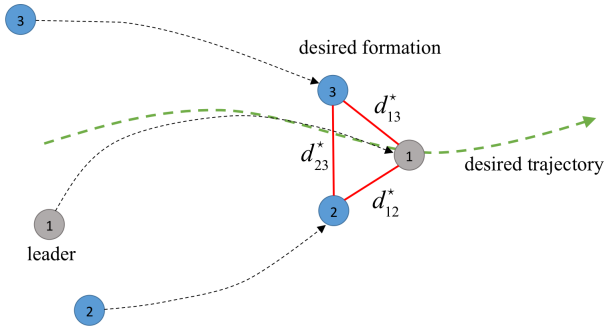

Figure 4.1: Leader-following distance-based formation control where the leader follows desired trajectory and the followers establish the desired formation.

agent is the leader and others are followers. While the leader is assigned a reference trajectory p^* to follow, it is desired for the followers to keep the predefined formation.

Consider an undirected, minimally infinitesimally rigid (MIR), graph $G = (V, E)$ that models a desired distance-based formation. Here, rigidity is a necessary condition for consistency of the formation. Let d^*_{ij} be the desired distance between agents i and j. The desired formation vector can be defined as

$$\mathbf{d}^* = [..., d^*_{ij}, ...]. \tag{4.1}$$

Note that the order of components of $\mathbf{d}^*$ is same as the edge function $\mathcal{E}_G(\mathbf{p})$.

The leader's tracking error is

$$e_t = \|p_1 - p^*\|. \tag{4.2}$$

Let us define the relative position of neighboring agents as

$$p_{ij} = p_i - p_j, \quad (i, j) \in E. \tag{4.3}$$

The distance between the neighboring pair of agents is

$$d_{ij} = \|p_{ij}\|. \tag{4.4}$$

Let us define

$$\mathbf{d} = [..., d_{ij}, ...], \tag{4.5}$$

with the same order as the desired formation vector introduced in (4.1). Then, the error vector is given by

$$\begin{aligned} \mathbf{e} &= \mathbf{d} - \mathbf{d}^* \\ &= [..., e_{ij}, ...]^T, \end{aligned} \tag{4.6}$$

where

$$e_{ij} = d_{ij} - d^*_{ij}. \tag{4.7}$$

Remark 4.1. Note that for the graph $G = (V, E)$ with $|E| = m$ edges, we can rewrite (4.6) in the form:

$$\mathbf{e} = [e_1, ..., e_m]^T. \tag{4.8}$$

We propose a cost functional that includes three components related to tracking, formation stability, and energy consumption:

$$J = J_{tr} + J_{fm} + J_{en}. \tag{4.9}$$

The cost functional components are given by

$$J_{tr} = \frac{1}{2} \int_{t_0}^{\infty} \|p_1 - p^*\|^2 q_t dt, \tag{4.10}$$

$$J_{fm} = \frac{1}{2} \sum_{i=1}^{N} J_i, \tag{4.11}$$

$$J_i = \frac{1}{2} \sum_{j \in N_i} \int_{t_0}^{\infty} (\|p_i - p_j\| - d^*_{ij})^2 q_{ij} dt, \tag{4.12}$$

$$J_{en} = \frac{1}{2} \sum_{i=1}^{N} \int_{t_0}^{\infty} \|\alpha_i v_i\|^2 \rho_i dt, \tag{4.13}$$

where q_t is the wighting factor of leader's tracking performance and q_{ij} is the weighting factor for the corresponding edge in the desired formation. Here, ρ_i is a weighting factor corresponding to v_i.

4.3 Formation Producing Control

We define the desired formation in a distance-based form that is modeled by an undirected MIR graph $G = (V, E)$. Furthermore, the connectivity of the communication graph is assumed. The distance-based formation control problem is formulated next.

4.3.1 Single-Integrator Model

For an agent which is modeled by the single-integrator model $\hat{\mathcal{W}}_s$, the error dynamics is given by

$$\begin{aligned} \dot{e}_{ij} &= \frac{d}{dt}\sqrt{(p_i - p_j)^T(p_i - p_j)} \\ &= \frac{(p_{ij})^T(u_i - u_j)}{e_{ij} + d^*_{ij}}. \end{aligned} \tag{4.14}$$

Substituting (4.14) in the time derivative of (4.6) yields

$$\begin{bmatrix} \vdots \\ \dot{e}_{ij} \\ \vdots \end{bmatrix} = \begin{bmatrix} \vdots & \vdots & \vdots & \vdots & \vdots \\ [\mathbf{0}] & \frac{p_{ij}^T}{e_{ij}+d^*_{ij}} & [\mathbf{0}] & \frac{p_{ji}^T}{e_{ij}+d^*_{ij}} & [\mathbf{0}] \\ \vdots & \vdots & \vdots & \vdots & \vdots \end{bmatrix} \begin{bmatrix} \vdots \\ u_i \\ \vdots \\ u_j \\ \vdots \end{bmatrix}, \tag{4.15}$$

where $[\mathbf{0}]$ denotes a row vector with all zeros of appropriate size. The matrix notation of (4.15) can be written as

$$\dot{\mathbf{e}} = B_s(\mathbf{p})\mathbf{u}. \tag{4.16}$$

Although B_s just depends on p_{ij}, for convenience, we use the notation of $B_s(\mathbf{p})$. Note that the structure of matrix $B_s(\mathbf{p})$ is similar to the rigidity matrix; hence, it contains weighted elements of the rigidity matrix. Thus, we introduce the normalized rigidity matrix of a graph as follows.

Definition 4.1. For an undirected graph $G(V, E)$, $\bar{\mathcal{R}}(\mathbf{p})$ is the *normalized rigidity matrix* of the graph which can be constructed using the following steps:

- Step 1. Find the rigidity matrix of $G : \mathcal{R}(\mathbf{p})$.
- Step 2. Normalize $\mathcal{R}(\mathbf{p})$ by dividing all elements of row l corresponding to the edge e_l (which is incident to vertices (i, j)), by the length of the edge $\|e_l\| = d_{ij}$. The normalized rigidity matrix is $\bar{\mathcal{R}}(\mathbf{p})$.

Remark 4.2. The normalized rigidity matrix is a special form of weighted rigidity matrix that is introduced in [7].

Based on (4.15), (4.16), and Definition 4.1, we can write

$$B_s(\mathbf{p}) = \bar{\mathcal{R}}(\mathbf{p}). \tag{4.17}$$

Now the optimal control problem can be formulated. Defining an augmented single-integrator error vector as $\mathbf{e}_s = \mathbf{e}$, we have

$$\begin{aligned} J = \min & \frac{1}{2}\int_{t_0}^{\infty} (\mathbf{e}_s{}^T Q \mathbf{e}_s + \mathbf{u}^T R \mathbf{u}) dt \\ & \text{s.t.} \\ & \dot{\mathbf{e}}_s = B_s(\mathbf{p})\mathbf{u} \\ & Q = \text{diag}[q_1, ..., q_m] > 0 \\ & R = \text{diag}[r_1, ..., r_N] \otimes I_n > 0, \end{aligned} \tag{4.18}$$

where q_i is the weighting factor corresponding to e_i in the error vector and r_i is the corresponding energy weighting factor of the agent i.

Assumption 4.1: The desired formation graph is minimally infinitesimally rigid (MIR).

The following theorem introduces a control law that guarantees local asymptotic stability of the formation.

Theorem 4.1. *Consider a set of agents described by the single-integrator model $\hat{\mathcal{W}}_s$ that operate under Assumption 4.1. The control law*

$$\boldsymbol{u} = -R^{-1} B_s(\boldsymbol{p})^T S(\boldsymbol{p}) \boldsymbol{e}_s, \tag{4.19}$$

where $S(\boldsymbol{p})$ is the positive definite solution of the following state-dependent Riccati equation

$$Q - S(\boldsymbol{p}) B_s(\boldsymbol{p}) R^{-1} B_s(\boldsymbol{p})^T S(\boldsymbol{p}) = 0, \tag{4.20}$$

achieves local asymptotic stability of the closed-loop system.

Proof. Since the desired formation is MIR, the normalized rigidity matrix is full row rank. Thus the system (4.16) is controllable. Selecting the positive definite Q, the conditions of Lemma 2.9 are satisfied. Thus, we use Lemma 2.9 to obtain the stabilizing SDRE control for the problem. The control law (4.19) is the SDRE solution of the nonlinear optimal control problem (4.18). Therefore, the proposed control law results in local asymptotic stability of the closed-loop system. □

Remark 4.3. For the agent i, the control law is given by

$$u_i = (\mathbf{z}_i \otimes \mathbf{1}_n)^T \mathbf{u}, \tag{4.21}$$

where $\mathbf{z}_i$ is a N-vector with 1 in its i-th element and all other elements equal to zero.

Remark 4.4. Since there are different SDC parametrization for non-scalar systems, we can use this property of SDRE method to improve the control performance.

In order to prevent complete depletion of agent's energy, we propose the following weighting factors.

Corollary 4.1.1. *Select input weighting factors as*

$$r_i = \bar{r}_i - log(l_i(t)), \tag{4.22}$$

where $\bar{r}_i > 0$ is a constant. Then, the control law (4.19) guarantees local asymptotic stability and prevents complete depletion of agents' energy.

Proof. Limitations on the energy consumption can be formulated as a constrained optimal control problem

$$\begin{aligned} J = \min & \frac{1}{2}\int_{t_0}^{\infty} (\mathbf{e}_s{}^T Q \mathbf{e}_s + \mathbf{u}^T \bar{R}\mathbf{u}) dt \\ & \text{s.t.} \\ & \dot{\mathbf{e}}_s = B_s(\mathbf{p})\mathbf{u} \\ & l_i > 0 \qquad 1 < i < N \\ & Q \geq 0 \\ & \bar{R} = \text{diag}[\bar{r}_1, ..., \bar{r}_N] \otimes I_n > 0. \end{aligned} \tag{4.23}$$

There are several standard methods to solve the constrained optimal control problem [123], [146]. Using the barrier function method we change constrained optimization into corresponding unconstrained one by adding an extra term called barrier function to the cost functional [147]. The proposed logarithmic barrier function is

$$\Psi = \mathbf{u}^T \hat{R}\mathbf{u}, \tag{4.24}$$

where

$$\hat{R} = -diag[log(l_1(t)), ..., log(l_N(t))] \otimes I_n. \tag{4.25}$$

The proposed barrier function (4.24) goes to infinity as an agent's energy level approaches zero. Hence, it prevents depleting the energy of the agents. It is straightforward to show that adding (4.24) to the cost functional in (4.23) results in a standard form of an SDRE problem where diagonal elements of the input weighting matrix are given by (4.22). Thus, the solution of the resulting SDRE problem with the weighting factor (4.22) satisfies the hard constraints of the optimal control problem (4.23). □

Now we provide a sufficient condition for the global stability.

Theorem 4.2. *Given Assumption 4.1, select the state weighting matrix as*

$$Q = \mathcal{H}(\boldsymbol{p}) I_m, \tag{4.26}$$

where $\mathcal{H}(\boldsymbol{p})$ is a positive scalar function. Then, for a set of agents described by the single-integrator model $\hat{\mathcal{W}}_s$, the proposed control law (4.19) results in the global asymptotic stability of the closed-loop system.

Proof. Substituting (4.19) in error dynamics (4.18), the closed-loop error dynamics is given by

$$\dot{\mathbf{e}}_s = A_{CS}(\mathbf{p})\mathbf{e}_s, \tag{4.27}$$

where

$$A_{CS}(\mathbf{p}) = -B_s(\mathbf{p})R^{-1}B_s(\mathbf{p})^T S(\mathbf{p}). \tag{4.28}$$

Rearranging equation (4.28) using (4.20) yields

$$A_{CS}(\mathbf{p}) = -S(\mathbf{p})^{-1}Q. \tag{4.29}$$

Since the inverse of a symmetric matrix is also symmetric, thus, selecting Q as in (4.26) ensures that the closed-loop SDC matrix $A_{CS}(\mathbf{p})$ is symmetric for all $\mathbf{e}_s$. According to Lemma 2.10, this implies global asymptotic stability of the closed-loop system. □

Theorem 4.2 provides a sufficient condition for global stability of the closed-loop system. The following corollary suggests a selection of the weighting matrix that prevents collision among the neighboring agents.

Corollary 4.2.1. *Select*

$$\mathcal{H}(\boldsymbol{p}) = \kappa + \mu(\boldsymbol{p}), \tag{4.30}$$

where $\kappa > 0$ is a constant and $\mu(\boldsymbol{p})$ is a positive barrier multiplier defined by

$$\mu(\boldsymbol{p}) = \sum_{(i,j)\in E} \left(\frac{d_{ij}^*}{d_{ij} - r_d}\right)^{\epsilon}, \tag{4.31}$$

for suitable $\epsilon \geq 1$, and r_d being a safe distance between pair of agents to prevent collision. Then, by using the weighting matrix (4.26), the control law (4.19), alongside global asymptotic stability, guarantees an inter-agent collision avoidance of the multi-agents system.

Proof. We write the collision avoidance problem in a form of a constrained optimal control problem with hard constraints and use the barrier function method to solve it as follows. Let us define the safety region of each agent as a ball with a radius $r_d/2$. Then, for preventing collision between neighboring agents it is required to have

$$d_{ij} > r_d, \quad (i,j) \in E. \tag{4.32}$$

The constraint (4.32) provides the sufficient condition for collision avoidance and can be added to the optimal control problem (4.18) as a hard constraint. The solution of

resulting constrained optimal control problem guarantees the collision avoidance. The resulted constrained optimal control problem is:

$$
\begin{aligned}
J = \min & \frac{1}{2}\int_{t_0}^{\infty} ({\mathbf{e}_s}^T \bar{Q}\mathbf{e}_s + \mathbf{u}^T R\mathbf{u})dt \\
& \text{s.t.} \\
& \dot{\mathbf{e}}_s = B_s(\mathbf{p})\mathbf{u} \\
& d_{ij} > r_d \qquad (i,j) \in E \\
& \bar{Q} = \kappa \times I_m > 0 \\
& R > 0.
\end{aligned}
\tag{4.33}
$$

In order to solve the constrained optimal control problem (4.33) we use the approach proposed by Friedland in [147]. The Friedland's approach is based on barrier function method to solve an SDRE problem with state constraints. Thus, the proposed inverse barrier function is

$$
\Phi(\mathbf{p}) = \mu(\mathbf{p})\mathbf{e}_s^T\mathbf{e}_s, \tag{4.34}
$$

where $\mu(\mathbf{p})$ is defined by (4.31). Adding the proposed inverse barrier function (4.34) to the cost functional of the optimal control problem (4.33) yields to the corresponding unconstrained problem. It is straightforward to show that the state weighting matrix of the resulted unconstrained problem can be written in form of (4.26), where $\mathcal{H}(\mathbf{p})$ is given by (4.30).

If the condition for collision avoidance (4.32) is violated, then the proposed barrier function (4.34) approaches infinity and based on [147] this prevents collision avoidance between neighboring agents. □

4.3.2 Double-Integrator Model

For an agent which is modeled by the double-integrator model $\hat{\mathcal{W}}_d$, the error dynamics is given by

$$
\begin{aligned}
\dot{e}_{ij} &= \frac{d}{dt}\sqrt{(p_i - p_j)^T(p_i - p_j)} \\
&= \frac{(p_{ij})^T(v_i - v_j)}{e_{ij} + d_{ij}^*}.
\end{aligned}
\tag{4.35}
$$

Let us define an aggregate error vector for the double-integrator model as

$$
\mathbf{e}_d = [\mathbf{e}^T, \mathbf{v}^T]^T, \tag{4.36}
$$

where $\mathbf{v}$ is the velocity vector. Using the normalized rigidity matrix, the error dynamics can be written as

$$\dot{\mathbf{e}} = \bar{\mathcal{R}}(\mathbf{p})\mathbf{v}. \tag{4.37}$$

A time derivative of (4.36) yields

$$\dot{\mathbf{e}}_d = A_d(\mathbf{p})\mathbf{e}_d + B_d\mathbf{u}, \tag{4.38}$$

with

$$A_d(\mathbf{p}) = \begin{bmatrix} \mathbf{0}_{m\times m} & \bar{\mathcal{R}}(\mathbf{p}) \\ \mathbf{0}_{(nN)\times m} & \mathbf{0}_{N\times N} \otimes I_n \end{bmatrix} \tag{4.39a}$$

$$B_d = \begin{bmatrix} \mathbf{0}_{m\times(nN)} \\ I_N \otimes I_n \end{bmatrix}. \tag{4.39b}$$

Similarly, for convenience, we use the notation of $A_d(\mathbf{p})$ while it depends on p_{ij}.

The corresponding optimal control problem is

$$\begin{aligned} J = \min & \frac{1}{2}\int_{t_0}^{\infty} (\mathbf{e}_d^T Q_d \mathbf{e}_d + \mathbf{u}^T R\mathbf{u})dt \\ & \text{s.t.} \\ & \dot{\mathbf{e}}_d = A_d(\mathbf{p})\mathbf{e}_d + B_d\mathbf{u}, \\ & Q = \text{diag}[Q_f, Q_v] \geq 0 \\ & R = \text{diag}[r_1, ..., r_N] \otimes I_n > 0, \end{aligned} \tag{4.40}$$

where $Q_f = [q_1, ..., q_m]$ and $Q_v = [\rho_1, ..., \rho_N] \otimes I_n$ are the corresponding weighting matrices. The next result proposes the control law that guarantees the local asymptotic stability of the distance-based formation for agents modeled as double-integrators.

Theorem 4.3. *Given Assumption 4.1 and a set of agents described by double-integrator model $\hat{\mathcal{W}}_d$, the control law*

$$\boldsymbol{u} = -R^{-1}B_d^T S(\boldsymbol{p})\boldsymbol{e}_d, \tag{4.41}$$

where $S(\boldsymbol{p})$ is the positive definite solution of the following state-dependent Riccati equation

$$Q + A_d(\boldsymbol{p})^T S(\boldsymbol{p}) + S(\boldsymbol{p})A_d(\boldsymbol{p}) - S(\boldsymbol{p})B_d R^{-1}B_d^T S(\boldsymbol{p}) = 0, \tag{4.42}$$

achieves local asymptotic stability of the closed-loop system.

Proof. Under Assumption 4.1, the normalized rigidity matrix $\bar{\mathcal{R}}(\mathbf{p})$ is a full row rank. Thus, double-integrator error dynamics (4.38) is controllable everywhere. This is straightforward to show by forming the controllability matrix. Given the positive definiteness

of R, all feasibility conditions of Lemma 2.9 are met. Thus, control signal (4.41) is a stabilizing SDRE control law according to Lemma 2.9. □

Remark 4.5. For the agent i, the control law is given by

$$u_i = (\mathbf{z}_i \otimes \mathbf{1}_n)^T \mathbf{u}, \tag{4.43}$$

where $\mathbf{z}_i$ is a N-vector with 1 in its i-th element and all other elements equal to zero.

Corollary 4.3.1. *By selecting the weighting factors as*

$$\rho_i = \bar{\rho}_i - log(l_i(t)), \tag{4.44}$$

where $\bar{\rho}_i > 0$ is a constant, the control law (4.41) prevents depleting the energy of the agents.

The proof sketch is same as the proof of Corollary 4.2.1. Theorem 4.3 provides a sufficient condition for the local asymptotic stability of the SDRE closed-loop system. The next result considers the *global* asymptotic stability of the closed-loop system.

Theorem 4.4. *Let $S(\boldsymbol{p})$ be the solution of*

$$P + A_d - B_d R^{-1} B_d^T S(\boldsymbol{p}) = 0, \tag{4.45}$$

where P is a desired, symmetric, and positive definite matrix with all eigenvalues $\lambda_i > 2\sqrt{3}$. Then, for a set of agents described by the double-integrator model $\hat{\mathcal{W}}_d$ and under Assumption 4.1, the control law (4.41) achieves the global asymptotic stability of the closed-loop system.

Proof. The closed-loop SDC matrix of the error dynamics is given by

$$A_{CD}(\mathbf{p}) = A_d - B_d(\mathbf{p}) R^{-1} B_d(\mathbf{p})^T S(\mathbf{p}). \tag{4.46}$$

Rearranging the equation (4.42) yields

$$A_{CD}(\mathbf{p}) = -S^{-1}(\mathbf{p}) Q - S^{-1}(\mathbf{p}) A_d(\mathbf{p})^T S(\mathbf{p}). \tag{4.47}$$

Since Q is a state-dependent design parameter, it can be selected as

$$Q = S(\mathbf{p}) P - A_d(\mathbf{p})^T S(\mathbf{p}), \tag{4.48}$$

where P is a desired, symmetric, and positive definite matrix with all eigenvalues $\lambda_i > 2\sqrt{3}$. The proof has two steps. First, we show that (4.48) has a unique solution. Second,

we show that the proposed P guarantees positive definiteness of Q, hence, existence of the SDRE solution.

Equation (4.48) is a well-known Sylvester equation. According to Sylvester-Rosenblum theorem [148], the equation (4.48) has a unique solution as long as $\Theta(P) \cap \Theta(A_d) = \emptyset$ [149]. Applying Cauchy–Schwarz inequality on $p_{ij}^T = [x_{ij}, y_{ij}, z_{ij}]$ yields

$$\frac{|x_{ij}|}{d_{ij}} + \frac{|y_{ij}|}{d_{ij}} + \frac{|z_{ij}|}{d_{ij}} \leq \sqrt{3}. \tag{4.49}$$

Due to the fact that all diagonal elements of A_d are zero and based on the well-known Gershgorin circle theorem [110], it follows that $\Theta(A_d) \leq 2\sqrt{3}$. The spectral mapping theorem[150], states that for (4.48) we have

$$\Theta(Q) = \Theta(P) - \Theta(A_d). \tag{4.50}$$

Selecting $\Theta(P) > 2\sqrt{3}$ ensures positive definiteness of Q and uniqueness of the solution (4.48). Substituting (4.48) in (4.42), Riccati equation yields to

$$P + A_d - B_d R^{-1} B_d^T S(\mathbf{p}) = 0. \tag{4.51}$$

Substituting (4.48) in (4.47), the closed-loop SDC matrix is given by

$$A_{CD}(\mathbf{p}) = -P, \tag{4.52}$$

which proves that the closed-loop system is globally asymptotically stable. □

Theorem 4.4 provides conditions under which SDRE closed-loop system becomes globally asymptotically stable. In fact, with matrix P we introduced an auxiliary design parameter for the formation control system. Note that at the same time we proved that the given control law is sub-optimal as a solution of the SDRE problem.

The following corollary describes how the proposed formation control can ensure a collision avoidance for the double-integrator model of agents.

Corollary 4.4.1. *Select*

$$P(\boldsymbol{p}) = \mathcal{K}(\boldsymbol{p})\bar{P}, \tag{4.53a}$$
$$\mathcal{K}(\boldsymbol{p}) = \sigma + \mu(\boldsymbol{p}), \tag{4.53b}$$

where $\sigma \geq 1$ is a positive constant and $\mu(\boldsymbol{p})$ is defined in (4.31) and $\bar{P}$ is a desired, symmetric positive definite matrix with all eigenvalues $\bar{\lambda}_i > 2\sqrt{3}$. Then Theorem 4.4 guarantees collision avoidance among the neighboring agents and the global asymptotic stability of the closed-loop system.

Proof. Since $\mathcal{K}(\mathbf{p})$ is a scalar function with $\mathcal{K}(\mathbf{p}) \geq 1$, all eigenvalues of $P(\mathbf{p})$ are greater or equal to the eigenvalues of $\bar{P}$ (all $\bar{\lambda}_i > 2\sqrt{3}$). This validates results of Theorem 4.4. The rest of the proof is as same as Corollary 4.3.1. □

Corollary 4.4.1 suggests a weighting matrix that ensures collision avoidance among neighboring agents for a set of agents modeled by double-integrator dynamics.

Remark 4.6. *(Global Stability of Desired Formation Realization)* The result of Theorem 4.2 (respectively Theorem 4.4) states that the origin $\mathbf{e}_s = 0$ (respectively $\mathbf{e}_d = 0$) is globally asymptotically stable equilibrium point of the closed-loop system when agents are modeled as single-integrators (respectively double-integrators). The set $\mathbf{e}_s = 0$ (respectively $\mathbf{e}_d = 0$) consists of all representations that are equivalent to the desired formation. Since the desired formation is MIR, this set has more than one element for $N \geq 4$. In order to resolve this issue, we can use the Friedland method [147] that is also used in collision avoidance. This adds a barrier function that drives the cost functional to infinity whenever agents approach an equivalent, but not a congruent realization. Such method prevents agents to converge to undesired realizations. Thus, the formation realization is *almost globally asymptotically stable* which means that the desired formation will be reached unless the initial positions of the agents constitute an equivalent but not a congruent realization [151].

4.4 Formation Tracking Control

Tracking is one of desired objectives in multi-agent systems. The whole formation can be translated or rotated following some given reference command while preserving the formation shape. Here, we consider a distance-based formation tracking problem where the leader agent is assigned a trajectory to follow.

4.4.1 Single-Integrator Model

Adding leader tracking to the distance-based formation control problem, we can combine the tracking error e_t and the formation error $\mathbf{e}_s$ to form an augmented error vector as $\hat{\mathbf{e}}_s = [e_t, \mathbf{e}_s^T]^T$. Thus, we have

$$\dot{\hat{\mathbf{e}}}_s = \hat{B}_s(\mathbf{p})\mathbf{u}, \tag{4.54}$$

where

$$\hat{B}_s(\mathbf{p}) = \begin{bmatrix} \mathbf{g} \\ \bar{\mathcal{R}}(\mathbf{p}) \end{bmatrix}, \tag{4.55}$$

and

$$\mathbf{g} = [\frac{(p_1 - p^*)^T}{\|p_1 - p^*\|}, [\mathbf{0}]]. \tag{4.56}$$

For an MIR graph $rank(\hat{B}_s(\mathbf{p})) = rank(\bar{\mathcal{R}}(\mathbf{p})) = m$. Therefore, it is not a full rank due to adding $\mathbf{g}$. Using the SDC factorization we can rewrite (4.54) as

$$\dot{\hat{\mathbf{e}}}_s = \hat{A}_s(\mathbf{p})\hat{\mathbf{e}}_s + \hat{B}_s(\mathbf{p})\mathbf{u}, \tag{4.57}$$

where $\hat{A}_s(\mathbf{p})$ has to be chosen such that $\hat{\mathbf{e}}_s$ lies in its null-space. Hence, the distance-based formation tracking optimal control problem becomes a SDRE control problem:

$$\begin{aligned} J = \min & \frac{1}{2}\int_{t_0}^{\infty} (\hat{\mathbf{e}}_s^T Q \hat{\mathbf{e}}_s + \mathbf{u}^T R \mathbf{u}) dt \\ & \text{s.t.} \\ & \dot{\hat{\mathbf{e}}}_s = \hat{A}_s(\mathbf{p})\hat{\mathbf{e}}_s + \hat{B}_s(\mathbf{p})\mathbf{u} \\ & Q > 0 \\ & R > 0. \end{aligned} \tag{4.58}$$

The following theorem introduces a hybrid control law that guarantees local stability of the formation tracking problem.

Theorem 4.5. *Consider a set of agents described by the single-integrator model $\hat{\mathcal{W}}_s$ that operate under Assumption 4.1. The HSDRE control law*

$$HSDRE: \begin{cases} \boldsymbol{u} = -R^{-1}\hat{B}_s(\boldsymbol{p})^T S(\boldsymbol{p})\hat{\boldsymbol{e}}_s & whenever \quad \|\hat{\boldsymbol{e}}_s\| > \varepsilon \\ \boldsymbol{u} = 0, & whenever \quad \|\hat{\boldsymbol{e}}_s\| \leq \varepsilon \end{cases} \tag{4.59}$$

where $\varepsilon > 0$ is sufficiently small and $S(\boldsymbol{p})$ is the positive definite solution of the following state-dependent Riccati equation

$$Q + \hat{A}_s(\boldsymbol{p})^T S(\boldsymbol{p}) + S(\boldsymbol{p})\hat{A}_s(\boldsymbol{p}) - S(\boldsymbol{p})\hat{B}_s(\boldsymbol{p})R^{-1}\hat{B}_s(\boldsymbol{p})^T S(\boldsymbol{p}) = 0, \tag{4.60}$$

achieves the local (practical) stability of the closed-loop system.

Proof. The system (4.57) is controllable and observable everywhere except at the origin. Thus, considering Lemma 2.13, the HSDRE control law given by (4.59) results in the local stability of the closed-loop system. □

4.4.2 Double-Integrator Model

Considering the double-integrator dynamics, we define relative velocity of the agent i as

$$\hat{v}_i = v_i - v^*, \tag{4.61}$$

where $v^* = \dot{p}^*$. The error dynamics (4.35) can be written as

$$\dot{e}_{ij} = \frac{(p_{ij})^T(\hat{v}_i - \hat{v}_j)}{e_{ij} + d_{ij}^*}. \tag{4.62}$$

Let us define an aggregate error vector for the double-integrator model as

$$\mathbf{e}_d = [\mathbf{e}^T, \hat{\mathbf{v}}^T]^T, \tag{4.63}$$

where $\hat{\mathbf{v}} = [\hat{v}_1, ..., \hat{v}_N]$ is the relative velocity vector. We combine leader's tracking error e_t and formation error $\mathbf{e}_d$ to obtain an augmented error vector as $\hat{\mathbf{e}}_d = [e_t, \mathbf{e}_d^T]^T$. The error dynamics can be written as

$$\dot{\hat{\mathbf{e}}}_d = \bar{A}_d(\mathbf{p})\hat{\mathbf{e}}_d + \hat{B}_d\mathbf{u}, \tag{4.64}$$

where

$$\bar{A}_d(\mathbf{p}) = \begin{bmatrix} \mathbf{0}_{(m+1)\times(m+1)} & \hat{B}_s(\mathbf{p}) \\ \mathbf{0}_{nN\times(m+1)} & \mathbf{0}_{N\times N} \otimes I_n \end{bmatrix} \tag{4.65a}$$

$$\hat{B}_d = \begin{bmatrix} \mathbf{0}_{(m+1)\times(nN)} \\ I_N \otimes I_n \end{bmatrix}, \tag{4.65b}$$

and $\hat{B}_s(\mathbf{p})$ is defined in (4.55). It should be noted that, as a result of augmenting e_t in the error vector, $\hat{B}_s(\mathbf{p})$ loses its full rank and the system (4.64) is not controllable anymore. Noting that $\hat{\mathbf{e}}_d = [\hat{\mathbf{e}}_s^T, \hat{\mathbf{v}}^T]^T$ and using SDC factorization we can rewrite (4.64) as

$$\dot{\hat{\mathbf{e}}}_d = \hat{A}_d(\mathbf{p})\hat{\mathbf{e}}_d + \hat{B}_d\mathbf{u}, \tag{4.66}$$

where

$$\hat{A}_d(\mathbf{p}) = \begin{bmatrix} A_{11} & \hat{B}_s(\mathbf{p}) \\ A_{21} & A_{22} \end{bmatrix}, \tag{4.67}$$

while $\hat{\mathbf{e}}_s$ should lie in the null-space of A_{11} and $A_{21}\hat{\mathbf{e}}_s + A_{22}\hat{\mathbf{v}} = 0$. The optimal, distance-based, formation tracking control problem becomes an SDRE-form control problem

$$\begin{aligned} J = \min & \frac{1}{2}\int_{t_0}^{\infty} (\hat{\mathbf{e}}_d^T Q \hat{\mathbf{e}}_d + \mathbf{u}^T R \mathbf{u}) dt \\ & \text{s.t.} \\ & \dot{\hat{\mathbf{e}}}_d = \hat{A}_d(\mathbf{p})\hat{\mathbf{e}}_d + \hat{B}_d\mathbf{u} \\ & Q > 0 \\ & R > 0. \end{aligned} \tag{4.68}$$

The next result proposes a hybrid control law that guarantees the local stability for distance-based formation tracking of agents modeled as double-integrators.

Theorem 4.6. *Given Assumption 4.1 and a set of agents described by double-integrator model $\hat{\mathcal{W}}_d$, for a sufficiently small $\varepsilon > 0$, the HSDRE control law*

$$HSDRE: \begin{cases} \boldsymbol{u} = -R^{-1}\hat{B}_d^T S(\boldsymbol{p})\hat{\boldsymbol{e}}_d & \text{whenever} \quad \|\hat{\boldsymbol{e}}_d\| > \varepsilon \\ \boldsymbol{u} = 0, & \text{whenever} \quad \|\hat{\boldsymbol{e}}_d\| \leq \varepsilon \end{cases} \tag{4.69}$$

where $S(\boldsymbol{p})$ is the positive definite solution of the following state-dependent Riccati equation:

$$Q + \hat{A}_d(\boldsymbol{p})^T S(\boldsymbol{p}) + S(\boldsymbol{p})\hat{A}_d(\boldsymbol{p}) - S(\boldsymbol{p})\hat{B}_d R^{-1}\hat{B}_d^T S(\boldsymbol{p}) = 0, \tag{4.70}$$

achieves local (practical) stability of the closed-loop, distance-based, formation tracking problem.

Proof. System (4.66) is controllable and observable everywhere except at the origin; thus, it meets the feasibility conditions of Lemma 2.13. HSDRE control law (4.69) is the stabilizing control law given by Lemma 2.13. □

4.5 Simulation Results

In this section we present simulation results based on the proposed control methods for different sets of agents. We first simulated the distance-based formation producing control with energy constraints in both 2-D and 3-D spaces, and then we presented results of the proposed method for the formation tracking problem.

Figure 4.2 shows results of the proposed SDRE-based control law (4.19) for a set of $N = 4$ agents that are modeled by the single-integrator dynamics in 2-D. We first simulated the scenario where all agents initially have fully charged batteries: $l_{0i} = 1$, for $i = 1, 2, 3, 4$ (top). Figure 4.2 (bottom) shows the case when one agent (agent #4) has less initial energy than other agents ($l_{04} = 0.2$). The weighting matrices Q and R are determined by (4.26) and (4.22), respectively. We chose the control parameters as $\bar{r}_i = 1$ for all i, $\kappa = 1$, $\epsilon = 2$, $r_d = 2$, and all desired distances $d_{ij}^* = 10$ for both simulations. The simulation shows that agents with full initial energy form the desired formation while compensating the weak agent (one with the lower initial energy). Figure 4.3 (top and bottom) shows the convergence of edge errors corresponding to Figure 4.2 (top and bottom), respectively.

Figure 4.4 (top and bottom) shows the L_2 norm of the control signals for each agent corresponding to the formation control in Figure 4.2 (top and bottom), respectively. Considering (2.25), one can see that the agent #4 has a notable reduction in the energy usage in the Figure 4.4 (bottom) compared to Figure 4.4 (top).

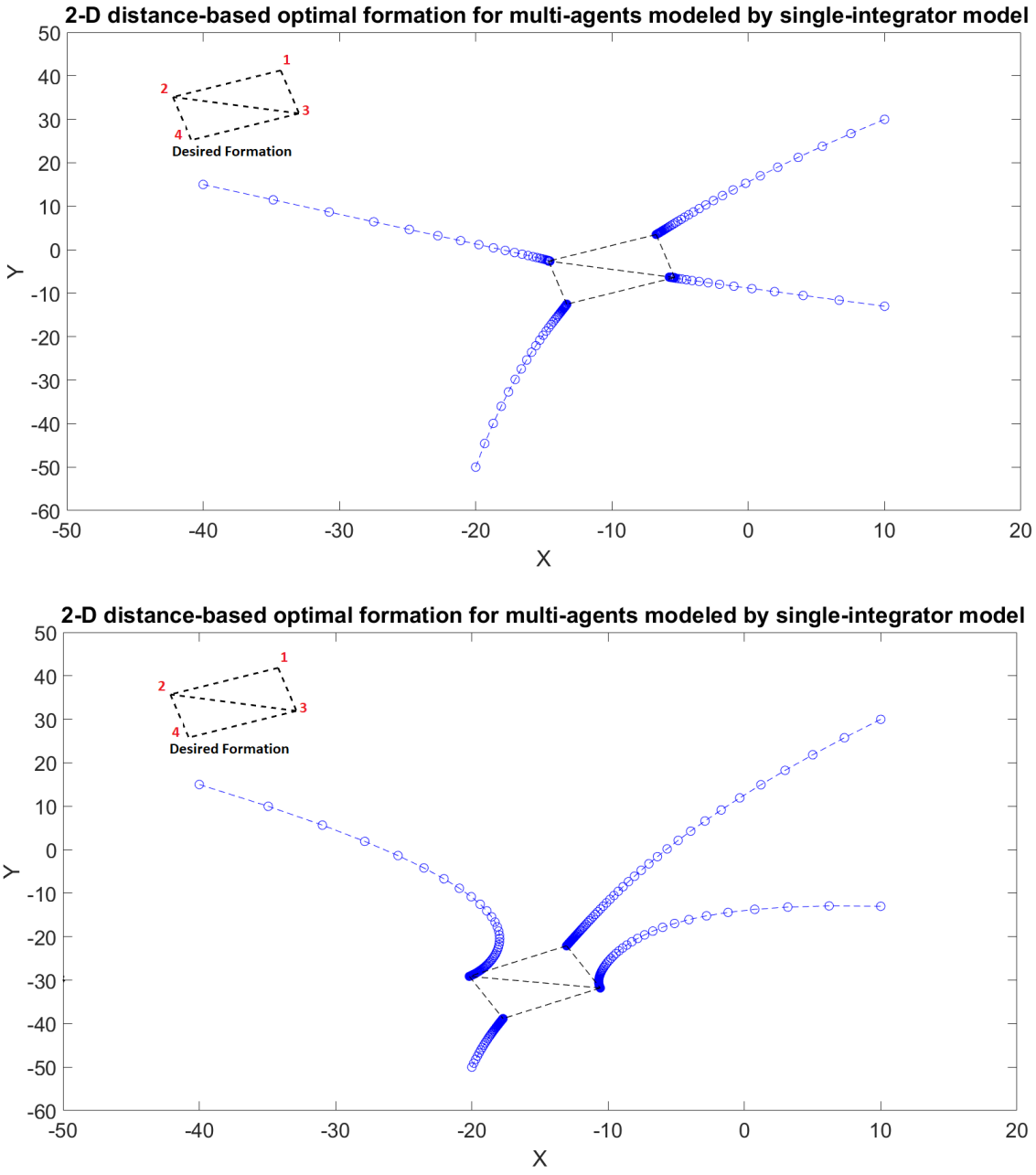

Figure 4.2: Distance-based optimal formation control for $N = 4$ agents modeled by the single-integrator dynamics; all agents have full initial energy levels (top). The agent #4 has a lower initial energy level, $l_{04} = 0.2$ (bottom).

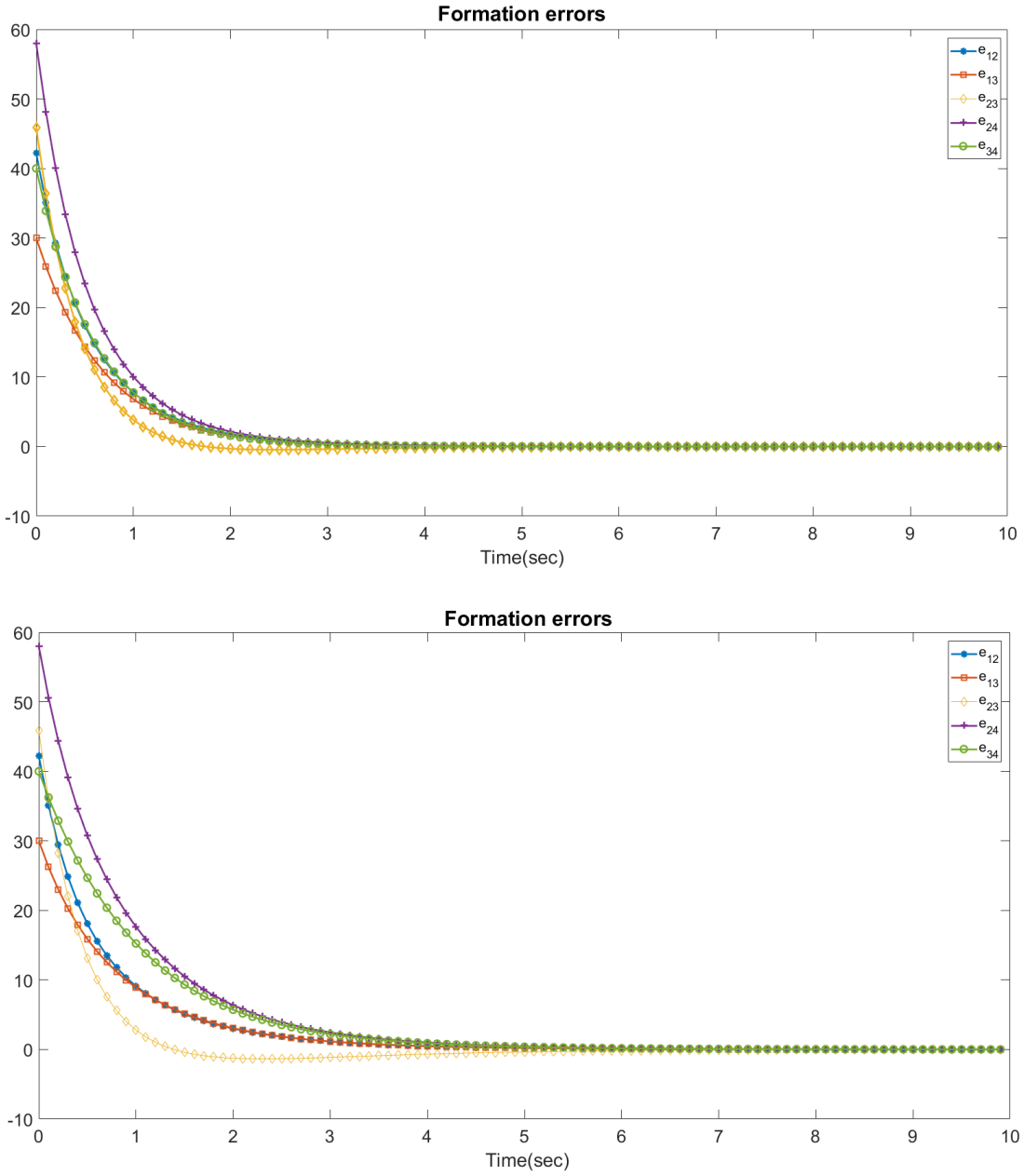

Figure 4.3: Convergence of the edge errors to zero, corresponding to the simulations in Figure 4.2.

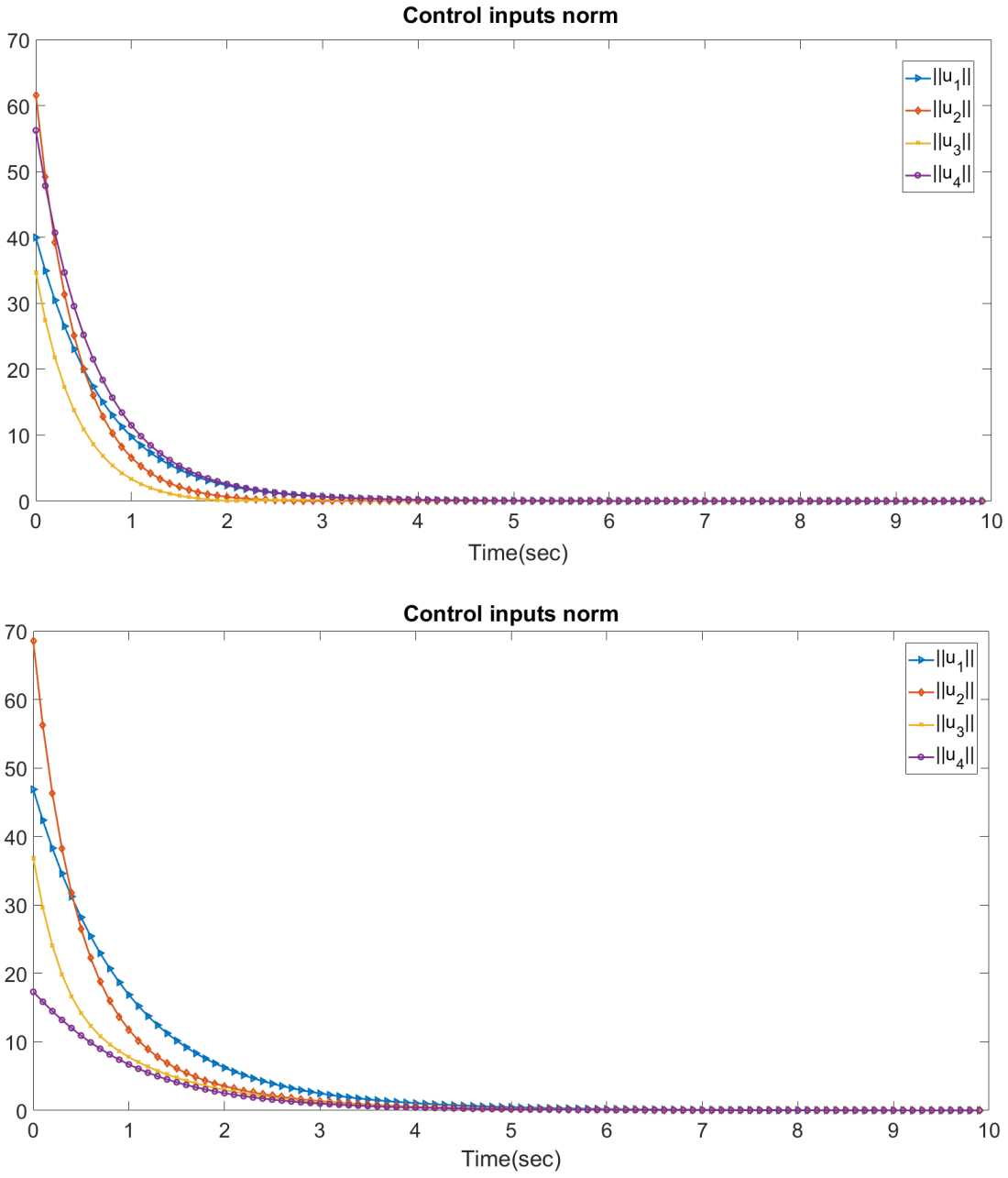

Figure 4.4: L_2 norm of the control inputs of the agents corresponding to Figure 4.2.

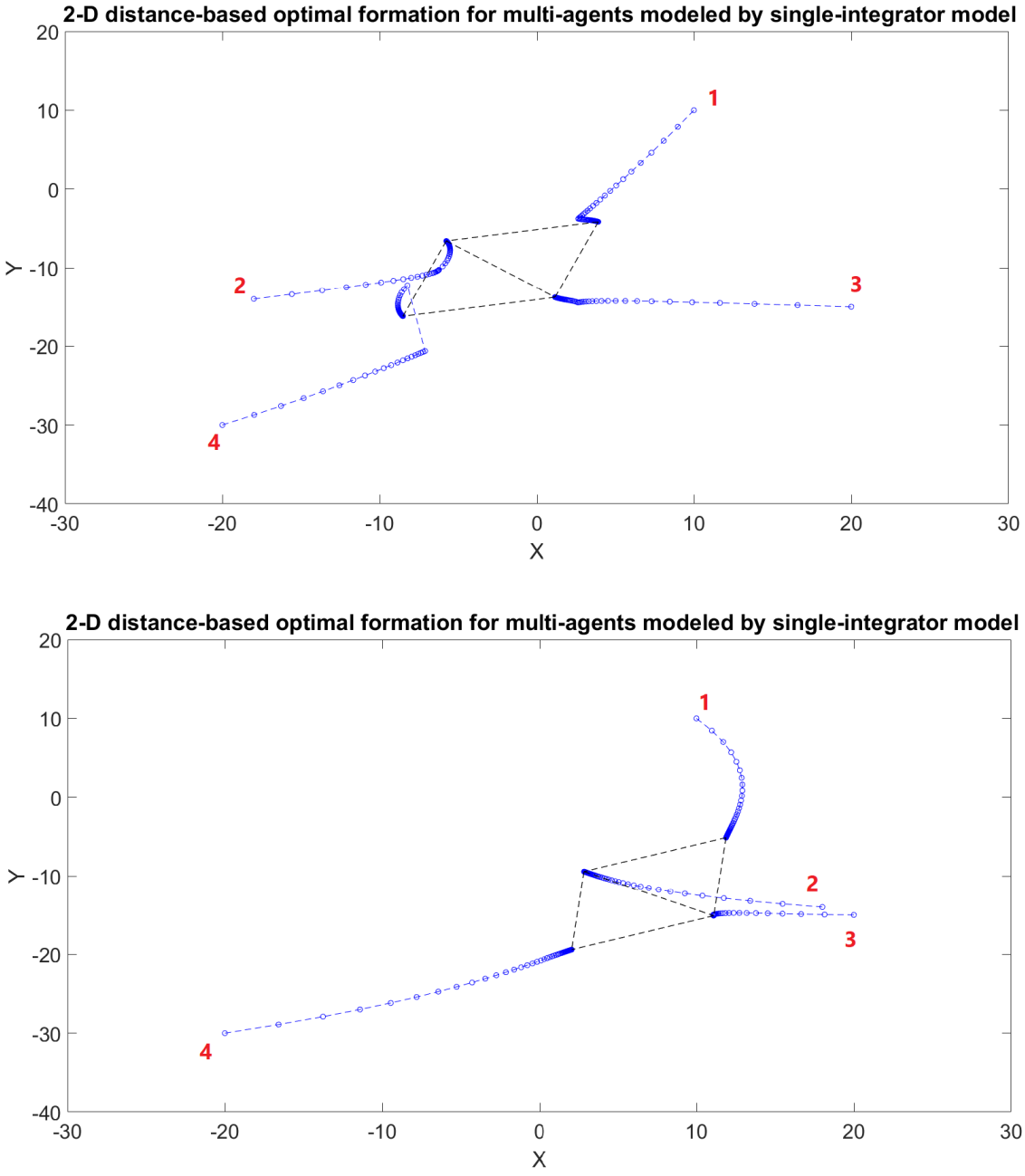

Figure 4.5: Collision avoidance in proposed formation control scheme.

Figure 4.5 shows the results of the proposed control law (4.19) for different initial positions as well as the collision avoidance capability. The simulation results show that for different initial positions the agents form the desired formation successfully. For collision avoidance, we developed two different scenarios. First, we assume that during the formation an external disturbance tries to push one agent (agent #4) very close to its neighboring agent (agent #2). Simulation shows that the control law successfully prevents collision between neighbors (top). Another scenario, depicted in the bottom, is when initial conditions of two neighboring agents are very close to each other. Again, the control law results in a successful formation without collision.

Figure 4.6 shows the optimal formation control of agents with double-integrator model in 3-D using control law (4.41). The formation producing is shown in top and the errors convergence in the bottom. All agents are assumed to have full initial energy levels ($l_{0i} = 1$, for $i = 1, 2, 3, 4, 5$). The controller and model parameters are selected as: $\bar{\rho}_i = 1$, $\bar{P} = 3I$, $\sigma = 1$, $r_d = 2$, $\epsilon = 2$, $\alpha_i = 0.0001$, and $r_i = 1$. Simulation results show the effectiveness of the method in 3-D space as well.

Figure 4.7 shows the results of the optimal formation tracking control (4.59) for a set of $N = 4$ agents with the single-integrator model in 2-D where all agents have full initial energy (top). The bottom shows the effect of the weak agent (when energy tends to zero) in formation tracking. The controller and model parameters are selected as $\varepsilon = 0.000001$, $\alpha_i = 0.0002$, and all other parameters remain the same. The SDC matrix $\hat{A}_s(\mathbf{p})$ is given in Appendix A. The simulation result shows that the controller manages to preserve the rest of the formation despite the low-energy follower. In addition, Figure 4.8 illustrates the successful formation tracking of a set of double-integrator agents in 3-D space with the same simulation parameters. We chose A_{11} and A_{22} zero matrices while A_{21} is given in the Appendix A.

In Figure 4.9 we present a comparison of the energy consumption between the proposed SDRE-based controller with different weighting matrix versus the widely used gradient-based controller [152] (the detailed information about the used gradient-based controller is given in Appendix B). Note that based on equation (2.24) the energy is proportional to the integral of absolute value of velocity in both cases. Therefore, we represent the integration of the absolute value of velocity as a measure of energy usage. In comparison with the gradient-based controller, the proposed method shows a notable reduction in energy consumption. Table 4.5 presents total energy usage of the both SDRE and gradient-based controllers for different initial positions of agents. The simulation results show the sensitivity of gradient-based controller to initial positions of the agents while the proposed SDRE controller shows the global asymptotic stability.

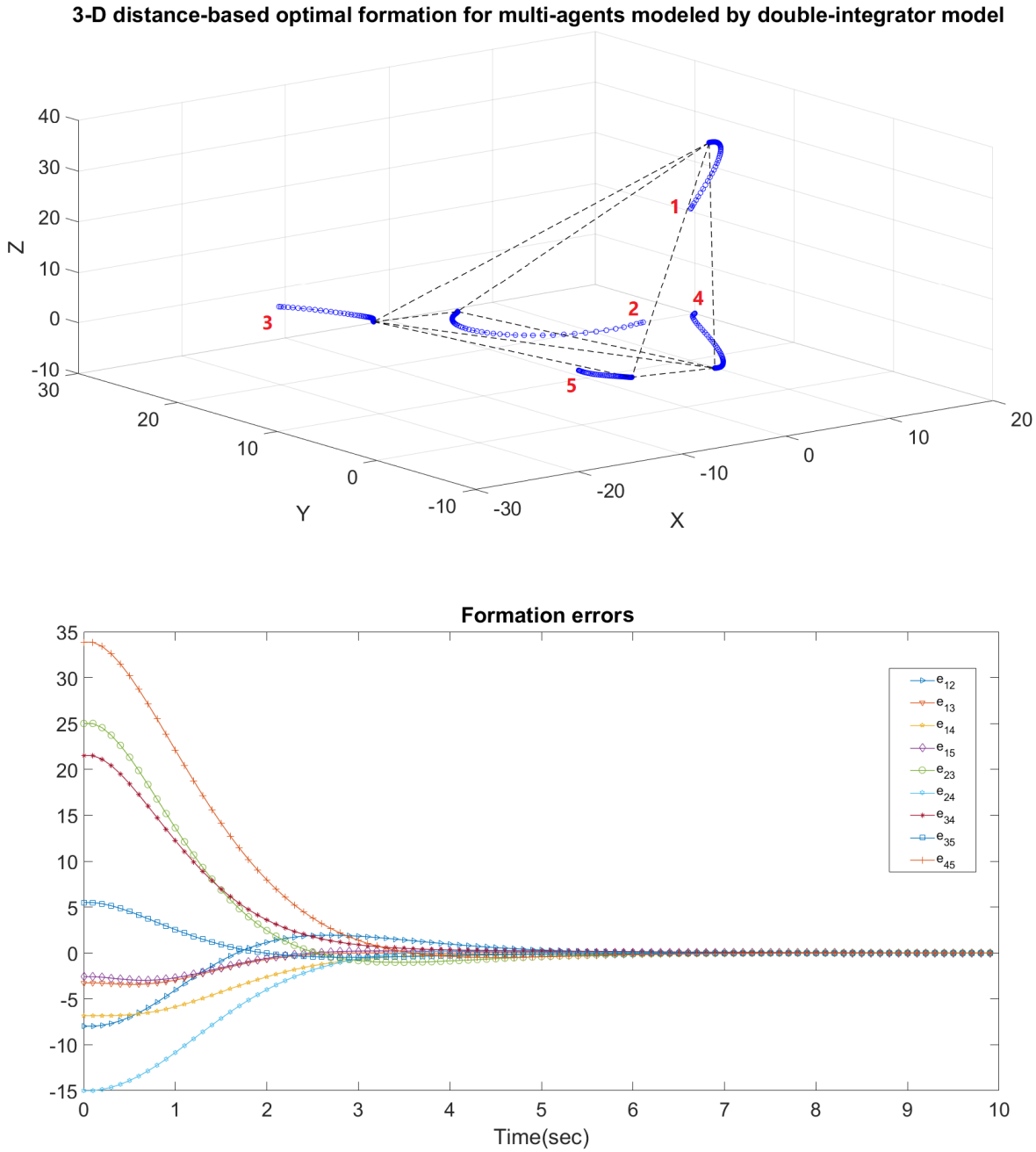

Figure 4.6: Distance-based optimal formation control for $N = 5$ agents modeled by the double-integrator dynamics (top). The corresponding edge errors convergence to zero (bottom).

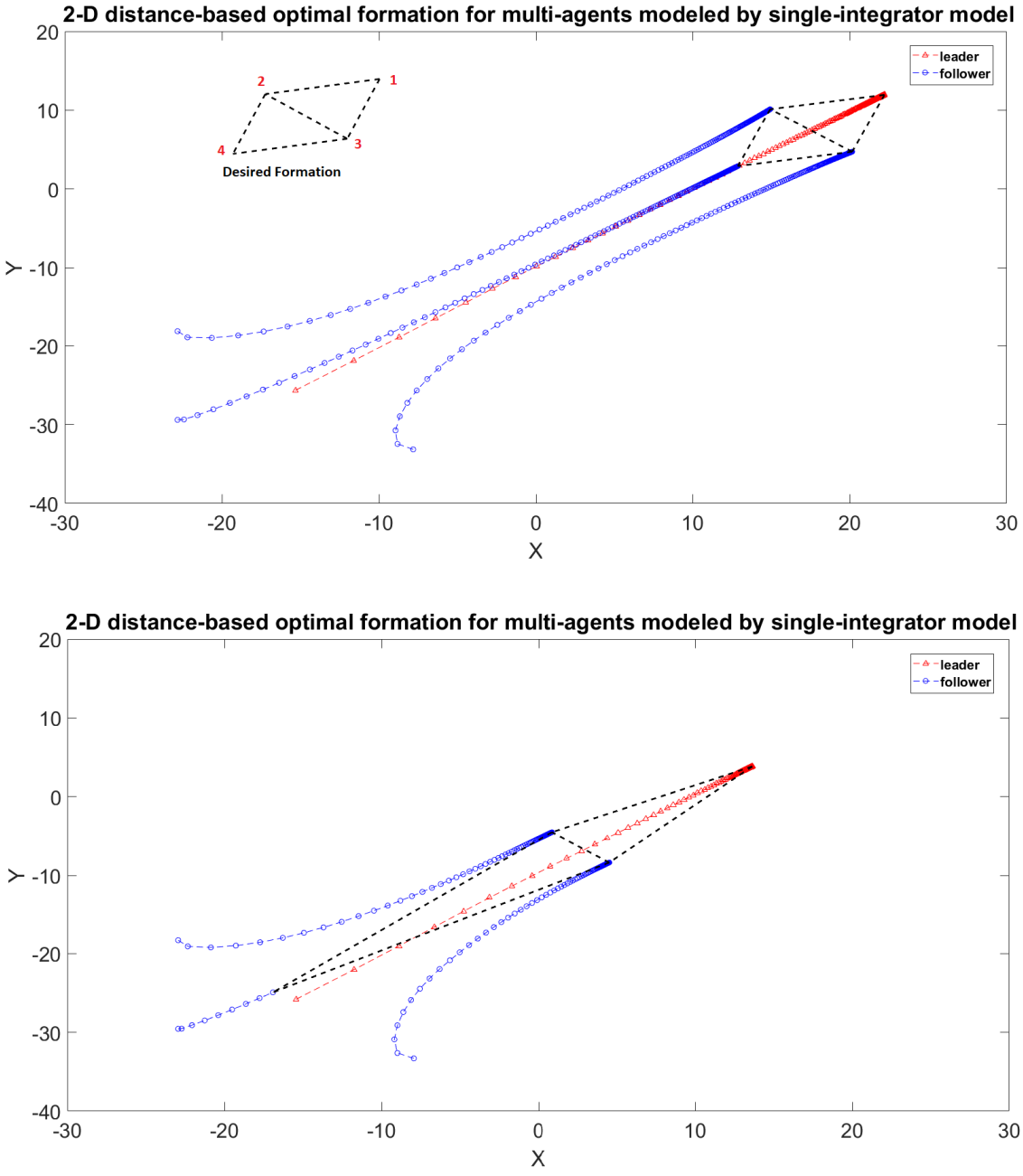

Figure 4.7: Distance-based optimal formation tracking control for $N = 4$ agents modeled by the single-integrator model; all agents have full initial energy levels (top). The follower number #4 at the bottom has a lower initial energy level, $l_{04} = 0.1$ (bottom).

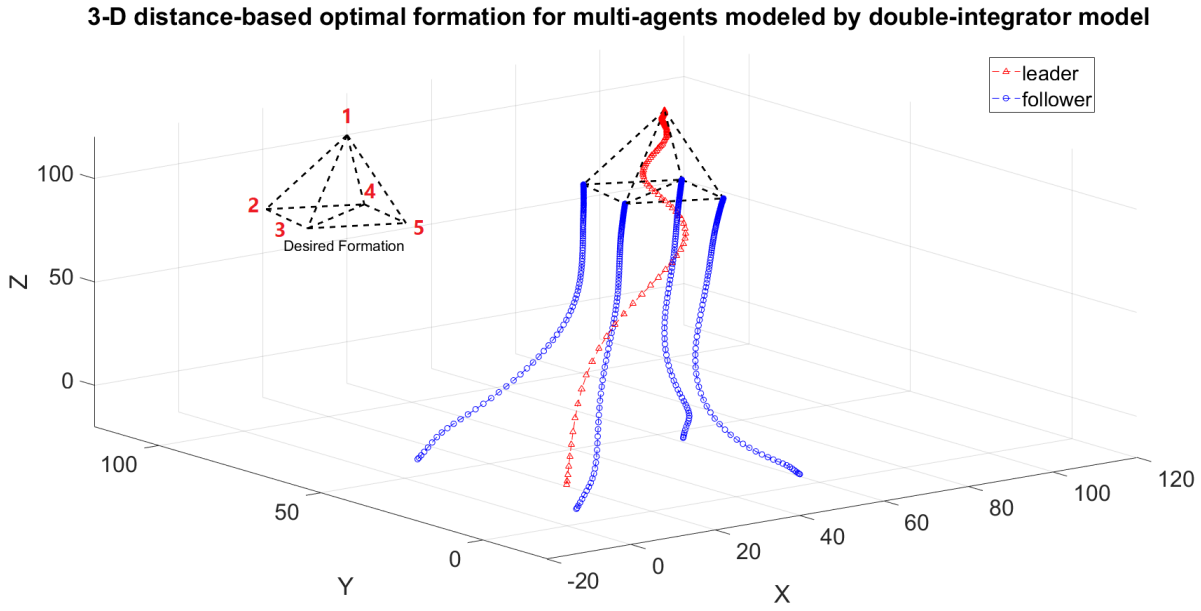

Figure 4.8: 3-Dimensional distance-based optimal formation tracking control for $N = 5$ agent modeled by double-integrator dynamics.

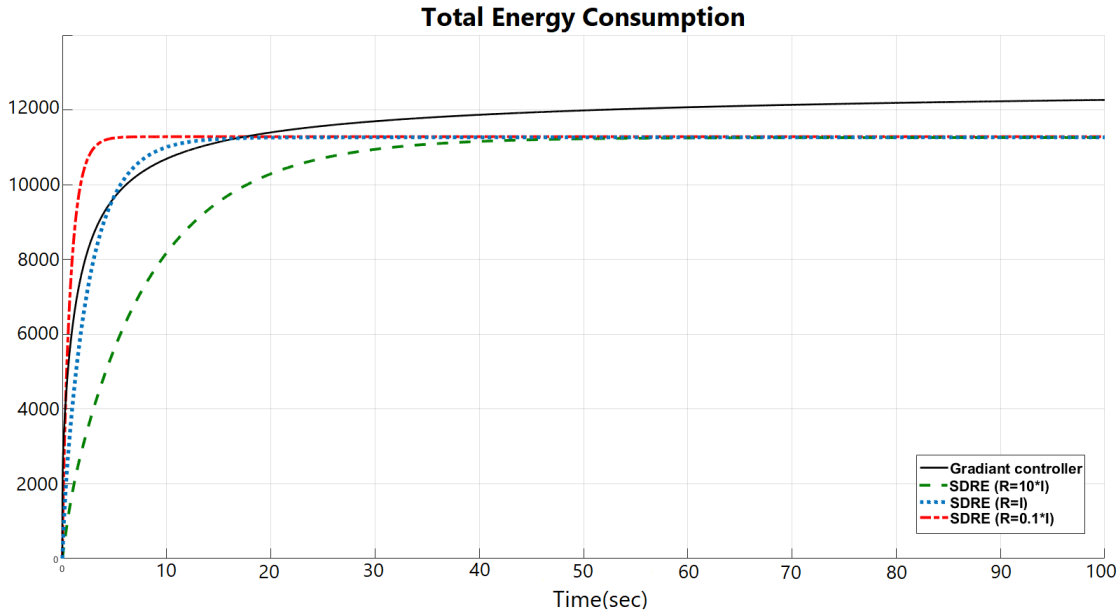

Figure 4.9: Comparison of the total energy consumption for the formation governed by various controllers. The formation consists of $N = 4$ agents modeled by the single-integrator model.

Table 4.1: Total energy usage for distance-based formations

Initial positions	Gradient-based controller	SDRE controller
$p_1 = (-3, 4), p_2 = (5, 7), p_3 = (-4, -6), p_4 = (6, -5)$	17189	14401
$p_1 = (-10, 14), p_2 = (5, 7), p_3 = (-4, -6), p_4 = (6, -5)$	41886	19338
$p_1 = (-10, 14), p_2 = (5, 7), p_3 = (-14, -16), p_4 = (6, -5)$	Unstable	42381
$p_1 = (-10, 14), p_2 = (5, 7), p_3 = (-14, -16), p_4 = (16, -15)$	Unstable	59347
$p_1 = (-10, 14), p_2 = (25, 30), p_3 = (-14, -16), p_4 = (16, -15)$	Unstable	103203

4.6 Conclusions

In this chapter, the undirected distance-based optimal formation control problem is considered. Based on the *normalized rigidity matrix*, we formulated the distance-based formation control problem. We developed an SDRE-based sub-optimal control scheme that asymptotically minimizes energy consumption and meets tracking and formation performances. The proposed control law guarantees local asymptotic stability of the system. Furthermore, we developed conditions for the global asymptotic stability of the closed-loop system and extended the results to ensure collision avoidance among neighboring agents. The proposed control method also allows users to adjust the trade-off between the formation control performance and the energy usage. The simulation results proved the effectiveness of the proposed solution while revealing an interesting behavior of the group (swarm) when some agents become low on energy while maintaining the desired formation. The simulation examples offer more insight into optimality in formation control and how distance-based formation adjusts due to weakness or a fault in one of the swarm members. The SDRE-based method shows a significant reduction in energy consumption compared to the gradient-based controller.

Chapter 5

Directed Distance-Based Formation Control

5.1 Introduction

In this chapter, the problem of distance-based formation control over directed graphs is studied. We consider the distance-based formation modeled as a directed graph, denoted by $\mathcal{G} = (\mathcal{V}, \mathcal{E})$, where each edge is assigned to only one of its adjacent agents to preserve the desired distance. We proposed a distributed control solution based on the state-dependent Riccati equation (SDRE) method that guarantees the global asymptotic stability of the formation for a set of agents models as single-integrators. Furthermore, the problem of flip ambiguity of distance-based formations is studied both in 2-D and 3-D spaces by using the combination of signed area and signed volume constraints. In this chapter, we use the directed graph notations introduced in Chapter 2.

5.2 Cost Functional

The relative position of neighboring agents is

$$p_{ij} = p_i - p_j, \quad (i,j) \in \mathcal{E}. \tag{5.1}$$

Thus, the distance between the pair of adjacent agents is given by

$$d_{ij} = \|p_{ij}\|. \tag{5.2}$$

The formation error vector of the agent i is given by

$$\mathbf{e}_i = [..., e_{ij}, ...]^T, \quad j \in \mathcal{N}_i, \tag{5.3}$$

where

$$e_{ij} = d_{ij} - d^*_{ij}, \tag{5.4}$$

and d^*_{ij} is the desired distance between agent i and agent j. Note that the formation error vector of the agent i depends only on the relative positions of agents' neighbors.

The proposed local cost functional of the agent i is

$$J_i = J_i^{fm} + J_i^{en}, \tag{5.5}$$

where J_i^{fm} and J_i^{en} are formation and energy cost, respectively, that are given by

$$J_i^{fm} = \frac{1}{2} \sum_{j \in \mathcal{N}_i} \int_0^\infty (\|p_i - p_j\| - d^*_{ij})^2 q_{ij} dt, \tag{5.6}$$

$$J_i^{en} = \frac{1}{2} \int_0^\infty \|\alpha_i v_i\|^2 \rho_i dt, \tag{5.7}$$

and q_{ij}, ρ_i are associated weighting factors. Note that $v_i = u_i$ for single-integrator model.

5.3 2-D Space

Distance-based formation over directed, triangulated Laman graphs is considered in this section. For the rest of the section, we assume that the following assumption is valid.

Assumption 5.1: The desired formation is in the form of directed triangulated Laman graph.

5.3.1 Single-Integrator Model

For an agent which is modeled by the single-integrator model, the error dynamics is given by

$$\begin{aligned} \dot{e}_{ij} &= \frac{d}{dt} \sqrt{(p_i - p_j)^T (p_i - p_j)} \\ &= \frac{(p_{ij})^T (u_i - u_j)}{e_{ij} + d^*_{ij}}. \end{aligned} \tag{5.8}$$

The first agent, the leader, is stationary since it is not responsible for any edge. Agent #2 (first-follower) is responsible for the edge e_{21}. The dynamics of error associated with

agent #2 is

$$\begin{aligned}\dot{\mathbf{e}}_2^s =& B_2^s u_2^s \\ =& \frac{p_{21}^T}{e_{21}+d_{21}^*} u_2^s,\end{aligned} \tag{5.9}$$

where $\mathbf{e}_2^s = e_{21}$. Note that hereafter in this chapter, we use the superscripts s and d to distinguish single- and double-integrator cases. Thus, the associated local optimal control problem with agent #2 is

$$\begin{aligned} J_2^s = \min & \frac{1}{2}\int_0^\infty \{\mathbf{e}_2^{sT} Q_2^s \mathbf{e}_2^s + u_2^{sT} R_2^s u_2^s\} dt \\ & \text{s.t.} \\ & \dot{\mathbf{e}}_2^s = B_2^s u_2^s \\ & Q_2^s = [q_{21}^s] > 0 \\ & R_2^s > 0. \end{aligned} \tag{5.10}$$

The following result provides the suboptimal SDRE control law that minimizes (5.10) and ensures that e_{21}^s asymptotically converges to zero.

Theorem 5.1. *For agent #2, described by the single-integrator model, the control law*

$$u_2^s = -R_2^{s-1} B_2^{sT} S_2^s \boldsymbol{e}_2^s, \tag{5.11}$$

in which S_2^s is the positive definite solution of the following Riccati equation

$$Q_2^s - S_2^s B_2^s R_2^{s-1} B_2^{sT} S_2^s = 0, \tag{5.12}$$

achieves global asymptotic stability of the closed-loop system.

Proof. Since B_2^s is full rank and $Q_2^s = [q_{21}^s] > 0$, Lemma 2.9 is applicable. Using the control law (5.11), the closed-loop system dynamics is

$$\Sigma_2^s : \quad \dot{\mathbf{e}}_2^s = -B_2^s R_2^{s-1} B_2^{sT} S_2^s \mathbf{e}_2^s, \tag{5.13}$$

which is scalar. Therefore, based on Lemma 2.10 and according to Remark 2.11, we conclude that the closed-loop system (5.13) is globally asymptotically stable. □

In a similar way, we can write the formation error dynamics of the agent #3 as

$$\begin{bmatrix} \dot{e}_{31} \\ \dot{e}_{32} \end{bmatrix} = \begin{bmatrix} \mathbf{0}_{1\times n} & \frac{p_{31}^T}{e_{31}+d_{31}^*} \\ \frac{p_{23}^T}{e_{32}+d_{32}^*} & \frac{p_{32}^T}{e_{32}+d_{32}^*} \end{bmatrix} \begin{bmatrix} u_2^s \\ u_3^s \end{bmatrix}, \tag{5.14}$$

where $n = 2$. Equation (5.14) can be written in the matrix form

$$\begin{aligned} \Xi_3^s: \quad \dot{\mathbf{e}}_3^s &= \hat{B}_3^s \hat{\mathbf{u}}_3^s \\ &= B_3^s u_3^s + \tilde{B}_3^s u_2^s. \end{aligned} \tag{5.15}$$

Let us take the nominal system as

$$\Sigma_3^s: \quad \dot{\mathbf{e}}_3^s = B_3^s u_3^s. \tag{5.16}$$

We can write the associated optimal control problem for agent #3 as

$$\begin{aligned} J_3^s = \min & \frac{1}{2} \int_0^\infty \{\mathbf{e}_3^{sT} Q_3^s \mathbf{e}_3^s + u_3^{sT} R_3^s u_3^s\} dt \\ & \text{s.t.} \\ & \dot{\mathbf{e}}_3^s = B_3^s u_3^s \\ & Q_3^s = \text{diag}[q_{31}^s, q_{32}^s] \geq 0 \\ & R_3^s > 0. \end{aligned} \tag{5.17}$$

The following theorem provides the control law that ensures the asymptotic stability of the closed-loop system and consequently, asymptotic convergence of $\mathbf{e}_3^s$ to zero.

Theorem 5.2. *For agent #3, described by the single-integrator model, the control law*

$$u_3^s = -R_3^{s-1} B_3^{sT} S_3^s \boldsymbol{e}_3^s, \tag{5.18}$$

where S_3^s is the positive definite solution of the following state-dependent Riccati equation

$$Q_3^s - S_3^s B_3^s R_3^{s-1} B_3^{sT} S_3^s = 0, \tag{5.19}$$

achieves local asymptotic stability of the closed-loop system.

Proof. Since the system Σ_2^s is asymptotically stable and control law (5.18) results in asymptotic stability of the system Σ_3^s, then the system Ξ_3^s is locally input-to-state stable with respect to u_2^s which is a function of $\mathbf{e}_2^s$ according to (5.11). Based on the Lemma 2.15, we conclude that the origin of the interconnected system

$$\Delta_3^s: \begin{cases} \Sigma_2^s \\ \Xi_3^s, \end{cases} \tag{5.20}$$

is locally asymptotically stable. □

Since the desired formation is given in the form of a directed triangulated Laman graph, it can be constructed by a sequence of directed vertex addition operations. We

have just provided the result for the agent i; however, the procedure is the same for all other agents. Consequently, for the next follower, denoted by agent i, which is added to an existing directed triangulated Laman graph via Henneberg directed vertex addition sequence, the error dynamic can be written as

$$\begin{bmatrix} \dot{e}_{ij} \\ \dot{e}_{ik} \end{bmatrix} = \begin{bmatrix} \frac{p_{ji}^T}{e_{ij}+d_{ij}^*} & \mathbf{0}_{1\times n} & \frac{p_{ij}^T}{e_{ij}+d_{ij}^*} \\ \mathbf{0}_{1\times n} & \frac{p_{ki}^T}{e_{ik}+d_{ik}^*} & \frac{p_{ik}^T}{e_{ik}+d_{ik}^*} \end{bmatrix} \begin{bmatrix} u_j^s \\ u_k^s \\ u_i^s \end{bmatrix}, \tag{5.21}$$

which can be written in the matrix form

$$\begin{aligned} \Xi_i^s : \quad \dot{\mathbf{e}}_i^s &= \hat{B}_i^s \hat{\mathbf{u}}_i^s \\ &= B_i^s u_i^s + \tilde{B}_i^s \tilde{u}_i^s, \end{aligned} \tag{5.22}$$

where $\tilde{u}_i^s = [u_j^{sT}, u_k^{sT}]^T$. The corresponding nominal optimal control problem can be formulated as

$$\begin{aligned} J_i^s = \min & \frac{1}{2} \int_0^\infty \{\mathbf{e}_i^{sT} Q_i^s \mathbf{e}_i^s + u_i^{sT} R_i^s u_i^s\} dt \\ & \text{s.t.} \\ & \dot{\mathbf{e}}_i^s = B_i^s u_i^s \\ & Q_i^s = \text{diag}[q_{ij}^s, q_{ik}^s] \geq 0 \\ & R_i^s > 0. \end{aligned} \tag{5.23}$$

The following theorem provides SDRE control law.

Theorem 5.3. *For the agent i described by the single-integrator model, distributed control law*

$$u_i^s = -R_i^{s-1} B_i^{sT} S_i^s \boldsymbol{e}_i^s, \tag{5.24}$$

where S_i^s is the positive definite solution of the following Riccati equation

$$Q_i^s - S_i^s B_i^s R_i^{s-1} B_i^{sT} S_i^s = 0, \tag{5.25}$$

achieves local asymptotic stability of the closed-loop directed distance-based formation.

Proof. The control law (5.24) is the stabilizing control of the nominal system $\Sigma_i^s : \dot{\mathbf{e}}_i^s = B_i^s u_i^s$. The stability analysis is similar to the one presented in the proof of Theorem 5.2 with similar arguments related to the stability analysis of interconnected systems. It is evident that the system Ξ_i^s is locally input-to-state stable with respect to $\tilde{u}_i^s$. Using induction method, the interconnected system of preceding $i-1$ agents, denoted by Δ_{i-1}^s,

is asymptotically stable. Thus, based on Lemma 2.15 the origin of interconnected system

$$\Delta_i^s : \begin{cases} \Delta_{i-1}^s \\ \Xi_i^s, \end{cases} \tag{5.26}$$

is locally asymptotically stable. □

5.3.2 Double-Integrator Model

In this case, the edge error dynamics is given by

$$\begin{aligned} \dot{e}_{ij} &= \frac{d}{dt}\sqrt{(p_i - p_j)^T(p_i - p_j)} \\ &= \frac{(p_{ij})^T(v_i - v_j)}{e_{ij} + d_{ij}^*}. \end{aligned} \tag{5.27}$$

The dynamics of error associated with the agent #2 is

$$\dot{e}_{21} = \frac{p_{21}^T}{e_{21} + d_{21}^*} v_2, \tag{5.28}$$

Let us define an aggregate error vector for the agent #2 as

$$\mathbf{e}_2^d = [e_{21}, v_2^T]^T. \tag{5.29}$$

A time-derivative of (5.29) is

$$\dot{\mathbf{e}}_2^d = A_2^d \mathbf{e}_2^d + B_2^d u_2^d, \tag{5.30}$$

with

$$A_2^d = \begin{bmatrix} 0 & \frac{p_{21}^T}{e_{21}+d_{21}^*} \\ \mathbf{0}_{n\times 1} & \mathbf{0}_{n\times n} \end{bmatrix} \tag{5.31a}$$

$$B_2^d = \begin{bmatrix} \mathbf{0}_{1\times n} \\ I_n \end{bmatrix}. \tag{5.31b}$$

Thus, the associated local optimal control problem with the agent #2 can be formulated as

$$\begin{aligned} J_2^d = \min & \frac{1}{2}\int_0^\infty \{\mathbf{e}_2^{dT} Q_2^d \mathbf{e}_2^d + u_2^{dT} R_2^d u_2^d\} dt \\ & \text{s.t.} \\ & \dot{\mathbf{e}}_2^d = A_2^d \mathbf{e}_2^d + B_2^d u_2^d, \\ & Q_2^d = \text{diag}[q_{21}^d, q_{v_2}^d] \geq 0 \\ & R_2^d > 0. \end{aligned} \tag{5.32}$$

The following result provides suboptimal SDRE control law that minimizes (5.32) and ensures that e_{21} asymptotically converges to zero.

Theorem 5.4. *The control law*

$$u_2^d = -R_2^{d^{-1}} B_2^{d^T} S_2^d e_2^d, \tag{5.33}$$

where S_2^d is the solution of the following Riccati equation

$$Q_2^d + A_2^{d^T} S_2^d + S_2^d A_2^d - S_2^d B_2^d R_2^{d^{-1}} B_2^{d^T} S_2^d = 0, \tag{5.34}$$

renders the closed-loop system asymptotically stable and steers e_{21} to zero.

Proof. The proof of the theorem is straightforward result of Lemma 2.9. □

Remark 5.1. Substituting the control law (5.33) in (5.30), the closed-loop dynamics is given by

$$\Sigma_2^d : \quad \dot{\mathbf{e}}_2^d = (A_2^d - B_2^d R_2^{d^{-1}} B_2^{d^T} S_2^d)\mathbf{e}_2^d. \tag{5.35}$$

For the agent #3, let us define $\mathbf{e}_3^d = [e_{31}, e_{32}, v_3^T]^T$. Thus, one has

$$\Xi_3^d : \quad \dot{\mathbf{e}}_3^d = A_3^d \mathbf{e}_3^d + \hat{B}_3^d \mathbf{u}_3^3, \tag{5.36}$$

$$A_3^d = \begin{bmatrix} 0 & 0 & \frac{p_{31}^T}{e_{31}+d_{31}^*} \\ 0 & 0 & \frac{p_{32}^T}{e_{32}+d_{32}^*} \\ \mathbf{0}_{n\times 1} & \mathbf{0}_{n\times 1} & \mathbf{0}_{n\times n} \end{bmatrix} \tag{5.37a}$$

$$\hat{B}_3^d = \begin{bmatrix} \mathbf{0}_{1\times n} & \mathbf{0}_{1\times n} \\ \frac{p_{23}^T}{e_{32}+d_{32}^*} & \mathbf{0}_{1\times n} \\ \mathbf{0}_{n\times n} & I_n \end{bmatrix}, \tag{5.37b}$$

where $\mathbf{u}_3^d = [{v_2}^T, {u_3^d}^T]^T$. Thus, the nominal system is given by

$$\Sigma_3^d : \quad \dot{\mathbf{e}}_3^d = A_3^d \mathbf{e}_3^d + B_3^d u_3^d, \tag{5.38}$$

where

$$B_3^d = \begin{bmatrix} \mathbf{0}_{1\times n} \\ \mathbf{0}_{1\times n} \\ I_n \end{bmatrix}. \tag{5.39a}$$

One can write the associated optimal control problem for the agent #3 as

$$\begin{aligned} J_3^d = \min & \frac{1}{2}\int_0^\infty \{\mathbf{e}_3^{dT} Q_3^d \mathbf{e}_3^d + u_3^{dT} R_3^d u_3^d\} dt \\ & \text{s.t.} \\ & \dot{\mathbf{e}}_3^d = A_3^d \mathbf{e}_3^d + B_3^d u_3^d \\ & Q_3^d = \text{diag}[q_{31}^d, q_{32}^d, q_{v_3}^d] \geq 0 \\ & R_3^d > 0. \end{aligned} \tag{5.40}$$

The following theorem provides the control law that ensures the asymptotic stability of the closed-loop system and consequently asymptotic convergence of $\mathbf{e}_3^d$ to zero.

Theorem 5.5. *For the agent #3, described by the augmented double-integrator model, the control law*

$$u_3^d = -R_3^{d^{-1}} B_3^{dT} S_3^d \boldsymbol{e}_3^d, \tag{5.41}$$

where S_3^d is the positive definite solution of the following state-dependent Riccati equation

$$Q_3^d + A_3^{dT} S_3^d + S_3^d A_3^d - S_3^d B_3^d R_3^{d^{-1}} B_3^{dT} S_3^d = 0, \tag{5.42}$$

achieves local asymptotic stability of the closed-loop system.

Proof. Since the system Σ_2^d is asymptotically stable and the control law (5.41) results in asymptotic stability of system Σ_3^d, then the system Ξ_3^d is locally input-to-state stable. Based on the Lemma 2.15 we conclude that the origin of the interconnected system

$$\Delta_3^d : \begin{cases} \Sigma_2^d \\ \Xi_3^d, \end{cases} \tag{5.43}$$

is locally asymptotically stable. □

Consequently, for the next follower, say agent i, which is added to an existing directed triangulated Laman graph via Henneberg directed vertex addition sequence the error vector is $\mathbf{e}_i^d = [e_{ij}, e_{ik}, v_i^T]^T$. The error dynamics can be written as

$$\Xi_i^d : \dot{\mathbf{e}}_i^d = A_i^d \mathbf{e}_i^d + \hat{B}_i^d \mathbf{u}_i^d \tag{5.44}$$

$$A_i^d = \begin{bmatrix} 0 & 0 & \frac{p_{ij}^T}{e_{ij}+d_{ij}^*} \\ 0 & 0 & \frac{p_{ik}^T}{e_{ik}+d_{ik}^*} \\ \mathbf{0}_{n\times 1} & \mathbf{0}_{n\times 1} & \mathbf{0}_{n\times n} \end{bmatrix} \tag{5.45a}$$

$$\hat{B}_i^d = \begin{bmatrix} \frac{p_{ji}^T}{e_{ij}+d_{ij}^*} & \mathbf{0}_{n\times n} & \mathbf{0}_{n\times n} \\ \mathbf{0}_{n\times n} & \frac{p_{ki}^T}{e_{ik}+d_{ik}^*} & \mathbf{0}_{n\times n} \\ \mathbf{0}_{n\times n} & \mathbf{0}_{n\times n} & I_n \end{bmatrix}, \tag{5.45b}$$

where $\mathbf{u}_i^d = [{v_j}^T, {v_k}^T, {u_i^d}^T]^T$. The corresponding nominal system is

$$\Sigma_i^d : \dot{\mathbf{e}}_i^d = A_i^d \mathbf{e}_i^d + B_i^d u_i^d, \tag{5.46}$$

where

$$B_i^d = \begin{bmatrix} \mathbf{0}_{1\times n} \\ \mathbf{0}_{1\times n} \\ I_n \end{bmatrix}. \tag{5.47a}$$

The associated nominal optimal control problem can be formulated as

$$\begin{aligned} J_i^d = \min \frac{1}{2} \int_0^\infty \{ & {\mathbf{e}_i^d}^T Q_i^d \mathbf{e}_i^d + {u_i^d}^T R_i^d u_i^d \} dt \\ \text{s.t.} \\ & \dot{\mathbf{e}}_i^d = A_i^d \mathbf{e}_i^d + B_i^d u_i^d \\ & Q_i^d = \text{diag}[q_{ij}^d, q_{ik}^d, q_{v_i}^d] \geq 0 \\ & R_i^d > 0. \end{aligned} \tag{5.48}$$

The following theorem offers the associated distributed controller for the agent i that guarantees convergence to the desired formation.

Theorem 5.6. *For the agent i, described by the double-integrator model, the distributed control law*

$$u_i^d = -{R_i^d}^{-1} {B_i^d}^T S_i^d \mathbf{e}_i^d, \tag{5.49}$$

where S_i^d is the unique solution of the equation

$$Q_i^d + {A_i^d}^T S_i^d + S_i^d A_i^d - S_i^d B_i^d {R_i^d}^{-1} {B_i^d}^T S_i^d = 0, \tag{5.50}$$

achieves local asymptotic stability of the closed-loop, directed, distance-based formation.

Proof. The control law (5.49) is the stabilizing control of the nominal system Σ_i^d. Thus,

the system Ξ_i^d is locally input-to-state stable. The stability analysis is similar to the procedure presented in the proof of Theorem 5.5 with equivalent argument about the stability analysis of interconnected systems. The system Δ_{i-1}^d which is the interconnected system of $i-1$ agents, is asymptotically stable. Thus, based on Lemma 2.15, the origin of interconnected system

$$\Delta_i^d : \begin{cases} \Delta_{i-1}^d \\ \Xi_i^d, \end{cases} \tag{5.51}$$

is locally asymptotically stable. □

5.3.3 Reflection Prevention and Collision Avoidance

In this section, based on the barrier function method, we propose a weight selection procedure such that considering the signed area of the triangle, it prevents the flip ambiguity of the desired formation and guarantees collision avoidance between the neighboring agents.

Theorem 5.7. *Select*

$$Q_i = \kappa_i diag[q_{ij}, q_{ik}], \tag{5.52}$$

$$\kappa_i = \frac{\mathbb{A}^* - \mathbb{A}}{\mathbb{A}^* + \mathbb{A}}, \tag{5.53}$$

where $\mathbb{A}^*$, $\mathbb{A}$ are desired and actual signed areas of the triangle corresponding to the clique (i, j, k), and

$$q_{im} = \kappa_{im} + \mu_{im} \quad m \in \{j, k\}, \tag{5.54}$$

where $\kappa_{im} > 0$ is a constant, μ_{im} is a positive barrier multiplier defined by

$$\mu_{im} = (\frac{d_{im}^*}{d_{im} - r_{d_{im}}})^{\epsilon}, \tag{5.55}$$

for suitable $\epsilon \geq 1$, and $r_{d_{im}}$ is a safe distance between pair of agents to prevent collision. Then, by using the weighting factor (5.52), the proposed SDRE control law prevents flip ambiguity of the directed distance-based formation and guarantees inter-agent collision avoidance between neighboring agents.

Proof. The proposed inverse barrier function is $\Phi_i = \mathbf{e}_i^T Q_i \mathbf{e}_i$ where Q_i is defined by (5.52). Adding the proposed inverse barrier function to the cost functional of the corresponding optimal control problem yields the corresponding unconstrained problem. If the condition for collision avoidance or reflection avoidance is violated, then the proposed barrier function approaches infinity and based on [147], this prevents collision avoidance between neighboring agents. □

Note that the result of Theorem 5.7 is applicable to both single- and double-integrator

cases.

5.4 3-D Space

Distance-based formation control problem over directed trilateral Laman graphs is considered in this section. According to the directed trilateral Laman graph structure, a leader is not responsible for any edge. The first-follower (or the agent #2 in the rest of the chapter) is required to preserve its distance from the leader. The agent #3 forms the LFF structure. The rest of the agents are added via the trilateration procedure. We first consider the single-integrator model and then the double-integrator case. The following assumption is supposed to be valid for the rest of the section.

Assumption 5.2: The desired formation is in the form of directed trilateral Laman graph.

5.4.1 Single-Integrator Model

For an agent that is modeled by the single-integrator model, the edge error dynamics is given by

$$\begin{aligned}\dot{e}_{ij} &= \frac{d}{dt}\sqrt{(p_i - p_j)^T(p_i - p_j)} \\ &= \frac{(p_{ij})^T(u_i - u_j)}{e_{ij} + d^*_{ij}}.\end{aligned} \tag{5.56}$$

Since the leader agent is not responsible for any edge, it remains stationary during the formation. Agent #2 (first-follower) is responsible for the edge e_{21}. The error dynamics associated with agent #2 is

$$\begin{aligned}\dot{\mathbf{e}}^s_2 =& B^s_2 u^s_2 \\ =& \frac{p^T_{21}}{e_{21} + d^*_{21}} u^s_2,\end{aligned} \tag{5.57}$$

where $\mathbf{e}^s_2 = e_{21}$. Thus, the associated local optimal control problem with agent #2 is

$$\begin{aligned} J^s_2 = \min & \frac{1}{2}\int_0^\infty \{\mathbf{e}^{sT}_2 Q^s_2 \mathbf{e}^s_2 + u^{sT}_2 R^s_2 u^s_2\} dt \\ & \text{s.t.} \\ & \dot{\mathbf{e}}^s_2 = B^s_2 u^s_2 \\ & Q^s_2 = [q^s_{21}] > 0 \\ & R^s_2 > 0. \end{aligned} \tag{5.58}$$

The following result provides the suboptimal SDRE control law that minimizes (5.58) and ensures that e_{21} globally asymptotically converges to zero.

Theorem 5.8. *For the agent #2 described by the single-integrator model (2.14), the control law*

$$u_2^s = -R_2^{s-1} B_2^{sT} S_2^s \boldsymbol{e}_2^s, \tag{5.59}$$

in which S_2^s is the positive definite solution of the following Riccati equation

$$Q_2^s - S_2^s B_2^s R_2^{s-1} B_2^{sT} S_2^s = 0, \tag{5.60}$$

ensures global asymptotic stability of the closed-loop system.

Proof. The system (5.57) is controllable; therefore, by selecting $Q_2^s = [q_{21}^s] > 0$, the system satisfies the SDRE feasibility conditions, and therefore, Lemma 2.9 is applicable. Using the control law (5.59), the closed-loop system dynamics is

$$\Sigma_2^s : \quad \dot{\mathbf{e}}_2^s = -B_2^s R_2^{s-1} B_2^{sT} S_2^s \mathbf{e}_2^s. \tag{5.61}$$

The error $\mathbf{e}_2^s$ in (5.61) is scalar. Thus, based on Lemma 2.10 and considering Remark 2.11, we conclude that the closed-loop system is globally asymptotically stable. □

Similarly, we can write the formation error dynamics of the agent #3 as

$$\begin{bmatrix} \dot{e}_{31} \\ \dot{e}_{32} \end{bmatrix} = \begin{bmatrix} \mathbf{0}_{1\times n} & \frac{p_{31}^T}{e_{31}+d_{31}^*} \\ \frac{p_{23}^T}{e_{32}+d_{32}^*} & \frac{p_{32}^T}{e_{32}+d_{32}^*} \end{bmatrix} \begin{bmatrix} u_2^s \\ u_3^s \end{bmatrix}, \tag{5.62}$$

where n is the space dimension. The equation (5.62) can be written in a form of

$$\begin{aligned} \Xi_3^s : \quad \dot{\mathbf{e}}_3^s &= \hat{B}_3^s \hat{\mathbf{u}}_3^s \\ &= B_3^s u_3^s + \tilde{B}_3^s u_2^s. \end{aligned} \tag{5.63}$$

Consider the nominal system as

$$\Sigma_3^s : \quad \dot{\mathbf{e}}_3^s = B_3^s u_3^s. \tag{5.64}$$

We can write an associated optimal control problem for agent #3 as

$$\begin{aligned} J_3^s = \min & \frac{1}{2}\int_0^\infty \{\mathbf{e}_3^{sT} Q_3^s \mathbf{e}_3^s + u_3^{sT} R_3^s u_3^s\} dt \\ & \text{s.t.} \\ & \dot{\mathbf{e}}_3^s = B_3^s u_3^s \\ & Q_3^s = \varrho_3 I_2 > 0 \\ & R_3^s > 0, \end{aligned} \tag{5.65}$$

where ϱ_3 is a positive scalar. The following theorem provides the control law that ensures global asymptotic stability of the closed-loop system and consequently, global asymptotic convergence of $\mathbf{e}_3^s$ to zero.

Theorem 5.9. *For the second-follower (agent #3), described by the single-integrator model (2.14), the control law*

$$u_3^s = -R_3^{s-1} B_3^{sT} S_3^s \boldsymbol{e}_3^s, \tag{5.66}$$

where S_3^s is the positive definite solution of the following state-dependent Riccati equation

$$Q_3^s - S_3^s B_3^s R_3^{s-1} B_3^{sT} S_3^s = 0, \tag{5.67}$$

results in the global asymptotic stability of the closed-loop system.

Proof. The origin of the system $\Sigma_2^s(\mathbf{e}_2^s)$ is globally asymptotically stable equilibrium point. The system (5.64) is stabilizable, and by selecting $Q_3^s > 0$ it is also detectable, which satisfies conditions of SDRE controller and guarantees Lemma 2.9's applicability. Replacing control law (5.66) in system dynamics (5.64), the closed-loop dynamic is given by

$$\begin{aligned} \Sigma_3^s : \quad & \dot{\mathbf{e}}_3^s = -A_{CL3} \mathbf{e}_3^s \\ & A_{CL3} = B_3^s R_3^{s-1} B_3^{sT} S_3^s. \end{aligned} \tag{5.68}$$

Rearranging equation (5.67), one has $A_{CL3} = B_3^s R_3^{s-1} B_3^{sT} S_3^s = \varrho_3 S_3^{s-1}$. Since S_3^s is symmetric and positive-definite and considering the fact that inverse of a symmetric matrix, also is symmetric, we demonstrate that A_{CL3} is symmetric. Thus, based on Lemma 2.10, we conclude that using the proposed SDRE controller (5.66), the nominal system (5.64) is globally asymptotically stable. To demonstrate the exponential stability of the (5.68), consider the following Lyapunov function

$$V_3(\mathbf{e}_3^s) = \frac{1}{2} \mathbf{e}_3^{sT} S_3^s \mathbf{e}_3^s, \tag{5.69}$$

for which, from the matrix theory, the following inequality holds

$$\frac{1}{2}\lambda_3^{min}||\mathbf{e}_3^s||^2 \leq V_3(\mathbf{e}_3^s) \leq \frac{1}{2}\lambda_3^{max}||\mathbf{e}_3^s||^2, \tag{5.70}$$

where λ_3^{min} and λ_3^{max} are the smallest and the largest eigenvalues in $\Theta(S_3^s)$. The derivative of Lyapunov function alongside state trajectory of the nominal system is

$$\begin{aligned}\dot{V}_3(\mathbf{e}_3^s) &= \frac{\partial V}{\partial \mathbf{e}_3^s}\dot{\mathbf{e}}_3^s \\ &= -\mathbf{e}_3^{sT} S_3^s B_3^s R_3^{s-1} B_3^{sT} S_3^s \mathbf{e}_3^s,\end{aligned} \tag{5.71}$$

which according to the Riccati equation (5.67), can be simplified to

$$\dot{V}_3(\mathbf{e}_3^s) = -\varrho_3||\mathbf{e}_3^s||^2. \tag{5.72}$$

Therefore, the proposed Lyapunov function (5.69) satisfies the conditions of Theorem 2.3, and thus, proves the exponential stability of the nominal system (5.68). Since control law (5.66) results in the global exponential stability of the nominal system Σ_3^s, then based on Theorem 2.5, the system $\Xi_3^s(\mathbf{e}_3^s, u_2^s)$ is globally input-to-state stable with respect to u_2^s where u_2^s is a function of $\mathbf{e}_2^s$. Therefore, based on the Lemma 2.16 and the result proven in the Theorem 5.8, we conclude that the origin of the interconnected system

$$\Delta_3^s : \begin{cases} \Sigma_2^s(\mathbf{e}_2^s) \\ \Xi_3^s(\mathbf{e}_3^s, \mathbf{e}_2^s), \end{cases} \tag{5.73}$$

is globally asymptotically stable. □

For the agent #4, which is the source of added edges e_{41}, e_{42}, e_{43}, we can write

$$\Xi_4^s : \quad \begin{bmatrix} \dot{e}_{41} \\ \dot{e}_{42} \\ \dot{e}_{43} \end{bmatrix} = \begin{bmatrix} \mathbf{0}_{1\times n} & \mathbf{0}_{1\times n} & \frac{p_{41}^T}{e_{41}+d_{41}^*} \\ \frac{p_{24}^T}{e_{42}+d_{42}^*} & \mathbf{0}_{1\times n} & \frac{p_{42}^T}{e_{42}+d_{42}^*} \\ \mathbf{0}_{1\times n} & \frac{p_{34}^T}{e_{43}+d_{43}^*} & \frac{p_{43}^T}{e_{43}+d_{43}^*} \end{bmatrix} \begin{bmatrix} u_2^s \\ u_3^s \\ u_4^s \end{bmatrix}, \tag{5.74}$$

The nominal system can be chosen as

$$\Sigma_4^s : \quad \dot{\mathbf{e}}_4^s = B_4^s u_4^s, \tag{5.75}$$

where

$$B_4^s = \begin{bmatrix} \frac{p_{41}^T}{e_{41}+d_{41}^*} \\ \frac{p_{42}^T}{e_{42}+d_{42}^*} \\ \frac{p_{43}^T}{e_{43}+d_{43}^*} \end{bmatrix}. \tag{5.76}$$

The associated optimal control problem is

$$
\begin{aligned}
J_4^s = \min & \frac{1}{2}\int_0^\infty \{\mathbf{e}_4^{sT} Q_4^s \mathbf{e}_4^s + u_4^{sT} R_4^s u_4^s\} dt \\
& \text{s.t.} \\
& \dot{\mathbf{e}}_4^s = B_4^s u_4^s \\
& Q_4^s = \varrho_4 I_3 > 0 \\
& R_4^s > 0.
\end{aligned}
\tag{5.77}
$$

Theorem 5.10. *For the third-follower (agent #4) described by the single-integrator model, the control law*

$$
u_4^s = -R_4^{s-1} B_4^{sT} S_4^s \boldsymbol{e}_4^s, \tag{5.78}
$$

where S_4^s is the positive definite solution of the following state-dependent Riccati equation

$$
Q_4^s - S_4^s B_4^s R_4^{s-1} B_4^{sT} S_4^s = 0, \tag{5.79}
$$

achieves global asymptotic stability of the closed-loop system.

Proof. For the system (5.75), the Conditions 1-3 are met by selecting $Q_4^s > 0$. Thus, Lemma 2.9 is applicable. The closed-loop dynamic matrix $A_{CL4} = B_4^s R_4^{s-1} B_4^{sT} S_4^s = \varrho_4 S_4^{s-1}$ is symmetric, considering the Riccati equation (5.79). Therefore, the closed-loop nominal system is globally asymptotically stable according to Lemma 2.10. It is easy to verify the exponential stability of the origin, considering the Lyapunov function $V_4(\mathbf{e}_4^s) = \frac{1}{2}\mathbf{e}_4^{sT} S_4^s \mathbf{e}_4^s$ following the same steps at the proof of the Theorem 5.9. Since the control law (5.83) results in the global exponential stability of the nominal system Σ_4^s, thus, based on Theorem 2.5, the system Ξ_4^s is globally input-to-state stable with respect to $[u_2^s, u_3^s]$. Also, Theorem 5.9 showed global asymptotic stability of the system Δ_3^s. Therefore, according to the Lemma 2.16, we can conclude that the origin of the interconnected system

$$
\Delta_4^s : \begin{cases} \Delta_3^s \\ \Xi_4^s \end{cases}, \tag{5.80}
$$

is globally asymptotically stable. □

Since the desired formation is given in the form of a directed trilateral Laman graph, it can be constructed by a sequence of trilateration operations as shown in Figure 2.5(c). We just provided the results for an agent i, and the procedure is repeatable for all other vertices in the same way. Consequently, for the next follower denoted by agent i, which is added to an existing directed trilateral Laman graph via Henneberg directed vertex

addition sequence, the error dynamic can be written as

$$\begin{bmatrix} \dot{e}_{ij} \\ \dot{e}_{il} \\ \dot{e}_{ik} \end{bmatrix} = \begin{bmatrix} \frac{p_{ji}^T}{e_{ij}+d_{ij}^*} & \mathbf{0}_{1\times n} & \mathbf{0}_{1\times n} & \frac{p_{ij}^T}{e_{ij}+d_{ij}^*} \\ \mathbf{0}_{1\times n} & \frac{p_{li}^T}{e_{il}+d_{il}^*} & \mathbf{0}_{1\times n} & \frac{p_{il}^T}{e_{il}+d_{il}^*} \\ \mathbf{0}_{1\times n} & \mathbf{0}_{1\times n} & \frac{p_{ki}^T}{e_{ik}+d_{ik}^*} & \frac{p_{ik}^T}{e_{ik}+d_{ik}^*} \end{bmatrix} \begin{bmatrix} u_j^s \\ u_l^s \\ u_k^s \\ u_i^s \end{bmatrix}, \tag{5.81}$$

which can be written in the matrix form

$$\begin{aligned} \Xi_i^s : \quad \dot{\mathbf{e}}_i^s &= \hat{B}_i^s \hat{\mathbf{u}}_i^s \\ &= B_i^s u_i^s + \tilde{B}_i^s \tilde{u}_i^s, \end{aligned} \tag{5.82}$$

where $\tilde{u}_i^s = [u_j^{sT}, u_l^{sT}, u_k^{sT}]^T$. The corresponding nominal optimal control problem can be formed as

$$\begin{aligned} J_i^s = \min & \frac{1}{2} \int_0^\infty \{\mathbf{e}_i^{sT} Q_i^s \mathbf{e}_i^s + u_i^{sT} R_i^s u_i^s\} dt \\ & \text{s.t.} \\ & \dot{\mathbf{e}}_i^s = B_i^s u_i^s \\ & Q_i^s = \varrho_i I_3 > 0 \\ & R_i^s > 0, \end{aligned} \tag{5.83}$$

where ϱ_i is a positive scalar. The following theorem provides the associated SDRE control law.

Theorem 5.11. *For the agent i, described by the single-integrator model, the distributed control law*

$$u_i^s = -R_i^{s-1} B_i^{sT} S_i^s \boldsymbol{e}_i^s, \tag{5.84}$$

where S_i^s is the unique, symmetric, positive definite solution of the following Riccati equation

$$Q_i^s - S_i^s B_i^s R_i^{s-1} B_i^{sT} S_i^s = 0, \tag{5.85}$$

results in the global asymptotic stability of the closed-loop, directed, distance-based formation.

Proof. The nominal system in (5.83) is stabilizable, therefore Lemma 2.9 is applicable by choosing $Q_i^s > 0$. The control law (5.84) is the stabilizing control of the nominal system $\Sigma_i^s : \dot{\mathbf{e}}_i^s = B_i^s u_i^s$. Substituting control law (5.84) in the nominal system dynamics, we have

$$\begin{aligned} \Sigma_i^s : \quad \dot{\mathbf{e}}_i^s &= -A_{CLi} \mathbf{e}_i^s \\ A_{CLi} &= B_i^s R_i^{s-1} B_i^{sT} S_i^s. \end{aligned} \tag{5.86}$$

After some mathematical manipulation, the Riccati equation (5.85) can be written as

$$B_i^s R_i^{s-1} B_i^{sT} S_i^s = \varrho_i S_i^{s-1}. \tag{5.87}$$

Since the inverse of a symmetric matrix is also symmetric, from (5.87) and (5.86) we can conclude that the closed-loop dynamic matrix, A_{CLi}, is symmetric for all $\mathbf{e}_i^s$. Therefore, based on Lemma 2.10, the global asymptotic stability of the closed-loop nominal system (5.86) is proven using the control law (5.84). To demonstrate the exponential stability of the (5.86), consider the following Lyapunov function

$$V_i(\mathbf{e}_i^s) = \frac{1}{2}\mathbf{e}_i^{sT} S_i^s \mathbf{e}_i^s. \tag{5.88}$$

The proposed Lyapunov function (5.88) satisfies

$$\frac{1}{2}\lambda_i^{min}||\mathbf{e}_i^s||^2 \leq V_i(\mathbf{e}_i^s) \leq \frac{1}{2}\lambda_i^{max}||\mathbf{e}_i^s||^2, \tag{5.89}$$

where λ_i^{min} and λ_i^{max} are the smallest and the biggest eigenvalues in $\Theta(S_i^s)$. The derivative of Lyapunov function alongside state trajectory is

$$\dot{V}_i(\mathbf{e}_i^s) = -\mathbf{e}_i^{sT} S_i^s B_i^s R_i^{s-1} B_i^{sT} S_i^s \mathbf{e}_3^s, \tag{5.90}$$

where according to the Riccati equation (5.87), can be simplified to

$$\dot{V}_i(\mathbf{e}_i^s) = -\varrho_i||\mathbf{e}_i^s||^2 \leq -\xi_i||\mathbf{e}_i^s||^2 \tag{5.91}$$

for some $\xi_i \geq \varrho_i$. Inequalities (5.91) and (5.89) show that the Lyapunov function $V_i(\mathbf{e}_i^s)$ meets the conditions of the Theorem 2.3. This proves the global exponential stability of the closed-loop nominal system (5.86) under the distributed SDRE control law (5.84).

The interconnected stability analysis is similar to the mathematical induction procedure presented in the proof of Theorem 5.10 with a similar argument about the stability analysis of interconnected systems. Based on the Theorem 2.5, it is evident that the system Ξ_i^s is globally input-to-state stable with respect to $\tilde{u}_i^s$. Using the mathematical induction, one can say that the interconnected system of preceding $i-1$ agents, denoted by Δ_{i-1}^s, is globally asymptotically stable. Thus, based on Lemma 2.16 the origin of the interconnected system

$$\Delta_i^s : \begin{cases} \Delta_{i-1}^s \\ \Xi_i^s \end{cases}, \tag{5.92}$$

is globally asymptotically stable. □

Remark 5.2. The global asymptotic stability results of this section are also valid for the single-integrator model case in the previous section.

5.4.2 Double-Integrator Model

In this case, the edge error dynamics is given by

$$\begin{aligned}\dot{e}_{ij} &= \frac{d}{dt}\sqrt{(p_i - p_j)^T(p_i - p_j)} \\ &= \frac{(p_{ij})^T(v_i - v_j)}{e_{ij} + d^*_{ij}}.\end{aligned} \tag{5.93}$$

The dynamics of the error associated with the agent #2 is

$$\dot{e}_{21} = \frac{p_{21}^T}{e_{21} + d^*_{21}} v_2. \tag{5.94}$$

Let us define an aggregate error vector for the agent #2 as

$$\mathbf{e}_2^d = [e_{21}, v_2^T]^T. \tag{5.95}$$

A time-derivative of (5.95) is

$$\dot{\mathbf{e}}_2^d = A_2^d \mathbf{e}_2^d + B_2^d u_2^d, \tag{5.96}$$

with

$$A_2^d = \begin{bmatrix} 0 & \frac{p_{21}^T}{e_{21}+d^*_{21}} \\ \mathbf{0}_{n\times 1} & \mathbf{0}_{n\times n} \end{bmatrix} \tag{5.97a}$$

$$B_2^d = \begin{bmatrix} \mathbf{0}_{1\times n} \\ I_n \end{bmatrix}. \tag{5.97b}$$

Thus, the associated local optimal control problem with the agent #2 can be formulated as

$$\begin{aligned} J_2^d = \min & \frac{1}{2}\int_0^\infty \{\mathbf{e}_2^{dT} Q_2^d \mathbf{e}_2^d + u_2^{dT} R_2^d u_2^d\} dt \\ & \text{s.t.} \\ & \dot{\mathbf{e}}_2^d = A_2^d \mathbf{e}_2^d + B_2^d u_2^d \\ & Q_2^d = \text{diag}[q_{21}^d, q_{v_2}^d] > 0 \\ & R_2^d > 0. \end{aligned} \tag{5.98}$$

The following result provides suboptimal SDRE control law that minimizes (5.98) and ensures that e_{21} asymptotically converges to zero.

Theorem 5.12. *The control law*

$$u_2^d = -R_2^{d^{-1}} B_2^{d^T} S_2^d \boldsymbol{e}_2^d, \tag{5.99}$$

where S_2^d is the solution of the following Riccati equation

$$Q_2^d + A_2^{d^T} S_2^d + S_2^d A_2^d - S_2^d B_2^d R_2^{d^{-1}} B_2^{d^T} S_2^d = 0, \tag{5.100}$$

renders the closed-loop system asymptotically stable and steers e_{21} to zero.

Proof. The system (5.96) is stabilizable, and by choosing $Q_2^d > 0$, it is detectable everywhere. Thus, Condition 1-3 are satisfied and that guarantees the Lemma 2.9's applicability. The control law (5.99) is a direct result of Lemma 2.9. □

Remark 5.3. Substituting the control law (5.99) in (5.96), the closed-loop dynamics is given by

$$\Sigma_2^d : \quad \dot{\mathbf{e}}_2^d = (A_2^d - B_2^d R_2^{d^{-1}} B_2^{d^T} S_2^d)\mathbf{e}_2^d. \tag{5.101}$$

For the agent #3, let us define $\mathbf{e}_3^d = [e_{31}, e_{32}, v_3^T]^T$. Thus, one has

$$\Xi_3^d : \quad \dot{\mathbf{e}}_3^d = A_3^d \mathbf{e}_3^d + \hat{B}_3^d \mathbf{u}_3^d, \tag{5.102}$$

$$A_3^d = \begin{bmatrix} 0 & 0 & \frac{p_{31}^T}{e_{31}+d_{31}^*} \\ 0 & 0 & \frac{p_{32}^T}{e_{32}+d_{32}^*} \\ \mathbf{0}_{n\times 1} & \mathbf{0}_{n\times 1} & \mathbf{0}_{n\times n} \end{bmatrix} \tag{5.103a}$$

$$\hat{B}_3^d = \begin{bmatrix} \mathbf{0}_{1\times n} & \mathbf{0}_{1\times n} \\ \frac{p_{23}^T}{e_{32}+d_{32}^*} & \mathbf{0}_{1\times n} \\ \mathbf{0}_{n\times n} & I_n \end{bmatrix}, \tag{5.103b}$$

where $\mathbf{u}_3^d = [{v_2}^T, {u_3^d}^T]^T$. Thus, the nominal system is given by

$$\Sigma_3^d : \quad \dot{\mathbf{e}}_3^d = A_3^d \mathbf{e}_3^d + B_3^d u_3^d, \tag{5.104}$$

where

$$B_3^d = \begin{bmatrix} \mathbf{0}_{1\times n} \\ \mathbf{0}_{1\times n} \\ I_n \end{bmatrix}. \tag{5.105a}$$

One can write the associated optimal control problem for the agent #3 as

$$\begin{aligned} J_3^d = \min & \frac{1}{2}\int_0^\infty \{\mathbf{e}_3^{dT} Q_3^d \mathbf{e}_3^d + u_3^{dT} R_3^d u_3^d\} dt \\ & \text{s.t.} \\ & \dot{\mathbf{e}}_3^d = A_3^d \mathbf{e}_3^d + B_3^d u_3^d \\ & Q_3^d = \text{diag}[q_{31}^d, q_{32}^d, q_{v_3}^d] > 0 \\ & R_3^d > 0. \end{aligned} \tag{5.106}$$

The following theorem provides the control law that ensures the asymptotic stability of the closed-loop system and consequently asymptotic convergence of $\mathbf{e}_3^d$ to zero.

Theorem 5.13. *For the second-follower (agent #3) that is described by the double-integrator model, the control law*

$$u_3^d = -R_3^{d^{-1}} B_3^{dT} S_3^d \boldsymbol{e}_3^d, \tag{5.107}$$

where S_3^d is the positive definite solution of the following state-dependent Riccati equation

$$Q_3^d + A_3^{dT} S_3^d + S_3^d A_3^d - S_3^d B_3^d R_3^{d^{-1}} B_3^{dT} S_3^d = 0, \tag{5.108}$$

results in the local asymptotic stability of the closed-loop system.

Proof. Conditions 1-3 are met as the system (5.104) is stabilizable and detectable. Since the system Σ_2^d is asymptotically stable and the control law (5.107) results in asymptotic stability of the system Σ_3^d, then the system Ξ_3^d is locally input-to-state stable. Based on the Lemma 2.15 we conclude that the origin of the interconnected system

$$\Delta_3^d : \begin{cases} \Sigma_2^d \\ \Xi_3^d, \end{cases} \tag{5.109}$$

is locally asymptotically stable. □

For the agent #4 the aggregate error vector is $\mathbf{e}_4^d = [e_{41}, e_{42}, e_{43}, {v_4}^T]^T$. The error dynamics can be written as

$$\Xi_4^d : \dot{\mathbf{e}}_4^d = A_4^d \mathbf{e}_4^d + \hat{B}_4^d \mathbf{u}_4^d \tag{5.110}$$

where

$$A_4^d = \begin{bmatrix} 0 & 0 & 0 & \frac{p_{41}^T}{e_{41}+d_{41}^*} \\ 0 & 0 & 0 & \frac{p_{42}^T}{e_{42}+d_{42}^*} \\ 0 & 0 & 0 & \frac{p_{43}^T}{e_{43}+d_{43}^*} \\ \mathbf{0}_{n\times 1} & \mathbf{0}_{n\times 1} & \mathbf{0}_{n\times 1} & \mathbf{0}_{n\times n} \end{bmatrix} \tag{5.111a}$$

$$\hat{B}_4^d = \begin{bmatrix} \mathbf{0}_{1\times n} & \mathbf{0}_{1\times n} & \mathbf{0}_{1\times n} \\ \frac{p_{24}^T}{e_{42}+d_{42}^*} & \mathbf{0}_{1\times n} & \mathbf{0}_{1\times n} \\ \mathbf{0}_{1\times n} & \frac{p_{34}^T}{e_{43}+d_{43}^*} & \mathbf{0}_{1\times n} \\ \mathbf{0}_{n\times n} & \mathbf{0}_{n\times n} & I_n \end{bmatrix}, \tag{5.111b}$$

and $\mathbf{u}_4^d = [{v_2}^T, {v_3}^T, {u_4^d}^T]^T$. The corresponding nominal system is

$$\Sigma_4^d : \dot{\mathbf{e}}_4^d = A_4^d \mathbf{e}_4^d + B_4^d u_4^d, \tag{5.112}$$

where

$$B_4^d = \begin{bmatrix} \mathbf{0}_{3\times n} \\ I_n \end{bmatrix}. \tag{5.113a}$$

The associated nominal optimal control problem can be formulated as

$$\begin{aligned} J_4^d = \min & \frac{1}{2}\int_0^\infty \{\mathbf{e}_4^{dT} Q_4^d \mathbf{e}_4^d + u_4^{dT} R_4^d u_4^d\} dt \\ & \text{s.t.} \\ & \dot{\mathbf{e}}_4^d = A_4^d \mathbf{e}_4^d + B_4^d u_4^d \\ & Q_4^d = \text{diag}[q_{41}^d, q_{42}^d, q_{43}^d, q_{v_4}^d] > 0 \\ & R_4^d > 0. \end{aligned} \tag{5.114}$$

The following theorem offers the associated distributed controller for agent #4 which can guarantees the convergence of the desired formation.

Theorem 5.14. *For the third-follower (agent #4) described by the double-integrator model, the distributed control law*

$$u_4^d = -R_4^{d^{-1}} B_4^{dT} S_4^d \boldsymbol{e}_4^d, \tag{5.115}$$

where S_4^d is the unique solution of the equation

$$Q_4^d + A_4^{dT} S_4^d + S_4^d A_4^d - S_4^d B_4^d R_4^{d^{-1}} B_4^{dT} S_4^d = 0, \tag{5.116}$$

achieves local asymptotic stability of the closed-loop directed distance-based formation.

Proof. Lemma 2.9 is applicable since Conditions 1-3 are satisfied for the nominal system (5.112) by selecting $Q_4^d > 0$. The control law (5.115) is the stabilizing control of the nominal system Σ_4^d, thus, one can conclude the local input-to-state stability of the system Ξ_4^d. Theorem 5.13 indicates asymptotic stability of the origin of the system Δ_3^d. Thus, based on Lemma 2.15 the origin of interconnected system

$$\Delta_4^d : \begin{cases} \Delta_3^d \\ \Xi_4^d, \end{cases} \tag{5.117}$$

is locally asymptotically stable. □

Consequently, for the next follower, denoted by agent i, which is added to an existing directed trilateral Laman graph via trilateration sequence the aggregate error vector is $\mathbf{e}_i^d = [e_{ij}, e_{il}, e_{ik}, {v_i}^T]^T$. The error dynamics can be written as

$$\Xi_i^d : \dot{\mathbf{e}}_i^d = A_i^d \mathbf{e}_i^d + \hat{B}_i^d \mathbf{u}_i^d, \tag{5.118}$$

where

$$A_i^d = \begin{bmatrix} 0 & 0 & 0 & \frac{p_{ij}^T}{e_{ij}+d_{ij}^*} \\ 0 & 0 & 0 & \frac{p_{il}^T}{e_{il}+d_{il}^*} \\ 0 & 0 & 0 & \frac{p_{ik}^T}{e_{ik}+d_{ik}^*} \\ \mathbf{0}_{n\times 1} & \mathbf{0}_{n\times 1} & \mathbf{0}_{n\times 1} & \mathbf{0}_{n\times n} \end{bmatrix} \tag{5.119a}$$

$$\hat{B}_i^d = \begin{bmatrix} \frac{p_{ji}^T}{e_{ij}+d_{ij}^*} & \mathbf{0}_{1\times n} & \mathbf{0}_{1\times n} & \mathbf{0}_{1\times n} \\ \mathbf{0}_{1\times n} & \frac{p_{li}^T}{e_{il}+d_{il}^*} & \mathbf{0}_{1\times n} & \mathbf{0}_{1\times n} \\ \mathbf{0}_{1\times n} & \mathbf{0}_{1\times n} & \frac{p_{ki}^T}{e_{ki}+d_{ik}^*} & \mathbf{0}_{1\times n} \\ \mathbf{0}_{n\times n} & \mathbf{0}_{n\times n} & \mathbf{0}_{n\times n} & I_n \end{bmatrix}, \tag{5.119b}$$

and $\mathbf{u}_i^d = [{v_j}^T, {v_l}^T, {v_k}^T, {u_i^d}^T]^T$. The corresponding nominal system is

$$\Sigma_i^d : \dot{\mathbf{e}}_i^d = A_i^d \mathbf{e}_i^d + B_i^d u_i^d, \tag{5.120}$$

where

$$B_i^d = \begin{bmatrix} \mathbf{0}_{1\times n} \\ \mathbf{0}_{1\times n} \\ \mathbf{0}_{1\times n} \\ I_n \end{bmatrix}. \tag{5.121a}$$

The associated nominal optimal control problem can be formulated as

$$\begin{aligned} J_i^d = \min & \frac{1}{2}\int_0^\infty \{\mathbf{e}_i^{dT} Q_i^d \mathbf{e}_i^d + u_i^{dT} R_i^d u_i^d\} dt \\ & \text{s.t.} \\ & \dot{\mathbf{e}}_i^d = A_i^d \mathbf{e}_i^d + B_i^d u_i^d \\ & Q_i^d = \text{diag}[q_{ij}^d, q_{il}^d, q_{ik}^d, q_{v_i}^d] > 0 \\ & R_i^d > 0. \end{aligned} \tag{5.122}$$

The following theorem offers the associated distributed controller for agent i which can guarantee the convergence of the desired formation.

Theorem 5.15. *For the agent i, described by the double-integrator model (2.17), the distributed control law*

$$u_i^d = -R_i^{d^{-1}} B_i^{dT} S_i^d \boldsymbol{e}_i^d, \tag{5.123}$$

where S_i^d is the unique solution of the equation

$$Q_i^d + A_i^{dT} S_i^d + S_i^d A_i^d - S_i^d B_i^d R_i^{d^{-1}} B_i^{dT} S_i^d = 0, \tag{5.124}$$

achieves the local asymptotic stability of the closed-loop, directed, distance-based formation.

Proof. By selecting $Q_i^d > 0$, Conditions 1-3 are satisfied for the system (5.120) and Lemma 2.9 can be applied. The control law (5.123) is the stabilizing control of the nominal system Σ_i^d. Thus, the system Ξ_i^d is locally input-to-state stable. Based on mathematical induction, the system Δ_{i-1}^d, which is the interconnected system of $i-1$ agents, is asymptotically stable. Based on Lemma 2.15, local asymptotic stability of the origin of the interconnected system

$$\Delta_i^d : \begin{cases} \Delta_{i-1}^d \\ \Xi_i^d, \end{cases} \tag{5.125}$$

is guaranteed. □

Remark 5.4. Note that each agent's SDRE state feedback control law, u_i, depends only on the agent's error vector, $\mathbf{e}_i$. Agent's error vector solely depends on the agent's velocity and the neighboring agents' relative positions in the agent's local coordinate system, to which the agent is assumed to have access. Therefore, the proposed control scheme is fully distributed.

5.4.3 Reflection Prevention and Collision Avoidance

Inspired by the seminal work [44] in 2-D space, we propose a formation control method that prevents reflection of formation configurations in 3-D. The proposed method prevents reflected configurations by considering the signed volume of a tetrahedron that is formed by the neighboring agents. Each added agent via directed vertex addition is responsible for controlling the volume of the tetrahedron formed by its associated edges. The method also prevents collision avoidance between the neighboring agents.

Theorem 5.16. *Select the state weighting matrices as*

$$Q_i = \vartheta_i \delta_i I, \quad i \geq 4 \tag{5.126}$$

$$\vartheta_i = \frac{\mathbb{V}^* - \mathbb{V}}{\mathbb{V}^* + \mathbb{V}}, \tag{5.127}$$

where $\mathbb{V}^*$ and $\mathbb{V}$ are desired and actual signed volume of the tetrahedron between the clique (j, l, k, i), respectively, and

$$\begin{aligned} \delta_i &= \sum_{m \in \mathcal{N}_i} q_{im} \\ q_{im} &= \varphi_{im} + \mu_{im}. \end{aligned} \tag{5.128}$$

Here, $\varphi_{im} > 0$ is a constant and μ_{im} is a positive barrier multiplier defined by

$$\mu_{im} = \left(\frac{d^*_{im}}{d_{im} - r_{d_{im}}}\right)^{\epsilon}, \tag{5.129}$$

for suitable $\epsilon \geq 1$, and $r_{d_{im}}$ being a safe distance between pair of agents to prevent collision. Then, by using the weighting factor (5.126), the proposed SDRE control law prevents flip ambiguity of the directed distance-based formation in 3-D space and guarantees inter-agent collision avoidance of the neighboring agents.

Proof. The proposed inverse barrier function is

$$\Phi_i = \mathbf{e}_i^T Q_i \mathbf{e}_i, \tag{5.130}$$

where Q_i is defined by (5.126). Adding the proposed inverse barrier function (5.130) to the cost functional of the corresponding optimal control problem yields the corresponding unconstrained problem. If the condition for collision avoidance or reflection avoidance is violated, then the proposed barrier function (5.130) approaches infinity and based on [147], this prevents flip ambiguity of the formation and guarantees collision avoidance between neighboring agents. □

Corollary 5.16.1. *Select the state weighting matrix as*

$$Q_3 = \kappa_3 \delta_3 I, \tag{5.131}$$

where

$$\kappa_3 = \frac{\mathbb{A}^* - \mathbb{A}}{\mathbb{A}^* + \mathbb{A}}, \tag{5.132}$$

and $\mathbb{A}^*$ *and* $\mathbb{A}$ *are desired and actual signed area of the LFF triangle between the clique* $(1, 2, 3)$*, and*

$$\begin{aligned} \delta_i &= \sum_{m \in \{1,2\}} q_{im} \\ q_{3m} &= \zeta_{3m} + \mu_{3m}, \end{aligned} \tag{5.133}$$

where $\zeta_{3m} > 0$ *is a constant and* μ_{3m} *is a positive barrier multiplier defined by*

$$\mu_{3m} = \left(\frac{d^*_{3m}}{d_{3m} - r_{d_{3m}}}\right)^{\epsilon}, \tag{5.134}$$

for suitable $\epsilon \geq 1$*, and* $r_{d_{3m}}$ *being a safe distance between pair of agents to prevent collision. Then, by using the weighting factor (5.131), the proposed SDRE control law prevents the flip ambiguity of the LFF triangle and guarantees inter-agent collision avoidance of the agent #3 with its neighboring agents.*

Proof. The proof is similar to the proof of Theorem (5.16). □

Note that the results of this section are applicable to both single- and double-integrator cases.

Remark 5.5. One can question the importance of reflection prevention methods for locally stable methods. As per simulation result shows, the region of attraction can include the reflected configurations. Therefore, it is still vital for agents not to converge to the reflected formations from a practical point of view.

Remark 5.6. Since the weighting matrices are state-dependent, the energy of the agent, l_i, can be used in the input weighting matrix R_i to control the energy usage.

5.5 Simulation Results

5.5.1 2-D Space

In this subsection, the simulation results of the proposed distance-based formation control over directed triangulated Laman graphs are presented. Figure 5.1 shows the desired directed distance-based formation shape. The desired configuration is in form of a directed

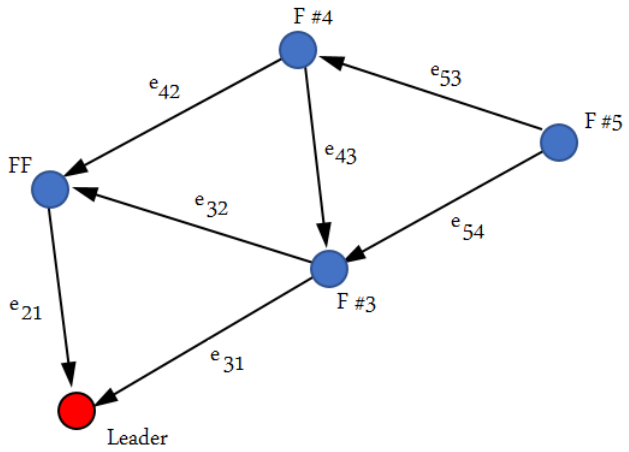

Figure 5.1: Desired distance-based formation in 2-D.

triangulated Laman graph. Note that the leader is not responsible for any edges, and thus it does not move. Figure 5.2 shows the trajectories of $N = 5$ agents modeled by single-integrator dynamics under the proposed controller. The agents are initially located at $p_1 = [-25, -5]^T, p_2 = [-29, 17]^T, p_3 = [-15, -20]^T, p_4 = [-20, 40]^T, p_5 = [5, 15]^T$.

Figure 5.3 shows how the proposed method prevents the reflection where the agent #5 was relocated to $p_5 = [-35, 45]^T$. Figure 5.3 (top) shows the controller performance without the signed area constraints. One can see that the agent #5 moves to the reflected position, which makes the configuration flip ambiguous. Figure 5.3 (bottom) shows the simulation results while the proposed method in Theorem 5.7 is utilized. The proposed controller, with signed area constraints, successfully prevents the convergence of the agent #5 to the reflected position. Figure 5.4 shows the trajectory of the set of $N = 4$ agents modeled by a double-integrator model.

5.5.2 3-D space

This subsection presents the simulation results of the proposed distance-based formation control over directed trilateral Laman graphs. Figure 2.6(b) depicts the desired directed distance-based formation shape in the form of a directed trilateral Laman graph in 3-D space. Note that the leader is not responsible for any edges.

Figure 5.5 shows the simulation results of the proposed distributed controller for a set of $N = 5$ agents. The agents initial positions were selected as $p_1 = [20, 20, 30]^T, p_2 = [20, -20, -10]^T, p_3 = [-20, -30, 20]^T, p_4 = [-10, 20, -10]^T, p_5 = [20, 20, -20]^T$. For simplicity all R_i^s were selected as identity matrices. Matrices Q_i were selected according to the Theorem 5.16 and Corollary 5.16.1 with parameters selected as $\varphi_{im} = 1$, $\zeta_{3m} = 1$, $r_{d_{im}} = 3$, and $\epsilon = 1$. The simulation result shows that all agents satisfied their assigned distance constraints.

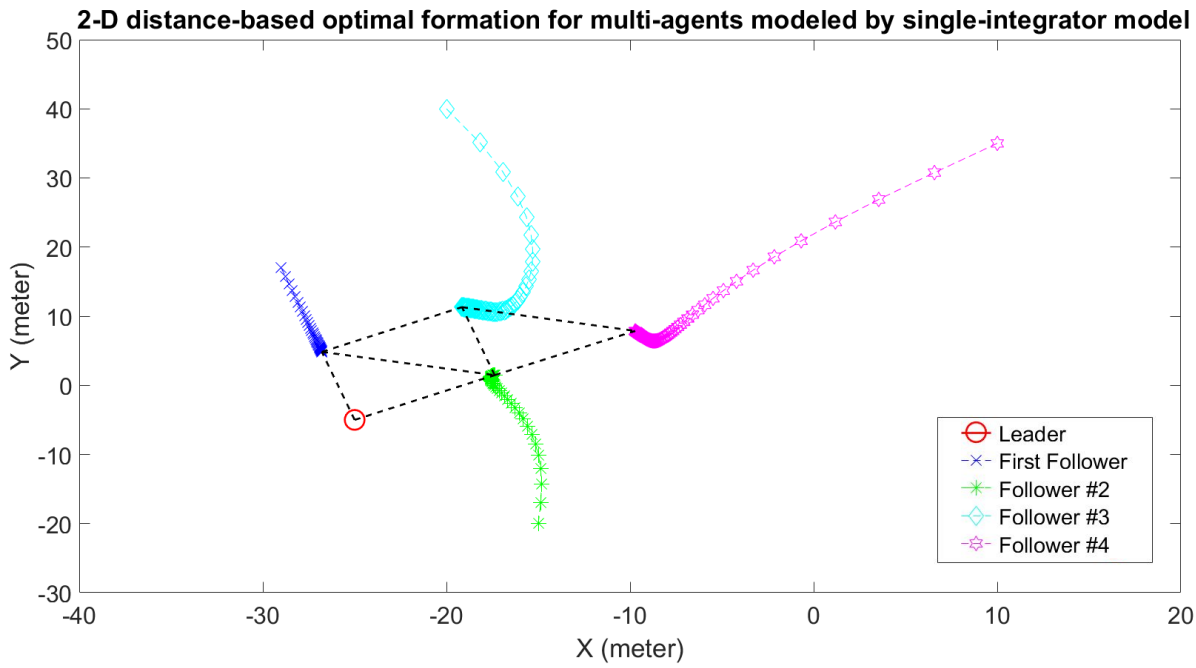

Figure 5.2: A distributed distance-based formation for $N = 5$ agents using the proposed controller. The desired formation is given in Figure 5.1.

Figure 5.6 shows the convergence of edge errors. Figure 5.7 (top) shows the controller performance without the signed volume constraints where $p_5 = [20, -20, 140]^T$ and Q_i matrices were selected as constant identity matrix. All other parameters remained unchanged. It shows that agent #5 moved to the reflected position, which makes the configuration flip ambiguous. Figure 5.7 (bottom) shows the simulation results while the proposed method in Theorem 5.16 is utilized. The simulation results show that the proposed controller, with signed volume constraints, prevented the convergence of the agent #5 to the reflected position. Figure 5.8 shows the trajectory of the set of $N = 5$ agents modeled by double-integrator model. The agents initial positions were selected as $p_1 = [20, 20, 30]^T, p_2 = [20, -20, -10]^T, p_3 = [-20, -30, 20]^T, p_4 = [5, 20, -10]^T, p_5 = [20, -20, 0]^T$. All other simulation parameters remained unchanged. The simulation results prove the effectiveness of the proposed controller.

5.5.3 Control Performance Function

In order to compare the performance of the proposed method with other methods in the literature, based on integral of the absolute magnitude of the error (IAE) criteria, we introduce the control performance function (CPF) as

$$\upsilon(t) = \frac{1}{|\mathcal{E}|} \sum_{(i,j)\in\mathcal{E}} \int_0^t |\|p_i - p_j\| - d_{ij}^*| dt + \frac{1}{|\mathcal{V}|} \sum_{i\in\mathcal{V}} \int_0^t \|u_i\| dt, \tag{5.135}$$

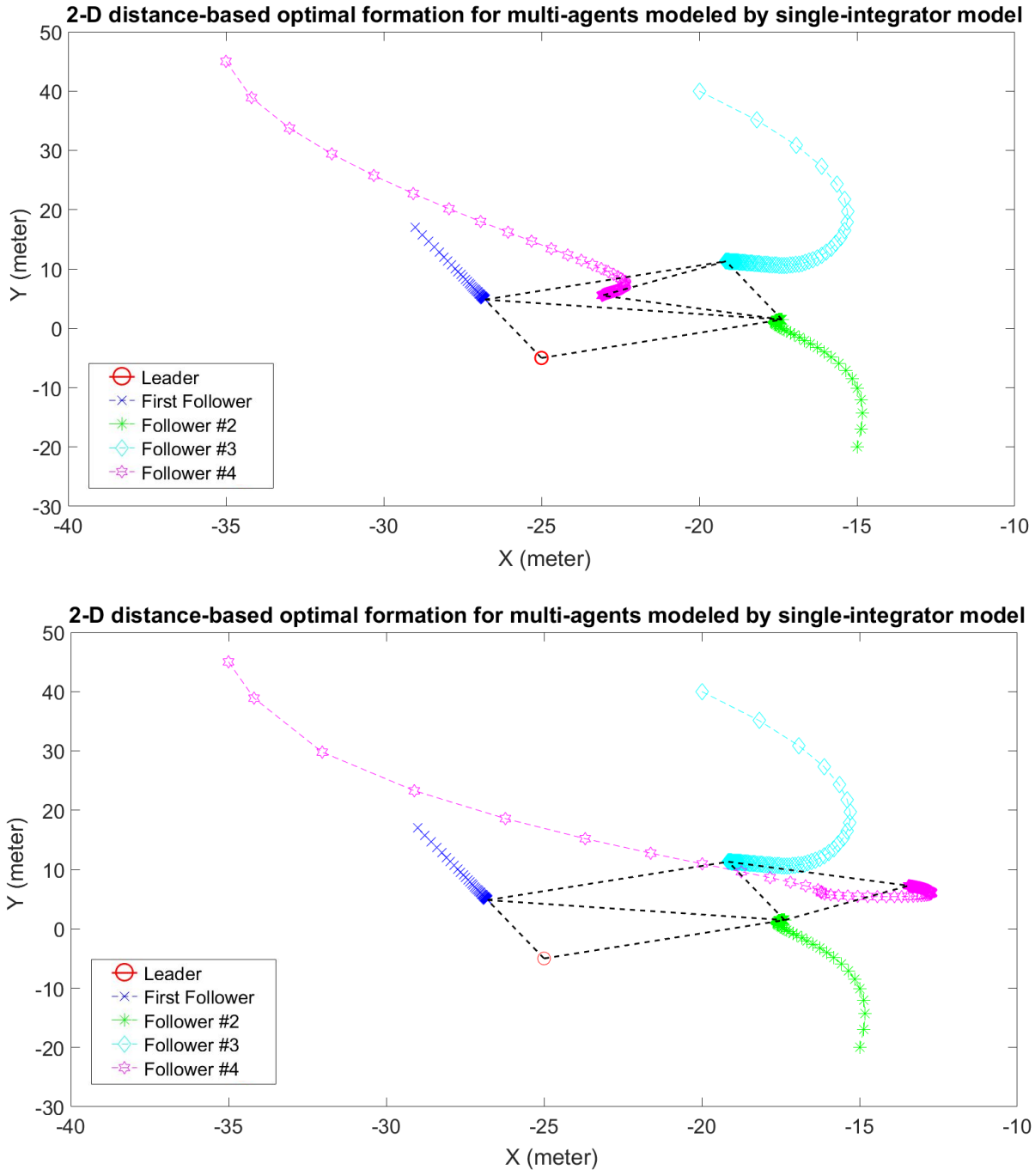

Figure 5.3: Simulation result of the proposed controller without signed area constraints (top) and with the signed area constraints that prevents flip ambiguity of the formation (bottom).

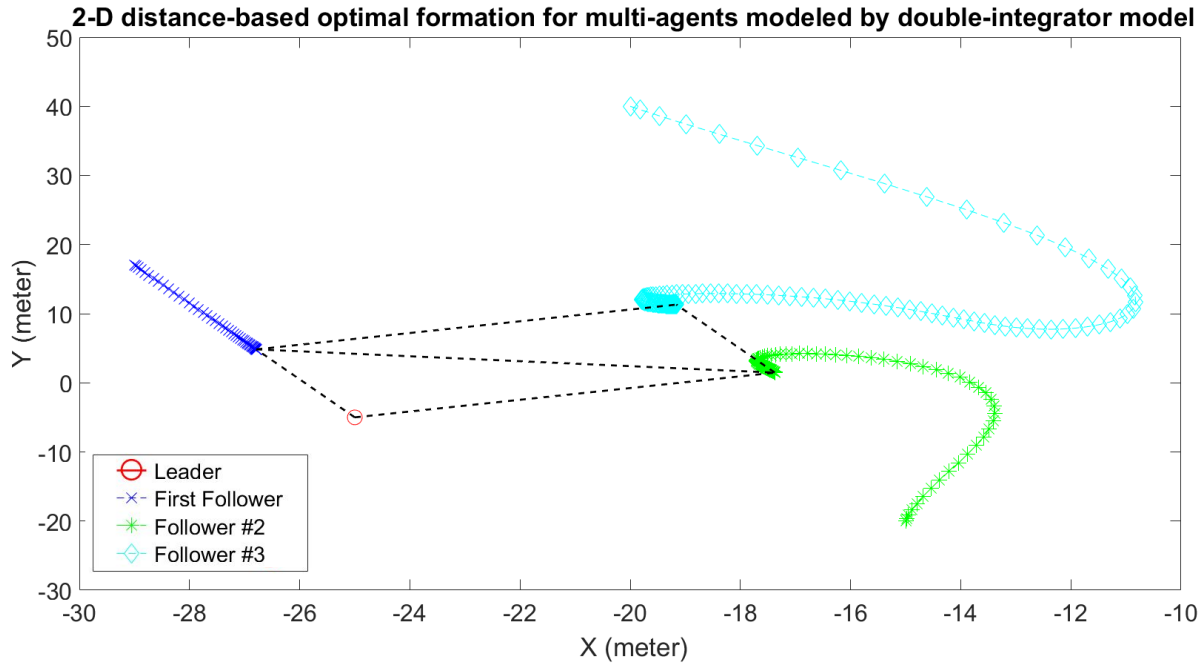

Figure 5.4: Simulation results of the proposed controller for a set of $N = 4$ agents modeled by double-integrator dynamics.

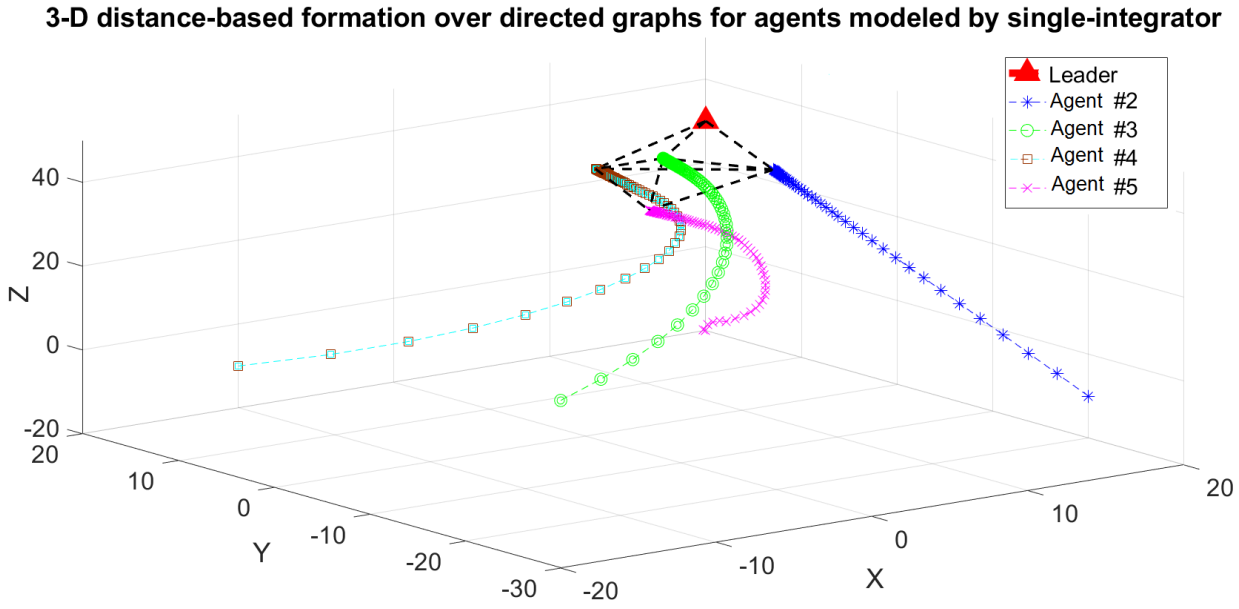

Figure 5.5: A distributed distance-based formation for $N = 5$ agents using the proposed controller. The desired formation is given in Figure 2.6 (b).

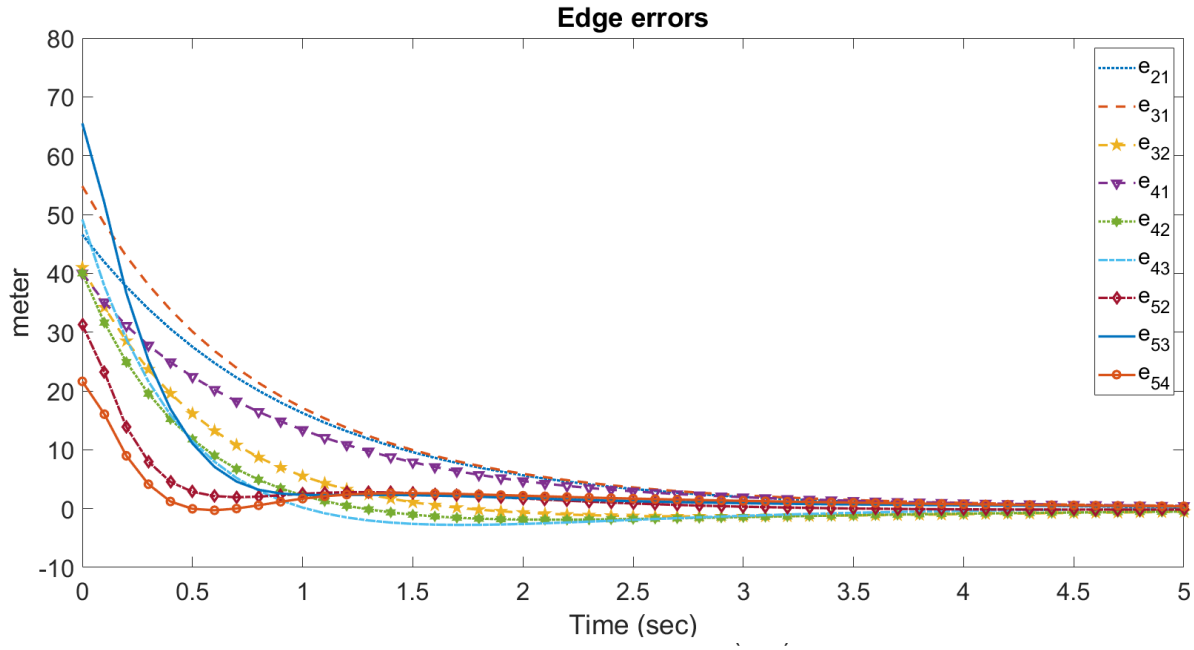

Figure 5.6: Convergence of the edge errors to zero in the simulation corresponding to Figure 5.5.

and control performance index (CPI), Υ, as $\Upsilon = \lim_{t\to\infty} \upsilon(t)$. The first term in the CPF indicates how fast the formation converges, while the second term measures how much control effort is used for the overall formation. We run simulations in 3-D space where the desired formation is given by Figure 2.6(b). The initial positions of the agents were selected as $p_1 = [2, 2, 3]^T, p_2 = [2, -2, -1]^T, p_3 = [-2, -3, 2]^T, p_4 = [1, 2, -1]^T, p_5 = [2, -2, 14]^T$ while the desired formation shape and the desired distances remained unchanged.

We implemented three different controllers: (i) the controller with our proposed method; (ii) a directed, gradient-based controller proposed in [56]; and (iii) an undirected, gradient-based controller proposed in [44]. Figure 5.9 shows the corresponding CPFs for all three methods. Also, CPIs for all simulations are presented in Table 5.1. The simulation results show that the proposed method has a better CPI compared to the other two methods. It is worth mentioning that, through extensive simulations, we found that our method is less sensitive to simulation parameters such as sampling time and initial positions of agents in comparison with the other two methods. However, the method requires more computational time. For real-time solving of the SDRE control, there are several methods proposed in literature [124].

Table 5.1: CPI for different methods

Method proposed in this chapter	Method in [56]	Method in [44]
6.15	7.67	7.86

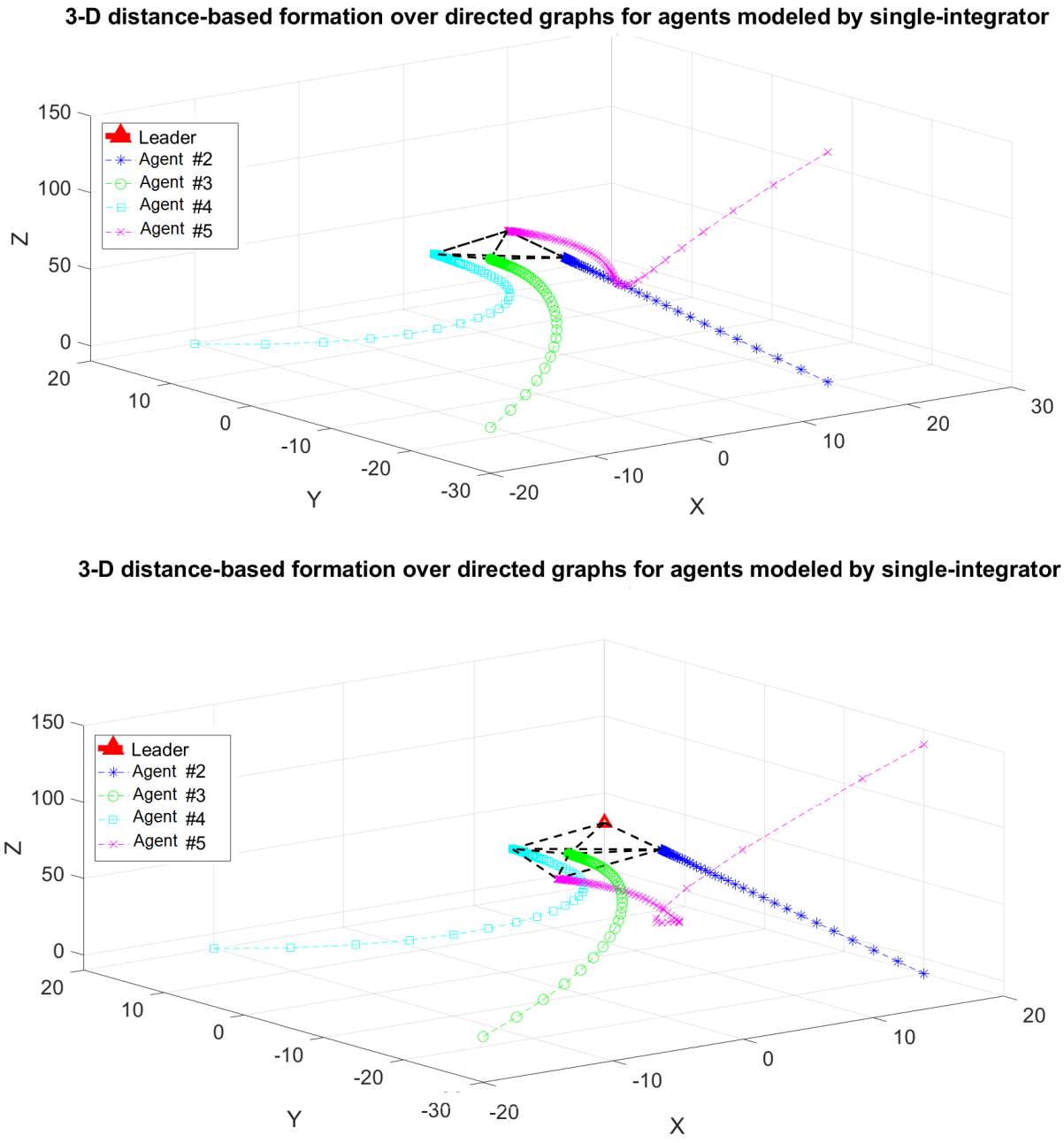

Figure 5.7: Simulation result of the proposed controller without signed volume constraints (top) and with the signed volume constraints that prevents flip ambiguity of the formation (bottom).

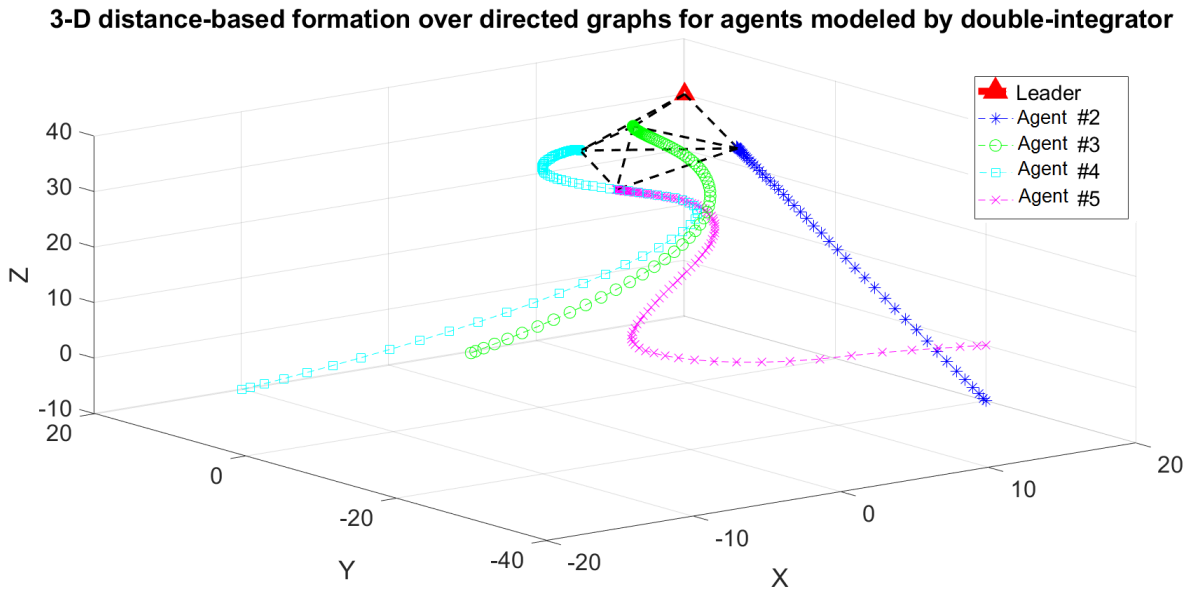

Figure 5.8: Simulation result of the proposed controller for a set of $N = 5$ agent modeled by double-integrator dynamics.

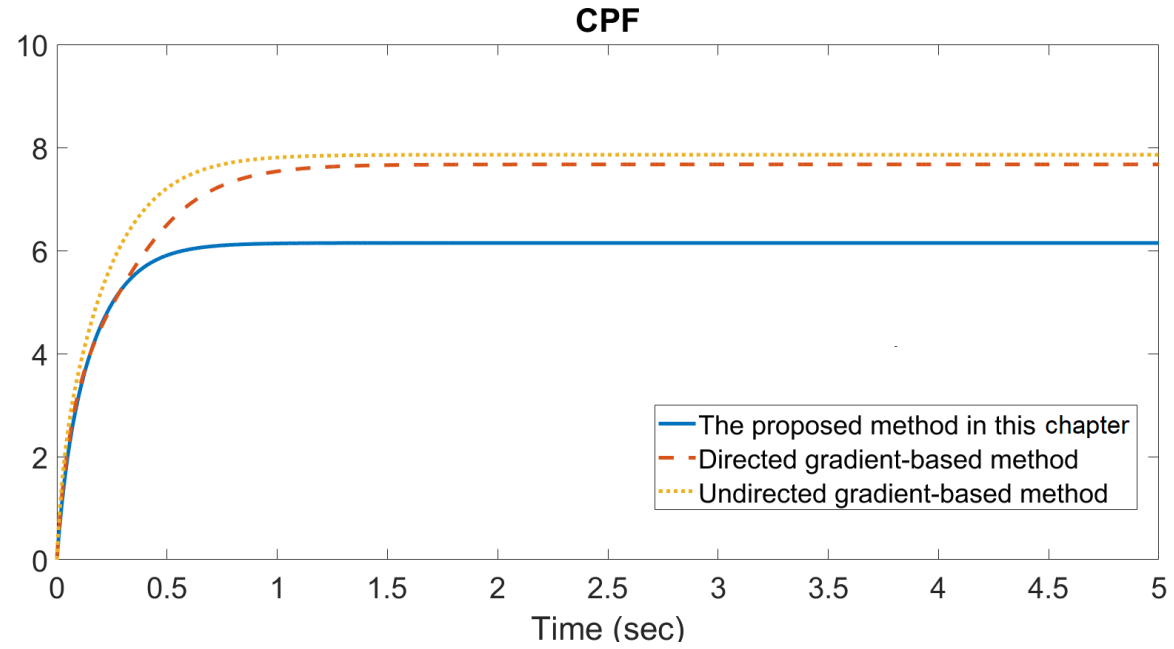

Figure 5.9: Control performance function for three different controller proposed for distance-based formation control problem.

5.6 Conclusions

In this chapter, the distributed distance-based formation control problem over directed graphs is studied. It is shown that the distance-based formation control over directed graphs has several advantages compared to the undirected graph configurations. We formulated the distance-based formation control problem for special classes of directed graphs, namely directed triangulated and trilateral Laman graphs. In this case, only one of the neighboring pair of agents is responsible for preserving the desired distance. We then developed a distributed control scheme for the distance-based formation problem. The proposed controller is based on the state-dependent Riccati equation (SDRE) method that ensures the global asymptotic stability of the desired formation for the single-integrator case.

Furthermore, an additional problem in a distance-based formation control is the existence of the reflected configurations that satisfy the distance constraints while the configuration is not the desired one. To address this issue, we introduced a method based on a barrier function that prevents such flip-ambiguous configurations. The solution also prevents collisions among neighboring agents. In addition, we introduced a novel index, called the control performance function, that measures and indicates the formation controller's overall performance.

Chapter 6

Distance-Based Formation Control of Nonlinear Agents

6.1 Introduction

Distance-based formation control is a challenging problem due to its mathematical complexity, especially in the case of nonlinear agent dynamics. We propose a distributed distance-based formation control scheme for a set of affine, nonlinear agents over a particular class of directed graphs. By using the state-dependent Riccati equation, the proposed control method can effectively cope with nonlinearities in the agent's dynamics.

The majority of the research in distance-based control considered the single-integrator model, to name a few [56], [64], [65], [42], [57], [44] and few considered the double-integrator case, e.g., [50], [62], [35]. Authors in [68] considered the second-order nonlinear dynamics where they showed the uniform ultimate boundedness of the formation. Since the practical systems have complex and nonlinear dynamics, we are motivated to study distance-based formation control of nonlinear agents. This chapter's main contribution is a new, distributed, distance-based formation control for a set of agents with affine, nonlinear models where the desired topology is a directed triangulated or trilateral Laman graph.

6.2 Nonlinear Homogeneous Agents in 2-D Space

For a set of nonlinear agents, the distance-based formation control problem is to find distributed control signals such that agents converge to the desired framework asymptotically. In other words, all the desired distance constraints between pairs of agents are required to be satisfied. In this section, we assign the responsibility of controlling a distance between two agents to one of them (the source of the corresponding edge). Thus, the desired topology is modeled as a digraph. In particular, we assume that the

desired topology is a directed triangulated Laman graph.

6.2.1 Agent Model

Suppose that each agent is described by an affine nonlinear model

$$\dot{x} = f(x) + B(x)u, \tag{6.1}$$

where functions $f(.)$ and $B(.)$ are C^1 and C^0 mappings, respectively. Agents' states vector can be written as $x = [p^T, v^T, z^T]^T$ where p, v, and z are agents' position, velocity, and the vector of other states, respectively. Therefore, (6.1) can be rewritten as

$$\dot{p} = v \tag{6.2a}$$
$$\dot{v} = \hat{f}(v, z) + \hat{B}(v, z)u \tag{6.2b}$$
$$\dot{z} = \check{f}(v, z) + \check{B}(v, z)u. \tag{6.2c}$$

The agent's model (6.2) can be written in a linear-like form as

$$\dot{x} = A(x)x + B(x)u. \tag{6.3}$$

Assumption 6.1: For an agent described by (6.3), corresponding pairs $\{A(x), B(x), \sqrt{Q(x)}\}$, where $Q(x)$ is associated weighting factor in SDRE problem, are point-wise stabilizable and detectable in linear sense for all x in some nonempty neighborhood of the origin.

Remark 6.1. For a general system (6.3), Assumption 6.1 is a common assumption in literature [123], [124], [153]. By selecting a positive definite state weighting matrix $Q(x)$, detectability of the pair$\{A(x), C(x)\}$ is assured. Hence, the stabilizability of the pair $\{A(x), B(x)\}$ greatly depends on the selection of SDC matrices [134]. Reference [154] proves that there always exists a stablizable and detectable SDC representation of the system (6.1) if $\{x, f(x)\}$ be linearly independent or $C(x)x \neq 0$. Therefore, by proper selection of $Q(x)$ we can guarantee the existence of such a stablizable and detectable SDC representation.

For agent i, the relative position of its neighboring agents is

$$p_{ij}^{\Sigma^i} = p_i^{\Sigma^i} - p_j^{\Sigma^i}, \quad i \in \mathcal{N}_i \tag{6.4}$$

where Σ^i is the local coordinate system of the agent i. Since all measurements are in agents' local coordinate systems, we drop the Σ^i notation for simplification. Thus, the corresponding distance between agent i and agent j is

$$d_{ij} = \|p_{ij}\|. \tag{6.5}$$

The error of the edge between agent i and agent j is

$$e_{ij} = d_{ij} - d^*_{ij}, \tag{6.6}$$

where d^*_{ij} is the desired distance between agent i and agent j. The edge error dynamics is then given by

$$\begin{aligned} \dot{e}_{ij} &= \frac{d}{dt}\sqrt{(p_i - p_j)^T(p_i - p_j)} \\ &= \frac{(p_{ij})^T(\dot{p}_i - \dot{p}_j)}{p_{ij}}. \end{aligned} \tag{6.7}$$

Since the desired topology is in form of a directed triangulated Laman graph, the leader will remains stationary. The first-follower (agent #2) has one distance constraints to satisfy, i.e. edge e_{21}. Dynamics of the edge associated with agent #2 is

$$\dot{e}_{21} = \frac{p_{21}^T}{\|p_{21}\|} v_2. \tag{6.8}$$

Let us define the normalizing operator, also known as relative bearing, as $\eta(p_{ij}) = \frac{p_{ij}^T}{\|p_{ij}\|}$. The aggregate error vector for the agent #2 is

$$\dot{\mathbf{e}}_2 = [e_{21}, v_2^T, z_2^T]^T. \tag{6.9}$$

Therefore, the time-derivative of (6.9) is

$$\dot{e}_{21} = \eta(p_{21})v_2 \tag{6.10a}$$
$$\dot{v}_2 = \hat{f}_2(v_2, z_2) + \hat{B}_2(v_2, z_2)u_2 \tag{6.10b}$$
$$\dot{z}_2 = \check{f}_2(v_2, z_2) + \check{B}_2(v_2, z_2)u_2. \tag{6.10c}$$

We can write (6.10) in a semi-linear form as

$$\dot{\mathbf{e}}_2 = A_2\mathbf{e}_2 + B_2u_2. \tag{6.11}$$

Now we can define the distance-based control problem as a nonlinear optimal control

problem. The associated SDRE problem with agent #2 is

$$
\begin{aligned}
J_2 = \min & \frac{1}{2}\int_0^\infty \{\mathbf{e}_2{}^T Q_2 \mathbf{e}_2 + u_2{}^T R_2 u_2\} dt \\
& \text{s.t.} \\
& \dot{\mathbf{e}}_2 = A_2 \mathbf{e}_2 + B_2 u_2 \\
& Q_2 \geq 0 \\
& R_2 > 0.
\end{aligned}
\tag{6.12}
$$

The following theorem introduces the control law that is the solution of the SDRE problem (6.12). The control law ensures that e_{21} asymptotically converges to zero.

Theorem 6.1. *For agent #2 modeled with nonlinear dynamics (6.2), under Assumption 6.1, the SDRE control law*

$$u_2 = -R_2{}^{-1} B_2{}^T S_2 \boldsymbol{e}_2, \tag{6.13}$$

where S_2 is the positive definite solution of the following Riccati equation

$$Q_2 + A_2{}^T S_2 + S_2 A_2 - S_2 B_2 R_2{}^{-1} B_2{}^T S_2 = 0, \tag{6.14}$$

steers formation error $\boldsymbol{e}_2$ to zero and results in asymptotic stability of the closed-loop system.

Proof. The proof of the theorem is straightforward result of Lemma 2.9. □

Remark 6.2. Substituting the control law (6.13) in (6.11), the closed-loop dynamic is

$$\dot{\mathbf{e}}_2 = (A_2 - B_2 R_2{}^{-1} B_2{}^T S_2)\mathbf{e}_2. \tag{6.15}$$

The next follower, agent #3, is responsible for controlling its distance with the leader e_{31} and first-follower e_{32}. Therefore, for agent #3 we define $\mathbf{e}_3 = [e_{31}, e_{32}, v_3^T, z_3^T]^T$. Then, one has

$$\dot{e}_{31} = \eta(p_{31}) v_3 \tag{6.16a}$$
$$\dot{e}_{32} = \eta(p_{32})(v_3 - v_2) \tag{6.16b}$$
$$\dot{v}_3 = \hat{f}_3(v_3, z_3) + \hat{B}_3(v_3, z_3) u_3 \tag{6.16c}$$
$$\dot{z}_3 = \check{f}_3(v_3, z_3) + \check{B}_3(v_3, z_3) u_3. \tag{6.16d}$$

System (6.16) can be written in a linear-like matrix form

$$\dot{\mathbf{e}}_3 = A_3 \mathbf{e}_3 + \tilde{B}_3 \mathbf{u}_3, \tag{6.17}$$

where $\mathbf{u}_3 = [v_2, u_3]$. Suppose that the system is unforced with respect to v_2, ($v_2 = 0$),

then the nominal system is

$$\dot{e}_{31} = \eta(p_{31})v_3 \tag{6.18a}$$
$$\dot{e}_{32} = \eta(p_{32})v_3 \tag{6.18b}$$
$$\dot{v}_3 = \hat{f}_3(v_3, z_3) + \hat{B}_3(v_3, z_3)u_3 \tag{6.18c}$$
$$\dot{z}_3 = \check{f}_3(v_3, z_3) + \check{B}_3(v_3, z_3)u_3, \tag{6.18d}$$

where it can be written in linear-like form as

$$\dot{\mathbf{e}}_3 = A_3\mathbf{e}_3 + B_3u_3. \tag{6.19}$$

The distance-based formation control for agent #3 now can be stated as an SDRE problem. We can write the associated nominal optimal control problem for the agent #3 as

$$\begin{aligned} J_3 = \min & \frac{1}{2}\int_0^\infty \{{\mathbf{e}_3}^T Q_3\mathbf{e}_3 + {u_3}^T R_3u_3\}dt \\ & \text{s.t.} \\ & \dot{\mathbf{e}}_3 = A_3\mathbf{e}_3 + B_3u_3 \\ & Q_3 \geq 0 \\ & R_3 > 0. \end{aligned} \tag{6.20}$$

The following theorem provides the SDRE control law that is the solution of the optimal control problem (6.20). The proposed control law guarantees the asymptotic convergence of $\mathbf{e}_3$ to zero and asymptotic stability of the LFF formation.

Theorem 6.2. *For the agent #3 described by the nonlinear affine model (6.2), under Assumption 6.1, the SDRE control law*

$$u_3 = -{R_3}^{-1}{B_3}^T S_3\boldsymbol{e}_3, \tag{6.21}$$

where S_3 is the positive definite solution of the following state-dependent Riccati equation

$$Q_3 + {A_3}^T S_3 + S_3A_3 - S_3B_3{R_3}^{-1}{B_3}^T S_3 = 0, \tag{6.22}$$

drives $\boldsymbol{e}_3$ asymptotically to zero and guarantees local asymptotic stability of the origin of the closed-loop LFF system.

Proof. The control law (6.21) results in asymptotic stability of system $\dot{\mathbf{e}}_3 = f_3(\mathbf{e}_3, 0)$. Since $v_2 = [0\ 1_n\ \mathbf{0}]\mathbf{e}_2$ and according to Theorem 2.4, this implies local input-to-state stability of the system $\dot{\mathbf{e}}_3 = f_3(\mathbf{e}_3, \mathbf{e}_2)$ with respect to $\mathbf{e}_2$. Also, Theorem 6.1 ensures

asymptotically stability of the origin of the system $\dot{\mathbf{e}}_2 = f_2(\mathbf{e}_2)$. Therefore, according to Theorem 2.7 we can conclude that the origin of the LFF system

$$\begin{aligned} \dot{\mathbf{e}}_2 &= f_2(\mathbf{e}_2) \\ \dot{\mathbf{e}}_3 &= f_3(\mathbf{e}_3, \mathbf{e}_2), \end{aligned} \tag{6.23}$$

is locally asymptotically stable. □

For the desired signed area $\mathbb{A}_3^*$ and the actual signed area $\mathbb{A}_3$ of the triangle, formed by the agents $(1, 2, 3)$, let us define the LFF signed area coefficient κ_3 as follows:

$$\kappa_3 = \frac{\mathbb{A}_3^* - \mathbb{A}_3}{\mathbb{A}_3^* + \mathbb{A}_3}. \tag{6.24}$$

The formation edge weighting factors q_{3m}, $m \in \{1, 2\}$, are given by

$$q_{3m} = \varrho_{3m} + \mu_{3m}, \tag{6.25}$$

where ϱ_{3m} is a positive constant. We propose the positive barrier multiplier given by

$$\mu_{3m} = \left(\frac{d_{3m}^*}{d_{3m} - r_{d_{3m}}}\right)^{\epsilon}, \tag{6.26}$$

where $\epsilon \geq 1$, and $r_{d_{3m}}$ is a safe distance that prevents collisions between agent #3 and agent #m, $m \in \{1, 2\}$. Also, q_{v_3} and q_{z_3} are appropriate positive definite weighting matrices corresponding to v_3 and z_3.

Corollary 6.2.1. *For the SDRE problem (6.20), the state weighting matrix*

$$Q_3 = \kappa_3 diag[q_{31}, q_{32}, q_{v_3}, q_{z_3}], \tag{6.27}$$

ensures that the proposed SDRE control law (6.21) prevents flip ambiguity of the directed distance-based LFF formation and guarantees inter-agent collision avoidance.

Proof. The proposed state weighting matrix (6.27) is an integrated barrier function for the optimal control (6.20). The weighting matrix Q_3 approaches infinity if the collision avoidance condition or signed area condition are violated. Thus, based on the method proposed in [147], we conclude that the control law prevents collision avoidance of agent #3 with the leader and the first-follower. Also, it prevents agent #3 from converging to the reflected position. □

The topology of the desired formation is assumed to be a directed triangulated Laman graph. As shown in Figure 2.5(b), the next follower, say agent i, is added to an existing directed triangulated Laman graph via Henneberg directed vertex addition sequence.

Therefore, the agent i connects to pre-existing agents j and k using two outgoing edges e_{ij} and e_{ik}. The aggregate error vector of agent i is $\mathbf{e}_i = [e_{ij}, e_{ik}, {v_i}^T, {z_i}^T]^T$ and the error dynamics can be written as

$$\dot{e}_{ij} = \eta(p_{ij})(v_i - v_j) \tag{6.28a}$$
$$\dot{e}_{ik} = \eta(p_{ik})(v_i - v_k) \tag{6.28b}$$
$$\dot{v}_i = \hat{f}_i(v_i, z_i) + \hat{B}_i(v_i, z_i)u_i \tag{6.28c}$$
$$\dot{z}_i = \check{f}_i(v_i, z_i) + \check{B}_i(v_i, z_i)u_i. \tag{6.28d}$$

The system (6.28) can be rewritten in a linear-like form

$$\dot{\mathbf{e}}_i = A_i\mathbf{e}_i + \tilde{B}_i\mathbf{u}_i, \tag{6.29}$$

where $\mathbf{u}_i = [{v_j}^T, {v_k}^T, {u_i}^T]^T$. The corresponding unforced nominal system is

$$\dot{e}_{ij} = \eta(p_{ij})v_i \tag{6.30a}$$
$$\dot{e}_{ik} = \eta(p_{ik})v_i \tag{6.30b}$$
$$\dot{v}_i = \hat{f}_i(v_i, z_i) + \hat{B}_i(v_i, z_i)u_i \tag{6.30c}$$
$$\dot{z}_i = \check{f}_i(v_i, z_i) + \check{B}_i(v_i, z_i)u_i, \tag{6.30d}$$

or in a linear-like form

$$\dot{\mathbf{e}}_i = A_i\mathbf{e}_i + B_iu_i. \tag{6.31}$$

The desired directed distance-based formation control problem for the agent i can be formulated as an SDRE optimal control problem:

$$\begin{aligned} J_i = \min & \frac{1}{2}\int_0^\infty \{{\mathbf{e}_i}^T Q_i\mathbf{e}_i + {u_i}^T R_iu_i\}dt \\ & \text{s.t.} \\ & \dot{\mathbf{e}}_i = A_i\mathbf{e}_i + B_iu_i \\ & Q_i \geq 0 \\ & R_i > 0. \end{aligned} \tag{6.32}$$

Theorem 6.3. *For the agent i that is described by the nonlinear model (6.2), under Assumption 6.1, the distributed SDRE control law*

$$u_i = -{R_i}^{-1}{B_i}^T S_i\boldsymbol{e}_i, \tag{6.33}$$

where S_i is the unique, symmetric, positive definite solution of the Riccati equation

$$Q_i + {A_i}^T S_i + S_i A_i - S_i B_i {R_i}^{-1} {B_i}^T S_i = 0, \tag{6.34}$$

steers $\boldsymbol{e}_i$ asymptotically to zero and ensures convergence of the desired formation.

Proof. The control law (6.33) is a stabilizing control of the unforced system (6.31). Thus, based on Theorem 2.4, the system (6.29) is locally ISS with respect to $v_j = [0\ 0\ 1_n\ \mathbf{0}]\mathbf{e}_j$ and $v_k = [0\ 0\ 1_n\ \mathbf{0}]\mathbf{e}_k$. Using the mathematical induction, one can show that the system made of previous $1, 2, ..., i-1$ agents is asymptotically stable. Thus, based on Theorem 2.7 the origin of the system

$$\begin{aligned} \dot{\mathbf{e}}_2 &= f_2(\mathbf{e}_2) \\ \dot{\mathbf{e}}_3 &= f_3(\mathbf{e}_3, \mathbf{e}_2) \\ &\vdots \\ \dot{\mathbf{e}}_i &= f_i(\mathbf{e}_i, ..., \mathbf{e}_2), \end{aligned} \tag{6.35}$$

is locally asymptotically stable. □

Let $r_{d_{im}}$ be a safe distance that prevents collision between the agents i and m, $m \in \{j, k\}$. Thus, collision avoidance constraint can be stated as

$$d_{im} > r_{d_{im}}. \tag{6.36}$$

For a triangle that is associated with agent i and formed between the agents (i, j, k), the desired and actual signed areas of the triangle are denoted by $\mathbb{A}_i^*$ and $\mathbb{A}_i$, respectively. Therefore, the reflection prevention can be stated as a constraint

$$\mathbb{A}_i(T_f) = \mathbb{A}_i^*, \tag{6.37}$$

where $\mathbb{A}_i(T_f)$ is a signed area of the triangle at final time $T_f \to \infty$. To address reflection and collision avoidance problems, the constraints (6.36) and (6.37) are added to the nonlinear optimal control problem (6.32). We use the inverse barrier function method, proposed in [147], to solve the obtained constrained SDRE problem.

Let us define the agent i's signed area coefficient as

$$\kappa_i = \frac{\mathbb{A}_i^* - \mathbb{A}_i}{\mathbb{A}_i^* + \mathbb{A}_i}. \tag{6.38}$$

The formation edge weighting factors for the agent i are given by

$$q_{im} = \varrho_{im} + \mu_{im} \quad m \in \{j, k\}, \tag{6.39}$$

where ϱ_{im} is a positive constant and μ_{im} is a positive barrier multiplier given by

$$\mu_{im} = (\frac{d^*_{im}}{d_{im} - r_{d_{im}}})^{\epsilon}. \tag{6.40}$$

Similarly, q_{v_i} and q_{z_i} are appropriate positive definite state weighting matrices.

Corollary 6.3.1. *For the SDRE problem (6.32), selecting the state weighting matrix*

$$Q_i = \kappa_i diag[q_{ij}, q_{ik}, q_{v_i}, q_{z_i}], \tag{6.41}$$

ensures that the proposed SDRE control law (6.33) prevents flip ambiguity of the directed triangulated distance-based formation and guarantees collision avoidance among the neighboring agents.

Proof. The barrier function

$$\Phi_i = \mathbf{e}_i^T Q_i \mathbf{e}_i, \tag{6.42}$$

approaches infinity if the conditions for collision avoidance and/or reflection avoidance are violated. Thus, based on [147], it prevents flip ambiguity and collision between neighboring agents. □

6.3 Nonlinear Heterogeneous Agents in 3-D Space

We present here a distance-based formation control over directed graphs in 3-D space. The desired topology is assumed to be given in the form of a directed trilateral Laman graph. Each agent is assumed to have access to the relative positions of its neighbors in the agent's own local coordinate system and the agent's states, excluding its own position in the global coordinate frame.

6.3.1 Agent Model

Suppose that each agent is described by an affine nonlinear model

$$\dot{x}_i = f_i(x_i) + h_i(x_i)u_i, \tag{6.43}$$

where functions f_i, h_i are C^1, C^0 mappings, respectively. For the formation control purposes, it is necessary that the state vector includes the agent's position p_i. Therefore, the agent's model can be written as

$$\dot{p}_i = v_i \tag{6.44a}$$
$$\dot{v}_i = \hat{f}_i(v_i, w_i) + \hat{h}_i(v_i, w_i)u_i \tag{6.44b}$$
$$\dot{w}_i = \check{f}_i(v_i, w_i) + \check{h}_i(v_i, w_i)u_i, \tag{6.44c}$$

where v_i is the velocity of the agent and w_i is the vector of other states. The agent's model (6.43) can be written in a linear-like form as

$$\dot{x}_i = \tilde{A}_i(x_i)x_i + \tilde{B}_i(x_i)u_i, \tag{6.45}$$

where $x_i = [p_i^T, v_i^T, w_i^T]^T$ is the state vector of the agent i and $\tilde{B}_i(x_i) = h_i(x_i)$.

The relative position of neighboring agents is

$$p_{ij} = p_i - p_j, \quad (i,j) \in \mathcal{E}. \tag{6.46}$$

Thus, the distance between the pair of adjacent agents is

$$d_{ij} = \|p_{ij}\|. \tag{6.47}$$

The edge error is given by

$$e_{ij} = d_{ij} - d_{ij}^*, \tag{6.48}$$

where d_{ij}^* is the desired distance between agent i and agent j. The edge error dynamics is given by

$$\begin{aligned} \dot{e}_{ij} &= \frac{d}{dt}\sqrt{(p_i - p_j)^T(p_i - p_j)} \\ &= \frac{(p_{ij})^T(\dot{p}_i - \dot{p}_j)}{d_{ij}}. \end{aligned} \tag{6.49}$$

In a directed trilateral Laman topology, the leader is stationary since it has no constraint to satisfy. The first follower (agent #2) is assigned the edge (e_{21}) to control. Thus, the dynamics of the edge associated with agent #2 is

$$\dot{e}_{21} = \frac{p_{21}^T}{\|p_{21}\|}v_2. \tag{6.50}$$

The aggregate error vector for the agent #2 is

$$\mathbf{e}_2 = [e_{21}, v_2^T, w_2^T]^T. \tag{6.51}$$

The time-derivative of (6.51) is given by

$$\dot{e}_{21} = \eta(p_{21})v_2 \tag{6.52a}$$

$$\dot{v}_2 = \hat{f}_2(v_2, w_2) + \hat{h}_2(v_2, w_2)u_2 \tag{6.52b}$$

$$\dot{w}_2 = \check{f}_2(v_2, w_2) + \check{h}_2(v_2, w_2)u_2. \tag{6.52c}$$

We can write (6.52) in a semi-linear form as

$$\dot{\mathbf{e}}_2 = A_2\mathbf{e}_2 + B_2u_2. \tag{6.53}$$

Thus, the associated local optimal control problem with agent #2 is given by

$$\begin{aligned} J_2 = \min & \frac{1}{2}\int_0^\infty \{\mathbf{e}_2{}^T Q_2\mathbf{e}_2 + u_2{}^T R_2 u_2\}dt \\ & \text{s.t.} \\ & \dot{\mathbf{e}}_2 = A_2\mathbf{e}_2 + B_2u_2 \\ & Q_2 \geq 0 \\ & R_2 > 0. \end{aligned} \tag{6.54}$$

The following result provides the suboptimal SDRE control law that minimizes (6.54) and ensures that e_{21} asymptotically converges to zero.

Theorem 6.4. *For the agent #2 described by the nonlinear affine model (6.43) under Assumption 6.1, the control law*

$$u_2 = -R_2{}^{-1}B_2{}^T S_2\boldsymbol{e}_2, \tag{6.55}$$

where S_2 is the solution of the following Riccati equation

$$Q_2 + A_2{}^T S_2 + S_2A_2 - S_2B_2R_2{}^{-1}B_2{}^T S_2 = 0, \tag{6.56}$$

renders the origin of the closed-loop system asymptotically stable and steers agent #2 to the desired position; hence, e_{21} converges to zero.

Proof. Given Assumption 6.1, the proof of the theorem is straightforward result of Lemma 2.9. □

Remark 6.3. Substituting the control law (6.55) in (6.53), the closed-loop dynamics is

$$\Delta_2: \quad \dot{\mathbf{e}}_2 = (A_2 - B_2R_2{}^{-1}B_2{}^T S_2)\mathbf{e}_2. \tag{6.57}$$

For the agent #3, we define $\mathbf{e}_3 = [e_{31}, e_{32}, v_3^T, w_3^T]^T$. Thus, one has

$$\dot{e}_{31} = \eta(p_{31})v_3 \tag{6.58a}$$
$$\dot{e}_{32} = \eta(p_{32})(v_3 - v_2) \tag{6.58b}$$
$$\dot{v}_3 = \hat{f}_3(v_3, w_3) + \hat{h}_3(v_3, w_3)u_3 \tag{6.58c}$$
$$\dot{w}_3 = \check{f}_3(v_3, w_3) + \check{h}_3(v_3, w_3)u_3. \tag{6.58d}$$

The equation (6.58) can be written in the matrix form

$$\Xi_3: \quad \dot{\mathbf{e}}_3 = \hat{A}_3\mathbf{e}_3 + \hat{B}_3\mathbf{u}_3, \tag{6.59}$$

where $\mathbf{u}_3 = [v_2, u_3]$. Suppose that the system is unforced with respect to v_2, the nominal system is

$$\dot{e}_{31} = \eta(p_{31})v_3 \tag{6.60a}$$
$$\dot{e}_{32} = \eta(p_{32})v_3 \tag{6.60b}$$
$$\dot{v}_3 = \hat{f}_3(v_3, w_3) + \hat{h}_3(v_3, w_3)u_3 \tag{6.60c}$$
$$\dot{w}_3 = \check{f}_3(v_3, w_3) + \check{h}_3(v_3, w_3)u_3, \tag{6.60d}$$

and it can be written in a linear-like form as

$$\Sigma_3: \quad \dot{\mathbf{e}}_3 = A_3\mathbf{e}_3 + B_3u_3. \tag{6.61}$$

One can write the associated nominal optimal control problem for the agent #3 as

$$\begin{aligned} J_3 = \min & \frac{1}{2}\int_0^\infty \{\mathbf{e}_3{}^T Q_3 \mathbf{e}_3 + u_3{}^T R_3 u_3\} dt \\ & \text{s.t.} \\ & \dot{\mathbf{e}}_3 = A_3\mathbf{e}_3 + B_3u_3 \\ & Q_3 \geq 0 \\ & R_3 > 0. \end{aligned} \tag{6.62}$$

The following theorem provides the control law that guarantees the asymptotic stability of the closed-loop system's origin and, consequently, the asymptotic convergence of $\mathbf{e}_3$ to zero.

Theorem 6.5. *For the agent #3, described by the nonlinear affine model (6.43), under Assumption 6.1, the control law*

$$u_3 = -R_3{}^{-1}B_3{}^T S_3 \boldsymbol{e}_3, \tag{6.63}$$

where S_3 is the positive definite solution of the following state-dependent Riccati equation

$$Q_3 + A_3{}^T S_3 + S_3 A_3 - S_3 B_3 R_3{}^{-1} B_3{}^T S_3 = 0, \tag{6.64}$$

achieves local asymptotic stability of the origin of the closed-loop system, hence the desired distance-based formation.

Proof. The origin of the system $\Delta_2: \quad \dot{\mathbf{e}}_2 = f_2(\mathbf{e}_2)$ is asymptotically stable. Given

Assumption 6.1, the control law (6.63) results in an asymptotic stability of the system $\Sigma_3 : \dot{\mathbf{e}}_3 = f_3(\mathbf{e}_3, 0)$. Thus, the system $\Xi_3 : \dot{\mathbf{e}}_3 = f_3(\mathbf{e}_3, \mathbf{e}_2)$ is locally input-to-state stable. Based on Theorem 2.7, we conclude that the origin of the interconnected system

$$\Delta_3 : \begin{cases} \dot{\mathbf{e}}_2 = f_2(\mathbf{e}_2) \\ \dot{\mathbf{e}}_3 = f_3(\mathbf{e}_3, \mathbf{e}_2), \end{cases} \tag{6.65}$$

is locally asymptotically stable. □

Corollary 6.5.1. *Let us select*

$$Q_3 = \kappa_3 diag[q_{31}, q_{32}, q_{v_3}, q_{w_3}], \tag{6.66}$$

where

$$\kappa_3 = \frac{\mathbb{A}^* - \mathbb{A}}{\mathbb{A}^* + \mathbb{A}}, \tag{6.67}$$

and $\mathbb{A}^*$ and $\mathbb{A}$ are desired and actual signed area of the triangle between the agents $(1, 2, 3)$, and

$$q_{3m} = \kappa_{3m} + \mu_{3m} \quad m \in \{1, 2\}, \tag{6.68}$$

where κ_{3m} is a positive constant and μ_{3m} is a positive barrier multiplier defined by

$$\mu_{3m} = (\frac{d^*_{3m}}{d_{3m} - r_{d_{3m}}})^{\epsilon}, \tag{6.69}$$

for suitable $\epsilon \geq 1$, and $r_{d_{3m}}$ being a safe distance between pair of agents to prevent collision. Also, q_{v_3} and q_{w_3} are appropriate positive definite matrices. Then, by using the weighting factor (6.66), the proposed SDRE control law (6.63) guarantees an inter-agent collision avoidance and prevents a flip ambiguity of the agent #3 in the directed, distance-based formation.

Proof. The weighting matrix Q_3 approaches infinity if the collision avoidance condition or signed area condition are violated. Thus, based on the method proposed in [147], we conclude that the SDRE control law prevents the collision of agent #3 with the leader and the first-follower. Moreover, it prevents agent #3 from converging to the reflected position. □

For the agent #4, the aggregate error vector is $\mathbf{e}_4 = [e_{41}, e_{42}, e_{43}, {v_4}^T, {w_4}^T]$. The

formation error dynamics can be written as

$$\dot{e}_{41} = \eta(p_{41})v_4 \tag{6.70a}$$
$$\dot{e}_{42} = \eta(p_{42})(v_4 - v_2) \tag{6.70b}$$
$$\dot{e}_{43} = \eta(p_{43})(v_4 - v_3) \tag{6.70c}$$
$$\dot{v}_4 = \hat{f}_4(v_4, w_4) + \hat{h}_4(v_4, w_4)u_4 \tag{6.70d}$$
$$\dot{w}_4 = \check{f}_4(v_4, w_4) + \check{h}_4(v_4, w_4)u_4. \tag{6.70e}$$

It can also be written in a matrix form as

$$\Xi_4 : \dot{\mathbf{e}}_4 = \hat{A}_4\mathbf{e}_4 + \hat{B}_4\mathbf{u}_4, \tag{6.71}$$

where $\mathbf{u}_4 = [{v_2}^T, {v_3}^T, {u_4}^T]^T$. The corresponding unforced nominal system is

$$\dot{e}_{41} = \eta(p_{41})v_4 \tag{6.72a}$$
$$\dot{e}_{42} = \eta(p_{42})v_4 \tag{6.72b}$$
$$\dot{e}_{43} = \eta(p_{43})v_4 \tag{6.72c}$$
$$\dot{v}_4 = \hat{f}_4(v_4, w_4) + \hat{h}_4(v_4, w_4)u_4 \tag{6.72d}$$
$$\dot{w}_4 = \check{f}_4(v_4, w_4) + \check{h}_4(v_4, w_4)u_4, \tag{6.72e}$$

and can be written in the linear-like form as

$$\Sigma_4 : \dot{\mathbf{e}}_4 = A_4\mathbf{e}_4 + B_4u_4. \tag{6.73}$$

The associated nominal optimal control problem can be formulated as

$$\begin{aligned} J_4 = \min & \frac{1}{2}\int_0^\infty \{{\mathbf{e}_4}^T Q_4 \mathbf{e}_4 + {u_4}^T R_4 u_4\} dt \\ & \text{s.t.} \\ & \dot{\mathbf{e}}_4 = A_4\mathbf{e}_4 + B_4u_4 \\ & Q_4 \geq 0 \\ & R_4 > 0. \end{aligned} \tag{6.74}$$

The following theorem specifies the control law for agent #4 that guarantees the convergence to the desired formation.

Theorem 6.6. *For the agent #4 described by the nonlinear model (6.43) under Assumption 6.1, the distributed control law*

$$u_4 = -{R_4}^{-1}{B_4}^T S_4 \boldsymbol{e}_4, \tag{6.75}$$

where S_4 is the unique solution of the equation

$$Q_4 + {A_4}^T S_4 + S_4 A_4 - S_4 B_4 {R_4}^{-1} {B_4}^T S_4 = 0, \tag{6.76}$$

achieves local asymptotic stability of the origin for the closed-loop, directed, distance-based formation system.

Proof. The control law (6.75) is the stabilizing control of the nominal system $\Sigma_4 : \quad \dot{\mathbf{e}}_4 = f_4(\mathbf{e}_4, 0, 0)$ provided that Assumption 6.1 is satisfied. Thus, according to the Theorem 2.4, the system $\Xi_4 : \quad \dot{\mathbf{e}}_4 = f_3(\mathbf{e}_4, \mathbf{e}_3, \mathbf{e}_2)$ is input-to-state stable with respect to $(\mathbf{e}_3, \mathbf{e}_2)$. We have shown that the system Δ_3 is asymptotically stable. Thus, based on the Theorem 2.7 the origin of interconnected system

$$\Delta_4 : \begin{cases} \dot{\mathbf{e}}_2 = f_2(\mathbf{e}_2) \\ \dot{\mathbf{e}}_3 = f_3(\mathbf{e}_3, \mathbf{e}_2) \\ \dot{\mathbf{e}}_4 = f_4(\mathbf{e}_4, \mathbf{e}_3, \mathbf{e}_2), \end{cases} \tag{6.77}$$

is locally asymptotically stable. □

Corollary 6.6.1. *Select*

$$Q_4 = \kappa_4 diag[q_{41}, q_{42}, q_{43}, q_{v_4}, q_{w_4}], \tag{6.78}$$

where

$$\kappa_4 = \frac{\mathbb{V}_4^* - \mathbb{V}_4}{\mathbb{V}_4^* + \mathbb{V}_4}, \tag{6.79}$$

and $\mathbb{V}_4^*$ and $\mathbb{V}_4$ are desired and actual signed volume of the tetrahedron between the clique $(1, 2, 3, 4)$, and

$$q_{4m} = \kappa_{4m} + \mu_{4m} \quad m \in \{1, 2, 3\}, \tag{6.80}$$

where $\kappa_{4m} > 0$ is a constant and μ_{4m} is a positive barrier multiplier defined by

$$\mu_{4m} = (\frac{d_{4m}^*}{d_{4m} - r_{d_{4m}}})^{\epsilon}, \tag{6.81}$$

for suitable $\epsilon \geq 1$, $r_{d_{4m}}$ is a safe distance between pair of agents to prevent collision, and q_{v_4}, q_{z_4} are the appropriate weighting matrices. Then, by using the weighting factor (6.78), the proposed SDRE control law (6.75) guarantees an inter-agent collision avoidance of the neighboring agents and prevents a flip ambiguity of the directed, distance-based formation.

Proof. The proof is similar to the proof of the Corollary 6.5.1. □

Since the topology of the desired formation is assumed to be a directed trilateral Laman graph, it can be constructed via a sequence of directed vertex addition operations.

Consequently, for the next follower, say agent i, which is added to an existing directed trilateral Laman graph via Henneberg directed vertex addition sequence, the error vector is $\mathbf{e}_i = [e_{ij}, e_{il}, e_{ik}, {v_i}^T, {w_i}^T]^T$. The aggregate error dynamics can be written as

$$\dot{e}_{ij} = \eta(p_{ij})(v_i - v_j) \tag{6.82a}$$
$$\dot{e}_{il} = \eta(p_{il})(v_i - v_l) \tag{6.82b}$$
$$\dot{e}_{ik} = \eta(p_{ik})(v_i - v_k) \tag{6.82c}$$
$$\dot{v}_i = \hat{f}_i(v_i, w_i) + \hat{h}_i(v_i, w_i)u_i \tag{6.82d}$$
$$\dot{w}_i = \check{f}_i(v_i, w_i) + \check{h}_i(v_i, w_i)u_i. \tag{6.82e}$$

The equation (6.82) can be written in the matrix form as

$$\Xi_i : \dot{\mathbf{e}}_i = \hat{A}_i\mathbf{e}_i + \hat{B}_i\mathbf{u}_i \tag{6.83}$$

where $\mathbf{u}_i = [{v_j}^T, {v_l}^T, {v_k}^T, {u_i}^T]^T$. The corresponding unforced nominal system is

$$\dot{e}_{ij} = \eta(p_{ij})v_i \tag{6.84a}$$
$$\dot{e}_{il} = \eta(p_{il})v_i \tag{6.84b}$$
$$\dot{e}_{ik} = \eta(p_{ik})v_i \tag{6.84c}$$
$$\dot{v}_i = \hat{f}_i(v_i, w_i) + \hat{h}_i(v_i, w_i)u_i \tag{6.84d}$$
$$\dot{w}_i = \check{f}_i(v_i, w_i) + \check{h}_i(v_i, w_i)u_i. \tag{6.84e}$$

In a linear-like form it can be written as

$$\Sigma_i : \dot{\mathbf{e}}_i = A_i\mathbf{e}_i + B_iu_i. \tag{6.85}$$

The associated nominal optimal control problem can be formed as

$$\begin{aligned} J_i = \min & \frac{1}{2}\int_0^\infty \{{\mathbf{e}_i}^T Q_i \mathbf{e}_i + {u_i}^T R_i u_i\}dt \\ & \text{s.t.} \\ & \dot{\mathbf{e}}_i = A_i\mathbf{e}_i + B_iu_i \\ & Q_i \geq 0 \\ & R_i > 0. \end{aligned} \tag{6.86}$$

The following theorem offers the associated distributed controller for agent i which guarantees the convergence of the desired formation.

Theorem 6.7. *For the agent i described by the nonlinear model (6.43), under Assump-*

tion 6.1, the distributed control law

$$u_i = -{R_i}^{-1}{B_i}^T S_i \boldsymbol{e}_i, \tag{6.87}$$

where S_i is the unique solution of the equation

$$Q_i + {A_i}^T S_i + S_i A_i - S_i B_i {R_i}^{-1}{B_i}^T S_i = 0, \tag{6.88}$$

achieves the local asymptotic stability of the origin of the closed-loop, directed, distance-based formation.

Proof. The control law (6.87) is the stabilizing control of the nominal system Σ_i under Assumption 6.1; thus, the system Ξ_i is locally input-to-state stable. The stability analysis is based on induction method and similar to the proof of Theorem 6.6 with similar argument about the stability analysis of interconnected systems. Using the mathematical induction, one can show that the system Δ_{i-1}, which is the interconnected system of $i-1$ agents, is asymptotically stable. Thus, based on Theorem 2.7 the origin of the interconnected system

$$\Delta_i : \begin{cases} \dot{\mathbf{e}}_2 = f_2(\mathbf{e}_2) \\ \dot{\mathbf{e}}_3 = f_3(\mathbf{e}_3, \mathbf{e}_2) \\ \vdots \\ \dot{\mathbf{e}}_i = f_i(\mathbf{e}_i, ..., \mathbf{e}_2) \end{cases} \tag{6.89}$$

is locally asymptotically stable. □

Remark 2: The error vector of the agent i, $\mathbf{e}_i$, is consisted of associated edge errors that are being measured in the agent's local coordinate frame and the agent's states except its global position p_i. Therefore, the proposed control method is distributed.

Remark 3: The analytical solution of the SDRE equation is extremely challenging except for very simple scalar systems as shown in [123], [124]. However, there are very effective numerical methods for solving SDRE proposed in the literature [124].

Corollary 6.7.1. *Select*

$$Q_i = \kappa_i diag[q_{ij}, q_{il}, q_{ik}, q_{v_i}, q_{z_i}], \quad i \geq 4 \tag{6.90}$$

where

$$\kappa_i = \frac{\mathbb{V}_i^* - \mathbb{V}_i}{\mathbb{V}_i^* + \mathbb{V}_i}, \tag{6.91}$$

and $\mathbb{V}_i^*$ and $\mathbb{V}_i$ are desired and actual signed volume of the tetrahedron between the clique

(i, j, l, k), *and*

$$q_{im} = \kappa_{im} + \mu_{im} \quad m \in \{j, l, k\}, \tag{6.92}$$

where $\kappa_{im} > 0$ *is a constant and* μ_{im} *is a positive barrier multiplier defined by*

$$\mu_{im} = (\frac{d^*_{im}}{d_{im} - r_{d_{im}}})^{\epsilon}, \tag{6.93}$$

for suitable $\epsilon \geq 1$, *and* $r_{d_{im}}$ *being a safe distance between pair of agents to prevent collision. Then, by using the weighting factor (6.90), the proposed SDRE control law (6.87) guarantees inter-agent collision avoidance of the neighboring agents and prevents the flip ambiguity of the directed distance-based formation.*

Proof. The proposed inverse barrier function is

$$\Phi_i = \mathbf{e}_i^T Q_i \mathbf{e}_i, \tag{6.94}$$

where Q_i is defined by (6.90). Adding the proposed inverse barrier function (6.94) to the cost functional of the corresponding optimal control problem yields the corresponding unconstrained problem. If conditions for collision avoidance or reflection avoidance have been violated, then the proposed barrier function (6.94) will approach infinity, and based on [147], it will prevent collision avoidance between neighboring agents. □

Remark 5: Although the stability results of the proposed method are local, the domain of attraction may include reflected configurations. Therefore, using the proposed reflection prevention method has both practical and theoretical significance.

6.4 Simulation Results

6.4.1 2-D Space

We present here the simulation results of the proposed distributed control law for two different topologies. The desired formation is assumed to be a directed triangulated Laman graph in both cases.

Figure 6.1 shows the desired directed distance-based formation topology for a set of $N = 4$ agents, a rectangle with a side length of $d = 10$. Accordingly, the desired length of the edge e_{32} is $d_{32} = \sqrt{200}$. The leader is stationary since it has no constraint to satisfy. The controllers' parameters are selected as $\mu_{im} = 1$, $r_{d_{im}} = 2$, and $\epsilon = 2$ for all simulations.

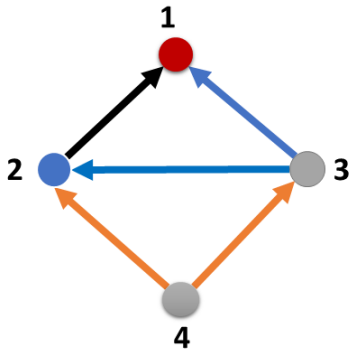

Figure 6.1: Desired directed distance-based formation for $N = 4$ agents.

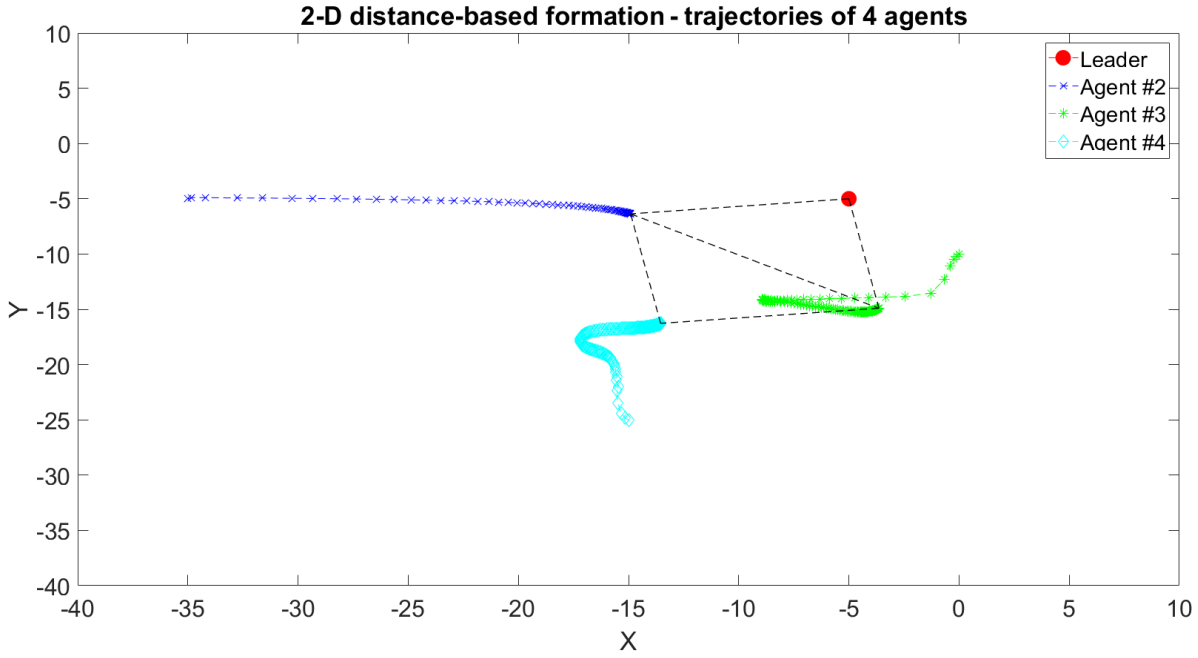

Figure 6.2: Trajectories of $N = 4$ agents modeled by nonlinear dynamics (6.95) using the proposed control method.

The agents are modeled as

$$\begin{aligned} \dot{x} &= v_x \\ \dot{y} &= v_y \\ \dot{v_x} &= v_x^2 + 2v_y + (1 + v_x)u_x \\ \dot{v_y} &= v_x v_y + (1 + v_y)u_y \\ \dot{z} &= -z + u_x + u_y \end{aligned} \tag{6.95}$$

Figure 6.2 shows the result of proposed controller, i.e. agents' trajectories in 2-D space. The leader is placed at $p_1 = [-5, -5]$. Initial locations of the agents are selected as $p_2 = [-35, -5]$, $p_3 = [0; -10]$, and $p_4 = [-15; -25]$. Figure 6.3 shows the formation

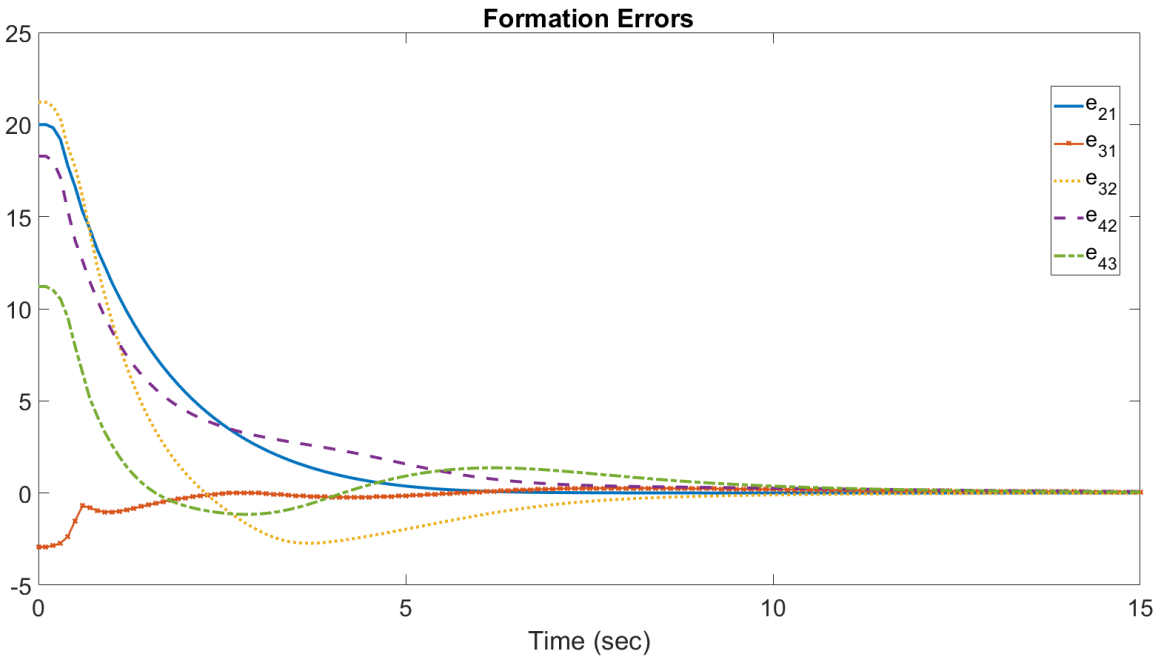

Figure 6.3: Formation errors for $N = 4$ agents.

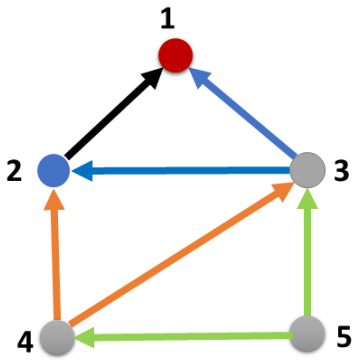

Figure 6.4: Desired directed distance-based formation for $N = 5$ agents.

errors corresponding to simulation in Figure 6.2.

Next, we simulated a proposed control scheme for a set of $N = 5$ nonlinear agents. The new desired topology is shown in Figure 6.4. The desired distances between agents are selected as: $d_{21} = 10$, $d_{31} = 10$, $d_{32} = \sqrt{200}$, $d_{42} = \sqrt{200}$, $d_{43} = \sqrt{400}$, $d_{53} = \sqrt{200}$, $d_{54} = \sqrt{200}$. The initial position of the agents are selected as $p_2 = [-35, -5]$, $p_3 = [-20; -30], p_4 = [-30, -25]$, and $p_5 = [-10; -30]$. The leader's position was remained unchanged.

Figure 6.5 shows the agents' trajectory for $N = 5$ agents. Despite changes in the agents' initial positions, the proposed method successfully achieves the desired distance-based formation topology for highly nonlinear agents.

Figure 6.6(top) shows the formation error of the edge e_{21} corresponding to the simulation of Figure 6.5 while Figure 6.6(bottom) shows the inputs of the agent 2, u_x and u_y,

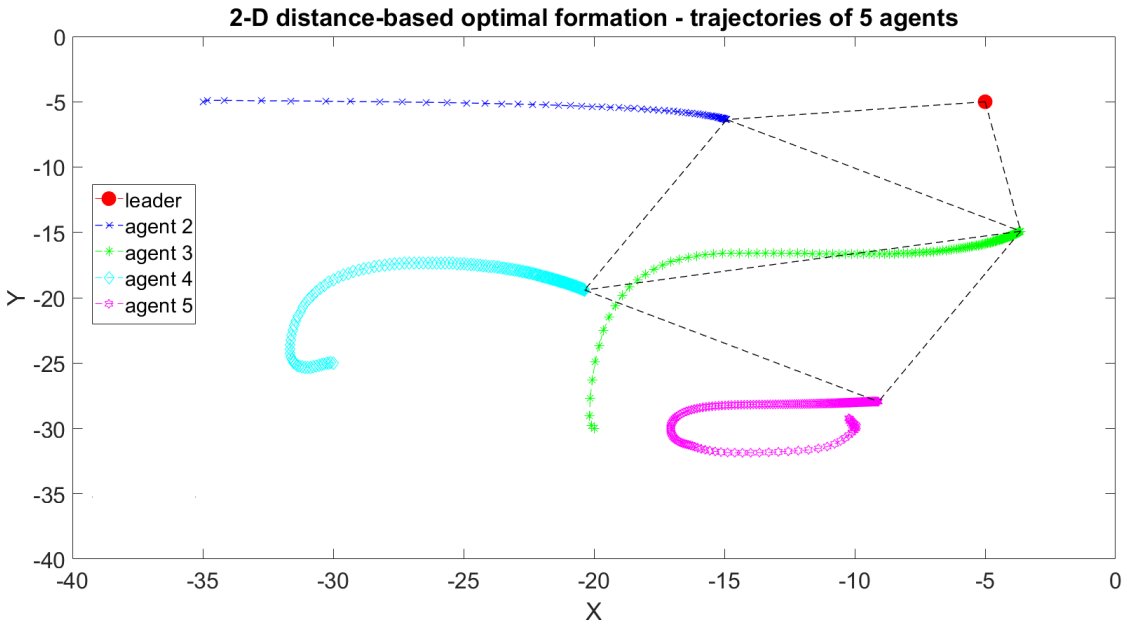

Figure 6.5: Trajectories of the set of $N = 5$ agents using the proposed controller.

respectively. Figure 6.7, Figure 6.8, and Figure 6.9 depict the convergence of the edge errors and input controls of the agent #3, agent #4, and agent #5, respectively.

6.4.2 3-D Space

This subsection presents simulation results of the proposed distance-based formation control over directed trilateral Laman graphs.

Figure 2.12(a) shows the desired, distance-based formation shape in 3-D space. The desired configuration is in the form of a directed trilateral Laman graph. Note that the leader is not responsible for any edges; thus, it is stationary. The simulation results for a set of nonlinear heterogeneous agents are provided. Since this work is the first study considering heterogeneous nonlinear dynamics, we chose a set of complex, highly nonlinear models that satisfy the SDRE feasibility conditions. The agents' models are as follows.

The leader is placed at $p_1 = [20, 20, 30]$. The agent #2 (first follower) is modeled as

$$\begin{aligned}
\dot{x}_2 &= v_{2_x} \\
\dot{y}_2 &= v_{2_y} \\
\dot{z}_2 &= v_{2_z} \\
\dot{v}_{2_x} &= 2v_{2_x} + (1 + v_{2_x})u_{2_x} \\
\dot{v}_{2_y} &= 2v_{2_y} + (1 + v_{2_y})u_{2_y} \\
\dot{v}_{2_z} &= 2v_{2_z} + (1 + v_{2_z})u_{2_z}
\end{aligned} \tag{6.96}$$

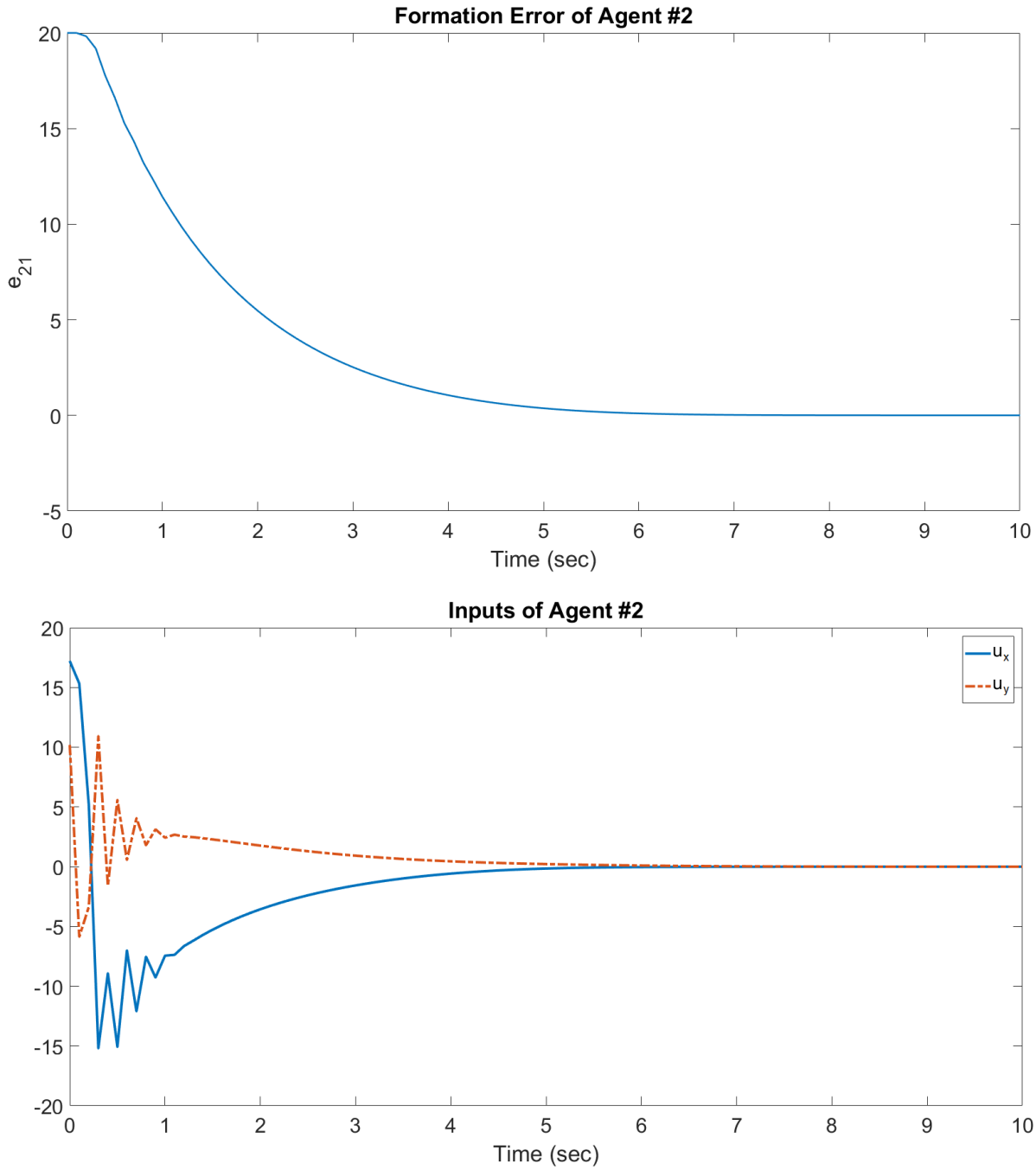

Figure 6.6: Formation error and control inputs of the agent #2 associated with the simulation of Figure 6.5

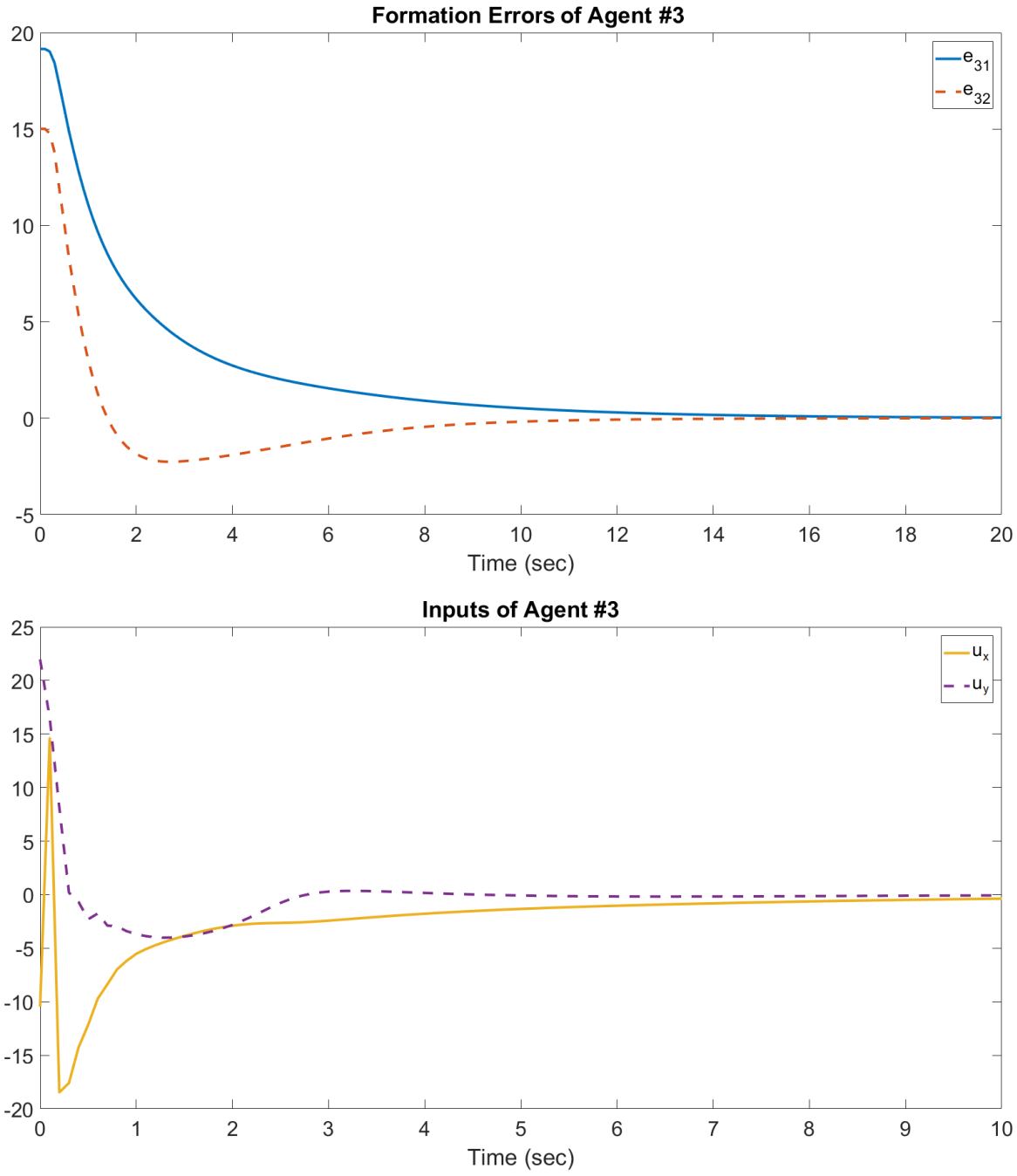

Figure 6.7: Formation errors and control inputs of the agent #3 associated with the simulation of Figure 6.5

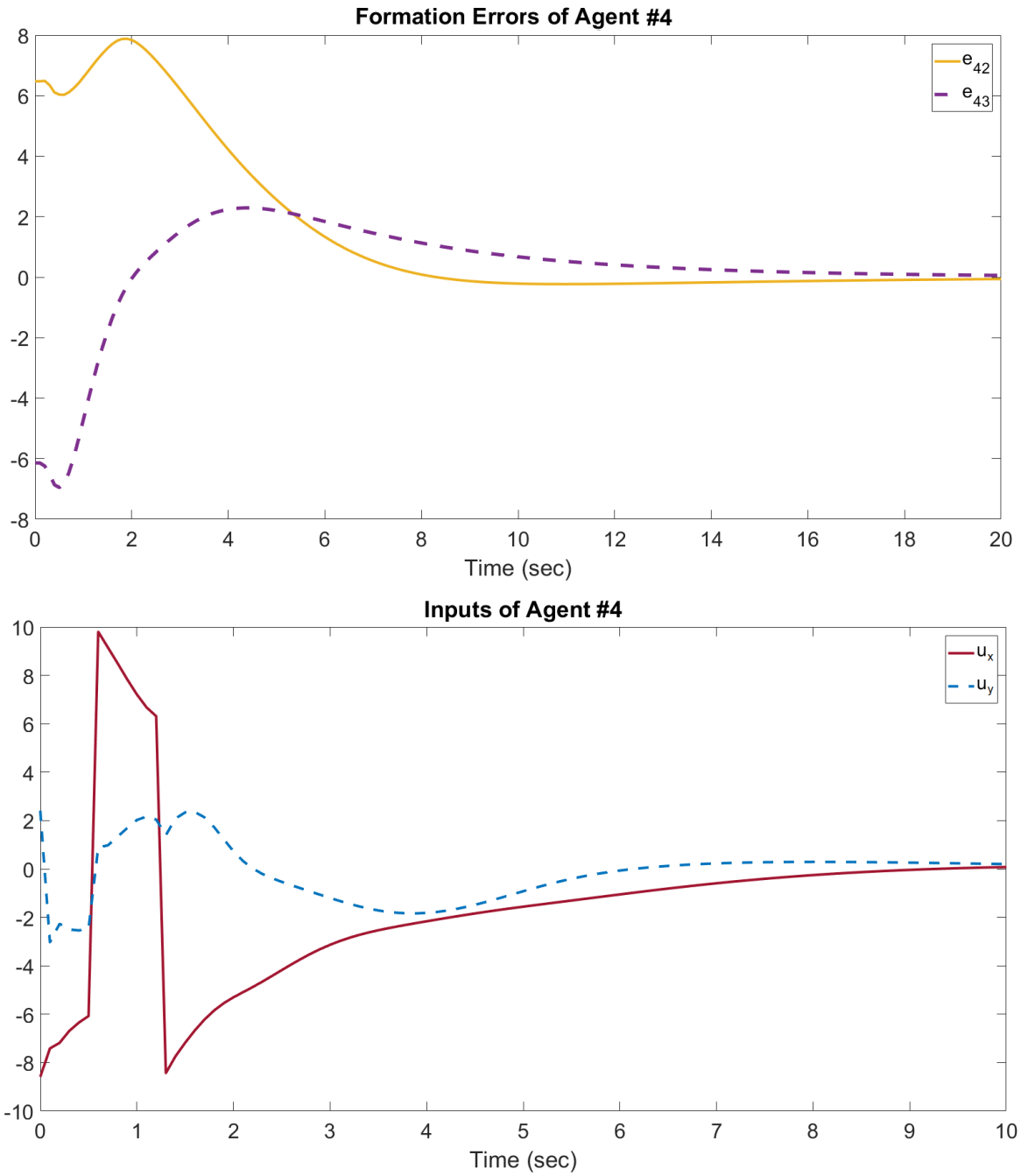

Figure 6.8: Formation errors and control inputs of the agent #4 associated with the simulation of Figure 6.5

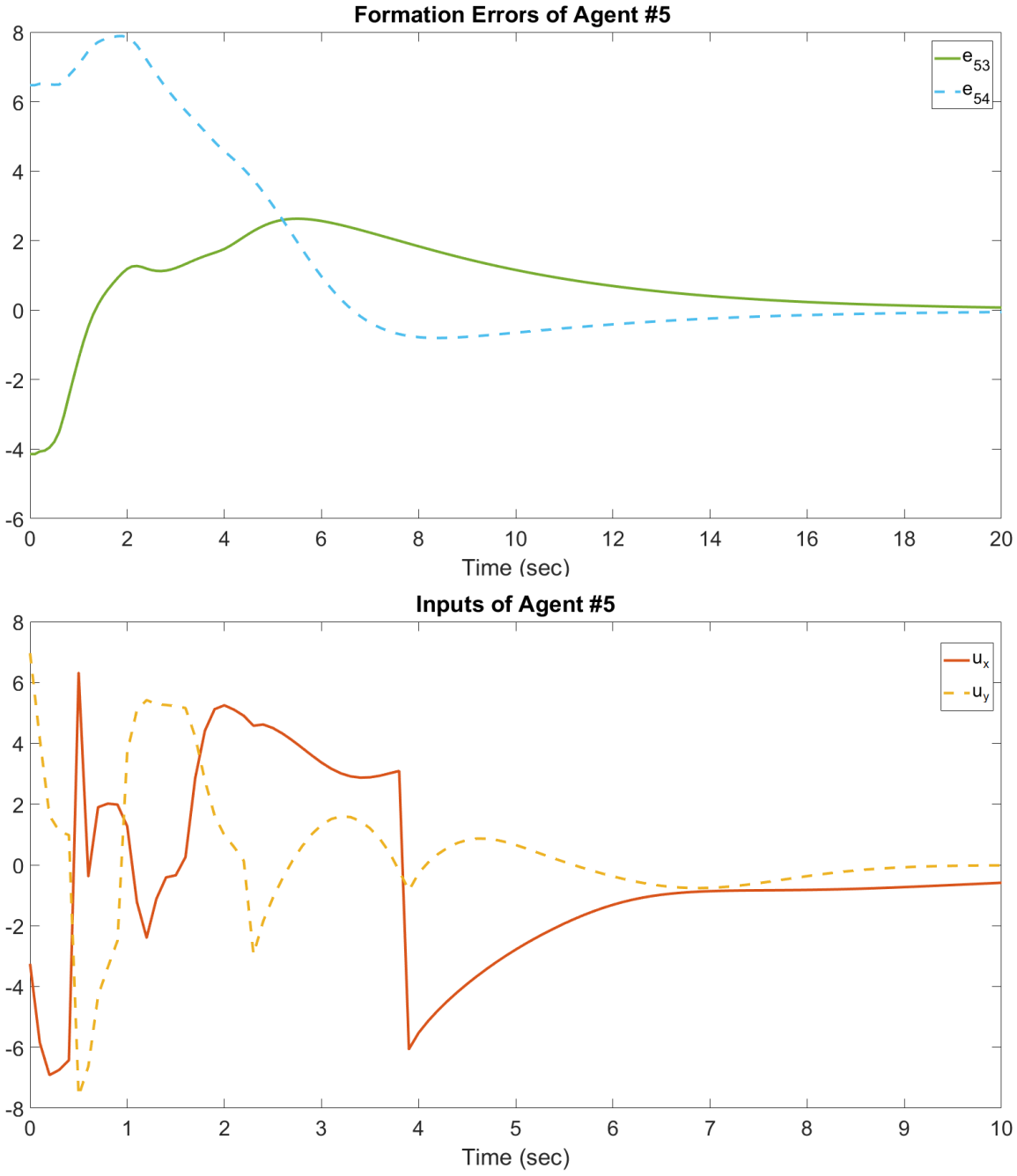

Figure 6.9: Formation errors and control inputs of the agent #5 associated with the simulation of Figure 6.5

where the initial position of the agent #2 is $p_2 = [50, 20, 30]$. The agent #3 is modeled as

$$\begin{aligned}
\dot{x}_3 &= v_{3_x} \\
\dot{y}_3 &= v_{3_y} \\
\dot{z}_3 &= v_{3_z} \\
\dot{v}_{3_x} &= v_{3_x} + u_{3_x} \\
\dot{v}_{3_y} &= v_{3_y} + u_{3_y} \\
\dot{v}_{3_z} &= v_{3_z} + u_{3_z} \\
\dot{w}_3 &= -w_3 + u_{3_x} + u_{3_y} + u_{3_z}
\end{aligned} \tag{6.97}$$

where the initial position of the follower #3 is $p_3 = [50, -30, 20]$. The agent #4 is modeled as

$$\begin{aligned}
\dot{x}_4 &= v_{4_x} \\
\dot{y}_4 &= v_{4_y} \\
\dot{z}_4 &= v_{4_z} \\
\dot{v}_{4_x} &= v_{4_x}^2 + u_{4_x} \\
\dot{v}_{4_y} &= v_{4_y}^2 + u_{4_y} \\
\dot{v}_{4_z} &= v_{4_z}^2 + u_{4_z}
\end{aligned} \tag{6.98}$$

where the initial position of the follower #4 is $p_4 = [-10, 20, -10]$.

Figure 6.10 shows trajectories for a set of $N = 4$ agents in 3-D space using the proposed controller. Figure 6.11 shows the formation errors corresponding to the formation shown in Figure 6.10. Figure 6.12 shows the control inputs of agent #2, agent #3, and agent #4.

Next, we add agent #5 to the desired formation using the directed vertex addition operation. The new desired formation is shown in Figure 2.6(b). Agent #5 is modeled as

$$\begin{aligned}
\dot{x}_5 &= v_{5_x} \\
\dot{y}_5 &= v_{5_y} \\
\dot{z}_5 &= v_{5_z} \\
\dot{v}_{5_x} &= v_{5_z} v_{5_x} + u_{5_x} \\
\dot{v}_{5_y} &= v_{5_y}^2 + u_{5_y} \\
\dot{v}_{5_z} &= v_{5_x} v_{5_z} + u_{5_z}
\end{aligned} \tag{6.99}$$

where the initial position of the follower #5 was selected as $p_5 = [30, -20, 50]$.

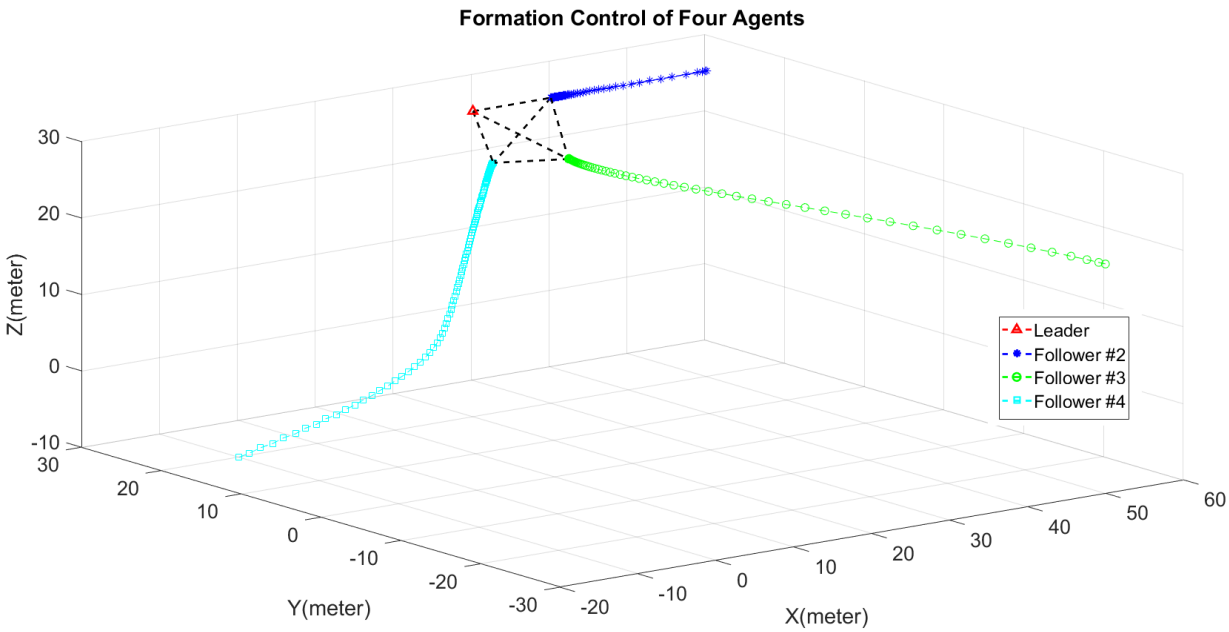

Figure 6.10: A distributed directed distance-based formation for $N = 4$ agents using the proposed controller.

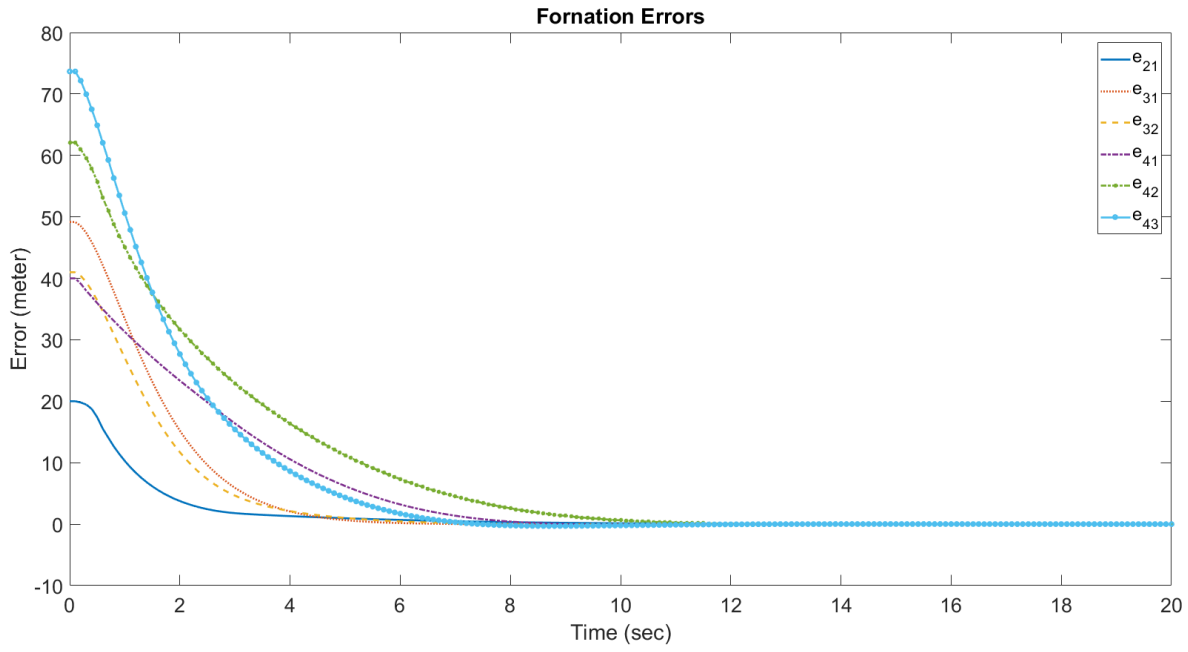

Figure 6.11: Formation errors of the simulation 6.10.

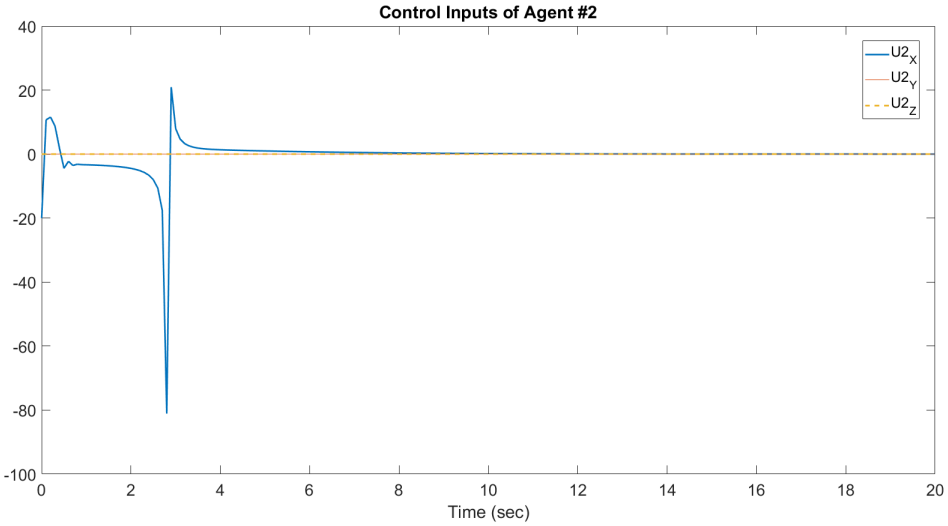

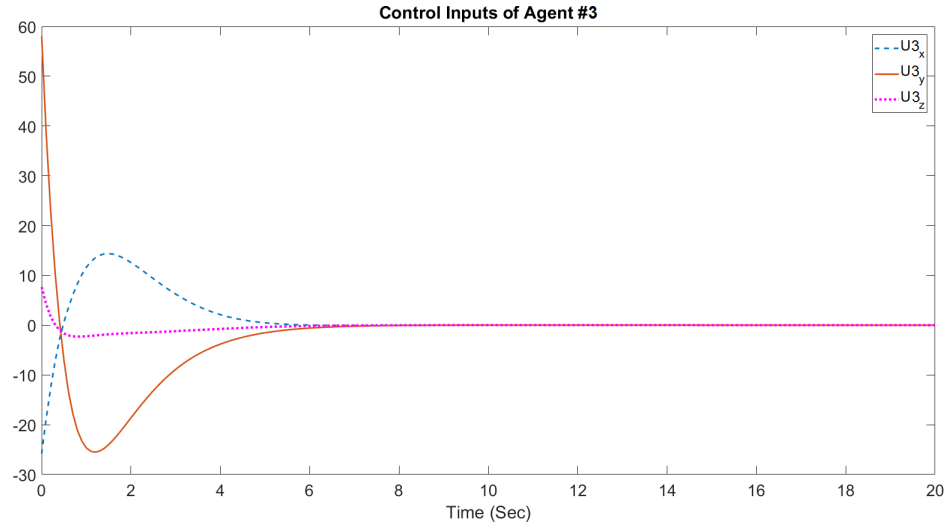

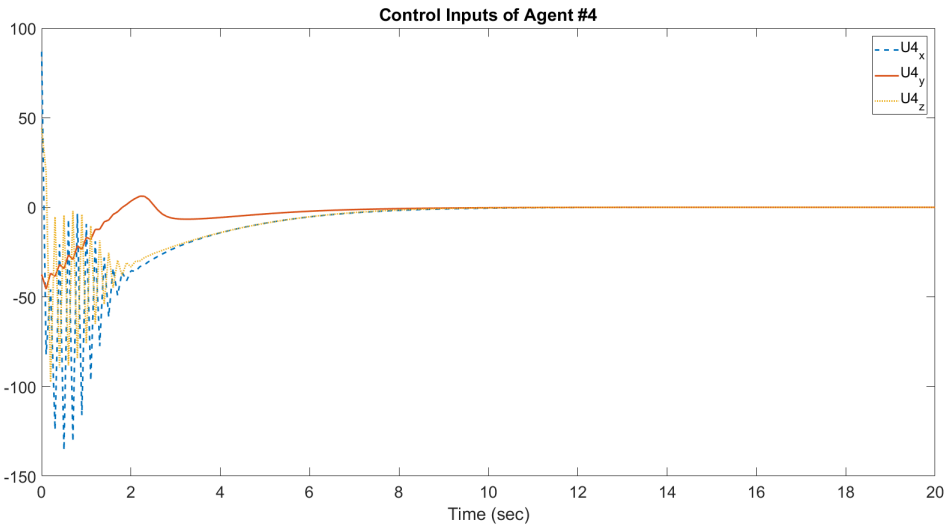

Figure 6.12: Control inputs of the agent #2, agent #3, and agent #4 corresponding to the formation in Figure 6.10.

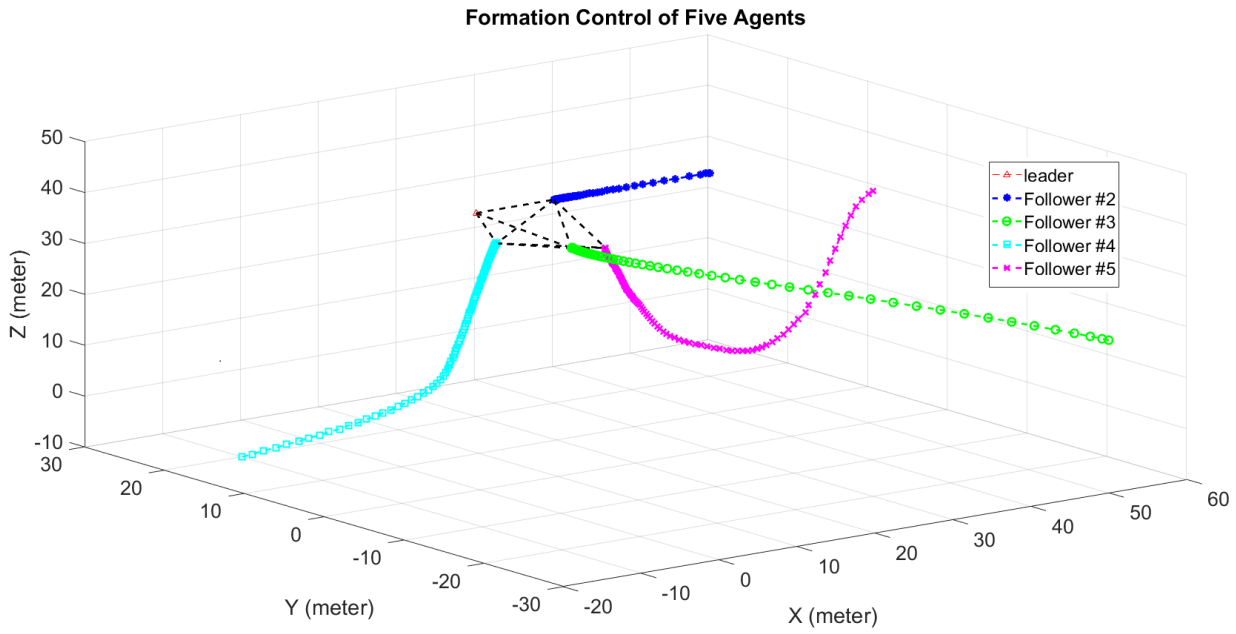

Figure 6.13: Trajectories of the agents for $N = 5$ agents using the proposed controller.

Figure 6.13 shows the agents' trajectory where the agent #5 is added. Figure 6.14 shows the formation errors of the edges that were assigned to the agent #5. Figure 6.15 shows the input signals of the agent #5.

To validate the results of the proposed reflection prevention method, we run a set of simulations. We first simulated the proposed controller without signed volume constraints. The results show the flip ambiguity of the formation. Afterward, the signed area constraints are added to the controller. Figure 6.16 (top) shows the controller performance without the signed volume constraints where $p_5 = [10, 60, 10]^T$ and Q_i matrices were selected as constant identity matrix. All other parameters remained unchanged. It shows that agent #5 moved to the reflected position, making the configuration flip ambiguous. Figure 6.16 (bottom) shows the simulation results while the proposed weighting matrix in Corollary 6.7.1 is utilized. The simulation results show that the proposed controller, with signed volume constraints, prevented the convergence of the agent #5 to the reflected position.

6.5 Conclusions

In this chapter, a distributed, distance-based formation control problem for a set of nonlinear agents is studied. We modeled the desired formation topology as directed triangulated or trilateral Laman graphs and agents as a general, affine, nonlinear dynamics. We formulated the distance-based formation control in a nonlinear optimal control framework and proposed a state-dependent Riccati equation (SDRE) method-based controller

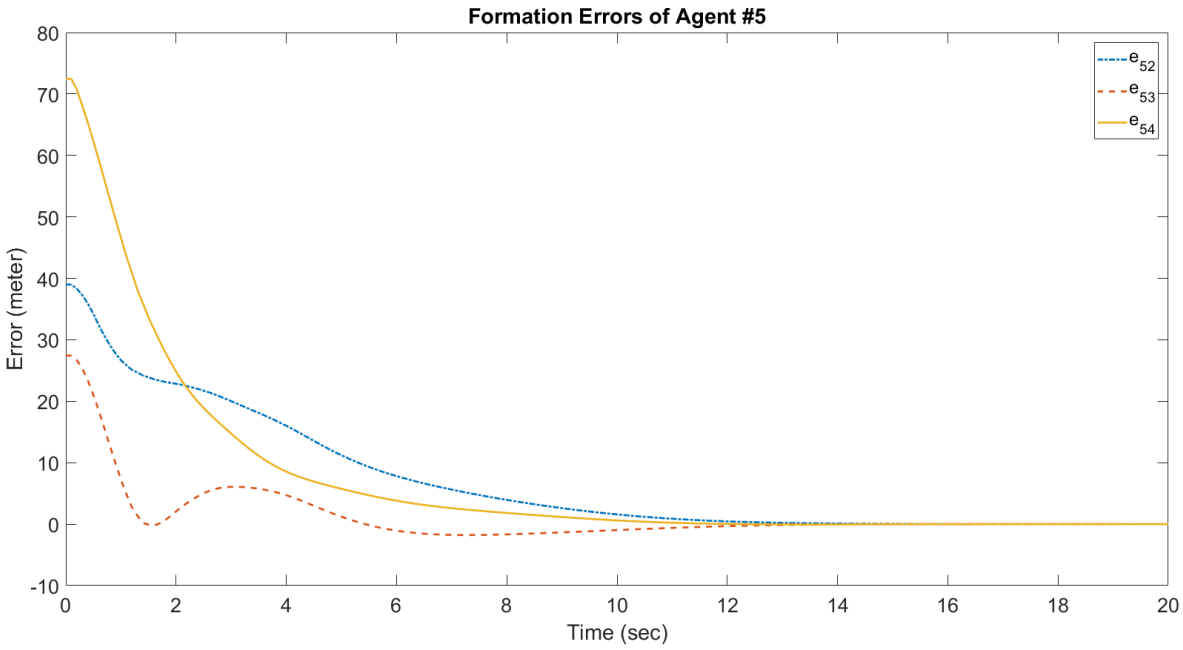

Figure 6.14: Formation errors assigned to the agent #5.

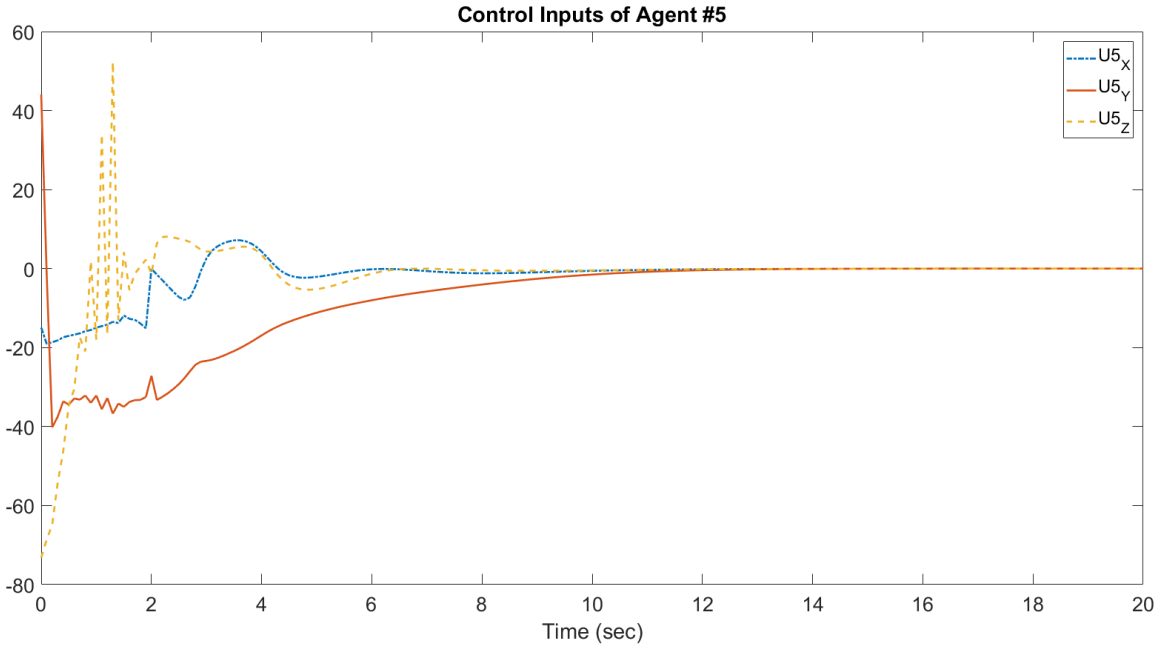

Figure 6.15: Input signals of the agent #5.

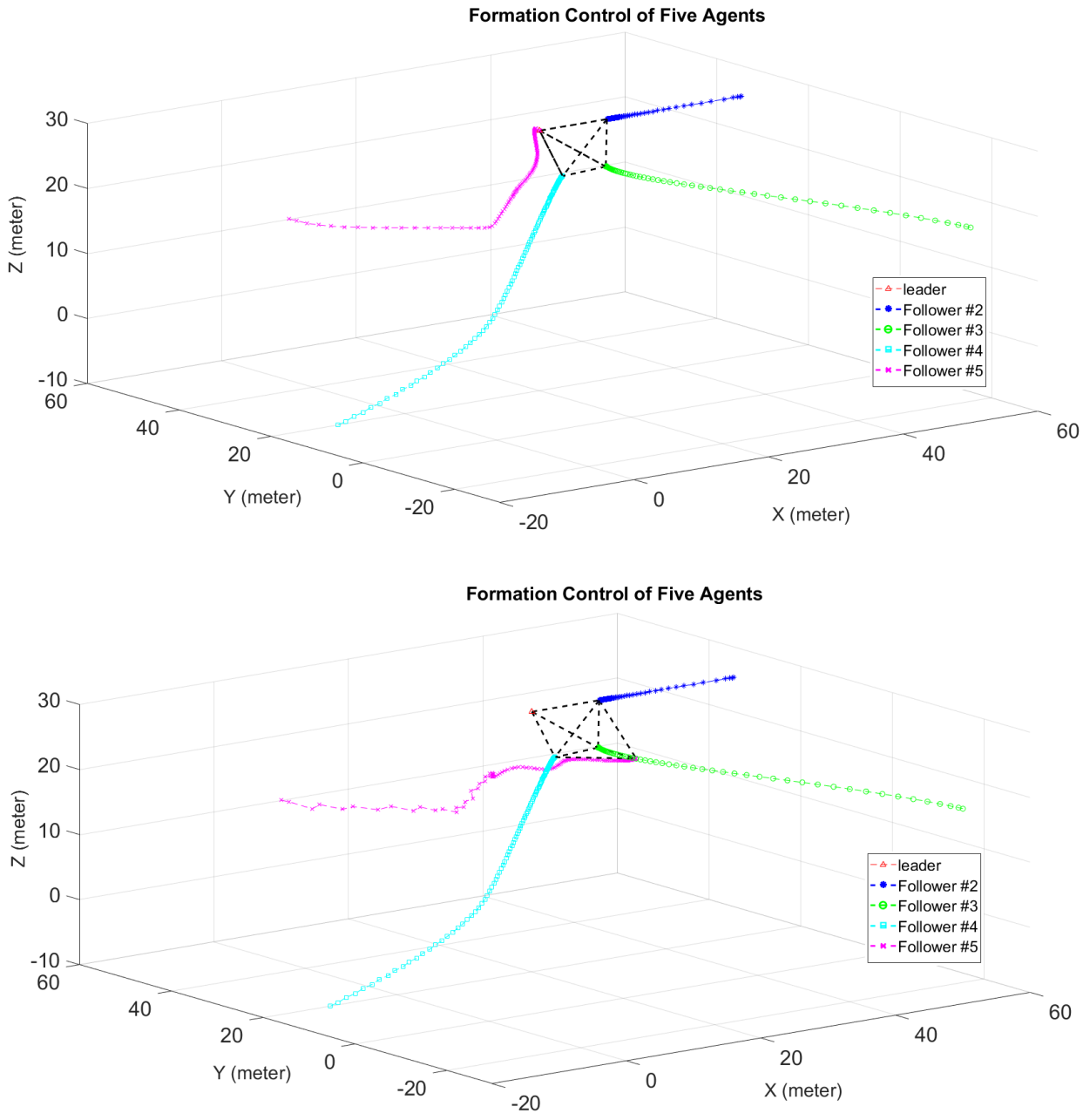

Figure 6.16: Simulation result of the proposed controller without signed volume constraints (top) and with the signed volume constraints that prevents flip ambiguity of the formation (bottom).

which ensures that all agents asymptotically converge to the desired framework. The rigorous stability analysis is presented for the proposed control scheme. Furthermore, to solve the problem of reflection of the desired formation, the proposed control law uses a signed area and signed volume constraints to prevent the formation's flip ambiguity. The proposed method also guarantees collision avoidance between the neighboring agent pairs.

Chapter 7

Robust Optimal Distance-Based Formation Control

7.1 Introduction

Nonlinear systems are often subject to uncertainties such as unmodeled dynamics or model perturbation. Although the SDRE method offers a handy tool for optimal control of nonlinear systems, it is not robust against uncertainties and disturbances. Therefore, the controller might have poor performance or even be unstable in the presence of uncertainty. There are several proposed methods to make an optimal controller robust, including the robust LQR [155], H_2/H_∞ [156], adaptive dynamic programming [157], and sliding mode control [158], [159]. The integral sliding mode method is introduced in [160] and combined with optimal control in [161], [162] and [163].

This chapter studies the formation control problem with distance constraints for a set of nonlinear agents where agents' dynamics are affected by uncertainties. The responsibility of controlling an edge is assigned to only one of its adjacent agents; therefore, directed graph theory is used to represent the desired formation topology.

7.2 Controller Design

In this section, we study the distributed, directed, distance-based formation control under uncertainty. We research formations with agents subject to various unknown uncertainties. We proposed a robust controller that can overcome the effect of uncertainty and stir the agent to the desired framework. Furthermore, the proposed robust optimal control scheme guarantees the asymptotic stability of the overall formation. The results presented in this section are applicable to both 2-D and 3-D spaces, where the desired topology is assumed to be given as a directed triangulated Laman graph (in 2-D) or a directed trilateral Laman graph (in 3-D).

Suppose that each agent model is described by an affine nonlinear model

$$\dot{x}_i = f_i(x_i) + h_i(x_i)u_i + \phi_i(x_i, t), \tag{7.1}$$

where $x_i \in \mathbb{R}^p$ and $u_i \in \mathbb{R}^q$ are agent's state and input vectors. The functions f_i and h_i are C^1 and C^0 mappings, respectively. Function $\phi_i(x_i, t) \in \mathbb{R}^p$ represents all additive uncertainties such as unmodeled dynamics and model perturbations and assumed to have a bounded 1-norm, $\|\phi_i\|_1 < \varepsilon_i$. Provided that $f_i(0) = 0$, the agent's model (7.1) can be written in the following linear-like form

$$\dot{x}_i = \mathcal{A}_i(x_i)x_i + \mathcal{B}_i(x_i)u_i + \phi_i(x_i, t), \tag{7.2}$$

where $f_i(x_i) = \mathcal{A}_i(x_i)x_i$ and $h_i(x_i) = \mathcal{B}_i(x_i)$.

Since the desired formation is described as a set of distance constraints, the state vector should include the agent's position p_i. Thus, the state vector of the agent i can be partitioned as $x_i = [p_i^T, w_i^T]^T$, where w_i is the vector of remaining states. We can write the agent's model (7.1) as

$$\dot{p}_i = \hat{f}_i(x_i) + \hat{h}_i(x_i)u_i + \hat{\phi}_i \tag{7.3a}$$

$$\dot{w}_i = \check{f}_i(x_i) + \check{h}_i(x_i)u_i + \check{\phi}_i, \tag{7.3b}$$

where functions $\hat{f}_i$, $\check{f}_i$, $\hat{h}_i$, $\check{h}_i$, $\hat{\phi}_i$, and $\check{\phi}_i$ are corresponding parts of f_i, h_i, and ϕ_i, respectively.

For a pair of neigbouring agents, the relative position is

$$p_{ij} = p_i - p_j, \quad (i, j) \in \mathcal{E}. \tag{7.4}$$

Note that p_{ij} can be measured by the source agent i in its own coordinate system. Thus, the distance between the pair of adjacent agents is given by

$$d_{ij} = \|p_{ij}\|. \tag{7.5}$$

It is assumed that the desired distance-based formation is specified in terms of a set of distance constraints, where d_{ij}^* is the desired distance between agent i and agent j. Consequently, the edge error can be written as

$$e_{ij} = d_{ij} - d_{ij}^*. \tag{7.6}$$

The objective of formation control is to control agents such that they form and preserve a specific geometric shape. A distance-based formation control problem for a set of nonlinear, heterogeneous agents modeled as (7.1) is to design a distributed stabilizing

control law u_i such that

$$\lim_{t\to\infty} e_{ij} \longrightarrow 0 \quad \forall (i,j) \in \mathcal{E}. \tag{7.7}$$

Note that, for the sake of having a stable, persistent formation, in addition to (7.7), the overall formation should also be stable.

The edge error is defined in (7.6). Thus, the edge error dynamics is

$$\begin{aligned} \dot{e}_{ij} &= \frac{d}{dt}\sqrt{(p_{ij})^T(p_{ij})} \\ &= \frac{p_{ij}^T \dot{p}_{ij}}{\|p_{ij}\|}. \end{aligned} \tag{7.8}$$

Substituting the agent dynamics (7.3) in the edge error dynamics (7.8) yields

$$\dot{e}_{ij} = \eta(p_{ij})\{\hat{f}_i(x_i) + \hat{h}_i(x_i)u_i + \hat{\phi}_i - (\hat{f}_j(x_j) + \hat{h}_j(x_j)u_j + \hat{\phi}_j)\}, \tag{7.9}$$

where $\eta(p_{ij}) = \frac{(p_{ij})^T}{\|p_{ij}\|}$ is the relative bearing function. Rearranging the equation (7.9), the edge error dynamics can be written as

$$\dot{e}_{ij} = \eta(p_{ij})\hat{f}_i(x_i) + \eta(p_{ij})\hat{h}_i(x_i)u_i + l_{ij} + \phi_{ij}, \tag{7.10}$$

where

$$l_{ij} = -\eta(p_{ij})(\hat{f}_j + \hat{h}_j u_j), \tag{7.11}$$

and

$$\phi_{ij} = \eta(p_{ij})(\hat{\phi}_i - \hat{\phi}_j), \tag{7.12}$$

is an auxiliary uncertainty function.

For the agent i that is responsible for preserving its distance to its neighbors, the formation error vector is

$$\hat{\mathbf{e}}_i = [..., e_{ij}, ...]^T, \quad j \in \mathcal{N}_i. \tag{7.13}$$

Remark 7.1. It is to be noted that the formation error vector of the agent i depends only on the relative positions of agents' neighbors since agent i only requires to have access to its neighbors' relative positions on its local coordinate system.

Remark 7.2. Since the agent #1 (the leader) is not responsible for any edge, it is stationary. For the agent #2, that is responsible for preserving its distance with the leader, $\hat{\mathbf{e}}_2 = [e_{12}]$. For the agent #3, the error vector is $\hat{\mathbf{e}}_3 = [e_{31}, e_{32}]^T$. For the next follower, agent i in a triangulated Laman graph topology the error vector is $\hat{\mathbf{e}}_i = [e_{ij}, e_{ik}]^T$ where $\{j,k\} \in \mathcal{N}_i$. Accordingly, in trilateral Laman topologies we can write $\hat{\mathbf{e}}_i = [e_{ij}, e_{ik}, e_{il}]^T$ where $\{j,k,l\} \in \mathcal{N}_i$.

Since the topology of the desired formation is assumed to be directed triangulated or trilateral Laman graphs, it can be constructed via a sequence of triangulation or trilateration operations, respectively. Consequently, for the next follower, say agent i, which is added to an existing directed Laman graph via Henneberg directed vertex addition sequence, the aggregate error vector is $\mathbf{e}_i = [\hat{\mathbf{e}}_i^T, {w_i}^T]^T$. The aggregate error dynamics can be written as

$$\dot{\hat{\mathbf{e}}}_i = F_i(\mathbf{e}_i) + H_i(\mathbf{e}_i)u_i + \varphi_i + L_i \tag{7.14a}$$

$$\dot{w}_i = \check{f}_i(\mathbf{e}_i) + \check{h}_i(\mathbf{e}_i)u_i + \check{\phi}_i, \tag{7.14b}$$

where φ_i and L_i are matrix form functions of ϕ_{ij} and l_{ij} for $\forall j \in \mathcal{N}_i$. Also, F_i and H_i are corresponding matrix valued functions. Neglecting the effect of neighbors L_i, the equation (7.14) can be written in the following matrix form

$$\dot{\mathbf{e}}_i = A_i\mathbf{e}_i + B_iu_i + \Phi_i. \tag{7.15}$$

The uncertainty function Φ_i is bounded since its every component is bounded. Thus, equation (7.15) represents the dynamics of the formation error and states of the agent i. The objective is to design a control law such that under bounded uncertainty, the origin of the system (7.15), which corresponds to the desired formation, becomes asymptotically stable.

The proposed control method has three steps. First, for the nominal system without uncertainties, we design an optimal, infinite horizon SDRE controller that can asymptotically stabilize the nominal system. Second, to design the controller that can handle uncertainties, we propose the SDRE controller in combination with an integral sliding mode control scheme that can stabilize the uncertain system. Stability analysis is driven based on the Lyapunov stability theory. Third, using the stability theory of cascade-connected systems, we show that the overall directed distance-based formation of N nonlinear, heterogeneous agents, subjected to bounded uncertainties, is asymptotically stable.

Neglecting the uncertainty of the system (7.15), the nominal system is

$$\dot{\mathbf{e}}_i = A_i\mathbf{e}_i + B_iu_i. \tag{7.16}$$

We propose a nonlinear, infinite horizon SDRE controller for the nominal system that asymptotically stabilizes the system. To meet SDRE feasibility condition we establish the following assumption.

Assumption 7.1: The pair $\{A_i, B_i\}$ is point-wise stabilizable in the linear sense for all x in some non-empty neighborhood of the origin.

Remark 7.3. Reference [154] proves that there always exist a stablizable and detectable

SDC representation of the system (7.14) unless $\{\mathbf{e}_i, [F_i^T(\mathbf{e}_i), \check{f}_i^T(\mathbf{e}_i)]^T\}$ be linearly dependent and $Q_i^{1/2}\mathbf{e}_i = 0$. Therefore, by proper selection of Q_i we can guarantee the existence of such a stablizable and detectable SDC representation.

The distributed optimal control problem for the agent i is

$$\begin{aligned} J_i = \min & \frac{1}{2}\int_{t_0}^{\infty} \{\mathbf{e}_i^T Q_i \mathbf{e}_i + u_i^T R_i u_i\} dt \\ & \text{s.t.} \\ & \dot{\mathbf{e}}_i = A_i \mathbf{e}_i + B_i u_i \\ & Q_i = \text{diag}[Q_{\hat{\mathbf{e}}_i}, Q_{w_i}] > 0 \\ & R_i > 0. \end{aligned} \tag{7.17}$$

where $Q_{\hat{\mathbf{e}}_i} = \text{diag}[..., q_{ij}, ...]$ for $j \in \mathcal{N}_i$ and Q_{w_i} is the weighting matrix of remaining states.

Remark 7.4. For any matrix E_i that $\mathbf{e}_i$ lies in its null space, $\dot{\mathbf{e}}_i = (A_i + E_i)\mathbf{e}_i + B_i u_i$ is also another SDC representation of the system (7.15).

Remark 7.5. By choosing a positive definite Q_i, detectability of the pair $\{Q_i^{1/2}, A_i\}$ is guaranteed [127].

Theorem 7.1. *Given Assumption 7.1, the distributed control law*

$$u_i^{SDRE} = -R_i^{-1} B_i^T S_i \boldsymbol{e}_i, \tag{7.18}$$

where S_i is a unique and positive-definite solution of the corresponding state-dependent Riccati equation

$$Q_i + A_i^T S_i + S_i A_i = S_i B_i R_i^{-1} B_i^T S_i, \tag{7.19}$$

guarantees asymptotic stability of the origin of the nominal system (7.16).

Proof. Given Assumption 7.1, the Lemma 2.9 is applicable to the nominal system (7.16), and thus the control law (7.18) is the stabilizing control of the nominal system. □

Remark 7.6. Substituting the control law (7.18) in the nominal system (7.16), the nominal closed-loop dynamics is

$$\dot{\mathbf{e}}_i = \{A_i - B_i R^{-1} B_i^T S_i\}\mathbf{e}_i. \tag{7.20}$$

Theorem 7.1 provides solution of the nonlinear optimal control problem (7.17) where the SDRE control law (7.18) stabilizes the nominal system (7.16). However, this does not guarantee the stability of the uncertain system (7.15). In order to stabilize the uncertain system, we propose the robust optimal controller presented next.

Let us define an integral sliding surface, $\mathbf{s}_i$, as

$$\mathbf{s}_i = G_i[\mathbf{e}_i(t) - \mathbf{e}_i(t_0) - \int_{t_0}^{t} \{A_i\mathbf{e}_i + B_i u_i^{SDRE}\} d\tau], \tag{7.21}$$

where the matrix G_i is to be selected such that (G_iB_i) is nonsingular. The following theorem represents our main result, which provides a robust optimal controller as a combination of SDRE and ISMC.

Theorem 7.2. *Given Assumption 7.1, the distributed robust optimal control law of the agent i*

$$u_i = u_i^{SDRE} + u_i^{ISMC}, \tag{7.22}$$

where u_i^{SDRE} is the SDRE based control law of the nominal system, obtained in (7.18), and u_i^{ISMC} is a integral sliding mode control law, defined as

$$u_i^{ISMC} = -(G_iB_i)^{-1}(\alpha_i \boldsymbol{s}_i + \beta_i \|G_i\|_1 sgn(\boldsymbol{s}_i)), \tag{7.23}$$

in which positive scalars α_i, β_i to be designed appropriately, results in the asymptotic stability of the uncertain system (7.15) and ensures that the agent i converges to its predefined distance-based formation.

Proof. The derivative of the integral sliding surface is

$$\dot{\mathbf{s}}_i = G_i\{\dot{\mathbf{e}}_i - A_i\mathbf{e}_i - B_i u_i^{SDRE}\}. \tag{7.24}$$

Substituting the aggregate error dynamics (7.15) in derivative of the sliding surface (7.24), one can write

$$\dot{\mathbf{s}}_i = G_i\{A_i\mathbf{e}_i + B_i u_i + \Phi_i - A_i\mathbf{e}_i - B_i u_i^{SDRE}\}. \tag{7.25}$$

Substituting (7.18) in (7.25) results in

$$\dot{\mathbf{s}}_i = G_i\{B_i u_i + \Phi_i + B_i R_i^{-1} B_i^T S_i \mathbf{e}_i\}. \tag{7.26}$$

The proposed positive definite Lyapunov candidate function is

$$V_i = \frac{1}{2}\mathbf{s}_i^T \mathbf{s}_i. \tag{7.27}$$

Thus, the derivative of proposed Lyapunov candidate function is

$$\dot{V}_i = \mathbf{s}_i^T \dot{\mathbf{s}}_i. \tag{7.28}$$

Therefore, by showing

$$\dot{V}_i < 0 \qquad \text{for all} \quad \mathbf{s}_i \neq 0, \tag{7.29}$$

it is proven that the integral sliding surface is globally asymptotically reachable.

Substituting (7.26) in (7.28), with some mathematical manipulation, one can write

$$\dot{V}_i = \mathbf{s}_i^T \Big\{ G_i B_i u_i + G_i \Phi_i + G_i B_i R_i^{-1} B_i^T S_i \mathbf{e}_i \Big\}. \tag{7.30}$$

Substituting (7.22) in (7.30) yields

$$\begin{aligned}
\dot{V}_i &= \mathbf{s}_i^T \Big\{ G_i B_i u_i^{SDRE} + G_i B_i u_i^{ISMC} \\
&\qquad + G_i \Phi_i + G_i B_i R_i^{-1} B_i^T S_i \mathbf{e}_i \Big\} \\
&= \mathbf{s}_i^T \Big\{ - G_i B_i R_i^{-1} B_i^T S_i \mathbf{e}_i \\
&\qquad - G_i B_i (G_i B_i)^{-1} (\alpha_i \mathbf{s}_i + \beta_i \|G_i\|_1 \mathrm{sgn}(\mathbf{s}_i)) \\
&\qquad + G_i \Phi_i + G_i B_i R_i^{-1} B_i^T S_i \mathbf{e}_i \Big\} \\
&= \mathbf{s}_i^T \Big(G_i \Phi_i - \alpha_i \mathbf{s}_i - \beta_i \|G_i\|_1 \mathrm{sgn}(\mathbf{s}_i) \Big) \\
&= \mathbf{s}_i^T G_i \Phi_i - \alpha_i \mathbf{s}_i^T \mathbf{s}_i - \beta_i \|G_i\|_1 \mathbf{s}_i^T \mathrm{sgn}(\mathbf{s}_i) \\
&= \mathbf{s}_i^T G_i \Phi_i - \alpha_i \|\mathbf{s}_i\|_2^2 - \beta_i \|G_i\|_1 \|\mathbf{s}_i\|_1.
\end{aligned} \tag{7.31}$$

The Lyapunov candidate function is scalar, thus, $\mathbf{s}_i^T G_i \Phi_i$ is scalar and from the properties of the l_1-norm we can write

$$\|\mathbf{s}_i^T G_i \Phi_i\|_1 \leq \|\mathbf{s}_i\|_1 \|G_i\|_1 \|\Phi_i\|_1. \tag{7.32}$$

Replacing (7.32) in derivative of Lyapunov candidate function, one can show

$$\begin{aligned}
\dot{V}_i &= \mathbf{s}_i^T G_i \Phi_i - \beta_i \|G_i\|_1 \|\mathbf{s}_i\|_1 - \alpha_i \|\mathbf{s}_i\|_2^2 \\
&\leq \|\mathbf{s}_i\|_1 \|G_i\|_1 \|\Phi_i\|_1 - \beta_i \|G_i\|_1 \|\mathbf{s}_i\|_1 - \alpha_i \|\mathbf{s}_i\|_2^2
\end{aligned} \tag{7.33}$$

Therefore, for any β_i satisfying the following inequality

$$\beta_i > \|\Phi_i\|_1, \tag{7.34}$$

$\dot{V}_i$ is strictly negative and therefore under the proposed robust optimal controller (7.22), the integral sliding surface $\mathbf{s}_i$ is globally asymptotically reachable. This proves that the proposed control law (7.22) drives the system trajectories toward the integral sliding surface and remains on it regardless of the initial conditions of the system. □

Remark 7.7. One can show that

$$\|\Phi_i\|_1 < \varepsilon_i + \sum_{j \in \mathcal{N}_i} \varepsilon_j. \tag{7.35}$$

7.2.1 Matched Uncertainty

The uncertainty is said to be matched if the uncertainty function can be written as $\Phi_i = B_i \Pi_i$. In other words, if uncertainty is applied through the input channel, it is matched; otherwise, it is unmatched. It is well-known that generally compensating the effect of matched uncertainty is easier than unmatched one [159].

For the system on the sliding surface, we have

$$\begin{aligned} \mathbf{s}_i &= 0 \\ \dot{\mathbf{s}}_i &= 0. \end{aligned} \tag{7.36}$$

From (7.26), for a system with a matched uncertainty on the sliding surface, we can write

$$\begin{aligned} \dot{\mathbf{s}}_i &= 0 \\ &= G_i B_i u_i^\star + G_i B_i \Pi_i + G_i B_i R_i^{-1} B_i^T S_i \mathbf{e}_i = 0, \end{aligned} \tag{7.37}$$

where $u_i^\star$ is the control on the integral sliding surface. Thus

$$u_i^\star = -\Pi_i - R_i^{-1} B_i^T S_i \mathbf{e}_i. \tag{7.38}$$

Substituting $u_i^\star$ in system dynamics (7.15), the closed-loop dynamics of the system with matched uncertainty is

$$\dot{\mathbf{e}}_i = \{A_i - B_i R^{-1} B_i^T S_i\} \mathbf{e}_i. \tag{7.39}$$

One can see that for a system with matched uncertainty, the closed-loop system dynamics (7.39) is precisely the same as the closed-loop dynamics of the SDRE controlled nominal system (7.20). In other words, for a system with a matched uncertainty, the proposed controller can completely compensate the effect of the uncertainty. Furthermore, from (7.21) one can see that $\mathbf{s}_i(t_0) = 0$. Thus, a system with matched uncertainty will stay on the sliding surface for $t > t_0$, which means that the trajectories of the uncertain system (7.15) with the proposed control law (7.22) are the same as the state trajectories of the nominal system (7.16) under the SDRE controller (7.18).

Theorem 7.2 provides a controller that makes the closed-loop system asymptotically stable and ensures achieving the desired distance constraints. Note that, based on the ISMC theorem, we showed that the given control law in (7.22) preserves the asymptotic optimality of the SDRE controller for the multi-agent systems with matched uncertainty.

7.3 Formation Stability

In the previous section, we designed a distributed robust optimal controller that steers agent i to its desired formation and satisfies the distance constraints assigned to it. This section shows that the proposed distributed controller also results in the asymptotic stability of the overall formation. In other words, the collective objective of the group of agents will be reached based on action of individual controllers for each agent.

Theorem 7.3. *Suppose that the desired formation is specified in the form of a directed triangulated Laman graph in 2-D or a directed trilateral Laman graph in 3-D space and Assumption 7.1 is valid for all $2 \leq i \leq N$. Then, for a set of uncertain nonlinear multi-agent systems that is modeled as (7.1), the distributed robust optimal control law (7.22) guarantees the asymptotic stability of the overall distance-based formation.*

Proof. We use the mathematical induction method to show the asymptotic stability of the overall formation of N nonlinear, heterogeneous agents. First, we show the stability of agent #2. Next, we show the stability of the overall system of agent #3 and agent #2. Finally, repeating this induction-based procedure, we prove that the overall formation of the agent i,..., agent #2 is asymptomatically stable.

Theorem 7.1 provides the asymptotic stabilizing control for the nominal system (7.16) where $2 \leq i \leq N$. Since the agent #2 (first-follower) is only responsible for controlling its distance toward agent #1 (the leader), therefore we have $\phi_{21} = \eta(p_{21})\hat{\phi}_2$. Since the uncertainty function $\hat{\phi}_2$ is assumed to be bounded, therefore the boundedness of φ_2 is assured and the boundedness of Φ_2 is guaranteed. This guarantees the applicability of Theorem 7.2 which guarantees the asymptotic stability of agent #2 under uncertainty. For the agent #3, from (7.12), one can confirm that $\phi_{31} = \eta(p_{31})\hat{\phi}_3$ and $\phi_{32} = \eta(p_{32})(\hat{\phi}_3 - \hat{\phi}_2)$. This guarantees the boundedness of φ_3, Φ_3, and thus applicability of Theorem 7.2. Also, from the equation (7.11) and (7.22) one can verify that L_3 solely depends on $\mathbf{e}_2$ and $\mathbf{s}_2$. Based on Theorem 7.2 where $i = 3$ and according to the Theorem 2.4, it is obvious that the system (7.14) where $i = 3$ is ISS with respect to L_3. Then, based on Lemma 2.15 we can conclude that the origin of the following interconnected system (overall LFF triangle formation)

$$\Delta_3 : \begin{cases} \dot{\mathbf{e}}_2 = f_2(\mathbf{e}_2, \mathbf{s}_2, \Phi_2) \\ \dot{\mathbf{e}}_3 = f_3(\mathbf{e}_3, \mathbf{s}_3, \Phi_3, \mathbf{e}_2, \mathbf{s}_2, \Phi_2) \end{cases} \tag{7.40}$$

is asymptotically stable.

Using the mathematical induction, one can show that the overall system of cascade interconnected $i-1$ agents, Δ_{i-1}, is asymptotically stable. We show that for the last agent i, the interconnected system is also asymptotically stable, and then the proof is

finished. The control law (7.18) is the stabilizing control of the nominal system (7.16). According to (7.12), the uncertainty function φ_i depends on $\hat{\phi}_i$ and $\hat{\phi}_j \quad \forall j \in \mathcal{N}_i$. Therefore, boundedness of Φ_i is guaranteed and consequently Theorem 7.2 is applicable. Thus, the system (7.15) is asymptotically stable, and therefore, based on theorem 2.3, it is obvious that the system (7.14) is locally ISS with respect to L_i. Then according to Theorem 2.7 the origin of interconnected system

$$\Delta_i : \begin{cases} \dot{\mathbf{e}}_2 = f_2(\mathbf{e}_2, \mathbf{s}_2, \Phi_2) \\ \dot{\mathbf{e}}_3 = f_3(\mathbf{e}_3, \mathbf{s}_3, \Phi_3, \mathbf{e}_2, \mathbf{s}_2, \Phi_2) \\ \vdots \\ \dot{\mathbf{e}}_i = f_i(\mathbf{e}_i, \mathbf{s}_i, \Phi_i, ..., \mathbf{e}_j, \mathbf{s}_j, \Phi_j, ...) \end{cases} \tag{7.41}$$

where $j \in \mathcal{N}_i$, is locally asymptotically stable. □

7.4 Selection of Weighting Matrices

Selection of state-dependent weighting matrices of the cost functional provides a very effective tool to include some desired constraints and/or performance adjustments [146], [147]. Thus, the weighting matrices of the cost functional can be chosen accordingly. In Chapter 4, we proposed an input weighting selection procedure that prevents from depleting the energy of the electrically sourced agents. We also proposed state weighting matrix selection procedures in Chapter 5, that prevent from flip ambiguity in distance-based formations in 2-D and 3-D spaces, respectively.

For a formation edge e_{ij}, let us define the corresponding weighting factor as

$$q_{ij} = \varrho_{ij} + \mu_{ij} \quad \forall j \in \mathcal{N}_i, \tag{7.42}$$

where $\varrho_{ij} \in \mathbb{R}_+$ is a constant and μ_{ij} is a positive barrier multiplier defined by

$$\mu_{ij} = (\frac{d_{ij}^*}{d_{ij} - r_{d_{ij}}})^{\epsilon}, \tag{7.43}$$

for suitable $\epsilon \geq 1$, and $r_{d_{ij}}$ being a safe distance between pair of agents i and j to prevent the collision. Then, the following theorem, which offers the weighting matrices selection procedure for preventing the collision of the neighboring agents and reflection of the formation, can be presented.

Theorem 7.4. *For a nominal SDRE controller in Theorem 7.1, let state weighting matrix be selected as*

$$Q_i = \kappa_i diag[..., q_{ij}, ..., q_{w_i}], \quad \forall j \in \mathcal{N}_i \tag{7.44}$$

where

$$\kappa_i = \begin{cases} \frac{\mathbb{A}_i^* - \mathbb{A}_i}{\mathbb{A}_i^* + \mathbb{A}_i}, & \text{if} \quad dg_i^+ = 2 \\ \frac{\mathbb{V}_i^* - \mathbb{V}_i}{\mathbb{V}_i^* + \mathbb{V}_i}, & \text{if} \quad dg_i^+ = 3 \end{cases} \tag{7.45}$$

and $\mathbb{A}_i^*$, $\mathbb{A}_i$, $\mathbb{V}_i^*$ and $\mathbb{V}_i$ are desired signed area, actual signed area, desired signed volume and actual signed volume of the corresponding triangle or tetrahedron formed by agent i and its neighbors. Then, the proposed control law (7.22), alongside asymptotic stability of the desired formation, prevents flip ambiguity of the directed distance-based formation and guarantees inter-agent collision avoidance of the neighboring agents.

Proof. Proof can be found in Chapter 5, thus omitted here. □

7.5 Simulation Results

In this section, we present simulation results of the proposed robust optimal controller for different scenarios. We studied different desired formation shapes in both 2-D and 3-D spaces for different sets of multi-agent systems. Moreover, we considered the formation control problem for groups of homogeneous agents and heterogeneous agents with different nonlinear dynamics. Finally, we also considered both matched and unmatched uncertainty situations. To prevent chattering of control, we can use a sigmoid function or a saturation function instead of the signum function [164]. In simulations, we used the saturation function where it is defined as

$$\text{sat}(x) = \begin{cases} x & |x| \leq 1 \\ \text{sgn}(x) & |x| > 1 \end{cases} . \tag{7.46}$$

It is easy to show that the results and proof of the Theorem 7.2 are still valid under this modification [165].

7.5.1 2-D Space

Figure 7.1 shows the desired directed distance-based formation topology for a set of $N = 6$ agents in 2-D space. All desired distances between agents are selected as $d_{ij} = 10$. Since the desired formation is directed triangulated Laman graph, the leader is not responsible for any edge and therefore leader is stationary. The SDRE controllers' parameters are selected as $\varrho_{ij} = 1$, $r_{d_{ij}} = 2$, $\epsilon = 2$, and $R_i = I$ for all simulations. The agents are

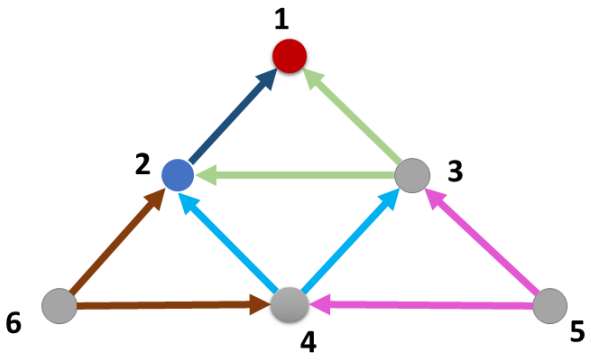

Figure 7.1: Desired formation topology for $N = 6$ agents in 2-D.

homogeneous and we use the model proposed in Chapter 6 to represent the agents as

$$\begin{aligned}
\dot{x}_i &= v_{x_i} \\
\dot{y}_i &= v_{y_i} \\
\dot{v}_{x_i} &= v_{x_i}^2 + 2v_{y_i} + (1 + v_{x_i})(u_{x_i} + d_i) \\
\dot{v}_{y_i} &= v_{x_i} v_{y_i} + (1 + v_{y_i})(u_{y_i} - d_i) \\
\dot{w}_i &= -w_i + u_{x_i} + u_{y_i},
\end{aligned} \tag{7.47}$$

where uncertainty assumed to be matched and selected as $d_2 = 2cos(0.2t)$, $d_3 = sin(0.2t)$, $d_4 = 2sin(0.1t)$, $d_5 = 3cos(0.3t)$, and $d_6 = 3sin(0.3t)$. The initial position of the agents are selected as $p_1 = [-5, -5]$. $p_2 = [-35, -5]$, $p_3 = [-5; -30], p_4 = [-25, -25]$, $p_5 = [-10; -30]$, and $p_6 = [-35; -20]$.

First, we simulated the scenario where just the nominal SDRE controller is applied, without the robust ISMC part. This is to examine what happens to the nominal formation under the uncertainty condition without having a robust controller. Figure 7.2 shows the trajectories of agents with the SDRE controller, u^{SDRE}, of the nominal system proposed in Theorem 7.1. Figure 7.3 depicts the corresponding formation errors. It is evident that although the SDRE controller asymptotically stabilizes the nominal system, it can not stabilize the system under uncertainty. The formation is distorted, and error signals do not converge.

Next, we simulate the system with the proposed robust optimal control in Theorem 7.2. Figure 7.4 depicts the trajectories of agents with the proposed ISMC-SDRE controller. It can be seen that the agents converge to the desired framework using the proposed controller. The corresponding formation errors and control signals are shown in Figure 7.5 and Figure 7.6, respectively.

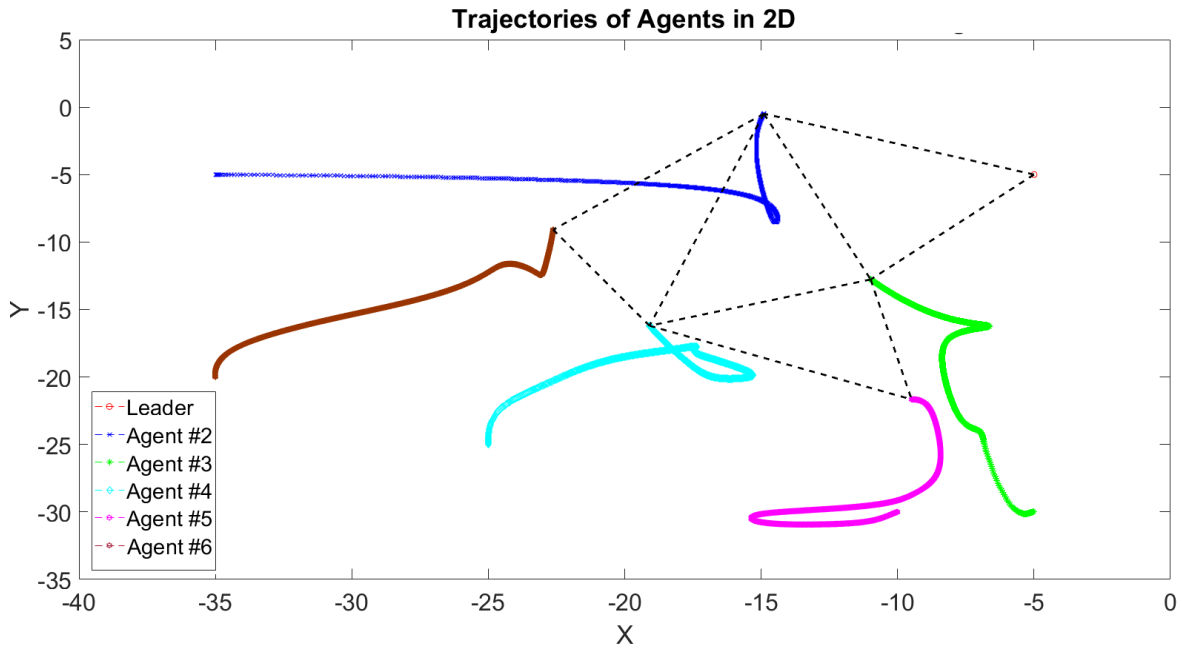

Figure 7.2: Trajectories of the agents with only nominal SDRE controller under matched uncertainty.

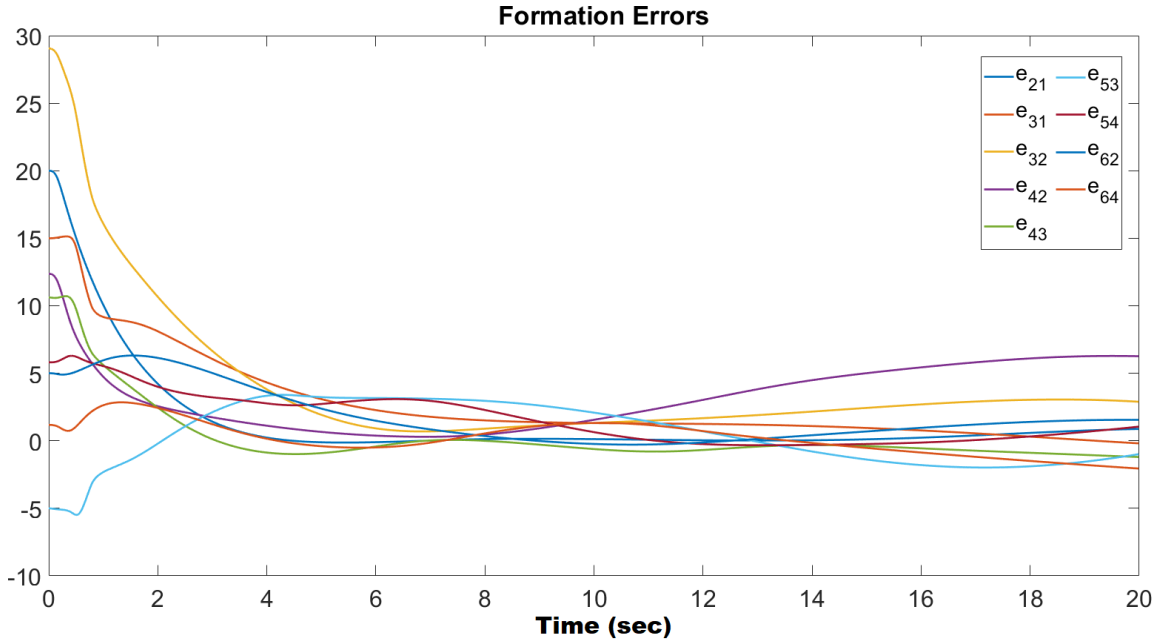

Figure 7.3: Corresponding formation errors in simulation Figure 7.2.

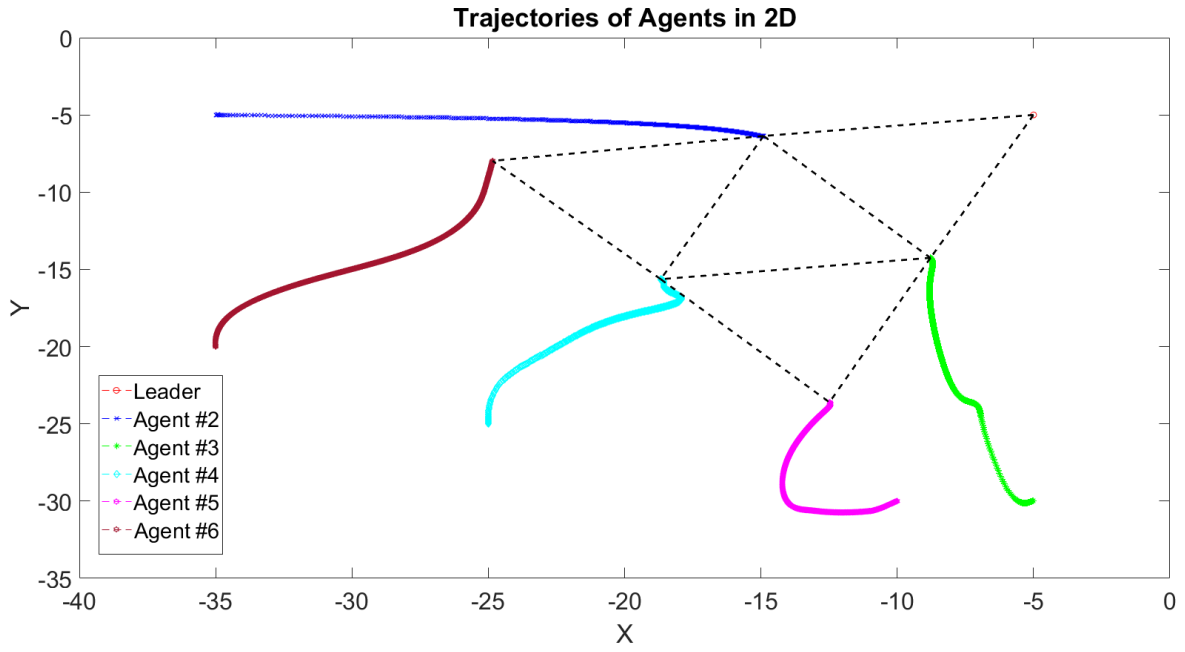

Figure 7.4: Trajectories of the agents with proposed ISMC-SDRE controller under matched uncertainty.

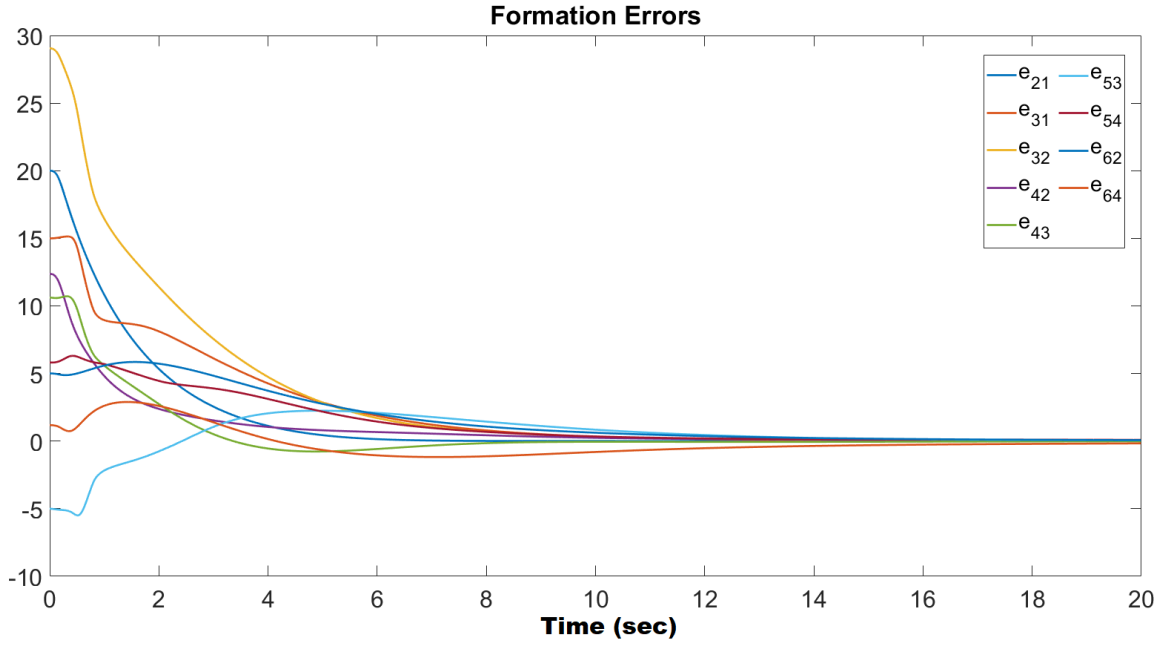

Figure 7.5: Corresponding formation errors in simulation Figure 7.4.

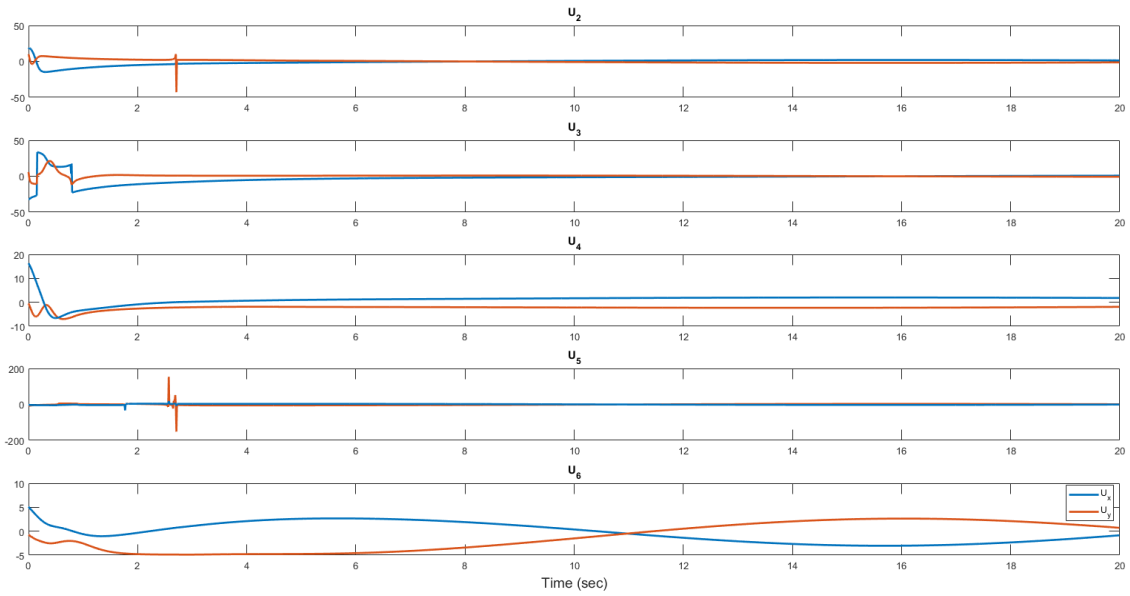

Figure 7.6: Agents control signals in simulation Figure 7.4.

7.5.2 3-D Space

Figure 2.6(b) depicts the desired directed trilateral Laman graph. Here, agents are supposed to be heterogeneous. Also, the uncertainties are assumed to be matched. The heterogeneous models from Chapter 6, is used to represent the agents. The leader is placed at $p_1 = [20, 20, 30]$. The agent #2 (first follower) is modeled as

$$\begin{aligned}
\dot{x}_2 &= v_{2_x} \\
\dot{y}_2 &= v_{2_y} \\
\dot{z}_2 &= v_{2_z} \\
\dot{v}_{2_x} &= 2v_{2_x} + (1 + v_{2_x})(u_{2_x} + d_2) \\
\dot{v}_{2_y} &= 2v_{2_y} + (1 + v_{2_y})(u_{2_y} - d_2) \\
\dot{v}_{2_z} &= 2v_{2_z} + (1 + v_{2_z})(u_{2_z} - d_2),
\end{aligned} \tag{7.48}$$

where the initial position of the agent #2 is $p_2 = [30, 10, -10]$ and the uncertainty is $d_2 = 0.5cos(0.2t)$. The agent #3 is modeled as

$$\begin{aligned}
\dot{x}_3 &= v_{3_x} \\
\dot{y}_3 &= v_{3_y} \\
\dot{z}_3 &= v_{3_z} \\
\dot{v}_{3_x} &= v_{3_x} + u_{3_x} + d_3 \\
\dot{v}_{3_y} &= v_{3_y} + u_{3_y} - d_3 \\
\dot{v}_{3_z} &= v_{3_z} + u_{3_z} - d_3 \\
\dot{w}_3 &= -w_3 + u_{3_x} + u_{3_y} + u_{3_z} - d_3,
\end{aligned} \tag{7.49}$$

where the uncertainty is $d_3 = 0.6sin(0.2t)$ and the initial position of the follower #3 is $p_3 = [50, -30, 20]$. The agent #4 is modeled as

$$\begin{aligned}
\dot{x}_4 &= v_{4_x} \\
\dot{y}_4 &= v_{4_y} \\
\dot{z}_4 &= v_{4_z} \\
\dot{v}_{4_x} &= v_{4_x}^2 + u_{4_x} + d_4 \\
\dot{v}_{4_y} &= v_{4_y}^2 + u_{4_y} \\
\dot{v}_{4_z} &= v_{4_z}^2 + u_{4_z} - d_4,
\end{aligned} \tag{7.50}$$

where $d_4 = 0.5sin(0.1t)$ and the initial position of the follower #4 is $p_4 = [-10, 20, -10]$. Agent #5 is modeled as

$$\begin{aligned}
\dot{x}_5 &= v_{5_x} \\
\dot{y}_5 &= v_{5_y} \\
\dot{z}_5 &= v_{5_z} \\
\dot{v}_{5_x} &= v_{5_z} v_{5_x} + u_{5_x} - d_5 \\
\dot{v}_{5_y} &= v_{5_y}^2 + u_{5_y} + d_5 \\
\dot{v}_{5_z} &= v_{5_x} v_{5_z} + u_{5_z} - d_5,
\end{aligned} \tag{7.51}$$

where the initial position of the follower #5 was selected as $p_5 = [50, -20, 20]$ and uncertainty is $d_5 = sin(0.15t)$.

Figure 7.7 shows the trajectories of $N = 5$ agents with proposed ISMC-SDRE controller. The agents converge to the desired distance-based formation shape successfully. Figure 7.8 presents the formation errors of the simulation that converges to zero.

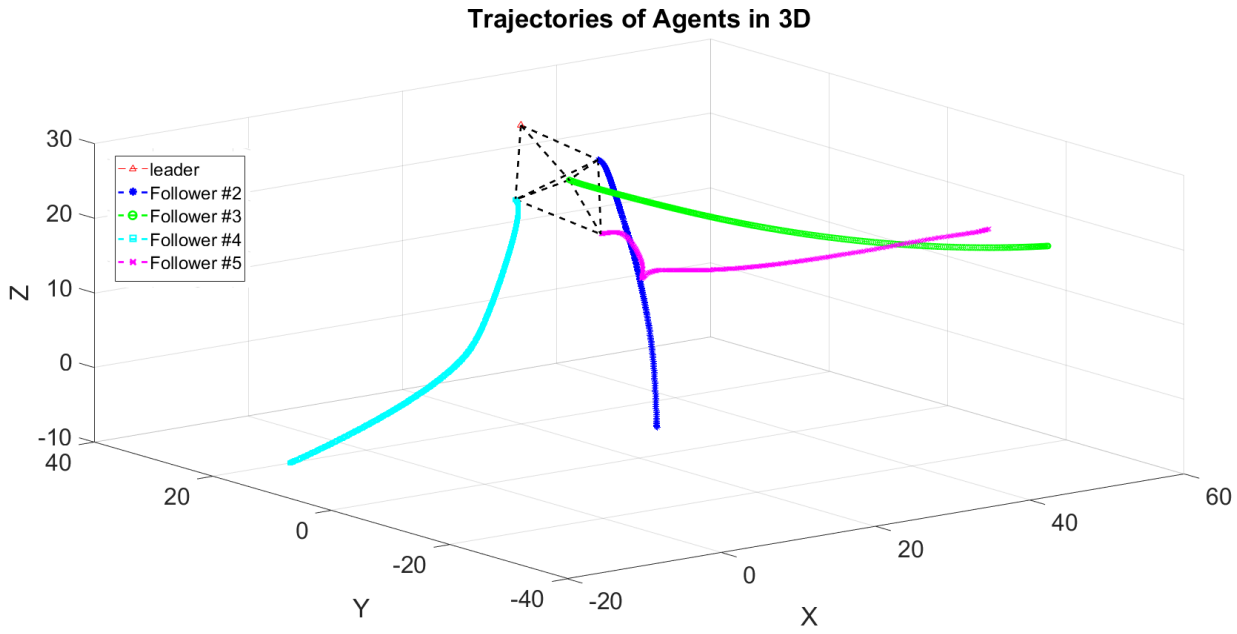

Figure 7.7: Trajectories of the agents using ISMC-SDRE based proposed controller in 3-D space.

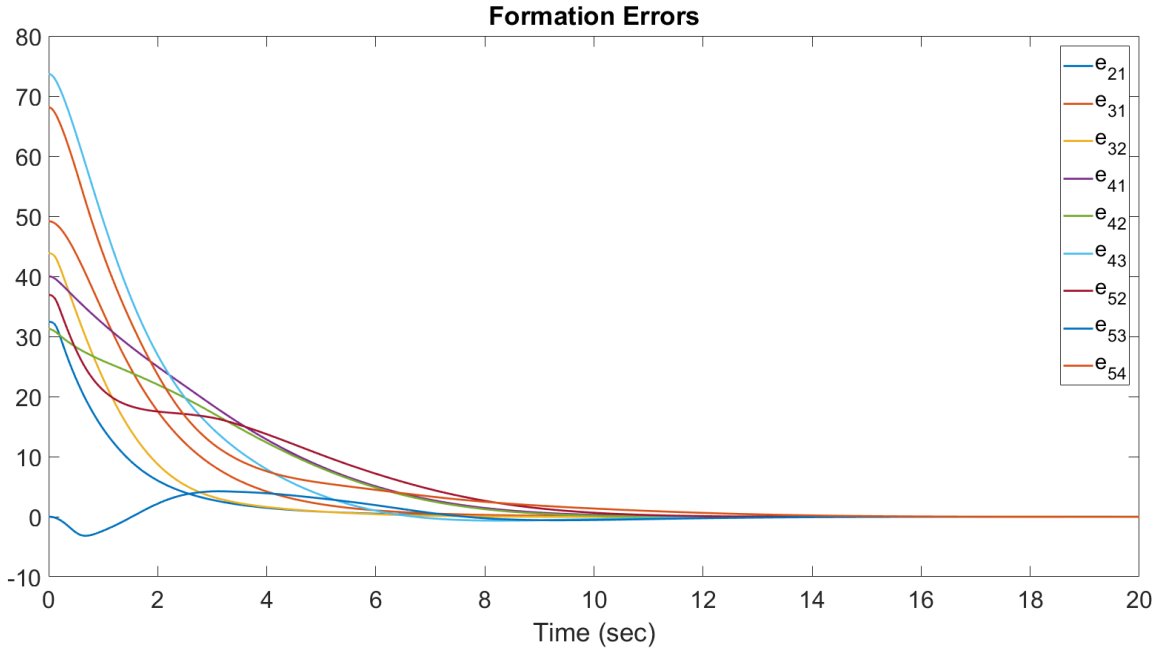

Figure 7.8: Corresponding formation errors in simulation Figure 7.7.

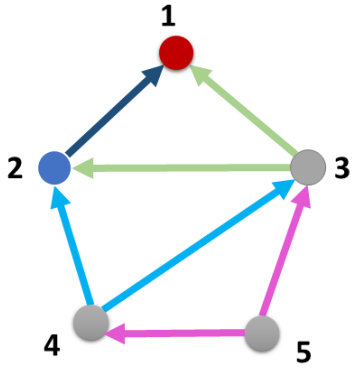

Figure 7.9: Desired formation topology for $N = 5$ agents in 2-D space.

7.5.3 Unmatched Uncertainty

In this subsection, we consider the unmatched uncertainties. From the mathematical analysis we anticipate that the control of unmatched uncertainties be more challenging and the controller loses its optimality. Figure 7.9 shows the desired formation topology. The desired distance constraints are selected as $d_{21} = 10$, $d_{31} = 10$, $d_{32} = \sqrt{200}$, $d_{42} = 10$, $d_{43} = \sqrt{200}$, $d_{53} = 10$ and $d_{54} = 10$. For simplicity and comparison purposes, we assume that the agents are homogeneous and modeled as

$$\begin{aligned}
\dot{x}_i &= v_{x_i} + d_i \\
\dot{y}_i &= v_{y_i} - d_i \\
\dot{v}_{x_i} &= v_{x_i}^2 + 2v_{y_i} + (1 + v_{x_i})u_{x_i} + d_i \\
\dot{v}_{y_i} &= v_{x_i}v_{y_i} + (1 + v_{y_i})u_{y_i} - d_i \\
\dot{w}_i &= -w_i + u_{x_i} + u_{y_i} + d_i.
\end{aligned} \tag{7.52}$$

the uncertainties are selected as $d_2 = 0.1 * cos(0.1 * t)$, $d_3 = 15 * sin(0.2 * t)$, $d_4 = 0.25 * sin(0.25 * t)$, and $d_5 = 0.2 * cos(0.1 * t)$. The initial position of the agents were selected as $p_1 = [-5, -5]$. $p_2 = [-35, -10]$, $p_3 = [-5; -30]$, $p_4 = [-30, -25]$, and $p_5 = [-10; -30]$. Figure 7.10 depicts the trajectories of the agents with unmatched uncertainty over the plane where the proposed ISMC-SDRE controllers successfully steer all agents to form the desired formation. Fig. 7.11 shows the corresponding control signals of the agents. The simulation is run for another desired wheel graph given in directed triangulated Laman form, Figure 7.12, and a different set of initial conditions to verify the performance of the proposed controller. The new initial positions were $p_1 = [-5, -5]$. $p_2 = [-35, -10]$, $p_3 = [-5; -35], p_4 = [-20, 15]$, and $p_5 = [10; 10]$. Figure 7.13 results demonstrate the effectiveness of the proposed controller.

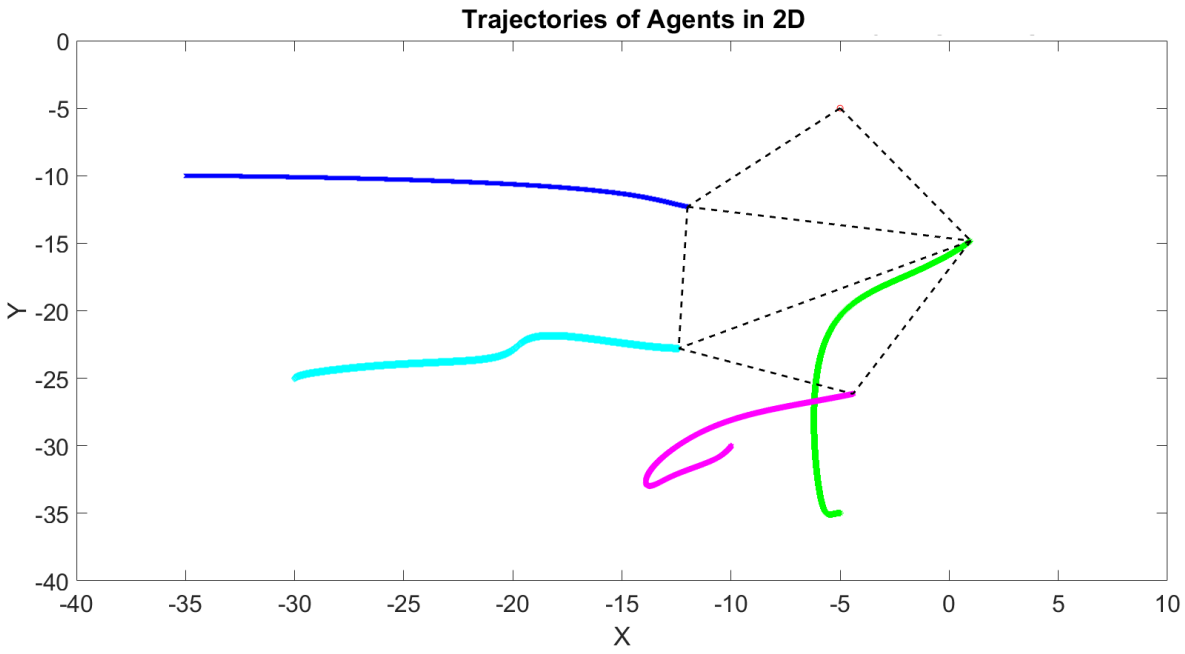

Figure 7.10: Trajectories of the agents with proposed ISMC-SDRE controller under unmatched uncertainty.

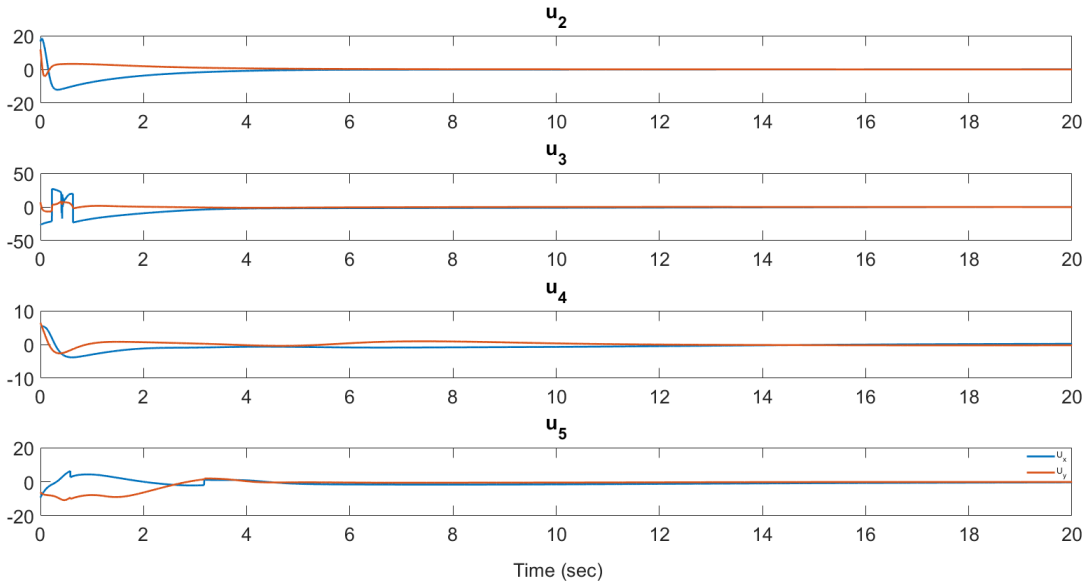

Figure 7.11: Agents control signals in simulation of Fig. 7.10.

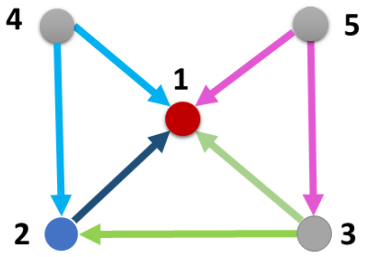

Figure 7.12: Desired formation topology for $N = 4$ agents in 2-D space.

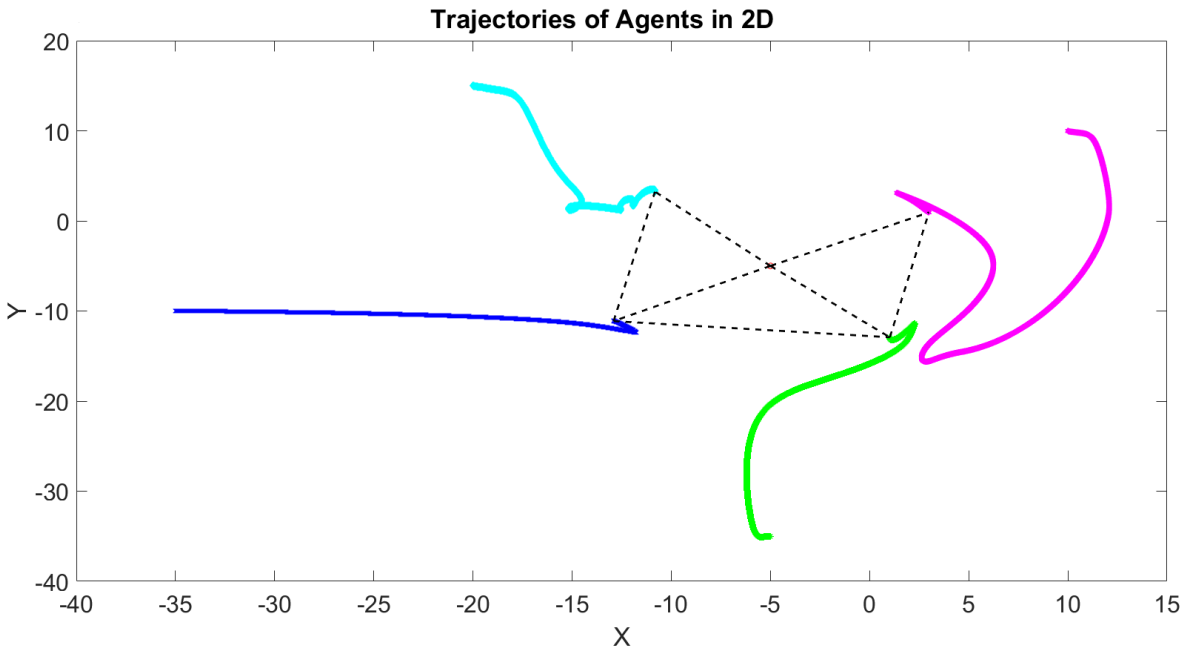

Figure 7.13: Trajectories of the agents with proposed ISMC-SDRE controller under unmatched uncertainty.

7.6 Conclusions

Physical systems are subject to uncertainties due to imperfections in modeling, internal noise, disturbances, etc. In this chapter, we studied a distance-based formation control of uncertain nonlinear agents. For a set of nonlinear agents with additive uncertainties, we developed a robust optimal formation control scheme that can guarantee asymptotic stability of the desired distance-based formation. The target formation is a directed triangulated Laman graph in 2-D space or a directed trilateral Laman graph in 3-D space, which are particular classes of directed acyclic minimally persistent or minimally structurally persistent graphs, respectively.

We developed a robust optimal control scheme that guarantees the asymptotic stability of the formation in the presence of bounded uncertainties. We have shown that the proposed controller can completely compensate for the effect of matched uncertainty on the formation. The proposed control scheme is based on the integral sliding mode control (ISMC) theory in combination with the state-dependent Riccati equation (SDRE) method. We also presented a discussion on weight selection policy that can include several constraints in the optimal control problem, including collision avoidance, reflection prevention, energy depletion prevention. The proposed weight selection procedure also allows users to adjust the trade-off between the formation control performance and control input energy usage. Simulation results are provided to back up the effectiveness of the theoretical results.

Chapter 8

Summary and Future Works

8.1 Summary

In this dissertation, we developed a new framework for distance-based formation control. Unlike the majority of the research on distance-based formation control, which used gradient-based control, as a novel approach, we developed a nonlinear optimal control-based methodology for the distance-based formation control problem. We studied distance-based formation control in different setups and developed a systematic approach for controlling the agents toward the desired objective. Due to the nonlinear nature of the distance-based formation problem, we used the well-matured state-dependent Riccati equation (SDRE) method as a backbone of the proposed solution. The SDRE method is a systematic approach that has great capability to control nonlinear systems alongside its ability to adjust the control performance directly and handle the state and input constraints.

The distance-based formation could be undirected or directed where controlling the distance between a pair of agents is assigned to both adjacent agents or just one of them, respectively. The desired distance between a pair of neighboring agents is controlled by the mutual effort of both adjacent agents in undirected formation. In contrast, in directed formation, only the source agent tries to preserve the edge. The appropriate mathematical framework for the directed and undirected distance-based formation problems are directed persistent and undirected rigid graph theories. We studied distance-based formation for both directed and undirected topologies. Accordingly, the proper rigid graph theory and persistent graph theory are used toward this aim.

We studied undirected distance-based formation control in Chapter 4. Introducing a particular form of rigidity matrix, named as normalized rigidity matrix, we formulated the distance-based formation control via dynamics of the edge function and used the SDRE controller to stabilize it. The proposed method assures global asymptotic stability of the desired formation for a set of agents models as single and double-integrators. Also, using

hybrid SDRE, we studied a leader-follower tracking problem where the leader tracks the desired trajectory and the followers preserve the desired formation shape. Using the barrier function method and including the collision avoidance in the cost function, the proposed method guarantees collision-free convergence of all agents to the desired framework. Furthermore, we introduced an energy dynamic for agents and used it to add a constraint to the optimal control problem that also prevents agents' energy depletion. It is worth mentioning that, through extensive simulations, we found that our method is less sensitive to simulation parameters such as sampling time, and it has a broader region of attraction compared to the other gradient-based controller. However, the method requires more computational time since it requires solving an SDRE equation in each step.

For directed topologies in which each edge is controlled by just one agent, we proposed a distributed control law that guarantees the global stability of the desired formation for agents modeled as the single-integrator. We introduced special classes of the directed graphs: directed triangulated and trilateral Laman graphs. The desired formation is supposed to be in the form of a directed triangulated Laman graph in 2-D or a directed trilateral Laman graph in 3-D. The control design process is established in accordance with cascade systems' stability that guarantees the stability of the desired formation. In order to prevent flip ambiguity of the formation, using signed area and signed volume constraints, we proposed a solution that prevents agents from converging to the undesired equilibrium set (reflected configurations).

We also studied the distance-based formation control for nonlinear systems. The proposed methodology applies to a broad class of homogeneous and heterogeneous affine nonlinear systems in both 2-D and 3-D space. In addition, the robustness of distance-based formation control of uncertain nonlinear systems is studied. Using the integral sliding mode control (ISMC) method combined with SDRE, we propose a robust controller that can stabilize the desired formation for a set of agents affected by bounded uncertainties. The proposed method is effective for both matched and unmatched uncertainties where it preserves the optimality of the controller for the matched case.

8.2 Future Work

The possible future work related to this theses can be

- Implementation of the methods developed in this dissertation:

  A real-time experimental setup for the controllers proposed in this thesis can be the next step. The methods proposed in this dissertation can be implemented on a set of UGVs or UAVs. Also, using the job assignment algorithm that is proposed in this work, several forms of the desired formations could be converted

to a persistent, directed, distance-based formation control. Then, the proposed control approaches can be used to control the formation. Also, there could be other potential applications such as autonomous vehicles, commercial planes, and drone shows.

- Combination of vision-based formation with distance-based formation:

  Vision-based control is a promising approach since it can be implemented by agents equipped with a camera sensor. Also, it is compatible with the formation control of LFF structures that are developed in this thesis. Therefore, plenty of applications can be defined for the combination of vision- and distance-based formation control approaches.

- Extending the optimal control framework to a vision- and bearing-based formations:

  The optimal control methods that are developed in this thesis can also be adopted for bearing-based, vision-based, or a combination of them with distance-based formation control. This might result in a unified platform for different approaches to formation control problems.

- Artificial intelligence controller design for the distance-based formation problem:

  Artificial intelligence and machine learning techniques are recently gained interest in different engineering fields, including control systems. There are few studies on the formation control of multi-agent systems with neural networks, but there are still open problems to study; for instance, asymptotic stability of the distance-based formation with neural-network-based controller needs to be addressed.

Bibliography

[1] PeopleTek, "What's a good leader." available online at: https://www.peopletekcoaching.com/whats-good-leader/. Accessed: 2021-10-14.

[2] K.-K. Oh, M.-C. Park, and H.-S. Ahn, "A survey of multi-agent formation control," *Automatica*, vol. 53, pp. 424–440, 2015.

[3] B. D. O. Anderson, C. Yu, B. Fidan, and J. M. Hendrickx, "Rigid graph control architectures for autonomous formations," *IEEE Control Syst. Mag.*, vol. 28, no. 6, pp. 48–63, 2008.

[4] P. Lissaman and C. A. Shollenberger, "Formation flight of birds," *Science*, vol. 168, no. 3934, pp. 1003–1005, 1970.

[5] Airbus, "Airlines are looking to reduce fuel consumption. wake-energy retrieval could help." available online at: https://www.airbus.com/newsroom/stories/airlines-are-looking-to-reduce-fuel-consumption-wake-energy-retrieval-could-help.html. Accessed: 2021-10-14.

[6] X. Li, D. Zhu, and Y. Qian, "A survey on formation control algorithms for multi-AUV system," *Unmanned Syst.*, vol. 2, no. 04, pp. 351–359, 2014.

[7] D. Zelazo, A. Franchi, H. H. Bülthoff, and P. R. Giordano, "Decentralized rigidity maintenance control with range measurements for multi-robot systems," *Int. J. Rob. Res.*, vol. 34, no. 1, pp. 105–128, 2015.

[8] D. Zelazo, P. R. Giordano, and A. Franchi, "Bearing-only formation control using an SE(2) rigidity theory," in *Proc. 54th IEEE Conf. Decis. Control (CDC)*, (Osaka, Japan), pp. 6121–6126, Dec. 2015.

[9] S. Ramazani, R. Selmic, and M. de Queiroz, "Rigidity-based multiagent layered formation control," *IEEE Trans. Cybern.*, vol. 47, no. 8, pp. 1902–1913, 2017.

[10] S. M. Kang, M. C. Park, B. H. Lee, and H. S. Ahn, "Distance-based formation control with a single moving leader," in *Proc. Amer. Control Conf. (ACC)*, (Portland, OR, USA), pp. 305–310, June 2014.

[11] J. Ma, Y. Zheng, and L. Wang, "LQR-based optimal topology of leader-following consensus," *Int. J. Robust Nonlin. Control*, vol. 25, no. 17, pp. 3404–3421, 2015.

[12] C. I. G. Chinelato and L. S. Martins-Filho, "SDRE based leader-follower formation control of multiple mobile robots," *TEMA (São Carlos)*, vol. 15, no. 2, pp. 195–202, 2014.

[13] Y. Chen and J. Sun, "Distributed optimal control for multi-agent systems with obstacle avoidance," *Neurocomputing*, vol. 173, pp. 2014–2021, 2016.

[14] R. Rajasree and V. Jisha, "Optimal formation control of unmanned aerial vehicles with obstacle avoidance," in *Proc. Int. Conf. Control Instrum. Commun. Comput. Technol. (ICCICCT)*, (Kumaracoil, India), pp. 163–168, Dec. 2015.

[15] C. B. Low and Q. San Ng, "A flexible virtual structure formation keeping control for fixed-wing UAVs," in *Proc. 9th IEEE Int. Conf. Control Autom. (ICCA)*, (Santiago, Chile), pp. 621–626, Dec. 2011.

[16] R. W. Beard and W. Ren, "Virtual structure based spacecraft formation control with formation feedback," in *Proc. AIAA Guid. Navig. Control Conf.*, p. 4963, 2002.

[17] S. Mou, M.-A. Belabbas, A. S. Morse, Z. Sun, and B. D. O. Anderson, "Undirected rigid formations are problematic," *IEEE Trans. Autom. Control*, vol. 61, no. 10, pp. 2821–2836, 2015.

[18] B. Fidan, C. Yu, and B. D. O. Anderson, "Acquiring and maintaining persistence of autonomous multi-vehicle formations," *IET Control Theory & Appl.*, vol. 1, no. 2, pp. 452–460, 2007.

[19] K.-K. Oh and H.-S. Ahn, "Distance-based formation control using euclidean distance dynamics matrix: Three-agent case," in *Proc. Amer. Control Conf. (ACC)*, pp. 4810–4815, 2011.

[20] K. K. Oh and H. S. Ahn, "Distance-based formation control using Euclidean distance dynamics matrix: General cases," in *Proc. Amer. Control Conf.*, pp. 4816–4821, 2011.

[21] Z. Lin, L. Wang, Z. Han, and M. Fu, "A graph Laplacian approach to coordinate-free formation stabilization for directed networks," *IEEE Trans. Autom. Control*, vol. 61, no. 5, pp. 1269–1280, 2015.

[22] B. H. Lee, S. J. Lee, M. C. Park, K. K. Oh, and H. S. Ahn, "Nonholonomic control of distance-based cyclic polygon formation," in *Proc. 9th Asian Control Conf. (ASCC)*, pp. 1–4, 2013.

[23] K. Aryankia and R. R. Selmic, "Neuro-adaptive formation control and target tracking for nonlinear multi-agent systems with time-delay," *IEEE Control Systems Letters*, vol. 5, no. 3, pp. 791–796, 2021.

[24] Y. Hou and C. Yu, "Distance-based control of formations with hybrid communication topology," *Int. J. Robust and Nonlinear Control*, vol. 28, no. 3, pp. 881–900, 2018.

[25] S. A. Barogh and H. Werner, "Cascaded formation control using angle and distance between agents with orientation control (part 2)," in *Proc. UKACC 11th Int. Conf. Control*, pp. 1–6, 2016.

[26] K. Fathian, D. I. Rachinskii, M. W. Spong, and N. R. Gans, "Globally asymptotically stable distributed control for distance and bearing based multi-agent formations," in *Proc. Amer. Control Conf.*, pp. 4642–4648, 2016.

[27] T. Liu and M. de Queiroz, "Distance + angle-based control of 2-D rigid formations," *IEEE Trans. Cybern.*, 2020.

[28] O. Rozenheck, S. Zhao, and D. Zelazo, "A proportional-integral controller for distance-based formation tracking," in *Proc. Eur. Control Conf. (ECC),*, pp. 1693–1698, 2015.

[29] R. Olfati-Saber and R. M. Murray, "Distributed cooperative control of multiple vehicle formations using structural potential functions," in *IFAC world congress*, vol. 15, pp. 242–248, Citeseer, 2002.

[30] D. V. Dimarogonas and K. H. Johansson, "On the stability of distance-based formation control," in *Proc. 47th IEEE Conf. Decis. Control (CDC)*, pp. 1200–1205, 2008.

[31] K.-K. Oh and H.-S. Ahn, "Distance-based undirected formations of single-integrator and double-integrator modeled agents in n-dimensional space," *Int. J. Robust Nonlinear Control*, vol. 24, no. 12, pp. 1809–1820, 2014.

[32] Z. Sun, S. Mou, B. D. O. Anderson, and M. Cao, "Exponential stability for formation control systems with generalized controllers: A unified approach," *Syst. & Control Lett.*, vol. 93, pp. 50–57, 2016.

[33] B. D. O. Anderson, Z. Lin, M. Deghat, *et al.*, "Combining distance-based formation shape control with formation translation," *Developments in Control Theory Towards Glocal Control*, vol. 1, pp. 121–130, 2012.

[34] Y. Zou, C. Wen, and M. Guan, "Distributed adaptive control for distance-based formation and flocking control of multi-agent systems," *IET Control Theory & Appl.*, vol. 13, no. 6, pp. 878–885, 2019.

[35] R. Babazadeh and R. Selmic, "Distance-based multiagent formation control with energy constraints using SDRE," *IEEE Trans. Aerosp. Electron. Syst.*, vol. 56, no. 1, pp. 41–56, 2019.

[36] K.-K. Oh and H.-S. Ahn, "Formation control of mobile agents based on inter-agent distance dynamics," *Automatica*, vol. 47, no. 10, pp. 2306–2312, 2011.

[37] T. Eren, P. N. Belhumeur, B. D. O. Anderson, and A. S. Morse, "A framework for maintaining formations based on rigidity," *IFAC Proceedings Volumes*, vol. 35, no. 1, pp. 499–504, 2002.

[38] A. Nikou, C. K. Verginis, and D. V. Dimarogonas, "Robust distance-based formation control of multiple rigid bodies with orientation alignment," *IFAC-PapersOnLine*, vol. 50, no. 1, pp. 15458–15463, 2017.

[39] A. P. Popov and H. Werner, "A robust control approach to formation control," in *Proc. Eur. Control Conf. (ECC)*, pp. 4428–4433, 2009.

[40] L. Wang and Q. Guo, "Distance-based formation stabilization and flocking control for distributed multi-agent systems," in *2018 IEEE Int. Conf. Mechatronics Autom. (ICMA)*, pp. 1580–1585, 2018.

[41] M. Deghat, B. D. O. Anderson, and Z. Lin, "Combined flocking and distance-based shape control of multi-agent formations," *IEEE Trans. Autom. Control*, vol. 61, no. 7, pp. 1824–1837, 2016.

[42] T. Liu, M. de Queiroz, P. Zhang, and M. Khaledyan, "Directed formation control of n planar agents with distance and area constraints," *arXiv preprint arXiv:1901.10564*, 2019.

[43] E. G. Hernandez-Martinez, E. D. Ferreira-Vazquez, G. Fernandez-Anaya, and J. J. Flores-Godoy, "Formation tracking of heterogeneous mobile agents using distance and area constraints," *Complexity*, vol. 2017, Article ID 9404193, 2017.

[44] B. D. O. Anderson, Z. Sun, T. Sugie, S.-i. Azuma, and K. Sakurama, "Formation shape control with distance and area constraints," *IFAC J. of Syst. and Control*, vol. 1, pp. 2–12, 2017.

[45] S. H. Kwon, Z. Sun, B. D. O. Anderson, and H. S. Ahn, "Hybrid distance-angle rigidity theory with signed constraints and its applications to formation shape control," *arXiv preprint arXiv:1912.12952*, 2019.

[46] E. Montijano, E. Cristofalo, M. Schwager, and C. Sagues, "Distributed formation control of non-holonomic robots without a global reference frame," in *Proc. 2016 IEEE Int. Conf. Robot. Autom. (ICRA)*, pp. 5248–5254, IEE, 2016.

[47] T. Sugie, B. D. O. Anderson, Z. Sun, and H. Dong, "On a hierarchical control strategy for multi-agent formation without reflection," in *Proc. 57th IEEE Conf. Decis. Control (CDC)*, pp. 2023–2028, 2018.

[48] Y. Cao, Z. Sun, B. D. O. Anderson, and T. Sugie, "Almost global convergence for distance-and area-constrained hierarchical formations without reflection," in *Proc. 15th IEEE Int. Conf. Control Autom.*, 2019.

[49] X. Chen, M. A. Belabbas, and T. Başar, "Global stabilization of triangulated formations," *SIAM J. Control Optim.*, vol. 55, no. 1, pp. 172–199, 2017.

[50] E. D. Ferreira-Vazquez, E. G. Hernandez-Martinez, J. J. Flores-Godoy, and G. Fernandez-Anaya, "Spatial formation control with volume information: Application to quadcopter UAV's," *IFAC-PapersOnLine*, vol. 49, no. 18, pp. 302–307, 2016.

[51] E. D. Ferreira-Vazquez, J. J. Flores-Godoy, E. G. Hernandez-Martinez, and G. Fernandez-Anaya, "Adaptive control of distance-based spatial formations with planar and volume restrictions," in *Proc. IEEE Conf. Control Appl.*, pp. 905–910, 2016.

[52] J. M. Hendrickx, B. D. O. Anderson, J.-C. Delvenne, and V. D. Blondel, "Directed graphs for the analysis of rigidity and persistence in autonomous agent systems," *Int. J. of Robust and Nonlinear Control*, vol. 17, no. 10-11, pp. 960–981, 2007.

[53] K.-K. Oh and H.-S. Ahn, "Distance-based control of cycle-free persistent formations," in *2011 IEEE Int. Symp. on Intelligent Control*, pp. 816–821, 2011.

[54] B. D. O. Anderson, S. Dasgupta, and C. Yu, "Control of directed formations with a leader-first follower structure," in *Proc. 46th IEEE Conf. Decis. Control*, pp. 2882–2887, 2007.

[55] M. C. Park and H. S. Ahn, "Stabilisation of directed cycle formations and application to two-wheeled mobile robots," *IET Control Theory & Appl.*, vol. 9, no. 9, pp. 1338–1346, 2015.

[56] V. H. Pham, M. H. Trinh, and H.-S. Ahn, "Distance-based directed formation control in three-dimensional space," in *56th Proc. SICE Annu. Conf.*, pp. 886–891, 2017.

[57] T. Han, Z. Lin, R. Zheng, and M. Fu, "A barycentric coordinate-based approach to formation control under directed and switching sensing graphs," *IEEE Trans. Cybern.*, vol. 48, no. 4, pp. 1202–1215, 2018.

[58] S.-M. Kang and H.-S. Ahn, "Design and realization of distributed adaptive formation control law for multi-agent systems with moving leader," *IEEE Trans. Ind. Electron.*, vol. 63, no. 2, pp. 1268–1279, 2015.

[59] O. Danesh Shahraki, "Optimal leader-follower formation control using dynamic games," Master's thesis, Concordia University, Montreal, Canada, 2015.

[60] S. Sedaghati, "Formation control and fault accommodation for a team of autonomous underwater vehicles," Master's thesis, Concordia University, Montreal, Canada, 2015.

[61] P. Zhang, M. de Queiroz, M. Khaledyan, and T. Liu, "Control of directed formations using interconnected systems stability," *J. Dyn. Syst. Meas. Control*, vol. 141, no. 4, 2019.

[62] T. Liu, M. de Queiroz, P. Zhang, and M. Khaledyan, "Further results on the distance and area control of planar formations," *Int. J. Control*, pp. 1–17, 2019.

[63] S. M. Kang, M. C. Park, and H. S. Ahn, "Distance-based cycle-free persistent formation: Global convergence and experimental test with a group of quadcopters," *IEEE Trans. Ind. Electron.*, vol. 64, no. 1, pp. 380–389, 2016.

[64] M. H. Trinh, S. Zhao, Z. Sun, D. Zelazo, B. D. O. Anderson, and H.-S. Ahn, "Bearing-based formation control of a group of agents with leader-first follower structure," *IEEE Trans. Autom. Control*, vol. 64, no. 2, pp. 598–613, 2019.

[65] V. H. Pham, M. H. Trinh, and H.-S. Ahn, "Finite-time convergence of acyclic generically persistent formations," in *Proc. Amer. Control Conf. (ACC)*, pp. 3642–3647, 2018.

[66] Z. Sun, H. G. de Marina, G. S. Seyboth, B. D. O. Anderson, and C. Yu, "Circular formation control of multiple unicycle-type agents with nonidentical constant speeds," *IEEE Trans. Control Syst. Tech.*, vol. 27, no. 1, pp. 192–205, 2018.

[67] S. Zhao, D. V. Dimarogonas, Z. Sun, and D. Bauso, "A general approach to coordination control of mobile agents with motion constraints," *IEEE Trans. Autom. Control*, vol. 63, no. 5, pp. 1509–1516, 2017.

[68] K. Aryankia and R. R. Selmic, "Neuro-adaptive formation control and target tracking for nonlinear multi-agent systems with time-delay," *IEEE Contr. Syst. Lett.*, vol. 5, no. 3, pp. 791–796, 2021.

[69] R. K. N. Vaddipalli, R. R. Selmic, and A. K. Rathore, "Multi-layered formation control of autonomous marine vehicles with nonlinear dynamics," in *Proc. IECON 44th Annu. Conf.*, pp. 2360–2366, 2018.

[70] S. J. Fu, "Aircraft guidance for formation flying based on optimal control theory," in *Proc. Amer. Control Conf. (ACC)*, (Minneapolis, MN, USA), pp. 393–394, June 1987.

[71] Z. Li, T. Zhang, and G. Xie, "LQR-based optimal leader-follower consensus of second-order multi-agent systems," in *Proc. 2015 Chin. Intell. Syst. Conf.*, (Yangzhou, China), pp. 353–361.

[72] G. Xu, D. Zhao, P. Liao, and G. Shi, "Optimal control of UAV elastic formation based on legendre pseudospectral method," in *Proc. Chin. Control Decis Conf. (CCDC)*, (Yinchuan, China), pp. 6389–6394, May 2016.

[73] Y. Wang, L. Cheng, Z. G. Hou, J. Yu, and M. Tan, "Optimal formation of multirobot systems based on a recurrent neural network," *IEEE Trans. Neural Netw. Learn. Syst*, vol. 27, no. 2, pp. 322–333, 2016.

[74] Y. Liu and Z. Geng, "Finite-time optimal formation control for linear multi-agent systems," in *Proc. 33rd Chin. Control Conf. (CCC)*, (Nanjing, China), pp. 8941–8946, July 2014.

[75] X. X. Yang, G. Y. Tang, Y. Li, and P. D. Wang, "Optimal formation control for multi-agents systems with external disturbances," in *Proc. 31st Chin. Control Conf. (CCC)*, (Hefei, China), pp. 2291–2295, July 2012.

[76] A. Imani, M. Bahrami, and B. Ebrahimi, "Optimal sliding mode control for spacecraft formation flying," in *Proc. 2nd Int. Conf. Control Instrum. Autom. (ICCIA)*, (Shiraz, Iran), pp. 38–43, Dec. 2011.

[77] H. Huang, C. Yu, and Q. Wu, "Distributed LQR design for multi-agent formations," in *Proc. 49th IEEE Conf. Decis. Control (CDC)*, (Atlanta, GA, USA), pp. 4535–4540, Dec. 2010.

[78] H. Zhenqi, Z. Ke, and L. Meibai, "Research on control method of keeping flight formation by using SDRE on the sun-earth libration points," *Advances in Astronomy*, 2017.

[79] H. Zhang, G. Zhao, and G. Xu, "Time-optimal control for formation reconfiguration of multiple unmanned aerial vehicles," in *Proc. 35th Chin. Control Conf. (CCC)*, (Chengdu, China), pp. 5630–5635, July 2016.

[80] W. Ren and Y. Cao, "Overview of recent research in distributed multi-agent coordination," in *Distributed Coordination of Multi-agent Networks*, pp. 23–41, Springer, 2011.

[81] K.-K. Oh and H.-S. Ahn, "Distance-based sequential formation control of mobile agents by using motion primitives," in *IEEE Int. Symp. Intell. Control (ISIC)*, pp. 1464–1469, 2010.

[82] E. Semsar-Kazerooni and K. Khorasani, "Optimal consensus algorithms for cooperative team of agents subject to partial information," *Automatica*, vol. 44, no. 11, pp. 2766–2777, 2008.

[83] P. Deshpande, P. P. Menon, C. Edwards, and I. Postlethwaite, "A distributed control law with guaranteed lqr cost for identical dynamically coupled linear systems," in *Proc. Amer. Control Conf. (ACC)*, pp. 5342–5347, 2011.

[84] F. Borrelli and T. Keviczky, "Distributed lqr design for identical dynamically decoupled systems," *IEEE Trans. Autom. Control*, vol. 53, no. 8, pp. 1901–1912, 2008.

[85] H. Zhang, T. Feng, G.-H. Yang, and H. Liang, "Distributed cooperative optimal control for multiagent systems on directed graphs: An inverse optimal approach," *IEEE Trans. Cybern.*, vol. 45, no. 7, pp. 1315–1326, 2015.

[86] W. B. Dunbar and R. M. Murray, "Distributed receding horizon control for multi-vehicle formation stabilization," *Automatica*, vol. 42, no. 4, pp. 549–558, 2006.

[87] A. Nedic and A. Ozdaglar, "Distributed subgradient methods for multi-agent optimization," *IEEE Trans. Autom. Control*, vol. 54, no. 1, pp. 48–61, 2009.

[88] T. Feng, H. Zhang, Y. Luo, and H. Liang, "Globally optimal distributed cooperative control for general linear multi-agent systems," *Neurocomputing*, vol. 203, pp. 12–21, 2016.

[89] O. A. Orqueda and R. Fierro, "Robust vision-based nonlinear formation control," in *Proc. Amer. Control Conf. (ACC)*, pp. 6–pp, 2006.

[90] Y. Lu, G. Zhang, Z. Sun, and W. Zhang, "Robust adaptive formation control of underactuated autonomous surface vessels based on MLP and DOB," *Nonlinear Dynamics*, vol. 94, no. 1, pp. 503–519, 2018.

[91] H. GarciadeMarina, "Maneuvering and robustness issues in undirected displacement-consensus-based formation control," *IEEE Trans. Autom. Control*, 2020.

[92] D. Liu, H. Liu, F. L. Lewis, and K. P. Valavanis, "Robust time-varying formation control for tail-sitters in flight mode transitions," *IEEE Trans. Syst., Man, Cybern. Syst.*, 2019.

[93] W. Jasim and D. Gu, "Robust team formation control for quadrotors," *IEEE Trans. Control Syst. Technol*, vol. 26, no. 4, pp. 1516–1523, 2017.

[94] K. Fathian, S. Safaoui, T. H. Summers, and N. R. Gans, "Robust distributed planar formation control for higher order holonomic and nonholonomic agents," *IEEE Trans. Robot.*, 2020.

[95] J. Chen, Z. Shi, and Y. Zhong, "Robust formation control for uncertain multi-agent systems," *J. Franklin Inst.*, vol. 356, no. 15, pp. 8237–8254, 2019.

[96] Z. Peng, D. Wang, and X. Hu, "Robust adaptive formation control of underactuated autonomous surface vehicles with uncertain dynamics," *IET Control Theory & Applic.*, vol. 5, no. 12, pp. 1378–1387, 2011.

[97] J. González-Sierra, H. Ríos, and A. Dzul, "Quad-rotor robust time-varying formation control: a continuous sliding-mode control approach," *Int. J. Control*, vol. 93, no. 7, pp. 1659–1676, 2020.

[98] W. Zhao, H. Liu, and F. L. Lewis, "Robust formation control for cooperative underactuated quadrotors via reinforcement learning," *IEEE Trans. Neural Netw. Learn. Syst*, 2020.

[99] N. Xuan-Mung and S. K. Hong, "Robust adaptive formation control of quadcopters based on a leader–follower approach," *Int. J. Adv. Robotic Sys.*, vol. 16, no. 4, 2019.

[100] N. Messai, D. H. Nguyen, N. Manamanni, *et al.*, "Robust formation control under state constraints of multi-agent systems in clustered networks," *Systems & Control Letters*, vol. 140, p. 104689, 2020.

[101] H. Liu, T. Ma, F. L. Lewis, and Y. Wan, "Robust formation control for multiple quadrotors with nonlinearities and disturbances," *IEEE Trans. Cybern.*, vol. 50, no. 4, pp. 1362–1371, 2018.

[102] D. Han and D. Panagou, "Robust multitask formation control via parametric Lyapunov-like barrier functions," *IEEE Trans. Autom. Control*, vol. 64, no. 11, pp. 4439–4453, 2019.

[103] D. Liu, H. Liu, F. L. Lewis, and Y. Wan, "Robust fault-tolerant formation control for tail-sitters in aggressive flight mode transitions," *IEEE Trans. Ind. Informat.*, vol. 16, no. 1, pp. 299–308, 2019.

[104] C. P. Bechlioulis and K. J. Kyriakopoulos, "Robust model-free formation control with prescribed performance and connectivity maintenance for nonlinear multi-agent systems," in *Proc. 53rd IEEE Conf. Decis. Control (CDC)*, pp. 4509–4514, 2014.

[105] Y. Fei, P. Shi, and C.-C. Lim, "Robust formation control for multi-agent systems: A reference correction based approach," *IEEE Trans. Circuits Syst. I, Reg. Papers*, vol. 68, no. 6, pp. 2616–2625, 2021.

[106] Y.-B. Bae, Y.-H. Lim, S.-M. Kang, and H.-S. Ahn, "Disturbance attenuation in distance-based formation control: A linear matrix inequality approach," in *IEEE Conf. Control Tech. Appl. (CCTA)*, pp. 1609–1614, 2018.

[107] F. Mehdifar, C. P. Bechlioulis, F. Hashemzadeh, and M. Baradarannia, "Prescribed performance distance-based formation control of multi-agent systems," *Automatica*, vol. 119, p. 109086, 2020.

[108] G. Jing and L. Wang, "Multi-agent flocking with angle-based formation shape control," *IEEE Trans. Autom. Control*, vol. 65, no. 2, pp. 817–823, 2019.

[109] D. Van Vu, M. H. Trinh, P. D. Nguyen, and H.-S. Ahn, "Distance-based formation control with bounded disturbances," *IEEE Contr. Syst. Lett.*, vol. 5, no. 2, pp. 451–456, 2020.

[110] M. Mesbahi and M. Egerstedt, *Graph theoretic methods in multiagent networks*. Princeton University Press, 2010.

[111] L. Asimow and B. Roth, "The rigidity of graphs, II," *J. Math. Anal. Appl.*, vol. 68, no. 1, pp. 171–190, 1979.

[112] B. Hendrickson, "Conditions for unique graph realizations," *SIAM j. Comput.*, vol. 21, no. 1, pp. 65–84, 1992.

[113] G. Laman, "On graphs and rigidity of plane skeletal structures," *J. Eng. Math.*, vol. 4, no. 4, pp. 331–340, 1970.

[114] X. Chen, M.-A. Belabbas, and T. Başar, "Formation control with triangulated laman graphs," in *Proc. 54th IEEE Conf. Decis. Control (CDC)*, pp. 4115–4120, 2015.

[115] R. Connelly and W. Whiteley, "Global rigidity: the effect of coning," *Discrete Comput. Geom.*, vol. 43, no. 4, pp. 717–735, 2010.

[116] T.-S. Tay and W. Whiteley, "Generating isostatic frameworks," *Structural Topology 1985 Núm 11*, 1985.

[117] C. Yu, J. M. Hendrickx, B. Fidan, B. D. O. Anderson, and V. D. Blondel, "Three and higher dimensional autonomous formations: Rigidity, persistence and structural persistence," *Automatica*, vol. 43, no. 3, pp. 387–402, 2007.

[118] J. M. Hendrickx, B. Fidan, C. Yu, B. D. O. Anderson, V. D. Blondel, *et al.*, "Elementary operations for the reorganization of minimally persistent formations," in *Proc. math. theory net. sys. (MTNS) conf.*, no. 17, pp. 859–873, 2006.

[119] P. Tokekar, N. Karnad, and V. Isler, "Energy-optimal velocity profiles for car-like robots," in *Proc. 2011 IEEE Int. Conf. Robot. Autom. (ICRA)*, (Shanghai, China), pp. 1457–1462, May 2011.

[120] A. Kwok and S. Martinez, "Energy-balancing cooperative strategies for sensor deployment," in *Proc. 46th IEEE Conf. Decis. Control (CDC)*, (New Orleans, LA, USA), pp. 6136–6141, Dec. 2007.

[121] Y. Mei, Y. H. Lu, Y. C. Hu, and C. G. Lee, "A case study of mobile robot's energy consumption and conservation techniques," in *Proc. 12th Int. Conf. Adv. Robot. (ICAR)*, (Seattle, WA, USA), pp. 492–497, July 2005.

[122] R. Parasuraman, K. Kershaw, P. Pagala, and M. Ferre, "Model based on-line energy prediction system for semi-autonomous mobile robots," in *Proc. 5th Int. Conf. Intell. Syst. Model. Simul. (ISMS)*, (Langkawi, Malaysia), pp. 411–416, Jan. 2014.

[123] T. Cimen, "Systematic and effective design of nonlinear feedback controllers via the state-dependent riccati equation (sdre) method," *Annu. Rev. Control*, vol. 34, no. 1, pp. 32–51, 2010.

[124] H. Banks, B. Lewis, and H. Tran, "Nonlinear feedback controllers and compensators: a state-dependent riccati equation approach," *Comput. Optim. Appl.*, vol. 37, no. 2, pp. 177–218, 2007.

[125] W. Baumann and W. Rugh, "Feedback control of nonlinear systems by extended linearization," *IEEE Trans. Autom. Control*, vol. 31, no. 1, pp. 40–46, 1986.

[126] F. Ornelas-Tellez, J. J. Rico, and R. Ruiz-Cruz, "Optimal tracking for state-dependent coefficient factorized nonlinear systems," *Asian J. Control*, vol. 16, no. 3, pp. 890–903, 2014.

[127] T. Cimen, "State-dependent riccati equation (SDRE) control: a survey," *IFAC Proceedings Volumes*, vol. 41, no. 2, pp. 3761–3775, 2008.

[128] J. R. Cloutier, C. N. D'Souza, and C. P. Mracek, "Nonlinear regulation and nonlinear H_∞ control via the state-dependent riccati equation technique: Part 1, theory," in *Proc. 1st Int. Conf. Nonlin. Probl. Aviat. Aerosp.*, (Daytona Beach, FL), pp. 117–130, 1996.

[129] K. A. Roudkenary, H. Khaloozadeh, and A. K. Sedigh, "SDRE control of non-affine systems," in *Proc. 4th Int. Conf. Control, Instrum., Automat. (ICCIA)*, pp. 239–244, 2016.

[130] F. Topputo, M. Miani, and F. Bernelli-Zazzera, "Optimal selection of the coefficient matrix in state-dependent control methods," *J. Guid., Control, Dyn.*, vol. 38, no. 5, pp. 861–873, 2015.

[131] L.-G. Lin and M. Xin, "Computational enhancement of the sdre scheme: general theory and robotic control system," *IEEE Trans. Robotics*, vol. 36, no. 3, pp. 875–893, 2020.

[132] J. S. Shamma and J. R. Cloutier, "Existence of sdre stabilizing feedback," *IEEE Trans. Autom. Control*, vol. 48, no. 3, pp. 513–517, 2003.

[133] Y.-W. Liang and L.-G. Lin, "Analysis of SDC matrices for successfully implementing the SDRE scheme," *Automatica*, vol. 49, no. 10, pp. 3120–3124, 2013.

[134] K. D. Hammett, C. D. Hall, and D. B. Ridgely, "Controllability issues in nonlinear state-dependent riccati equation control," *J. Guid., Control, Dyn.*, vol. 21, no. 5, pp. 767–773, 1998.

[135] L.-G. Lin, J. Vandewalle, and Y.-W. Liang, "Analytical representation of the state-dependent coefficients in the SDRE/SDDRE scheme for multivariable systems," *Automatica*, vol. 59, pp. 106–111, 2015.

[136] A. Bracci, M. Innocenti, and L. Pollini, "Estimation of the region of attraction for state-dependent riccati equation controllers," *J. Guidance, Control, and Dynamics*, vol. 29, no. 6, pp. 1427–1430, 2006.

[137] I. Chang and S.-J. Chung, "Exponential stability region estimates for the state-dependent riccati equation controllers," in *Proc. 48h IEEE Conf. Dec. Control (CDC)*, pp. 1974–1979, 2009.

[138] J. R. Cloutier and D. T. Stansbery, "Control of a continuously stirred tank reactor using an asymmetric solution of the state-dependent Riccati equation," in *Proc. of the IEEE Int. Conf. Control Appl.*, vol. 2, pp. 893–898, 1999.

[139] T. Çimen, "Approximate nonlinear optimal SDRE tracking control," in *17th IFAC Symp. Automat. Control Aerosp.*, pp. 147–152, 2007.

[140] A. Isidori, *Nonlinear control systems II*. Springer Science & Business Media, 2012.

[141] H. K. Khalil, "Nonlinear systems," *Upper Saddle River*, 2002.

[142] H. J. Marquez, *Nonlinear control systems: analysis and design*, vol. 1. Wiley-Interscience Hoboken, 2003.

[143] V. Sundarapandian, "Local and global asymptotic stability of nonlinear cascade interconnected systems," *Math. Comput. Model.*, vol. 40, no. 1-2, pp. 227–232, 2004.

[144] B. Joe, "Shape measures for quadrilaterals, pyramids, wedges, and hexahedra," 2008.

[145] J. Wang and M. Xin, "Integrated optimal formation control of multiple unmanned aerial vehicles," *IEEE Trans. Control Syst. Technol.*, vol. 21, no. 5, pp. 1731–1744, 2013.

[146] J. R. Cloutier and J. C. Cockburn, "The state-dependent nonlinear regulator with state constraints," in *Proc. Amer. Control Conf. (ACC)*, vol. 1, pp. 390–395, 2001.

[147] B. Friedland, "On controlling systems with state-variable constraints," in *Proc. Amer. Control Conf. (ACC)*, vol. 4, pp. 2123–2127, 1998.

[148] R. Bhatia and P. Rosenthal, "How and why to solve the operator equation AX-XB=Y," *Bull. London Math. Soc.*, vol. 29, no. 1, pp. 1–21, 1997.

[149] P. Benner, R.-C. Li, and N. Truhar, "On the ADI method for sylvester equations," *J. Comput. Appl. Math.*, vol. 233, no. 4, pp. 1035–1045, 2009.

[150] S. G. Lee and Q. P. Vu, "Simultaneous solutions of sylvester equations and idempotent matrices separating the joint spectrum," *Linear Algebra Appl*, vol. 435, no. 9, pp. 2097–2109, 2011.

[151] M. A. Belabbas, "On global stability of planar formations," *IEEE Trans. Autom. Control*, vol. 58, no. 8, pp. 2148–2153, 2013.

[152] O. Rozenheck, S. Zhao, and D. Zelazo, "Distance-constrained formation tracking control," in *Israel 55th Annu. Conf. Aero. Sci.*, 2015.

[153] S. R. Nekoo, "Tutorial and review on the state-dependent Riccati equation," *J. Appl. Nonlinear Dyn.*, vol. 8, no. 2, pp. 109–166, 2019.

[154] Y.-W. Liang and L.-G. Lin, "On factorization of the nonlinear drift term for SDRE approach," *IFAC Proceedings Volumes*, vol. 44, no. 1, pp. 9607–9612, 2011.

[155] F. Lin and A. W. Olbrot, "An lqr approach to robust control of linear systems with uncertain parameters," in *Proc. 35th IEEE Conf. Decis. Control,*, vol. 4, pp. 4158–4163, 1996.

[156] X. Wang, E. E. Yaz, S. C. Schneider, and Y. I. Yaz, "$h2-h\infty$ control of continuous-time nonlinear systems using the state-dependent riccati equation approach," *Sys. Science & Control Eng.*, vol. 5, no. 1, pp. 224–231, 2017.

[157] D. Wang, D. Liu, H. Li, and X. Yang, "Robust optimal control for a class of nonlinear dynamic systems using single network adaptive dynamic programming," in *Proc. 33rd Chin. Control Conf. (CCC)*, pp. 8711–8716, 2014.

[158] H. Pang and L. Wang, "Global robust optimal sliding mode control for a class of affine nonlinear systems with uncertainties based on sdre," in *2nd Int. Workshop on Comput. Sci. and Eng.*, pp. 276–280, 2009.

[159] H.-P. Pang and Q. Yang, "Optimal sliding mode control for a class of uncertain nonlinear systems based on feedback linearization," in *Robust Control, Theory Appl.*, InTech, 2011.

[160] V. Utkin and J. Shi, "Integral sliding mode in systems operating under uncertainty conditions," in *Proc. 35th IEEE Conf. Conf. Decis. Control*, vol. 4, pp. 4591–4596, 1996.

[161] H. Pang and X. Yang, "Robust optimal sliding-mode tracking control for a class of uncertain nonlinear mimo systems," *J. of Applied Mathematics*, vol. 2013, 2013.

[162] F. Castaños and L. Fridman, "Analysis and design of integral sliding manifolds for systems with unmatched perturbations," *IEEE Trans. Autom. Control*, vol. 51, no. 5, pp. 853–858, 2006.

[163] W.-J. Cao and J.-X. Xu, "Nonlinear integral-type sliding surface for both matched and unmatched uncertain systems," *IEEE Trans. Autom. Control*, vol. 49, no. 8, pp. 1355–1360, 2004.

[164] H. U. Suleiman, M. B. Mu'azu, T. A. Zarma, A. T. Salawudeen, S. Thomas, and A. A. Galadima, "Methods of chattering reduction in sliding mode control: a case study of ball and plate system," in *Proc. IEEE 7th Int. Conf. Adaptive Sci. & Tech. (ICAST)*, pp. 1–8, 2018.

[165] I. González, S. Salazar, and R. Lozano, "Chattering-free sliding mode altitude control for a quad-rotor aircraft: Real-time application," *J. Intell. & Robot. Sys.*, vol. 73, no. 1, pp. 137–155, 2014.

Appendices

Appendix A

SDC Parametrization

The SDC parametrization which is used for simulation in Figure 4.7 is

$$\hat{A}_s(\mathbf{p}) = 0.1 \begin{bmatrix} e_1 & -e_t & 0 & 0 & 0 & 0 \\ 0 & e_2 & -e_1 & 0 & 0 & 0 \\ 0 & 0 & e_3 & -e_2 & 0 & 0 \\ 0 & 0 & 0 & e_4 & -e_3 & 0 \\ 0 & 0 & 0 & 0 & e_5 & -e_4 \\ -e_5 & 0 & 0 & 0 & 0 & e_t \end{bmatrix}.$$

Also, the matrix A_{21} that is used for simulation in Figure 4.8 is

$$A_{21} = \frac{1}{20} \begin{bmatrix} e_1 & -e_t & 0 & 0 & 0 & 0 & 0 & 0 & 0 & 0 \\ 0 & e_2 & -e_1 & 0 & 0 & 0 & 0 & 0 & 0 & 0 \\ 0 & 0 & e_3 & -e_2 & 0 & 0 & 0 & 0 & 0 & 0 \\ 0 & 0 & 0 & e_4 & -e_3 & 0 & 0 & 0 & 0 & 0 \\ 0 & 0 & 0 & 0 & e_5 & -e_4 & 0 & 0 & 0 & 0 \\ 0 & 0 & 0 & 0 & 0 & e_6 & -e_5 & 0 & 0 & 0 \\ 0 & 0 & 0 & 0 & 0 & 0 & e_7 & -e_6 & 0 & 0 \\ 0 & 0 & 0 & 0 & 0 & 0 & 0 & e_8 & -e_7 & 0 \\ 0 & 0 & 0 & 0 & 0 & 0 & 0 & 0 & e_9 & -e_8 \\ -e_9 & 0 & 0 & 0 & 0 & 0 & 0 & 0 & 0 & e_t \end{bmatrix}.$$

Appendix B

Gradient-Based Controller

The gradient-based control law for the agent i law is

$$u_i = -\nabla_{p_i}\Phi(e) = -\sum_{j\in N_i}(\|d_{ij}\|^2 - {d^*_{ij}}^2)d_{ij},$$

where the corresponding positive semi-definite potential function is

$$\Phi(e) = \frac{1}{2}\sum_{(i,j)\in E}^{N}(\|d_{ij}\|^2 - {d^*_{ij}}^2)^2.$$

The local asymptotic stability of the controller is proved in [152].